



The  
University  
Of  
Sheffield.

**The Role of TRAIL in Pulmonary Arterial Hypertension  
And Pulmonary Fibrosis**

**By:**

**Adam Thomas Braithwaite**

A thesis submitted in partial fulfilment of the requirements for the degree of  
Doctor of Philosophy

The University of Sheffield  
Faculty of Faculty of Medicine, Dentistry and Health  
Department of Infection, Immunity & Cardiovascular Disease

Registration number: 150234861

September 2019

## Abstract

Pulmonary arterial hypertension (PAH) and pulmonary fibrosis (PF) are complex disorders with distinct pathobiology, but both feature progressive aberrant remodelling of the lung. PAH is characterised by pulmonary arterial remodelling – underpinned by vascular smooth muscle cell (VSMC) proliferation – and a progressive increase in pulmonary vascular resistance leading to right heart failure. In PF, expansion and activation of apoptosis-resistant fibroblasts and myofibroblasts leads to excessive collagen deposition and progressive decline in lung function. The tumour necrosis factor-related apoptosis-inducing ligand (TRAIL) is an apoptosis-inducing cytokine that can also promote cell survival, proliferation and migration via non-canonical kinase signalling pathways. TRAIL has previously been demonstrated as detrimental in PAH mice, but protective in the context of autoimmune disease and PF. I hypothesised that TRAIL specifically from fibroblasts confers a protective effect in PF, while VSMC-derived TRAIL drives PAH pathogenesis. To test this, *TRAIL* was genetically deleted in Cre/lox mice, which were subjected to models of PAH and PF. Deletion of *TRAIL* from fibroblasts worsened bleomycin-induced PF with no change in associated PAH. Deletion of VSMC-derived *TRAIL* led to a reduction in Sugen 5416/hypoxia-induced PAH determined by haemodynamics, right ventricular hypertrophy and remodelling of small pulmonary arteries. These data indicate that TRAIL produced by fibroblasts is protective in the development of PF induced by bleomycin, whereas TRAIL from VSMCs is pathogenic in the context of experimental PAH. Effects of TRAIL stimulation on cultured human pulmonary artery VSMCs were explored by measuring transcriptomic and protein phosphorylation changes. TGF $\beta$ /BMP signalling, focal adhesion and extracellular matrix regulation were key pathways regulated by TRAIL. Furthermore, expression of several TRAIL-regulated genes was altered in animal models of PF and PAH, and in serum of PAH patients. Together these data highlight new mechanisms for TRAIL involvement in PF and PAH and present new potential targets for therapeutic intervention.

## Acknowledgements

Firstly, I would like to thank my academic supervisors, Professor Allan Lawrie and Dr. Helen Marriott for their guidance and dedication to helping me succeed with this project. Their willingness to sacrifice their own time, and patience with me were instrumental in my accomplishments.

I would also like to thank all the members of the Sheffield Pulmonary Vascular Research Group (past and present at the time of writing) who helped me along the way. In particular, Dr. Josephine Pickworth, Dr. Laura West and Dr. Roger Thompson for their academic support and readiness for a helpful discussion whenever I needed it.

Furthermore I thank Professor Allan Lawrie and Dr. Laura West for carrying out cardiac catheterisation of mice, Nadine Arnold and Dr. Amira Zawia for performing and analysing echocardiography imaging, and all the Sheffield Biological Services Unit staff for their help with animal breeding and husbandry. Also I thank Nadine Arnold and Dr. Laura West for their invaluable help with animal experimental design and management.

I would like to thank Dr. Josephine Pickworth and Dr. Sarah Dawson for performing cell stimulation experiments and preparing protein lysates, and James Iremonger for performing microarray assays. Also I thank Fiona Wright for her advice and assistance with histology.

I would also like to thank Professor Stephan Offermanns, Professor Chris Denton, C. Hall and Professor George Bou-Gharios for providing transgenic mouse strains used in this project.

Finally, and most importantly I would like to thank Tanya. Your encouragement and support gave me the strength and confidence to embark on this journey and to see it through to the best of my ability until the end.

## Abbreviations

$\alpha$ -SMA	Alpha smooth muscle actin
5-HT	5-hydroxytryptamine
ABEVG	Miller's elastin stain with alcian blue and Curtis' modified van Gieson
ACVR1/2	Activin A receptor 1/2
AECs	Alveolar epithelial cells
ALK1	Activin receptor-like kinase type 1
ANOVA	Analysis of variation
ApoE	Apolipoprotein E
BMP	Bone morphogenetic protein
BMPR2	Bone morphogenetic protein receptor type 2
bp	Base pairs
CCB	Calcium channel blocker
cFLIP	(FADD-like interleukin-1 beta-converting enzyme)-inhibitory protein
cGMP	Cyclic guanosine monophosphate
COLx	Collagen species
CSA	Cross-sectional area (of vessels)
Ct	Threshold cycle
CTD	Connective tissue disease
CTEPH	Chronic thromboembolic pulmonary hypertension
DcR	(TRAIL) decoy receptor
dCt	Ct target gene normalised to Ct reference gene; delta Ct
ddCt	dCt target sample normalised to dCt reference sample; delta delta Ct
DE	Differentially expressed
DISC	Death-inducing signalling complex
dP/dt	Delta pressure/delta time; change in pressure over time
DR	(TRAIL) death receptor
ECs	Endothelial cells
ECM	Extracellular matrix
EMT	Epithelial to mesenchymal cell transition
ERA	Endothelin receptor antagonist
ERK	Extracellular signal-regulated kinase
ET	Endothelin
FADD	Fas-associated protein with death domain
FAK	Focal adhesion kinase
FDR	False discovery rate

FIGF	C-Fos induced growth factor; VEGFD
FGFR	Fibroblast growth factor receptor
FRT	Flippase recognition target
GAPDH	Glyceraldehyde 3-phosphate dehydrogenase
GO	Gene ontology
HIV	Human immunodeficiency virus
ICAM1	Intracellular adhesion molecule 1
Id	Inhibitor of DNA-binding
IGF1R	Insulin-like growth factor type 1 receptor
IKK- $\gamma$	Inhibitor of NF- $\kappa$ B kinase subunit gamma
IL	Interleukin
ILD	Interstitial lung disease
IPAH	Idiopathic pulmonary arterial hypertension
IPF	Idiopathic pulmonary fibrosis
ITGA/B $\alpha$	Integrin alpha/beta species
JNK	c-Jun N-terminal kinase
KEGG	Kyoto Encyclopaedia of Genes and Genomes
LIMMA	Linear models for microarray analysis
LV	Left ventricle
MAPK	Mitogen-activated protein kinase
MCT	Monocrotaline
mDR5	Mouse (TRAIL) death receptor 5
MEK1	MAPK/ERK protein-serine kinase 1
mPAP	Mean pulmonary artery pressure
mRNA	Messenger ribonucleic acid
MTC	Masson's Trichrome stain
NFAT	Nuclear factor of activated T cells
NF- $\kappa$ B	Nuclear factor kappa-light-chain-enhancer of activated B cells
NO	Nitric oxide
OPG	Osteoprotegerin; TNFRSF11B
p300	E1A-associated protein p300; Histone acetyltransferase p300
PA	Pulmonary artery
PAAT	Pulmonary artery acceleration time
PAECs	Pulmonary artery endothelial cells
PASMCs	Pulmonary arterial smooth muscle cells
PAH	Pulmonary arterial hypertension
PAKs	p21-activated kinases

PBS	Phosphate-buffered saline
PCR	Polymerase chain reaction
PDE-5	Phosphodiesterase type 5
PDGFD	Platelet-derived growth factor delta
PDGFRA/B	Platelet-derived growth factor receptor alpha/beta
PF	Pulmonary fibrosis
PH	Pulmonary hypertension
PI3K	Phosphatidylinositide 3-kinase
PKC	Protein kinase C
PTEN	Phosphatase and tensin homolog
RIPK1/3	Receptor-interacting serine/threonine-protein kinase 1/3
RA	Rheumatoid arthritis
RV	Right ventricle
RVEDP	Right ventricular end-diastolic pressure
RVESP	Right ventricular end-systolic pressure
RVH	Right ventricular hypertrophy
RT-qPCR	Reverse transcription with quantitative polymerase chain reaction
SDS-PAGE	Sodium dodecyl sulphate - polyacrylamide gel electrophoresis
SEM	Standard error of the mean
sGC	Soluble guanylate cyclase
siRNA	Small interfering RNA
SMCs	Smooth muscle cells
SOST	Sclerostin
SPIA	Signalling pathway impact analysis
sRANKL	(Soluble) receptor activator of NF- $\kappa$ B ligand; TNFSF11
SSc	Systemic sclerosis
SSc-PAH	Systemic sclerosis associated with PAH
SuHx	Sugen 5416/hypoxia
TGF $\beta$	Transforming growth factor beta
TGF $\beta$ R	Transforming growth factor beta receptor
TNF	Tumour necrosis factors
TLCo	Transfer factor of the lung for carbon monoxide
TRAF2	TNF receptor-associated factor 2
TRAIL	TNF-related apoptosis-inducing ligand; TNFSF10
TRAIL-R	TRAIL receptor
VEGF	Vascular endothelial growth factor
VEGFD	Vascular endothelial growth factor delta

VIPR1	Vasoactive intestinal polypeptide receptor 1
VSMCs	Vascular smooth muscle cells
VWF	Von Willebrand Factor

# Table of contents

<b>Abstract</b>	<b>i</b>
<b>Acknowledgements</b>	<b>ii</b>
<b>Abbreviations</b>	<b>iii</b>
<b>Table of contents</b>	<b>vii</b>
<b>List of figures</b>	<b>xii</b>
<b>List of tables</b>	<b>xiii</b>
<b>1 Introduction</b>	<b>1</b>
1.1 Pulmonary hypertension	1
1.2 Pulmonary arterial hypertension	1
1.2.1 PAH and lung disease	5
1.2.2 Pathobiology and molecular mechanisms of PAH	5
1.2.2.1 Pulmonary arterial vasoconstriction	6
1.2.2.2 Endothelial dysfunction	6
1.2.2.3 Genetic factors	7
1.2.2.4 Inflammation	7
1.2.3 Treatment of PAH	8
1.2.4 Animal models of PH/PAH	9
1.3 Pulmonary fibrosis	10
1.3.1 Pathobiology and molecular mechanisms of PF	11
1.3.2 Treatment of PF	13
1.3.3 Animal models of PF	14
1.4 Tumour necrosis factor-related apoptosis-inducing ligand	15
1.4.1 TRAIL molecular signalling	15
1.4.2 TRAIL in disease	19
1.4.2.1 TRAIL in cancer	19
1.4.2.2 TRAIL in PAH	21
1.4.2.3 TRAIL in autoimmune disease and fibrosis	22
1.4.2.4 Trail in airway inflammation	24
1.4.2.5 TRAIL in respiratory infection	25
1.5 Research hypothesis	26
<b>2 Materials and methods</b>	<b>28</b>
2.1 In vitro studies	28

2.1.1	Primary pulmonary artery smooth muscle cells	28
2.1.2	Stimulations	28
2.1.3	RNA extraction from cultured cells	28
2.1.4	Protein extraction from cultured cells	29
2.1.5	Synthesis of cDNA from mRNA	29
2.1.6	Quantitative RT-PCR	30
2.1.7	Array quantification of mRNA	30
2.1.8	Array quantification of protein	31
2.1.9	Differential mRNA analysis	31
2.1.10	Gene ontology analysis	31
2.1.11	Pathway topology analysis	32
2.1.12	Differential protein analysis	32
2.2	Animals	33
2.2.1	Licensing	33
2.2.2	Husbandry	33
2.2.3	Transgenic mouse lines	33
2.2.4	Breeding	36
2.2.5	Induction of Cre recombination	39
2.3	Genotyping	39
2.3.1	DNA extraction	40
2.3.2	Polymerase chain reaction	40
2.3.3	Agarose gel electrophoresis	41
2.4	Animal models	41
2.4.1	Animals	41
2.4.2	VSMC-specific TRAIL deletion in Sugen 5416/hypoxia	42
2.4.3	Bleomycin preliminary time-course model	43
2.4.4	Bleomycin final model	43
2.4.4.1	Global and fibroblast-specific TRAIL deletion in bleomycin model	44
2.4.5	Humane endpoints	44
2.5	Animal endpoint procedures	45
2.5.1	Echocardiography	45
2.5.2	Cardiac catheterisation	45
2.5.3	Sacrifice of animals	46
2.5.4	Lung perfusion formalin fixation	46
2.5.5	Tissue harvest	47
2.5.6	Harvest of frozen tissue for imaging	47
2.6	Animal tissue handling	47

2.6.1	Processing formalin fixed tissues for histology	47
2.6.2	Handling snap-frozen tissue for imaging	48
2.6.3	Grinding frozen lung tissue	48
2.6.4	RNA extraction from lung tissue	49
2.6.5	Protein extraction from lung tissue	49
2.6.6	Right ventricular hypertrophy measurement	50
2.7	Histological staining of tissue sections	50
2.7.1	General histological techniques	50
2.7.2	Miller's elastin stain	50
2.7.3	Masson's Trichrome stain	51
2.7.4	General immunohistochemistry method	52
2.7.5	Alpha smooth muscle actin immunostaining	52
2.7.6	TRAIL immunostaining	53
2.7.7	Von Willebrand Factor immunostaining	53
2.7.8	Imaging of histological sections	53
2.7.9	Imaging of fluorescence Cre reporter sections	54
2.7.10	Quantification of pulmonary vascular remodelling	54
2.7.11	Quantification of PF from images	55
2.8	Patient studies	56
2.8.1	Ethical approval	56
2.8.2	Participants	57
2.8.3	Serum protein measurement	57
2.9	Statistics	57
<b>3</b>	<b>The role of fibroblast-derived TRAIL in bleomycin-induced PF</b>	<b>58</b>
3.1	Generation of mice with global Cre-driven <i>TRAIL</i> knockout	60
3.1.1	Genotyping	60
3.1.2	Cre reporter demonstration of Cre recombination	63
3.2	Generation of mice with fibroblast-specific <i>TRAIL</i> deletion	65
3.2.1	Genotyping	65
3.2.2	Cre reporter demonstration of Cre recombination	66
3.3	Bleomycin mouse model of PF	68
3.3.1	Quantification of PF	70
3.3.2	Haemodynamics	72
3.3.3	Right ventricular hypertrophy	75
3.3.4	Pulmonary vascular remodelling	76
3.3.5	TRAIL mRNA expression in lungs	78

3.4	Fibroblast-specific <i>TRAIL</i> deleted mice have worsened PF	79
3.4.1	TRAIL expression in lungs	81
3.4.2	Quantification of PF	83
3.4.3	Haemodynamics	86
3.4.4	Right ventricular hypertrophy	89
3.4.5	Pulmonary vascular remodelling	90
3.5	Summary	94
3.6	Discussion	95
3.6.1	Fibroblasts are a protective source of TRAIL in PF	95
3.6.2	The role of TRAIL in bleomycin-induced PAH	96
3.6.3	The IP bleomycin mouse model of PF	97
<b>4</b>	<b>The role of VSMC-derived TRAIL in SuHx-induced PAH</b>	<b>100</b>
4.1	Generation of mice with VSMC-specific <i>TRAIL</i> deletion	101
4.1.1	Genotyping	101
4.1.2	Cre reporter demonstration of Cre recombination	103
4.2	VSMC-specific <i>TRAIL</i> deleted mice are protected from PAH	105
4.2.1	TRAIL expression in lungs	107
4.2.2	Haemodynamics	109
4.2.3	Right ventricular hypertrophy	112
4.2.4	Pulmonary vascular remodelling	113
4.3	Summary	117
4.4	Discussion	118
4.4.1	VSMCs are a protective source of TRAIL in PAH	118
4.4.2	The SuHx mouse model	120
<b>5</b>	<b>The role of TRAIL targets in PSMCs, animal models and human PAH</b>	<b>122</b>
5.1	TRAIL alters mRNA levels and protein phosphorylation in PSMCs	123
5.1.1	Microarray mRNA quantification	123
5.1.2	qPCR validation of differentially expressed genes	128
5.1.3	Gene ontology analysis	130
5.1.4	Protein kinase phosphorylation changes	132
5.1.5	Pathway topology analysis	135
5.2	Expression of TRAIL targets are altered in animal models and PAH patients	140
5.2.1	TRAIL-regulated genes in bleomycin mice	141
5.2.2	TRAIL-regulated genes in SuHx mice	143
5.2.3	TRAIL-regulated genes in patient serum	145
5.2.4	Correlation of serum sclerostin with PAH clinical severity	147

5.3	Summary	148
5.4	Discussion	149
5.4.1	TRAIL inhibits TGF $\beta$ /BMP signalling	149
5.4.2	TRAIL activates focal adhesion	151
5.4.3	A molecular signature of TRAIL stimulation in PSMCs	153
<b>6</b>	<b>General discussion</b>	<b>154</b>
6.1	Limitations	159
6.2	Future work	162
<b>7</b>	<b>Bibliography</b>	<b>165</b>
<b>8</b>	<b>Appendices</b>	<b>I</b>
8.1	Appendix A: Taqman RT-qPCR	I
8.1.1	Taqman RT-qPCR probes	I
8.1.2	Taqman RT-qPCR reaction	I
8.2	Appendix B: R scripts	II
8.2.1	LIMMA mRNA microarray analysis	II
8.2.2	SPIA pathway topology analysis	IV
8.3	Appendix C: Genotyping PCR	VI
8.3.1	Genotyping PCR primers	VI
8.3.2	TRAIL <sup>tm1c</sup> & TRAIL <sup>WT</sup> PCR reaction	VI
8.3.3	TRAIL <sup>tm1d</sup> & distal LoxP site PCR reaction	VII
8.3.4	COL1A2-Cre-ERT / PGK-Cre & WT control PCR reaction	VIII
8.3.5	SMMHC-Cre-ERT2 <sup>tg</sup> / SMMHC-Cre-ERT2 <sup>wt</sup> PCR reaction	IX

## List of figures

Figure 1.1: Molecular signalling of TRAIL. ....	18
Figure 1.2: TRAIL functions in lung diseases. ....	20
Figure 2.1: <i>TRAIL</i> TM1C transgene construct. ....	34
Figure 2.2: Transgenic breeding strategy. ....	38
Figure 2.2: Quantification of PF from images. ....	56
Figure 3.1: PCR genotyping of <i>TRAIL</i> <sup>tm1c</sup> , <i>TRAIL</i> <sup>tm1d</sup> and PGK-Cre transgenic alleles. ....	62
Figure 3.2: Cre reporter demonstrates ubiquitous Cre recombination. ....	64
Figure 3.3: PCR genotyping of <i>TRAIL</i> <sup>tm1c</sup> and Col1a2-Cre-ERT transgenic alleles. ....	65
Figure 3.4: Cre reporter demonstrates fibroblast-specific Cre recombination. ....	67
Figure 3.5: Experimental schematic for IP bleomycin time-course. ....	69
Figure 3.6: PF in bleomycin mice. ....	71
Figure 3.7: PAH determined by haemodynamic measures after bleomycin insult. ....	74
Figure 3.8: Right ventricular hypertrophy after bleomycin insult. ....	75
Figure 3.9: Pulmonary vascular remodelling in bleomycin mice. ....	77
Figure 3.10: <i>TRAIL</i> mRNA expression in lungs from bleomycin mice. ....	78
Figure 3.11: Experimental schematic for <i>TRAIL</i> genetic deletion in bleomycin mice. ....	80
Figure 3.12: <i>TRAIL</i> expression in lungs of <i>TRAIL</i> -deleted bleomycin mice. ....	82
Figure 3.13: PF in <i>TRAIL</i> -deleted bleomycin lungs. ....	85
Figure 3.14: Haemodynamic measures in <i>TRAIL</i> -deleted bleomycin mice. ....	88
Figure 3.15: Right ventricular hypertrophy in <i>TRAIL</i> -deleted bleomycin mice. ....	89
Figure 3.16: Pulmonary vascular remodelling in <i>TRAIL</i> -deleted bleomycin mice. ....	93
Figure 4.1: PCR genotyping of <i>TRAIL</i> <sup>tm1c</sup> and SMMHC-Cre-ERT2 transgenic alleles. ....	102
Figure 4.2: Cre reporter demonstrates VSMC-specific Cre recombination. ....	104
Figure 4.3: Experimental schematic for <i>TRAIL</i> genetic deletion in SuHx mice. ....	106
Figure 4.4: <i>TRAIL</i> expression in VSMC-specific <i>TRAIL</i> -deleted SuHx lungs. ....	108
Figure 4.5: Haemodynamic measures in VSMC-specific <i>TRAIL</i> -deleted SuHx mice. ....	111
Figure 4.6: Right ventricular hypertrophy in VSMC-specific <i>TRAIL</i> -deleted SuHx mice. ....	112
Figure 4.7: Vascular remodelling in VSMC-specific <i>TRAIL</i> -deleted SuHx lungs. ....	116
Figure 5.1: Differentially expressed mRNA after TRAIL stimulation of PASCs. ....	125
Figure 5.2: qPCR validation of microarrays. ....	129
Figure 5.3: Pathways activated by TRAIL stimulation of PASCs. ....	136
Figure 5.4: TGFβ signalling pathway is inhibited by TRAIL stimulation of PASCs. ....	138
Figure 5.5: Focal adhesion pathway is activated by TRAIL stimulation of PASCs. ....	139
Figure 5.6: Expression of TRAIL-regulated genes in lungs of bleomycin mice. ....	142
Figure 5.7: Expression of TRAIL-regulated genes in lungs of SuHx mice. ....	144

Figure 5.8: Expression of TRAIL-regulated genes in patient serum. ....	146
Figure 5.9: Correlation of serum sclerostin with PAH clinical severity. ....	147

## List of tables

Table 1.1: Clinical classification of pulmonary hypertension.....	3
Table 2.1: Transgenic mouse lines. ....	36
Table 5.1: Top differentially expressed genes after TRAIL stimulation of PSMCs .....	126
Table 5.2: Gene ontology analysis of TRAIL-induced mRNA changes in PSMCs .....	131
Table 5.3: Altered protein levels after TRAIL stimulation of PSMCs .....	133

# **1 Introduction**

## **1.1 Pulmonary hypertension**

Pulmonary hypertension (PH) is a disorder traditionally diagnosed by mean pulmonary arterial pressure (mPAP), obtained from right heart catheterisation, greater than or equal to 25 mmHg (Hatano and Strasser 1975). However, this definition has since been updated to specify PH should be diagnosed in patients with mPAP >20 mmHg (Simonneau and Montani 2019). PH is present in a range of disorders, and these are classified into five main groups: pulmonary arterial hypertension (PAH), PH due to left heart disease, PH due to lung disease and/or hypoxia, chronic thromboembolic PH (CTEPH) and PH with unclear or multifactorial mechanisms (Table 1; Simonneau and Montani 2019).

## **1.2 Pulmonary arterial hypertension**

Pulmonary arterial hypertension (PAH) is a particularly rare form of PH, with a prevalence of approximately 15–26 cases per million population (Humbert et al. 2006, Peacock et al. 2007). Unlike other forms of PH, PAH is characterised by the progressive remodelling of pulmonary arteries, in particular thickening of the vessel walls and occasionally the formation of obstructive plexiform lesions. Chronic pulmonary arterial pathology causes a progressive increase in pulmonary vascular resistance (PVR), leading to raised afterload on the right ventricle (RV) and ultimately right heart failure. The prognosis for PAH patients is poor: mean life expectancy of untreated PAH patients is 2.8 years (D'Alonzo et al. 1991) and with modern diagnosis and treatment, survival at 5 years is just 59% (Boucly et al. 2017). Although the incidence of PAH is approximately 4-fold higher in women, survival is worse in men – an effect that has been attributed to poorer response to treatment in men, measured by PVR and right ventricular ejection fraction (Jacobs et al. 2014). Interestingly there is widely varied severity within PAH patient cohorts, and risk stratification based on clinical characteristics and biomarkers has been demonstrated as beneficial in predicting survival (Boucly et al. 2017,

Hoepfer et al. 2017). Patients may present with symptoms including dyspnoea, fatigue, chest pain and coughing. Initial examination may be carried out by echocardiography, followed by diagnosis by cardiac catheterisation. Further to PH diagnosis based on mPAP of >20 mmHg, classification of PAH is recommended to include pulmonary capillary wedge pressure <15 mmHg and PVR  $\geq$ 3 Wood Units, to exclude the effects of cardiac output or left ventricular dysfunction (Simonneau and Montani 2019).

The diverse range of PAH clinical conditions may be further classified by recognised risk factors and co-morbidities, including drug and toxin-induced PAH, or associated diseases: connective tissue disease (CTD), HIV, portal hypertension, congenital heart disease or schistosomiasis (Table 1; Simonneau and Montani 2019). Heritable PAH refers to PAH in patients with family history and/or pathogenic mutations, of which those in bone morphogenetic protein receptor type 2 (*BMPR2*) are the most common. The remaining PAH cases, without a family history, known mutations, identified risk factors or relevant comorbidities, are classified as idiopathic PAH (IPAH). IPAH is relatively rare; estimates at the prevalence of IPAH vary from 6.5 cases per million (Humbert et al. 2006) to 9 cases per million (Peacock et al. 2007), representing 35–43% of total PAH cases.

**Table 1.1: Clinical classification of pulmonary hypertension.**

Group	Description
1	PAH
1.1	Idiopathic PAH
1.2	Heritable PAH
1.3	Drug- and toxin-induced PAH
1.4	PAH associated with:
1.4.1	Connective tissue disease
1.4.2	HIV infection
1.4.3	Portal hypertension
1.4.4	Congenital heart disease
1.4.5	Schistosomiasis
1.5	PAH long-term responders to calcium channel blockers
1.6	PAH with overt features of venous/capillaries (PVOD/PCH) involvement
1.7	Persistent PH of the newborn syndrome
2	PH due to left heart disease
2.1	PH due to heart failure with preserved LVEF
2.2	PH due to heart failure with reduced LVEF
2.3	Valvular heart disease
2.4	Congenital/acquired cardiovascular conditions leading to post-capillary PH
3	PH due to lung diseases and/or hypoxia
3.1	Obstructive lung disease
3.2	Restrictive lung disease
3.3	Other lung disease with mixed restrictive/obstructive pattern
3.4	Hypoxia without lung disease
3.5	Developmental lung disorders
4	PH due to pulmonary artery obstructions
4.1	Chronic thromboembolic PH
4.2	Other pulmonary artery obstructions
5	PH with unclear and/or multifactorial mechanisms
5.1	Haematological disorders
5.2	Systemic and metabolic disorders

5.3 Others

5.4 Complex congenital heart disease

---

PAH: pulmonary arterial hypertension; PVOD: pulmonary veno-occlusive disease; PCH: pulmonary capillary haemangiomatosis; LVEF: left ventricular ejection fraction. Classification established at the 6th World Symposium of pulmonary hypertension, Nice, France, 2018.

### **1.2.1 PAH and lung disease**

While IPAH is rare, PAH as a broader group is more prevalent in association with certain diseases including HIV, sickle cell disease and CTD. PAH is a complication sometimes found in CTD, in particular the prevalence of patients with systemic sclerosis (SSc) developing PAH (SSc-PAH) is 7–12% (Mukerjee et al. 2003, Hachulla et al. 2005). SSc is a heterogeneous autoimmune disorder, characterised by tissue fibrosis and vascular injury. The underlying autoimmune dysfunction and dysregulation of fibroblasts leads to abnormal accumulation of collagen and potential damage to the skin, gastrointestinal tract, kidneys, lungs and other organs. Disease outcome is generally poorer in SSc-PAH, with higher mortality than IPAH or SSc alone (Kawut et al. 2003, Hachulla et al. 2009, Le Pavec et al. 2011), and even more so in association with interstitial lung disease (ILD; SSc-ILD-PAH). Indeed, PAH is one of the leading causes of death in SSc patients, with one study finding PAH accounts for approximately 27% of mortalities (Steen and Medsger 2007).

### **1.2.2 Pathobiology and molecular mechanisms of PAH**

The pathobiology of PAH is complex, and many biological processes have so far been implicated. While the molecular pathogenesis of PAH has been studied extensively, the underlying mechanisms of PAH with lung disease, including SSc-PAH and SSc-ILD-PAH, are yet to be fully elucidated. Pathological changes in the pulmonary vasculature vary in the different forms of PAH, and may be found in the veins, capillaries and arterioles. The most frequent alterations are sustained pulmonary vasoconstriction and remodelling of the pulmonary arteries and arterioles. The arterial remodelling of PAH is characterised by medial hypertrophy, intimal fibrosis and often the development of thrombotic or plexiform lesions (Pietra et al. 1989). Together, these processes cause the occlusion of small pulmonary arteries. Combined with the muscularisation and progressive obliteration of distal vessels, the subsequent loss of cross-sectional area (CSA) generates increased right ventricular afterload. At the cellular level, the neoplastic pathologies of PAH are thought to be driven by cellular

processes including excessive proliferation of apoptosis-resistant endothelial cells (ECs), together with proliferation and migration of medial smooth muscle cells (SMCs) and adventitial fibroblasts.

### **1.2.2.1 Pulmonary arterial vasoconstriction**

Sustained vasoconstriction in PAH may be caused by impaired vasorelaxation and/or excessive vasoconstriction. Reduced circulating levels of vasodilatory mediators, including prostaglandin I<sub>2</sub>, NO and cyclic guanosine monophosphate (cGMP; Christman et al. 1992) are found in PAH patients. Additionally, elevated levels of the vasoconstrictors endothelin 1 (ET-1) and thromboxane are found in PAH patients (Christman et al. 1992, Kreymborg et al. 2010). 5-hydroxytryptamine (5-HT; serotonin) has been highlighted as another key mediator of vasoconstriction in PAH (Launay et al. 2002), and is thought to be involved in cross-talk between pulmonary arterial ECs (PAECs) and pulmonary arterial SMCs (PASMCs) (Eddahibi et al. 2006). Perturbation in K<sup>+</sup> and Ca<sup>2+</sup> channels have also been shown in PAH, and may affect processes such as medial hypertrophy and SMC proliferation (Yu et al. 2004).

### **1.2.2.2 Endothelial dysfunction**

Endothelial dysfunction is a key process in PAH, as illustrated by defective Von Willebrand Factor (VWF) in patients (Lopes et al. 1998). Endothelial dysfunction is thought to first occur early in PAH disease progression and the PAECs play an important role in mediating structural changes in the pulmonary vasculature (Thambiayya 2015), such as inducing SMC proliferation via 5-HT (Eddahibi et al. 2006, Launay et al. 2002). PAECs are also important later in disease, particularly in the plexiform lesions that are characteristic of – and in experimental PAH, demonstrably directly linked to – advanced haemodynamic disease (Abe et al. 2010a). These lesions are thought to originate due to abnormal clonal endothelial proliferation (Cool et al. 1999, Yeager et al. 2001). PAECs within plexiform lesions express vascular endothelium growth factor (VEGF) and its receptors (Cool et al. 1999, Geiger et al. 2000, Tuder et al. 2001),

highlighting a potential role for this growth factor in PAH pathogenesis. The transition of ECs to mesenchymal cells (EndoMT) is another mechanism; involved in several disease processes, which has also recently linked PAEC dysfunction to PAH pathogenesis (Good et al. 2015, Ranchoux et al. 2015).

### **1.2.2.3 Genetic factors**

In heritable forms of PAH, causative loss-of-function mutations have been found in genes including the bone morphogenetic protein (BMP) receptor and transforming growth factor  $\beta$  (TGF $\beta$ ) receptor superfamily, and activin receptor-like kinase type 1 (ALK1 or ACVRL1). It has been shown that 60% of patients with familial PAH and 10–20% of patients with IPAH have a heterozygous mutation in BMPR2 (International et al. 2000, Deng et al. 2000). Although these mutations have low penetrance of approximately 20% in familial PAH, the importance of BMPR2 is illustrated by reduced levels of both BMPR2 protein (Atkinson et al. 2002) and its co-receptor BMPR1A (Du et al. 2003) in IPAH patients. This suggests BMPR2 mutations increase susceptibility to a ‘second hit’ against key pathways. BMPR2 dysfunction is proposed to affect various processes of PAH pathobiology, including upregulation of p38 mitogen-activated protein kinase (MAPK)-dependent pro-proliferative pathways (Rudarakanchana et al. 2002), defective Smad signalling (Yang et al. 2005) and interleukin (IL)-6-mediated inflammation (Hagen et al. 2007). A recent whole genome sequencing study identified several rare variants associated with PAH, including mutations in *SOX17* and *GDF2*, a gene encoding a BMPR2 ligand (Gräf et al. 2018). Furthermore, loci within an enhancer near *SOX17* were subsequently demonstrated as the first common variants to be associated with PAH (Rhodes et al. 2019).

### **1.2.2.4 Inflammation**

Inflammation has an important role in PAH, with increased circulating levels of inflammatory cytokines such as IL-1 $\beta$  and IL-6 found in IPAH patients (Humbert et al. 1995). IL-6

overexpression in transgenic mice is sufficient to cause PH (Steiner et al. 2009), and conversely IL-6 knockout mice under chronic hypoxia had reduced numbers of recruited inflammatory cells – such as macrophages – in the lungs and were protected from PH (Savale et al. 2009). A potential mechanistic link between BMPR2 loss-of-function mutations and PAH is dysregulation of a negative feedback loop – which would normally regulate inflammation – between BMPR2 and IL-6 (Hagen et al. 2007). The role of inflammation as a potential cause of PAH, rather than merely a bystander to other biological processes, is highlighted by the relatively common occurrence of PAH in association with autoimmune diseases such as SSc. This is further supported by mouse models of schistosomiasis that develop PH including plexiform lesions, apparently mediated by inflammatory cytokines (Crosby et al. 2010).

### **1.2.3 Treatment of PAH**

Currently the only curative treatment for PAH is lung transplantation. A variety of drug treatment regimens have so far been developed to treat the symptoms of PAH. Patients who respond to acute vasodilators may undergo calcium channel blocker (CCB) treatment (Galie et al. 2013). However, these vasoreactive patients are a minority, and in a cohort of IPAH patients, less than half demonstrated long-term improvement after CCB treatment (Sitbon et al. 2005). Standard approved drug therapies for PAH are used in non-vasoreactive patients or vasoreactive patients whom are not responding well to CCBs. These drugs aim to induce vasodilation by targeting the endothelin, nitric oxide (NO) or prostacyclin pathways, increasingly in combination therapy (Galie et al. 2013). For patients with CTD as a comorbidity with PAH, the treatment regimen may be further complicated. A study of SSc-ILD-PAH patients found no clear benefit to PAH vasodilation drug therapy (Le Pavec et al. 2011). Aberrant endothelin signalling can cause excessive vasoconstriction in PAH, and several drugs target this pathway. The endothelin receptor antagonist (ERA) ambrisentan selectively targets the endothelin-A receptor, while bosentan and macitentan are dual ERAs – affecting both endothelin-A and -B receptors. Sustained vasoconstriction in PAH can also be caused by impaired vasorelaxation, in particular due to dysfunction in the prostacyclin and NO

pathways. Prostacyclin therapy aims to restore prostacyclin vasodilation activity to endogenous levels, as it is normally produced by vascular ECs. Prostacyclin replacement drugs include epoprostenol (synthetic prostacyclin) and prostacyclin analogues iloprost, treprostinil and beraprost. Selexipag is a selective prostacyclin IP-receptor antagonist that was recently approved for PAH (Sitbon et al. 2015). Alternatively to the prostacyclin drugs, the goal of drugs targeting the NO pathway in PAH is to upregulate cGMP, the second messenger downstream of NO. Phosphodiesterase type 5 (PDE-5) is an enzyme that degrades cGMP, and inhibitors of PDE-5 for treatment of PAH include sildenafil, tadalafil and vardenafil. Another drug, riociguat, acts as a stimulator of NO-soluble guanylate cyclase (sGC).

The common purpose with all current drug therapies for PAH – whether targeting the endothelin, NO or prostacyclin pathways – is inducing vasorelaxation. While there is evidence for anti-proliferative effects mediated by the NO pathway in particular (Wharton et al. 2005), reversal of the proliferative phenotype has not been demonstrated. Current PAH treatments may improve PVR metrics and quality of life for patients to some extent, but ultimately there is little to no change in survival (Macchia et al. 2007, Rich 2007). As such, there is a necessity for new drugs targeting the proliferative pathways driving PAH. Drugs targeting right heart failure may also show promise – for example, a recent clinical trial demonstrated that the  $\beta$ -blocker carvedilol could reduce RV deterioration and maintain cardiac output (Farha et al. 2017).

#### **1.2.4 Animal models of PH/PAH**

Experimental models are a key component of preclinical research, particularly in rare diseases such as PAH. Animal models can permit the dissection of disease processes, identification of potential drug targets and development of novel therapeutic interventions. However, with all preclinical models the quality of data produced (i.e. reproducibility and likelihood to successfully translate into humans) is dependent on the model utilised. For PAH research, multiple animal models are available, with the majority focused on rodents. It is notable that while animals

subjected to these experimental models may develop PH, there they vary in how closely the disease resembles human PAH (Stenmark et al. 2009). The chronic hypoxia model is one of the most commonly used in mice and rats (Lawrie 2014). Hypoxia can induce increased pulmonary arterial pressures in mice and rats, with associated right ventricular hypertrophy (RVH). However, the response varies between strains, and underlying pulmonary vascular remodelling is less severe in mice than in rats, with little evidence of obliterative lesion formation (Stenmark et al. 2009). Monocrotaline is a toxic plant-derived alkaloid that was discovered to cause PH in rats (Kay et al. 1967) and has since been developed and widely used as an experimental model of PH, predominantly in rats. Monocrotaline causes severe PH with remodelling, elevated pulmonary arterial pressure and RVH, suggested to be mediated via endothelial damage (Jasmin et al. 2001). However, other severe non-PAH related effects have been described, including liver and kidney toxicity (Roth et al. 1981). In the present study, the Sugen 5416 and hypoxia (SuHx) model was utilised as a model of PAH. The addition of Sugen 5416 with hypoxia causes increased pulmonary vascular remodelling in mice (Ciuclan et al. 2011). The SuHx model was developed in rats (Taraseviciene-Stewart et al. 2001) and subsequently adapted for mice (Ciuclan et al. 2011). Sugen 5416 is an inhibitor of VEGF receptors 1 and 2, and although this anti-angiogenic effect may appear paradoxical, in combination with experimental hypoxia it has been suggested to increase signalling through other receptors, e.g. VEGFR3 to cause pulmonary vascular remodelling (Roth et al. 1981). The SuHx model is now the second most commonly used by researchers in mice (Lawrie 2014). Furthermore, mouse models have the advantage of widely available transgenic strains and relatively simple options for genetic manipulation, which make the SuHx mouse a suitable experimental system for the present study.

### **1.3 Pulmonary fibrosis**

ILD is a term referring to a collection of rare diseases that share some common features but have diverse pathophysiology and outcomes. PF is the most common form of ILD, and it may

be idiopathic (IPF) or found in association with autoimmune disorders of the connective tissue, most often SSc and rheumatoid arthritis (Olson et al. 2012). IPF patients may present with chronic exertional dyspnoea, coughing and reduced lung function (Raghu et al. 2011). Diagnosis can include radiographic features, spirometry, bronchoscopy and surgical biopsy. IPF is rare, but more common in men and in older adults – a recent large meta-analysis of studies in Europe 1968–2012 determined that incidence is 3–9 cases per 100,000 per year (Hutchinson et al. 2015). Some studies have also found increased prevalence over time, although this effect has been linked to differences in diagnostic criteria and procedures (Strongman et al. 2018). Within Europe, the UK has the highest rates of reported IPF, with incidence of 4.6–8.7 per 100,000 people per year (Hutchinson et al. 2015). Risk factors associated with IPF include age, genetic factors, smoking and environmental exposure to pathogens or other damaging elements (Raghu et al. 2011). The prognosis for IPF patients is very poor – within a UK cohort, median survival was 2.7 years, and 5- and 10-year survival rates were 34% and 19%, respectively (Strongman et al. 2018). Additionally, no improvements in survival were observed between 2000 and 2012, suggesting a lack of meaningful treatment development during this period (Strongman et al. 2018).

### ***1.3.1 Pathobiology and molecular mechanisms of PF***

PF is characterised by chronic, progressive lung remodelling and excessive fibrosis leading to declining oxygen diffusion capacity. The aetiology of conditions causing PF is varied, although the most common form, IPF is less well understood. At the cellular level, fibrosis is mediated by deposition of extracellular matrix (ECM) proteins – in particular collagens – by activated fibroblasts and myofibroblasts within the lungs. The pro-fibrogenic response is considered to be an aberrant form of repair processes in response to injury of pulmonary cells, in particular alveolar epithelial cells (AECs). This effect has been highlighted by early dysfunction in AECs due to injury in explanted IPF patient lung tissue (Chilosi et al. 2002, Kasper and Haroske 1996). Furthermore, excessive apoptosis of AECs is observed in the lungs of IPF patients (Plataki et al. 2005, Uhal et al. 1998). AEC apoptosis has also been directly implicated in

experimental PF induced by the drug bleomycin, which is attenuated by blocking AEC apoptosis using caspase inhibitors (Kuwano et al. 2001, Wang et al. 2000). The triggers for this AEC dysfunction are not fully understood, although factors implicated include environmental exposures and genetic predisposition (Wang et al. 2009). Recently, single-cell RNA-sequencing of IPF epithelial cells has allowed characterisation of the aberrantly differentiated subpopulations of cells involved in driving IPF (Xu et al. 2016). These epithelial cells are distinct to healthy cells, and exhibit activation of multiple pro-fibrogenic pathways (Xu et al. 2016). Release of pro-fibrogenic factors from dysfunctional AECs can stimulate fibrotic phenotype in fibroblasts and myofibroblasts – e.g. a key factor implicated is TGF $\beta$ 1; activation of which can cause PF in mice, as well as further apoptosis in AECs (Lee et al. 2004). Activation of TGF $\beta$ -regulated pathways has been demonstrated in IPF airway epithelial cells, in particular basal cells – a subset of which appear to be abnormally activated and differentiated progenitor cells distinct to IPF patients (Xu et al. 2016). Airway progenitor cells have been demonstrated as activated after epithelial tissue damage induced by influenza infection (Zuo et al. 2015) or bleomycin insult (Vaughan et al. 2015). These abnormally activated regeneration processes in PF present a similarity to the pathological processes found in other progressive disorders such as cancer and notably in the pulmonary vascular remodelling underlying PAH.

In addition to dysfunctional AECs, pathogenic alterations in the key effector cells of PF – fibroblasts and myofibroblasts – have also been linked to the development and persistence of the chronic fibrotic state. These changes include apoptosis resistance (Moodley et al. 2004, Thannickal and Horowitz 2006), altered expression of apoptosis-inducing membrane death receptors (Hohmann et al. 2019) and senescence (Faner et al. 2012). Interestingly, mutations in genes associated with telomeres and senescence (that were previously implicated in heritable PF) have also been demonstrated in IPF patients (Petrovski et al. 2017). The growth factor TGF $\beta$ 1 has been also demonstrated to promote apoptosis resistance in fibroblasts (Horowitz et al. 2004, Zhang and Phan 1999). In addition to phenotypic changes observed in

lung resident pro-fibrogenic cells, PF has also been demonstrated to involve the influx of bone marrow-derived progenitor cells known as fibrocytes, which can differentiate to fibroblasts or myofibroblasts that then potentiate the fibrotic phenotype within the lung (Hashimoto et al. 2004, Phillips et al. 2004). Fibrocytes have also been implicated as drivers of fibrosis; by releasing growth factors and promoting proliferation of resident fibroblasts, and the inhibition of this process was suggested to be a mechanism of action for the anti-fibrotic drug nintedanib (Sato et al. 2017). The process of epithelial-mesenchymal transition (EMT) has also been indicated as a potential source of pathogenic myofibroblasts in PF. TGF $\beta$ 1 has also been demonstrated to cause EMT *in vitro*, and cells co-expressing markers of EMT (i.e. AEC markers and mesenchymal markers) are abundant in IPF lungs (Willis et al. 2005). Aberrant Wnt signalling has also been linked to EMT in IPF lungs (Chilosi et al. 2003). Interestingly aside from the cells of the airways, the vascular endothelium has been implicated in various forms of autoimmune and fibrotic diseases via the process of EndoMT, including SSc (Manetti et al. 2017) and experimental bleomycin-induced PF (Hashimoto et al. 2010). This suggests that the pulmonary vasculature may also be important in PF pathobiology.

### **1.3.2 Treatment of PF**

There are currently few treatments for PF, in particular for IPF where the causes are less clear. PF was initially thought to be caused primarily by chronic inflammation, so immunosuppressant and anti-inflammatory drugs – including corticosteroids such as prednisone and the anti-inflammatory colchicine – have been tested for treatment. However, the responses were variable (Douglas et al. 1998), and results suggest these kinds of therapy may be useful in a small number of cases of autoimmune associated PF, but not in IPF (Raghu et al. 2012). Recently, two anti-fibrotic therapies against IPF have been approved for use in the UK: pirfenidone in 2013 and nintedanib, in 2015. These treatments may be combined with oxygen therapy in addition to targeting specific symptoms such as coughing and dyspnoea. Pirfenidone has been demonstrated in clinical trials to reduce disease progression (measured by a reduction in the decline of forced vital capacity of the lungs) and to improve survival

(Fisher et al. 2017, King et al. 2014, Nathan et al. 2017). Its mechanism of action is not fully understood, but has been linked to reduction in fibroblast proliferation and inhibition of TGF $\beta$ -stimulated collagen production. Nintedanib is another anti-fibrotic drug, which is a small molecule tyrosine-kinase inhibitor, targeting VEGF receptors, fibroblast growth factor receptor (FGFR) and platelet-derived growth factor receptor (PDGFR) to reduce fibrosis. Nintedanib has also been demonstrated to slow the decline in forced vital capacity in IPF patients (Richeldi et al. 2014). The effectiveness of pirfenidone and nintedanib has not yet been compared directly in a clinical trial. Another drug recently shown in a phase II clinical trial to slow decline of lung function in IPF patients is pentraxin 2, a recombinant protein inhibitor of monocyte differentiation into fibrocytes or pro-inflammatory macrophages (Raghu et al. 2019, Raghu et al. 2018). Ultimately the drug therapies developed so far have at best only slowed the progression of PF, and the only potential curative option remains lung transplantation. There is therefore a need for development of new treatments to halt progression of PF or even improve lung function in PF patients.

### **1.3.3 Animal models of PF**

Many animal models of PF have been developed in order to study disease pathogenesis and discover or test new therapeutics. The majority of these models target AEC injury as a mechanism to induce fibrosis, and this may be achieved by exposure to physical substances mimicking environmental exposure (e.g. asbestos, silica), radiation or drug/chemical agents (e.g. bleomycin, fluorescein isothiocyanate) (Moore and Hogaboam 2008). Bleomycin is the most commonly used agent to induce PF in mice (Moore et al. 2013). The mechanism of action is the introduction of double-strand breaks in DNA, apoptosis/necrosis of cells leading to inflammation and fibrotic response (Moeller et al. 2008). Interestingly, bleomycin causes PF when administered by IP or IV injection as well as by oropharyngeal aspiration or surgically by intratracheal instillation in animal models (Adamson and Bowden 1974, Fleischman et al. 1971, Thrall et al. 1979). The induction of PF with bleomycin administered systemically demonstrates that the damaging effect of bleomycin can also induce PF via the pulmonary

vascular endothelium. In comparison to the possibly reversible fibrotic response post-intratracheal bleomycin instillation (Izbicki et al. 2002), the repeated IP bleomycin model has been described as producing more chronic vascular-associated inflammation and pulmonary remodelling, with associated PAH demonstrated by haemodynamic measures and pulmonary vascular remodelling (Bryant et al. 2016, Karmouty-Quintana et al. 2015, Karmouty-Quintana et al. 2012). For these reasons, the IP bleomycin model was selected rather than the intratracheal or oropharyngeal routes of administration for use in the present study.

## **1.4 Tumour necrosis factor-related apoptosis-inducing ligand**

The tumour necrosis factor-related apoptosis-inducing ligand (TRAIL) is a cytokine that can bind five different cell membrane receptors. TRAIL is widely expressed in most tissues (Berglund et al. 2008, Uhlen et al. 2017), most predominantly in lung, spleen and prostate (Wiley et al. 1995). TRAIL is also expressed in all hematopoietic cell lineages, particularly in myeloid cells and neutrophils (Berglund et al. 2008, Uhlen et al. 2017). Within the lung, TRAIL is expressed within vascular ECs and SMCs (VSMCs) (Gochuico et al. 2000, Lawrie et al. 2008). TRAIL has been of particular interest for its proposed ability to selectively induce apoptosis in tumour cells. However, it has also been found to regulate a wide variety of non-canonical cellular effects including survival, migration and proliferation via kinase signalling pathways. The widespread expression of TRAIL in most cell types suggests it plays an important role in normal biological processes. However, its expression and varied functions in cell types of the lung and involvement in pulmonary diseases such as PAH and PF make it an interesting candidate for targeting novel therapeutics for these conditions.

### **1.4.1 TRAIL molecular signalling**

TRAIL, a type II transmembrane protein, is a member of the death receptor ligand family; a subclass of the tumour necrosis factor family (Wiley et al. 1995). TRAIL is proteolytically cleaved and its extracellular domain can bind five TRAIL receptors: membrane-bound death

receptors DR4 (TRAIL-R1) and DR5 (TRAIL-R2), membrane-bound decoy receptors DcR1 (TRAIL-R3) and DcR2 (TRAIL-R4) and the soluble decoy osteoprotegerin (OPG) (Degli-Esposti et al. 1997, Emery et al. 1998, MacFarlane et al. 1997, Marsters et al. 1997, Pan et al. 1997a, Pan et al. 1997b, Screaton et al. 1997). TRAIL is conserved in mice – they have two decoy receptors and a single TRAIL death receptor, mDR5, which is more similar to DR5 than DR4 (Schneider et al. 2003).

TRAIL is composed of 281 amino acids and forms a homo-trimeric structure upon binding three receptor molecules (Hymowitz et al. 1999). The death receptors DR4 and DR5 are type I transmembrane proteins containing a cytoplasmic death domain. In the canonical TRAIL apoptosis signalling pathway (Figure 1.1A), binding of death receptors by TRAIL leads to recruitment of Fas-associated protein with death domain (FADD), formation of a complex known as death-inducing signalling complex (DISC), activation of caspase-8 and subsequently downstream caspase-3 dependent apoptosis of the cell (Figure 1A; Dickens et al. 2012, Pitti et al. 1996, Suliman et al. 2001). Unlike the TRAIL death receptors, the decoy receptor DcR1 has no death domain (Degli-Esposti et al. 1997, Pan et al. 1997a) and DcR2 has a truncated, non-functional death domain (Degli-Esposti et al. 1997, Marsters et al. 1997, Pan et al. 1998). These decoy receptors and additionally – binding with lower affinity – the soluble OPG are suggested to suppress apoptotic signalling by competitively binding TRAIL (Daniels et al. 2005, Miyashita et al. 2004). Interestingly it was later shown that while DcR1 acts by inhibiting formation of the DISC, DcR2 is co-recruited to the DISC with DR5, blocking initiation of caspase activation and also preventing recruitment of DR4 to the DISC (Merino et al. 2006).

Besides inducing cell death, conversely TRAIL can also promote cellular processes including survival, proliferation and migration via activation of kinase signalling pathways (Figure 1.1B) (Hameed et al. 2012). This non-canonical signalling may depend on the formation of a secondary signalling complex after initial DISC assembly (Varfolomeev et al. 2005), recruiting

other factors including FADD, caspase-8, RIPK1, TNF receptor-associated factor 2 (TRAF2) and inhibitor of NF- $\kappa$ B kinase subunit gamma (IKK- $\gamma$ ). Activation of non-canonical TRAIL signalling pathways may also be regulated by expression of DcR1, as antibody neutralisation of this decoy receptor can inhibit TRAIL-induced cell proliferation (Hameed et al. 2012). Downstream non-canonical signalling by TRAIL has been shown to be effected by activation of kinase signalling e.g. NF- $\kappa$ B, p38, c-Jun N-terminal kinase (JNK), phosphatidylinositide 3-kinases (PI3K), Akt and extracellular signal-regulated kinases (ERK); leading to activation of gene transcription (Daniels et al. 2005). By activating NF- $\kappa$ B, TRAIL can also modulate levels of FADD-like interleukin-1 $\beta$ -converting enzyme)-inhibitory protein (c-FLIP; Cantarella et al. 2014), a negative regulator of caspase-mediated apoptosis – a further mechanism by which a cell may deviate from pro-apoptotic to pro-survival signalling in response to TRAIL.

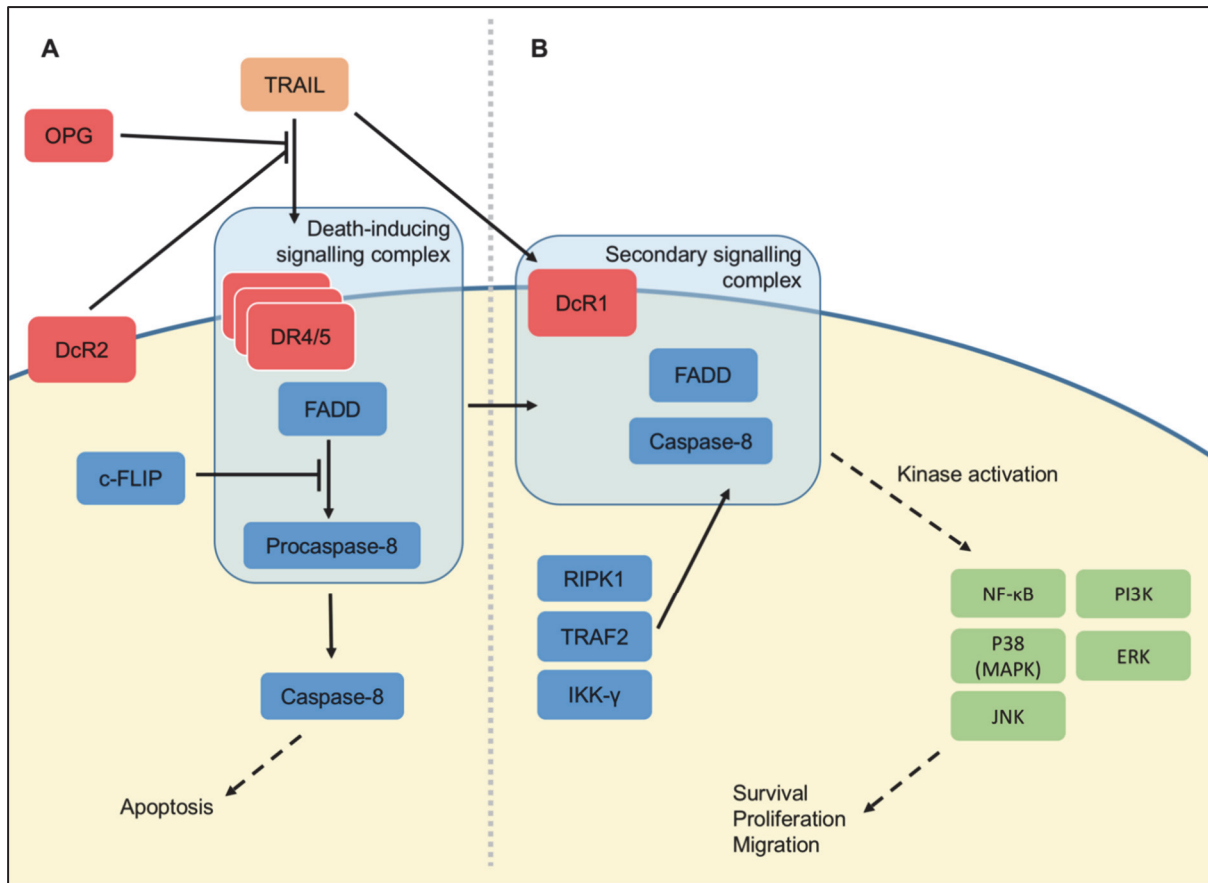


**Figure 1.1: Molecular signalling of TRAIL.** (A) Three proteolytically-cleaved tumour necrosis factor-related apoptosis-inducing ligand (TRAIL) proteins form a homo-trimeric structure when binding death receptor 4 (DR4) or death receptor 5 (DR5) at the cell membrane. These are joined by Fas-associated death domain (FADD) and procaspase-8 to form the death-inducing signalling complex (DISC). The DISC activates the caspase cascade, leading to apoptosis of the cell. TRAIL may also bind the membrane decoy receptors (DcR1/2) or soluble osteoprotegerin (OPG), which do not contain a death domain, thus preventing TRAIL-induced apoptosis. Apoptosis can also be suppressed by (FADD-like interleukin-1 $\beta$ -converting enzyme)-inhibitory protein (c-FLIP), which inhibits the function of the DISC. (B) In the non-canonical signalling pathway, the receptor and ligand are thought to be lost, leaving FADD and caspase-8 to be joined by receptor-interacting serine/threonine-protein kinase 1 (RIPK1), TNF receptor-associated factor 2 (TRAF2) and inhibitor of NF- $\kappa$ B kinase subunit gamma (IKK- $\gamma$ ). This secondary signalling complex initiates protein kinase signalling pathways, leading to activation of kinases including nuclear factor kappa-light-chain-enhancer of activated B cells (NF- $\kappa$ B), p38 (mitogen-activated protein kinase; MAPK), c-Jun N-terminal kinase (JNK), phosphatidylinositide 3-kinases (PI3K) and extracellular signal-regulated kinase (ERK). The cellular effects of these kinases include survival, proliferation and migration. Adapted from Braithwaite et al. (2018).

## **1.4.2 TRAIL in disease**

### **1.4.2.1 TRAIL in cancer**

As its name suggests, TRAIL was primarily of particular interest for its ability to selectively induce apoptosis in tumour cells *in vitro* and *in vivo*, while apparently exhibiting minimal off-target effects (Ashkenazi et al. 1999, Chinnaiyan et al. 2000, Walczak et al. 1999). Furthermore, *TRAIL*-deficient mice are also more susceptible to tumour formation and metastasis (Cretney et al. 2002), suggesting TRAIL has a protective role in cancer suppression. Consequently TRAIL signalling has been targeted for use in several anticancer therapies (Johnstone et al. 2008), however their success has been mixed, as several types of cancer cells are actually resistant to TRAIL-induced apoptosis. In these cells, TRAIL can activate pro-inflammatory signalling pathways (Berg et al. 2009, Nguyen et al. 2009), proliferation (Azijli et al. 2012, Baader et al. 2005, Ehrhardt et al. 2003, Nguyen et al. 2009) and metastasis (Trauzold et al. 2006). The known function of TRAIL has thus evolved beyond apoptosis to include these non-canonical effects and TRAIL is now known to have divergent roles in diseases affecting the lung (Figure 1.2; adapted from Braithwaite et al. (2018)), where TRAIL is widely expressed (Gochuico et al. 2000, Lawrie et al. 2008).

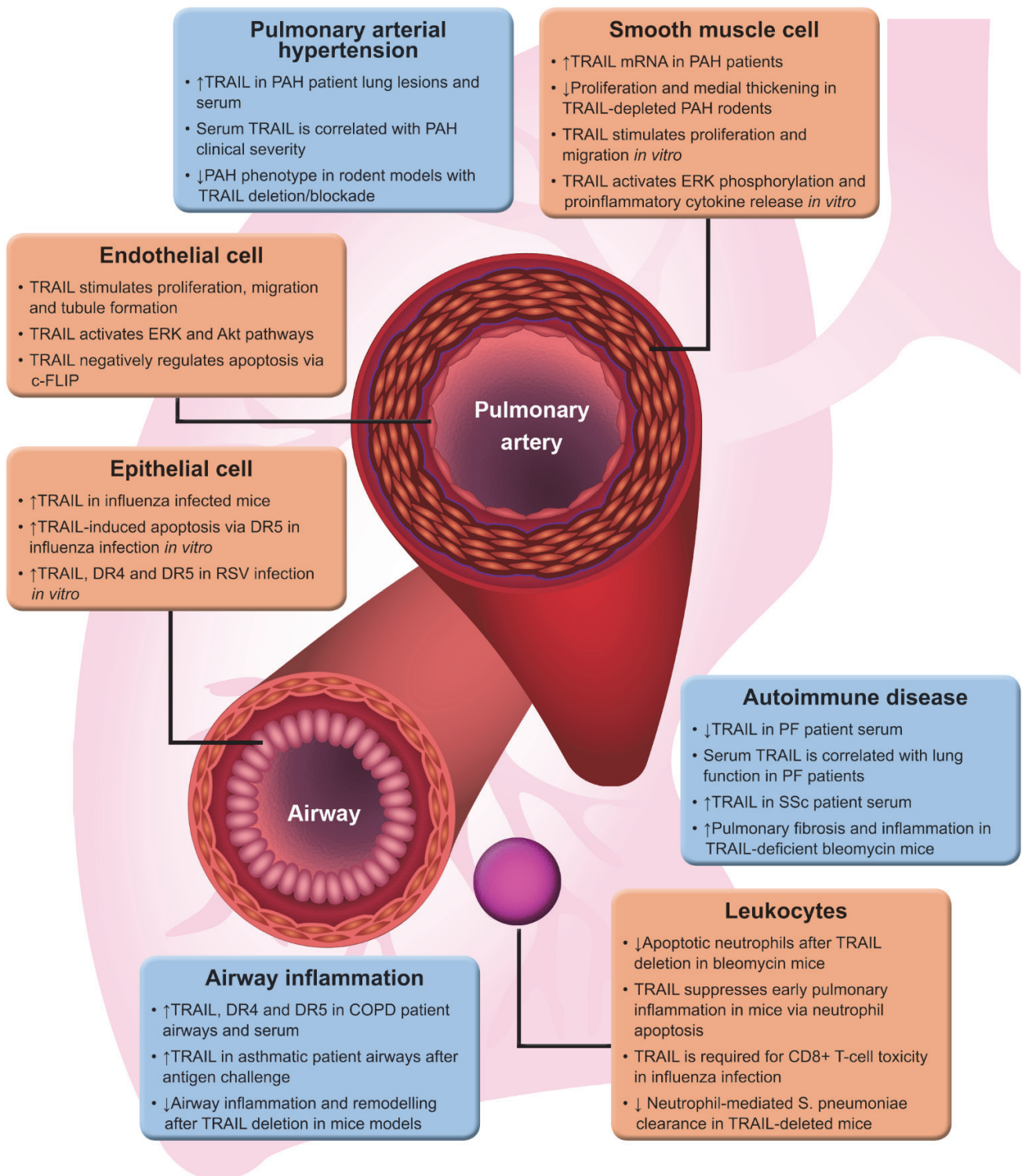


**Figure 1.2: TRAIL functions in lung diseases.** A brief summary of evidence for the varied roles of TRAIL in lung diseases. ↑ and ↓, up- and down-regulation, respectively. Akt, protein kinase B; COPD, chronic obstructive pulmonary disease; DR4/5, TRAIL death receptor 4/5; ERK, extracellular signal-regulated kinase; PAH, pulmonary arterial hypertension; PF, pulmonary fibrosis; RSV, respiratory syncytial virus; SSc, systemic sclerosis. Adapted from Braithwaite et al. (2018).

#### **1.4.2.2 TRAIL in PAH**

TRAIL has been implicated in the pathobiology of PAH (Dawson et al. 2014, Hameed et al. 2012). This is indicated by elevated levels of soluble TRAIL found in the serum of PAH patients, which is associated with worsened clinical severity (Liu et al. 2015). The pulmonary vasculature is complex, and many aberrant processes can lead to disease. PAH is a multifactorial disorder characterised by remodelling of the pulmonary arteries and a progressive increase in PVR, leading to raised afterload on the RV and ultimately right heart failure (Hoepfer et al. 2013). TRAIL immunoreactivity has been shown in pulmonary vascular lesions from IPAH patients (Lawrie et al. 2008) and increased *TRAIL* mRNA expression is detected in the lungs of rodent models of PAH (Lawrie et al. 2011, Liu et al. 2015). Furthermore, TRAIL has been demonstrated – by knockout and by inactivation – as necessary for the development of PAH in multiple pre-clinical models of PAH (Hameed et al. 2012). Reversal of established PAH in rodent models was also demonstrated by administration of an anti-TRAIL antibody (Hameed et al. 2012). *TRAIL* genetic deletion also had a similar protective effect in a SuHx mouse model of PAH (Dawson et al. 2014). Increased *TRAIL*, *DR4* and *DcR1* mRNA levels have been detected in explanted PSMCs from IPAH patients, compared to healthy control cells (Hameed et al. 2012). Additionally, TRAIL depletion or blockade in rodent models of PAH is associated with reduced pulmonary arterial remodelling with fewer proliferating PSMCs (Dawson et al. 2014, Hameed et al. 2012). This evidence indicates that TRAIL is a key promoter of the PSMC proliferation associated with the pathogenic vascular remodelling in PAH in animal models and human disease. Recombinant TRAIL was also shown to induce proliferation and migration of IPAH patient PSMCs *in vitro*, via phosphorylation of ERK1/2 (Hameed et al. 2012). The pro-proliferative effect of TRAIL was reversed by the addition of DcR1 neutralising antibody, suggesting this decoy receptor is essential to non-canonical TRAIL signalling in PSMCs. Other studies have similarly demonstrated that TRAIL can stimulate proliferation and migration of vascular SMCs via non-canonical kinase signalling cascades (Kavurma et al. 2008, Secchiero et al. 2004).

Additionally, following activation of NF- $\kappa$ B, TRAIL has been shown to stimulate production and release of pro-inflammatory cytokines in vascular SMCs (Song et al. 2011).

EC dysfunction is another key aspect of the angioproliferative state of pulmonary arteries in PAH. Several studies have demonstrated that TRAIL can stimulate angiogenic processes in vascular ECs *in vitro*, including proliferation (Cantarella et al. 2014, Cartland et al. 2016, Secchiero et al. 2003), migration (Cantarella et al. 2014, Cartland et al. 2016, Zauli et al. 2003) and tubule formation (Cartland et al. 2016). Similarly to non-canonical TRAIL signalling in SMCs, its angioproliferative effect in ECs has been linked to activation of Akt and ERK pathways (Secchiero et al. 2003), as well as upregulation of DcR2 (Harith et al. 2016). Conversely, TRAIL has also been demonstrated to have apoptotic (Alladina et al. 2005, Gochuico et al. 2000) and anti-angiogenic (Cantarella et al. 2006) effects on vascular ECs. The reason for this disparity is unclear, although each of these studies used a relatively high concentration of recombinant TRAIL (100 ng/ml), suggesting the pro-angiogenic signalling in ECs may preferentially occur at lower TRAIL concentrations. In Cantarella et al. (2014), high levels of TRAIL were shown to induce caspase 8-mediated apoptosis of ECs, whereas low levels of TRAIL were pro-angiogenic. Interestingly, these dose-dependent opposing effects of TRAIL in ECs were linked to modulation of levels of c-FLIP, a procaspase-8 homolog and negative regulator of TRAIL-mediated apoptosis (Cantarella et al. 2014).

#### **1.4.2.3 TRAIL in autoimmune disease and fibrosis**

TRAIL is now known to have crucial functions in regulation of inflammation and immune response. These systems are significant in the pathogenesis of many forms of lung disease, including autoimmune disorders and respiratory infection in addition to pulmonary vascular disease (Figure 1.2). A role for TRAIL in regulating inflammation via apoptosis was highlighted in a knockout of the mouse TRAIL death receptor, as in addition to tumour formation, the mice were prone to chronic inflammation (Finnberg et al. 2008). Additionally, TRAIL has been demonstrated to suppress the early inflammatory response via apoptosis of neutrophils

(McGrath et al. 2011). There is evidence of commonalities in disease aetiologies between PAH and autoimmune disease; for example, 7–12% of patients with systemic sclerosis (SSc) develop PAH (Hachulla et al. 2005, Mukerjee et al. 2003). SSc is a heterogeneous autoimmune disorder, characterised by tissue fibrosis and vascular injury. PF is the most common form of interstitial lung disease and it may be idiopathic (IPF) or often found in association with autoimmune disorders of the connective tissue, including SSc and rheumatoid arthritis. PF is characterised by pathogenic lung remodelling and deposition of ECM proteins – in particular various collagens – by activated fibroblasts and myofibroblasts. Elevated soluble TRAIL protein has been observed in plasma (Habel et al. 2018) and serum (Collison et al. 2019) of IPF patients compared to controls. Additionally, increased serum TRAIL levels have been found in SSc patients compared to healthy controls, as well as being elevated in SSc patients with either PAH or PF compared to those without pulmonary involvement (Azab et al. 2012), indicating that TRAIL may also play a key role in these disease processes. In contrast, an additional study found soluble TRAIL present at lower levels in the serum of patients with IPF than in healthy controls (McGrath et al. 2012). Within the IPF patient group in this study, lung function – shown by transfer factor of the lung for carbon monoxide – was correlated with serum levels of TRAIL, suggesting it may have a protective role in IPF (McGrath et al. 2012). The reason for the apparent discrepancy in circulating TRAIL levels is unclear – possible causes include differences in patient cohorts or timing of sample acquisition or technical variation between the studies described. Consideration may also be given to the potential lack of a direct relationship or correlation between soluble TRAIL levels and TRAIL expressed by cells within the lungs. Perhaps a more reliable inference for the role of TRAIL in PF is that differences in TRAIL immunostaining have also been demonstrated in the lungs of IPF patients compared to healthy controls (Habel et al. 2018, McGrath et al. 2012).

Furthermore, a direct link for TRAIL to PF pathobiology is illustrated in *TRAIL*-deficient mice, where fibrosis – measured by total lung collagen content – in the bleomycin model of PF was

enhanced in comparison to wild-type mice (McGrath et al. 2012). In this model, *TRAIL* genetic deletion also increased pulmonary inflammation (assessed by neutrophil counts in bronchoalveolar lavage fluid). The inflammatory phenotype in *TRAIL* knockout mice was accompanied by a reduced number of apoptotic cells in lung tissue, with a corresponding reduction of apoptotic neutrophils in bronchoalveolar lavage fluid. This suggests that TRAIL-mediated apoptosis of neutrophils is a protective process in this form of PF. Contrasting results were found in another study, in which *TRAIL* deletion was found to reduce the PF phenotype in bleomycin mice (Collison et al. 2019). However, the metric used for quantification of fibrosis was the area of collagen staining per micrometre length of basement membrane of major airways, i.e. only directly airway-associated collagen was assessed and only at a limited number (~10) of positions in each lung. In reality, PF induced by bleomycin in mice causes deposition of collagen throughout the lung and this may have been unaccounted for in this study (Collison et al. 2019). Another bleomycin mouse study demonstrated that delivery of a neutralising anti-TRAIL antibody by IP injection led to significantly increased procollagen 1 and procollagen 3 protein in the lung (Habel et al. 2018). A protective role of TRAIL against fibrosis was suggested in this work to be derived from TRAIL-expressing myeloid cells inducing apoptosis of pulmonary myofibroblasts, a process which was diminished by the anti-TRAIL antibody (Habel et al. 2018).

#### **1.4.2.4 *Trail in airway inflammation***

Contrary to its protective effect in IPF, TRAIL appears to have a detrimental role in the context of both acute and chronic airway inflammation, by upregulating inflammation and autoimmune responses (Figure 1.2). TRAIL is increased in bronchoalveolar lavage fluid from asthmatic patients following antigen challenge, and isolated eosinophils express more TRAIL and DcR2, but less DR4 and DR5 (Robertson et al. 2002). Deletion of the *TRAIL* gene in mice diminishes airway hyper-reactivity, inflammation and remodelling in an ovalbumin-induced model of allergic asthma (Collison et al. 2014, Weckmann et al. 2007) and a rhinovirus-induced asthma model (Girkin et al. 2017). Additionally, chronic asthmatic inflammation, remodelling and lung

function are worsened by *TRAIL* deletion in mice infected as neonates with chlamydia (Starkey et al. 2014).

Prolonged exposure to irritants and inflammation can lead to chronic obstructive pulmonary disease (COPD). A role for TRAIL in COPD has been highlighted by its elevated levels found in the lungs of COPD patients. One study found increased TRAIL, DR4, DR5 and DcR1 protein in lung parenchyma from COPD patients (Morissette et al. 2008). Higher levels of *TRAIL*, *DR4* and *DR5* mRNA were also found in airway epithelial brushings of COPD patients compared to healthy controls (Haw et al. 2016). Another study found increased levels of serum TRAIL and DR5 proteins in COPD patients compared to healthy controls (Wu et al. 2015). Additionally, with the COPD patient group serum levels of TRAIL and DR5 were found to be inversely correlated with forced expiratory volume, a measure of lung function (Wu et al. 2015). Inflammation and alveolar cell apoptosis are key processes in many forms of COPD. A pro-apoptotic function of TRAIL in COPD was originally suggested, as emphysematous lung tissue is more sensitive to TRAIL-induced apoptosis than health lung (Morissette et al. 2011). However, a pro-inflammatory element may also be important. In a chronic cigarette smoke-exposure mouse model of COPD, *TRAIL* mRNA and protein expression was increased in the airway epithelium and parenchyma, and in mice with *TRAIL* deletion, airway inflammation – as well as remodelling – was reduced (Haw et al. 2016). The activation by TRAIL of both apoptotic and inflammatory pathways within COPD highlights its varied roles and how specific cell types are targeted – whether or not this is mediated by differential receptor expression or some other mechanism remains unclear.

#### **1.4.2.5 *TRAIL* in respiratory infection**

In lower respiratory tract infections, TRAIL has differing roles in immune response and damage to host tissues (Figure 1.2). Apoptosis of virus-infected cells is a key mechanism for clearance of viral infection and *in vitro*. In the context of influenza infection, TRAIL-induced apoptosis of human lung AECs is enhanced; an effect which is inhibited by blocking DR5 (Brincks et al.

2008b). Similarly, *TRAIL*, *DR4* and *DR5* are strongly upregulated in response to respiratory syncytial virus infection in AECs, leading to increased sensitivity to apoptosis (Kotelkin et al. 2003). In animal models, *TRAIL* expressed by CD8<sup>+</sup> T-cells has been demonstrated as essential for viral immunity, with *TRAIL* knockout mice exhibiting increased influenza-associated morbidity and reduced CD8<sup>+</sup> T-cell cytotoxicity (Brincks et al. 2008a, Brincks et al. 2011, Ishikawa et al. 2005). *DR5* expression was also shown to be upregulated in influenza-infected AECs *in vivo* (Brincks et al. 2008b, Ishikawa et al. 2005).

In opposition to its protective role in viral clearance, other studies have shown that *TRAIL* expressed by macrophages is instrumental in damage to airways caused by apoptosis of AECs in influenza infection (Herold et al. 2008, Peteranderl et al. 2016). Deletion of *TRAIL* in mice led to a reduction in mortality and the alveolar epithelial apoptosis and alveolar leakage associated with influenza virus pneumonia (Herold et al. 2008). This highlights an interesting situation whereby *TRAIL* death signalling may be used for host for viral clearance, while also assisting in viral infection via tissue damage. *TRAIL* has also been demonstrated as important in immune response to bacterial respiratory infection. In the context of *Streptococcus pneumoniae* infection, deletion of *TRAIL* in mice reduces bacterial clearance in the lungs and worsens survival – an effect that is reversed by treatment with *TRAIL* or *DR5* agonist antibody (Steinwede et al. 2012). In the same study, neutrophils were found to be the key source of *TRAIL* (Steinwede et al. 2012).

## **1.5 Research hypothesis**

Together, these data suggest *TRAIL* is multifaceted in a variety of lung diseases. *TRAIL* also has the ability to function as either pro-apoptotic or pro-survival depending on the cell type, and receptor expression on local tissue to mediate either protective or pathogenic mechanisms. The exact mechanism by which *TRAIL* modulates these functions is not fully

understood, although regulation of TRAIL, and its cleavage, as well as the expression of receptors by specific cell types is clearly important in determining its effects.

Further work is required to fully elucidate the divergent roles of TRAIL to gain a better understanding of the role it plays in underlying processes of lung disease, and its potential as a therapeutic agent – or target – depending on disease context. Gaining new insights into the nature of TRAIL could help to disentangle the differences in molecular pathogenesis between IPAH and PAH with CTD such as SSc-PAH and SSc-ILD-PAH.

The main hypothesis of this work is that TRAIL derived from different cell types has varying roles in disease: TRAIL from VSMCs drives the pathogenic proliferative processes underlying PAH, whereas TRAIL expressed in fibroblasts promotes apoptosis of those or other cells, thus modulating the fibrotic processes. Previous studies suggest that TRAIL primarily drives pulmonary arterial remodelling in PAH via PASMC proliferation and migration. This could be mediated by the activation of the non-canonical kinase signalling pathways of TRAIL. Whereas in PF and potentially SSc-/SSc-ILD-PAH, the protective effect of TRAIL may be due to its immunosuppressive action via canonical stimulation of apoptosis in fibroblasts.

## **2 Materials and methods**

### **2.1 In vitro studies**

#### **2.1.1 Primary pulmonary artery smooth muscle cells**

Human primary PSMCs (Lonza, Basel, Switzerland) were grown in media produced with the Smooth Muscle Cell Growth Medium-2 BulletKit (Lonza, Basel, Switzerland). Standard cell culture techniques were used, and cells were passaged when they reached 80% confluence. Cells used in experiments were between p4–p8.

#### **2.1.2 Stimulations**

PSMCs were seeded on T25 flasks at approximately 80% density and given low serum medium (1:20 dilution of full growth media in basal media) for 48 hours before stimulations. Cells were then stimulated with 30 ng/ml recombinant TRAIL (R&D Systems, Minneapolis, MN, United States) or unstimulated as control. Stimulations were carried out for 6 hours for RNA and 10 and 60 minutes for protein with 6 replicates per condition.

#### **2.1.3 RNA extraction from cultured cells**

RNA was isolated using TRIzol extraction (Thermo Fisher Scientific, Waltham, MA, USA) according to the manufacturer's instructions. Cells were washed with PBS, then 500 µl TRIzol reagent was added directly to the culture flask and pipetted up and down several times to homogenise, then transferred to a tube and incubated for 5 minutes. All subsequent reagent volumes are per 1 ml of TRIzol reagent used for extraction. A 0.2 ml volume of chloroform was added and then samples incubated for 2–3 minutes. The sample was then centrifuged for 15 minutes at  $12,000 \times g$  at  $4^{\circ}\text{C}$ . The upper, colourless aqueous phase containing RNA was transferred to a clean tube. A 0.5 ml volume of isopropanol was added to the aqueous phase then samples were incubated for 10 minutes at room temperature. Samples were then centrifuged for 10 minutes at  $12,000 \times g$  at  $4^{\circ}\text{C}$  and the supernatant was discarded. Pellets

were resuspended in 1 ml of 75% (v/v) ethanol, vortexed briefly, then centrifuged for 5 minutes at  $7,500 \times g$  at  $4^{\circ}\text{C}$  and the supernatant was discarded. The RNA pellet was air dried for 5–10 minutes then resuspended in 50  $\mu\text{l}$  RNase-free water (Sigma-Aldrich, St. Louis, MO) by pipetting up and down several times, then incubating at  $55^{\circ}\text{C}$  for 10 minutes. RNA was quantified by absorbance at 260 nm using a NanoDrop Spectrophotometer (Thermo Fisher Scientific, Waltham, MA, USA). RNA was stored at  $-80^{\circ}\text{C}$  until use.

#### **2.1.4 Protein extraction from cultured cells**

Protein was extracted from cells using the Mammalian Protein Extraction Reagent (Thermo Fisher Scientific, Waltham, MA, USA) according to the manufacturer's instructions. Cells were washed with PBS, then 500  $\mu\text{l}$  extraction reagent was added directly to the flask. Flasks were shaken for 5 minutes then the lysate was transferred to a microcentrifuge tube and centrifuged at  $14,000 \times g$  for 10 minutes. The supernatant containing protein lysate was transferred to a clean tube and stored at  $-80^{\circ}\text{C}$  until use.

#### **2.1.5 Synthesis of cDNA from mRNA**

cDNA was produced from RNA using the high capacity cDNA reverse transcription kit (Applied Biosystems, Foster City, CA, United States). Briefly, a 20  $\mu\text{l}$  reaction mixture was set up for each sample in a well of a 96-well plate. The reaction mixture consisted of 1  $\mu\text{g}$  or 9  $\mu\text{l}$  (whichever was lower) of RNA, 10  $\mu\text{l}$  RT Buffer and 1  $\mu\text{l}$  RT Enzyme, with the remaining volume made up with RNase-free water. Control samples were also included with no RNA or no RT Enzyme. Samples were run in a thermal cycler for 60 minutes at  $37^{\circ}\text{C}$ , 5 minutes at  $95^{\circ}\text{C}$ , then held at  $4^{\circ}\text{C}$  until retrieval from the machine. The resulting cDNA was then stored at  $-20^{\circ}\text{C}$  until use.

### **2.1.6 Quantitative RT-PCR**

Quantitative RT-PCR utilising the TaqMan system (Applied Biosystems, Foster City, CA, United States) was carried out to measure levels of specific gene expression within cDNA samples. A 10 µl reaction mixture was made in duplicate wells of a 384-well plate for each sample and TaqMan probe combination. The reaction mix consisted of 0.5 µl TaqMan probe, 5 µl TaqMan Universal PCR Master Mix and 4.5 µl cDNA. The reaction was run and measured in a 7900HT Fast Real-Time PCR System (Applied Biosystems, Foster City, CA, United States) with the following thermal cycle: 2 minutes at 50°C, 10 minutes at 95°C, then 45 cycles of 15 seconds at 95°C and 1 minute at 60°C. An internal control probe (for *GAPDH*) was included for every cDNA sample for normalisation. Full details of probes used can be found in Appendix A: Taqman RT-qPCR. Thresholds were set for each probe in the SDS software (Applied Biosystems, Foster City, CA, United States) within the log-linear phase of amplification and threshold cycle (*Ct*) values exported. For each sample/probe combination, *Ct* values were averaged from technical duplicates, then a relative quantity was calculated using the delta delta *Ct* (*ddCt*) method to give expression data that are log normally distributed (Livak and Schmittgen 2001). In this method, the *Ct* value for each target gene is normalised to the reference gene (*GAPDH*), then each sample *dCt* is normalised to a calibrator sample *dCt* (from an untreated control group), as below:

$$dCt = Ct_{target} - Ct_{reference}$$

$$ddCt = dCt_{control} - dCt_{sample}$$

### **2.1.7 Array quantification of mRNA**

To measure transcriptome, cDNA was measured using Agilent SurePrint G3 Human Gene Expression v2 single colour microarrays (Agilent Technologies, Santa Clara, CA, USA). Samples for arrays were prepared and run by J. Iremonger according to the manufacturer's instructions and I performed all bioinformatics analyses.

### **2.1.8 Array quantification of protein**

Protein lysate samples for protein measurement were prepared by J. Pickworth and S. Dawson as described in Chapter 2.1.4. Kinex KAM-800 antibody arrays (Kinexus Bioinformatics, Vancouver, BC, Canada) for protein kinase signalling, containing 877 antibodies were run by Kinexus Bioinformatics (Vancouver, BC, Canada) according to the manufacturer's instructions for measurement of 518 pan-specific and 359 phosphorylated protein levels.

### **2.1.9 Differential mRNA analysis**

Microarray data were analysed using the linear models for microarray analysis (LIMMA) R package (Ritchie et al. 2015, Smyth 2004) to determine the differentially expressed (DE) genes. LIMMA uses empirical Bayesian methods to provide stable results even with smaller numbers of arrays. Raw Agilent microarray intensity data were read into the package, corrected for background and quantile normalised within and between arrays. Expression values were then calculated for each probe, and probes that were not expressed in at least three separate arrays were filtered out. Linear models were then constructed according to a single factor – TRAIL stimulation vs. unstimulated – and used to calculate differential expression of probes between these two conditions. A moderated *t*-statistic was used to determine significance, and Benjamini and Hochberg's method was used to control global false discovery (FDR) rate, for which the significance level was set to 5%, giving globally adjusted p-values. Full details are provided in Appendix B: R scripts.

### **2.1.10 Gene ontology analysis**

DE genes determined by LIMMA were assessed for enrichment of gene ontology (GO) terms using the DAVID web-based tool (Huang da et al. 2009) with the default settings. The categories included for testing were: Genetic Association Database diseases, biological process GO terms, molecular function GO terms and Kyoto Encyclopaedia of Genes and

Genomes (KEGG) pathways (Kanehisa and Goto 2000). GO terms with more than 500 gene hits were excluded as too broad to be informative. Significance threshold for enriched GO gene sets was set to  $p < 0.05$  (Benjamini-Hochberg adjusted p-value).

#### **2.1.11 Pathway topology analysis**

Pathway enrichment analysis of DE genes detected by LIMMA was carried out using the signalling pathway impact analysis (SPIA) R package (Tarca et al. 2009) with the default settings. SPIA matches DE genes to KEGG pathways (Kanehisa and Goto 2000) and takes into account both the number of genes altered within a pathway (NDE) and the perturbation of the pathway (PERT), based on the impact of these genes within the pathway topology. These metrics were combined using Fisher's combined probability test to give a global p-value for the probability of significantly altered pathways with cut-offs defined by FDR correction. Enriched pathways were plotted using the 'plotP' function within the SPIA package. Full details are provided in Appendix B: R scripts.

#### **2.1.12 Differential protein analysis**

Array protein quantification values were converted to Z-scores to account for inter-array variation and the array data were then combined. For each antibody, a Student's *t*-test was carried out to determine significantly altered protein levels between the control and 10- or 60-minute TRAIL-stimulated PSMCs. Significantly altered proteins and phosphorylated proteins determined by the Kinex arrays were overlaid on the signalling pathways highlighted by mRNA studies.

## **2.2 Animals**

### **2.2.1 Licensing**

All animal experiments were approved by the University of Sheffield Project Review Committee and conformed to the UK Home Office Animal (Scientific Procedures) Act 1986 and University of Sheffield guidelines for the care and use of animals.

### **2.2.2 Husbandry**

Mice were housed with up to 6 individuals in polypropylene cages containing bedding, nesting material and environmental enrichment. Cages were kept in a controlled environment with a 12-hour light/dark cycle at 22°C and a constant air pressure. Animals were fed standard laboratory chow (Harlan 18% protein rodent diet) and water *ad libitum*. Littermates were housed together where possible, and if non-littermates were combined, this was done shortly after weaning to minimise stress. Husbandry was kindly performed by the University of Sheffield Biological Services Unit staff and I performed regular welfare checks and husbandry tasks during procedures.

### **2.2.3 Transgenic mouse lines**

For the preliminary bleomycin time-course experiment, which did not require genetic modifications, male C57BL/6 mice were obtained from Charles River Laboratories (Wilmington, MA, USA).  $Tnfsf10^{tm1c(KOMP)Wtsi}$  (hereafter referred to as  $TRAIL^{tm1c}$ ) mice were produced from UC Davis EC Cells and obtained from MRC Harwell (all mouse strains are summarised in Table 2.1). The primary genetic modification in this allele is a pair of loxP sites flanking exon 3 of the *TRAIL* gene (Figure 2.1). Recombination at the loxP sites occurs in cells with Cre recombinase expression, causing excision of the exon and depletion of mRNA and protein expression. The deleted allele is referred to as  $TRAIL^{tm1d}$ .

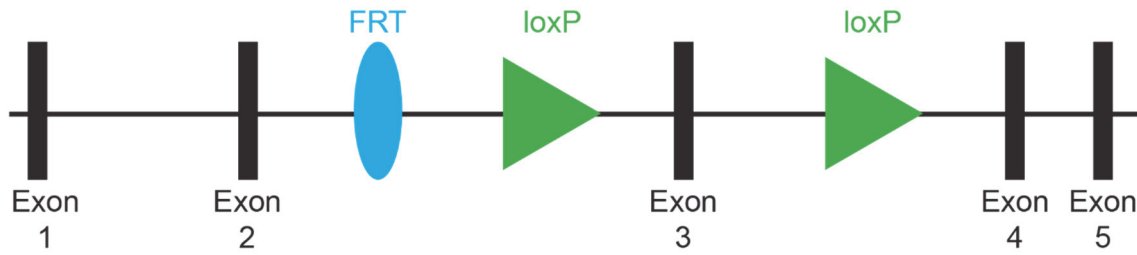


**Figure 2.1: *TRAIL* TM1C transgene construct.** Schematic illustrating the *TRAIL*<sup>tm1c</sup> conditional allele transgene construct. The mouse *TRAIL* gene has 5 exons and is located on chromosome 3. The *TRAIL*<sup>tm1c</sup> has loxP sites flanking exon 3, which can be recognised by Cre recombinase in order to excise exon 3 and prevent expression of TRAIL protein. A flippase recognition target (FRT) site remains between exons 2 and 3 from previous Flp-mediated excision of other elements to create the *TRAIL*<sup>tm1c</sup> allele.

Several cell type-specific Cre driver lines were crossed with the TRAIL<sup>tm1c</sup> line to produce double transgenic mice. The B6.FVB-Tg(Myh11-cre/ERT2)<sup>1Soff/J</sup> (hereafter referred to as SMMHC-Cre-ERT2) line has tamoxifen-inducible Cre expression, driven by the smooth muscle myosin heavy chain 11 (MYH11) promoter in VSMCs (Wirth et al. 2008). These mice were generated and provided by S. Offermanns at the Max-Planck-Institute for Heart and Lung Research. As the SMMHC-Cre-ERT2 allele is carried on the Y-chromosome, only male animals were used for breeding and experiments with this transgene. The B6.Cg-Tg(Col1a2-cre/ERT,-ALPP)<sup>7Cpd/J</sup> (hereafter referred to as Col1a2-Cre-ERT) line has a Cre recombinase driven by a tamoxifen-inducible fibroblast-specific collagen 1 a2 (COL1A2) promoter (Zheng et al. 2002), and was generated by and obtained from C. Denton at University College London. The Tg(Pgk1-cre)<sup>1Lni</sup> (hereafter referred to as PGK-Cre) line has constitutive, ubiquitous expression of Cre recombinase under the control of a phosphoglycerate kinase (PGK) promoter (Lallemand et al. 1998) and was obtained from C. Hall at Cancer Research UK. Due to an effect of maternal Cre expression during oogenesis, cells of non-transgenic offspring from a female carrying the PGK-Cre allele may have Cre-driven recombination (Lallemand et al. 1998). However, as we found this effect was inconsistent and may confound genotyping results, only male PGK-Cre carriers were used as breeders. Also used was the Gt(ROSA)<sup>26Sor<sup>tm1</sup>(CAG-Brainbow2.1)Cle</sup> strain (hereafter referred to as R26R-Brainbow2.1), which was produced by H. Clevers at the Hubrecht Institute and obtained from G. Bou-Gharios at the University of Liverpool. The R26R-Brainbow2.1 strain has a conditional allele with a CAG promoter followed by a floxed-STOP cassette and the Brainbow 2.1 construct inserted at the Gt(ROSA)<sup>26Sor</sup> locus (Livet et al. 2007, Weissman et al. 2011). This allele functions as a Cre recombinase reporter of multiple fluorescent proteins from a single genomic locus depending on the recombination event. All transgenic mouse lines used were based on a C57BL/6 background.

**Table 2.1: Transgenic mouse lines.**

Full strain name	Short name	Details
Tnfsf10 <sup>tm1c(KOMP)Wtsi</sup>	TRAIL <sup>tm1c</sup>	Floxed <i>TRAIL</i> conditional deletion allele
Gt(ROSA)26Sor <sup>tm1(CAG-Brainbow2.1)Cle</sup>	R26R-Brainbow2.1	Fluorescent conditional reporter allele
B6.FVB-Tg(Myh11-cre/ERT2)1Soff/J	SMMHC-Cre-ERT2	VSMC-specific tamoxifen-inducible Cre recombinase expression
B6.Cg-Tg(Col1a2-cre/ERT,-ALPP)7Cpd/J	Col1a2-Cre-ERT	Fibroblast-specific tamoxifen-inducible Cre recombinase expression
Tg(Pgk1-cre)1Lni	PGK-Cre	Global constitutive Cre recombinase expression

*TNFSF10*, TNF Superfamily Member 10; *TRAIL*, TNF-related apoptosis-inducing ligand; *SMMHC*, smooth muscle myosin heavy chain 11; *COL1A2*, collagen 1 a2; *PGK*, phosphoglycerate kinase.

#### 2.2.4 Breeding

TRAIL<sup>tm1c/wt</sup> mice were bred to homozygosity by pairing male and female heterozygous mice and selecting homozygous offspring as subsequent breeders. The SMMHC-Cre-ERT2 line was maintained by breeding a male SMMHC-Cre-ERT2<sup>tg/0</sup> with a female C57BL/6 wildtype mouse. All other Cre driver lines were maintained by pairing mice each possessing at least one Cre allele (producing offspring potentially heterozygous or homozygous for the Cre allele). For F1 crosses, TRAIL<sup>tm1c/tm1c</sup> mice were paired with mice carrying a heterozygous (Col1a2-Cre-ERT, PGK-Cre) or hemizygous (SMMHC-Cre-ERT2) Cre allele (Figure 2.2). For SMMHC-Cre-ERT2 and Col1a2-Cre-ERT experimental crosses, double transgenic F1 offspring were selected as breeders, and back-crossed with TRAIL<sup>tm1c/tm1c</sup> mice in F2 crosses to produce experimental animals possessing TRAIL<sup>tm1c/tm1c</sup> and a single Cre allele. For PGK-Cre F2 crosses, double transgenic offspring from the F1 cross (TRAIL<sup>tm1d/wt</sup>-PGK-Cre<sup>tg/wt</sup>) were back-crossed with parental strain TRAIL<sup>tm1c/tm1c</sup> mice to produce (among other allelic combinations) TRAIL<sup>tm1d/tm1d</sup>-PGK-Cre<sup>tg/wt</sup> and TRAIL<sup>tm1c/wt</sup> for use in experiments. R26R-Brainbow2.1<sup>tg/tg</sup> mice

were crossed with heterozygous Cre mice from each Cre line, to confirm the localisation of Cre recombinase expression and recombination. All breeders were paired at 6-8 weeks of age. I coordinated the breeding strategy and performed genotyping, and the setting up of matings, ear clipping and weaning was kindly performed by the University of Sheffield Biological Services Unit staff.

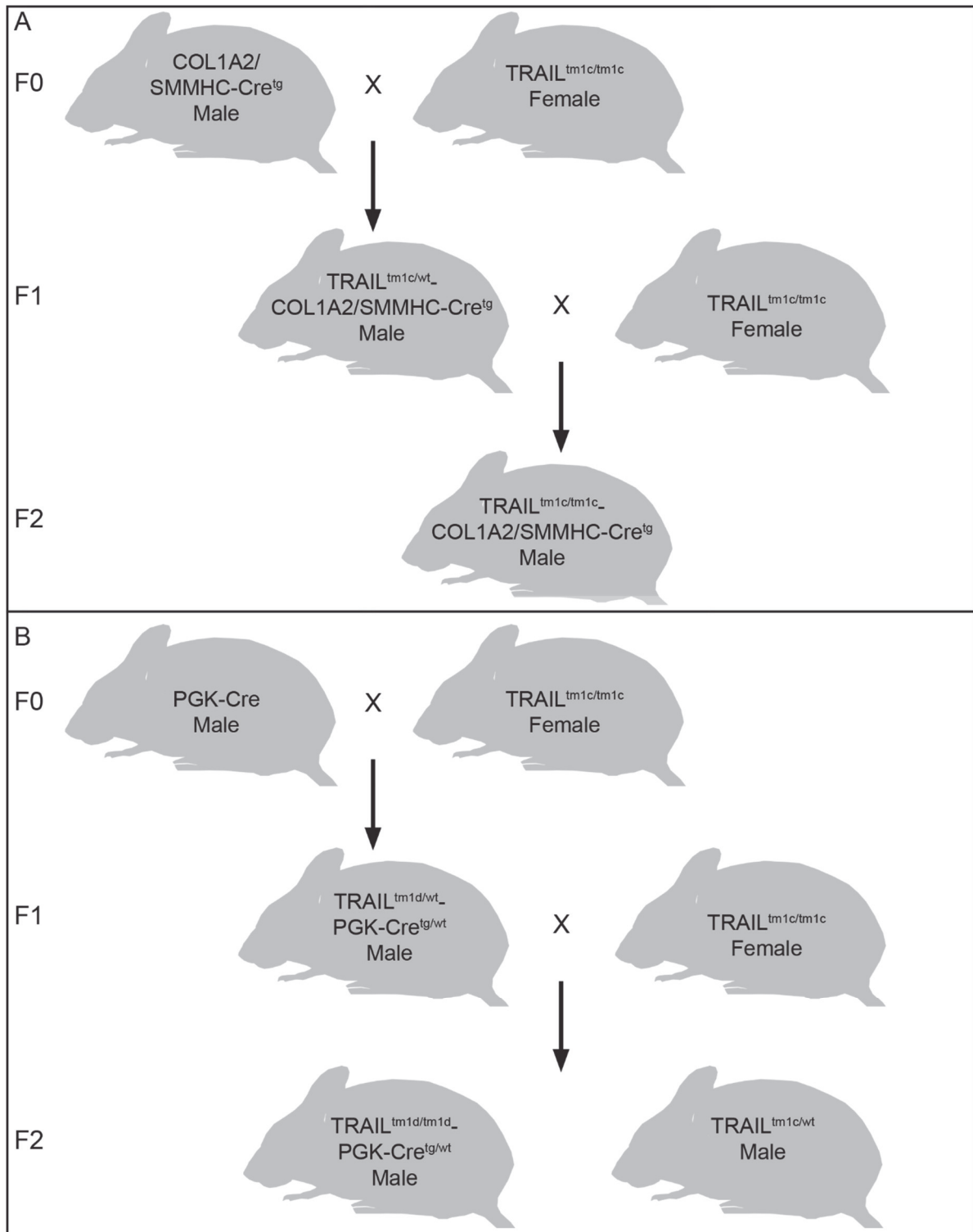


**Figure 2.2: Transgenic breeding strategy.** Schematic illustrating the breeding strategy to produce transgenic mice for experiments. Parental strain TRAIL<sup>tm1c/tm1c</sup> mice were crossed with COL1A2/SMMHC-Cre (A) or PGK-Cre (B) to produce F1 offspring. These were back-crossed with TRAIL<sup>tm1c/tm1c</sup> mice to produce F2 offspring for experimental use.

### **2.2.5 Induction of Cre recombination**

Cre recombinase activity was utilised to achieve genetic deletion of *TRAIL* in VSMCs (SMMHC-Cre-ERT2), fibroblasts (Col1a2-Cre-ERT) and globally (PGK-Cre). As the PGK-Cre promoter is constitutively active in all cells, mice inheriting one or two *TRAIL*<sup>tm1c</sup> alleles in addition to a PGK-Cre<sup>tg</sup> allele would have had Cre expression in all daughter cells since fertilisation, and therefore all cells in the adult mouse should have one or two copies of the deleted *TRAIL*<sup>tm1d</sup> allele respectively. As SMMHC-Cre-ERT2 and Col1a2-Cre-ERT promoters are both tamoxifen-inducible, tamoxifen was delivered to induce Cre expression in animals where this was required. A dose of 2 mg tamoxifen in corn oil (volume 100 µl) was given by intraperitoneal (IP) injection once daily for 5 days at 5–8 weeks old. To make the 20 mg/ml tamoxifen solution, 1 g tamoxifen (Sigma-Aldrich, St. Louis, MO) was dissolved in 50 ml corn oil (Sigma-Aldrich, St. Louis, MO) in a falcon tube overnight at 37°C with shaking. The tamoxifen solution was aliquoted into microcentrifuge tubes, which were transferred to -20°C storage until use. Tamoxifen aliquots were thawed and brought to approximately 37°C before injections. Where appropriate, 5x daily 100 µl corn oil IP injections were given as a control for animals not receiving tamoxifen.

## **2.3 Genotyping**

Parental strains and offspring from all crosses were genotyped to determine which animals could be used for subsequent breeding and experiments. Mice were genotyped by PCR detection of transgenic alleles, using DNA samples extracted from ear clips. Ear clips of approximately 1 mm diameter were taken when mice were weaned, transferred to individual microcentrifuge tubes and stored at 4°C until DNA extraction. Ear clipping was kindly performed by the University of Sheffield Biological Services Unit staff and samples sent to me for preparation and analysis.

### **2.3.1 DNA extraction**

DNA was extracted from ear clips using a REDExtract-N-Amp Tissue kit (Sigma Aldrich, St. Louis, MO, United States). All steps were performed at room temperature unless stated otherwise. Briefly, a master mix containing 100  $\mu$ l Extraction Solution and 20  $\mu$ l Tissue Preparation Solution for each ear clip was prepared and mixed thoroughly. 120  $\mu$ l of this solution was added to the microcentrifuge tube containing the ear clip, then incubated for 10 minutes at room temperature. The tube was then transferred to a heat block and incubated at 95°C for 3 minutes. After removing the tube from the heat block, 100  $\mu$ l of Neutralization Solution B was added to sample and mixed by vortexing. Samples were kept at 4°C for short term, or -20°C for long term storage.

### **2.3.2 Polymerase chain reaction**

PCR amplification was carried out with specific oligonucleotide primers and thermal cycle conditions for each transgenic allele, using a REDExtract-N-Amp PCR Reaction Mix (Sigma Aldrich, St. Louis, MO, United States) and a Veriti 96-Well Thermal Cycler (Thermo Fisher Scientific, Waltham, MA, USA). PCR primers were purchased from Sigma-Aldrich (St. Louis, MO) and 10  $\mu$ M stock solutions made up with nuclease-free water. PCR primer sequences are listed in Appendix C: Genotyping PCR. For each sample, a 20  $\mu$ l PCR reaction was assembled in a well of a 96-well PCR plate (Thermo Fisher Scientific, Waltham, MA, USA) using 10  $\mu$ l PCR Reaction Mix and 4  $\mu$ l of DNA, with primers and nuclease-free water making up the remaining volume (full details in Appendix C: Genotyping PCR). PCR plates were sealed with adhesive PCR plate sealer (Thermo Fisher Scientific, Waltham, MA, USA), mixed by vortexing then centrifuged briefly to 500 x g to collect all liquid at the base of the wells. PCR plates were transferred to the thermal cycler to carry out the PCR reaction (thermal cycle conditions are listed in Appendix C: Genotyping PCR) and removed when complete.

### **2.3.3 Agarose gel electrophoresis**

DNA products from PCR amplification were separated by agarose gel electrophoresis for visual assessment of results. A 2% (w/v) agarose (Sigma Aldrich, St. Louis, MO, United States) gel was produced containing 15  $\mu$ l of 10 mg/ml ethidium bromide (Thermo Fisher Scientific, Waltham, MA, USA) in 1X TAE buffer (Sigma Aldrich, St. Louis, MO, United States). A volume of 10  $\mu$ l from each PCR reaction (containing loading buffer and dye from the PCR Reaction Mix) was loaded into a well of the gel. 6  $\mu$ l of 100 bp DNA ladder (Invitrogen; Waltham, MA, USA), made up according to the manufacturer's specifications, was loaded into a well. Electrophoresis was carried out at 90 V for 45–60 minutes, then the gel removed and imaged under UV illumination using a Gel Doc system (Bio-Rad Laboratories, Hercules, CA, United States).

## **2.4 Animal models**

### **2.4.1 Animals**

Mice from C57BL/6N background, either wildtype or with the desired transgenic alleles were selected for use in SuHx and bleomycin models. Male mice were used for consistency across all experiments due to genetic considerations including the location of the SMMHC-Cre-ERT2 transgene on the Y-chromosome. Animals were allocated to groups based on their ages, in order to equalise the age range between groups as much as possible in addition to randomising the groups. To prevent unintended exposure to tamoxifen in animals from non-tamoxifen groups, the treatment groups were split into separate cages. To give 95% power at  $p < 0.05$ , an optimal group size of minimum 8 animals per genotype and/or treatment condition was determined based on a minimum effect size of 28% change in RVESP. This was conservatively defined as half of the effect seen in a previous study, whereby *TRAIL* deletion reduced mean RVESP from 97 mmHg (SD 11 mmHg) to 42 mmHg (SD 19 mmHg) (Dawson et al. 2014). However, sufficient numbers were not available for all experiments due to limitations with breeding, in particular litter sizes and number of animals with the correct

genotypes. In these cases, animals were allocated to treatment groups with the objective of equalising group sizes where possible and therefore maximising the opportunity for statistically informative data. Within each experiment or batch, model and treatment protocols were synchronised such that endpoint procedures would occur at the same time. The ear clipping used for genotyping was also utilised for animal identification, with each animal receiving a clip pattern consisting of up to two clips per ear (at the upper and/or lower section). Animals each had a unique ear clip pattern within their cage.

#### **2.4.2 VSMC-specific TRAIL deletion in Sugden 5416/hypoxia**

Mice were used in the SuHx model to determine the effect of VSMC-specific *TRAIL* deletion on PAH. Only mice from the  $TRAIL^{tm1c} \times SMMHC-Cre-ERT2$  cross were used in this model, due to the unavailability of sufficient numbers of animals from other Cre crosses. Strains used in the experiment were  $TRAIL^{tm1c/tm1c-SMMHC-Cre-ERT2^{tg/0}}$  from the F2 cross and  $TRAIL^{tm1c/tm1c}$  from the parental  $TRAIL^{tm1c}$  strain.  $TRAIL^{tm1c/tm1c-SMMHC-Cre-ERT2^{tg/0}}$  mice received either tamoxifen or corn oil injections at 5–8 weeks old and were all subjected to SuHx. Additionally, mice lacking the SMMHC-Cre-ERT2 allele ( $TRAIL^{tm1c/tm1c}$ ) were given tamoxifen at 5–8 weeks old and underwent SuHx. Mice from the parental  $TRAIL^{tm1c}$  strain were also used as a healthy control group and received corn oil injections at 5–8 weeks old, followed by normoxic conditions during the SuHx protocol. Mice entered the SuHx protocol at minimum 12-weeks old and weighed approximately 25 g at the first Sugden 5416 injection. Mice underwent 3 weekly subcutaneous injections of Sugden 5416 at a dose of 20 mg/kg, on days 1, 7 and 14. A 5 mg/ml Sugden 5416 solution was made fresh weekly by dissolving Sugden 5416 (Tocris Bioscience, Bristol, UK) in vehicle containing 0.5% (w/v) carboxymethylcellulose sodium, 0.9% (w/v) sodium chloride, 0.4% (v/v) polysorbate 80 and 0.9% (v/v) benzyl alcohol in deionized water (all components from Sigma Aldrich, St. Louis, MO, United States). Mice were kept in hypoxic chambers for 3 weeks (day 1–21), with oxygen concentration sustained by an electronic controller at 10% with addition of nitrogen and oxygen as required. Mice had free access to standard chow and water at all times. Cages were removed from the hypoxic

chambers and cages, bedding, food and water replaced twice weekly. Mice were weighed twice weekly, during cage changes and before injections. Animal endpoint procedures were followed at day 21.

#### **2.4.3 *Bleomycin preliminary time-course model***

The repeated IP injection of bleomycin model was chosen as a suitable model for PF (Bryant et al. 2016, Karmouty-Quintana et al. 2015, Karmouty-Quintana et al. 2012). A preliminary time-course experiment was undertaken to determine suitable length and endpoint for the final bleomycin experiments with Cre/lox transgenic mice. Male C57BL/6 mice, initially at median weight 23.5 g (range 20–25 g) were used for the experiment. Mice underwent IP injection with 35 mg/kg bleomycin (reconstituted with sterile saline 0.9% (w/v) and adjusted to pH 7 with sodium hydroxide; obtained from Sigma-Aldrich, St. Louis, MO) or 0.9% (w/v) saline twice weekly for 1, 3 or 4 weeks (6 groups, n=8 mice per group). Groups underwent endpoint procedures and were sacrificed at day 7, day 21 and day 32 respectively.

#### **2.4.4 *Bleomycin final model***

The repeated IP bleomycin model was used to determine the effect of Cre recombinase-mediated deletion of *TRAIL* globally or in VSMCs or fibroblasts on PF. Mice from the  $TRAIL^{tm1c}$  x PGK-Cre,  $TRAIL^{tm1c}$  x SMMHC-Cre-ERT2 and  $TRAIL^{tm1c}$  x Col1a2-Cre-ERT crosses respectively were used in this model to determine these effects. Due to the timing of breeding, two separate bleomycin experiments were run: one using  $TRAIL^{tm1c/tm1c}$ -SMMHC-Cre-ERT2<sup>tg/0</sup> animals from the F2 cross and  $TRAIL^{tm1c/tm1c}$  from the parental strain, and the other using  $TRAIL^{tm1c/tm1c}$ -Col1a2-Cre-ERT<sup>tg/wt</sup>,  $TRAIL^{tm1d/tm1d}$ -PGK-Cre<sup>tg/wt</sup>,  $TRAIL^{tm1c/wt}$  and  $TRAIL^{tm1c/tm1c}$  animals. Mice underwent IP injection with 35 mg/kg bleomycin (reconstituted with 0.9% (w/v) sterile saline and adjusted to pH 7 with sodium hydroxide; produced by Kyowo Kirin, Japan and purchased from Sheffield Teaching Hospitals pharmacy) or 0.9% (w/v) sterile saline twice weekly for 4 weeks. Animals underwent endpoint procedures and were sacrificed at day 35;

however, based on severity in the preliminary experiment mice were entered into the protocol with higher starting weights (median weight 26.4 g, range 21–31.3 g). Mice had free access to standard chow and water at all times. Mice were weighed twice weekly and endpoint procedures were followed at day 21.

#### **2.4.4.1 Global and fibroblast-specific TRAIL deletion in bleomycin model**

For the global and fibroblast-specific *TRAIL* deletion experiment,  $TRAIL^{tm1c/tm1c}$ -Col1a2-Cre-ERT<sup>tg/wt</sup> mice received tamoxifen IP injections at 5–8 weeks old and were all subjected to the bleomycin model. Additionally, mice lacking a Cre allele ( $TRAIL^{tm1c/tm1c}$ ) were given tamoxifen at 5–8 weeks old and underwent bleomycin.  $TRAIL^{tm1d/tm1d}$ -PGK-Cre<sup>tg/wt</sup> and  $TRAIL^{tm1c/wt}$  from the  $TRAIL^{tm1c}$  x PGK-Cre F2 cross also underwent bleomycin. Mice from the parental  $TRAIL^{tm1c}$  strain were also used as a healthy control group and received corn oil injections at 5–8 weeks old, followed by IP saline injections during the bleomycin protocol. These mice entered the bleomycin protocol at minimum 12-weeks old and weighed approximately 26 g at the first bleomycin injection. Due to the availability of animals with the correct genotypes, this experiment was run in two batches, with each group split approximately equally between batches. No differences due to batch were found in any measurement used in this study (data not shown), so the data were combined for all reported analyses.

#### **2.4.5 Humane endpoints**

Based on regular monitoring, on welfare grounds if animals displayed signs of distress or pain or loss of weight of greater than 20% of body weight over 5 days, animals were sacrificed according to Schedule 1 procedures.

## **2.5 Animal endpoint procedures**

### **2.5.1 Echocardiography**

For echocardiography, anaesthesia was induced by inhaled isoflurane in air and maintained at 1–1.5% (v/v) in air throughout. Heart rate, respiratory rate and rectal temperature were monitored, with anaesthetic dose adjusted to maintain a heart rate of 450–500 beats per minute. The procedure was performed with mice on a heated stage and covered to minimise heat loss. Mice were depilated and heated Aquasonics 100 ultrasound transmission gel (Parker Laboratories, Fairfield, NJ, USA) was used to minimise signal loss. A Vevo 770 echocardiography device with an RMV707B scan head (Visual Sonics, Toronto, Canada) was used to record data. For the LV, standard parameters were measured in the short axis view and M-mode measurements made for the LV wall and internal dimensions. Stroke volume derived from measurement of the velocity timed integral of aortic valve annulus was multiplied by heart rate to obtain the cardiac output, which was then normalised to body weight to give the cardiac index. M-Mode RV free wall measurements were recorded from the right parasternal long axis view. Doppler flow measurements were carried out at the proximal pulmonary artery, from which the time from onset of flow to peak velocity (PA acceleration time; PAAT) was derived. Echocardiography was performed by N. Arnold and A. Zawia.

### **2.5.2 Cardiac catheterisation**

Immediately after echocardiography, right and left ventricular catheterisation was carried out via the right external jugular vein and right internal carotid artery. Mice remained under inhaled isoflurane anaesthesia at 1–1.5% (v/v) in air. An incision was made from the neck to the clavicle to the right of the midline to expose the right external jugular vein. Using blunt dissection, the surrounding tissue was removed from the jugular vein. The vein at the end distal to the heart was ligated with 5-0 silk and the suture secured to the nose cone with tape. A second suture was placed around the jugular vein proximal to the heart, left loose and secured with a needle holder, which was positioned to keep tension on the suture and stretch

the jugular vein. A 25 G needle was used to puncture and hold open the jugular vein whilst simultaneously inserting a Millar ultra-miniature pressure-volume PVR-1030 catheter (Millar Instruments, Inc., Houston, TX) into the jugular vein. The tension on the proximal suture was then released as the catheter was advanced down the jugular vein, then through the right atrium and into the RV. The catheter was adjusted until an RV pressure-volume loop was observed, then left for 1 minute to stabilise before recording for an extra minute for data analysis. After RV catheterisation, the protocol was repeated to access the LV via the right internal carotid artery using a PVR-1045 1F catheter (Millar Instruments, Inc.). Data were collected using a PowerLab 8/30 data acquisition system (AD Instruments, Oxfordshire, UK) and recorded with Chart v7 software (AD Instruments). After data collection, a selection of high-quality trace was exported to PVAN v2.3 software (Millar Instruments, Inc.) for pressure-volume loop extraction and analysis. Cardiac catheterisation was performed by A. Lawrie and L. West.

### **2.5.3 Sacrifice of animals**

Immediately after cardiac catheterisation, mice were exsanguinated by cardiac puncture and sacrificed by cervical dislocation.

### **2.5.4 Lung perfusion formalin fixation**

A lateral incision was made below the diaphragm and the thoracic cavity was opened via a vertical incision along the centre of the rib cage. The descending aorta was cut and the RV was injected with 2 ml PBS to flush remaining blood from the pulmonary vasculature. The heart and lungs with trachea were then removed *en bloc*. The right lung was ligated and removed. The left lung was then inflated to 20 cm of H<sub>2</sub>O with 10% (v/v) neutral buffered formalin via a catheter inserted into the trachea. The left lung and heart were fixed for 24 hours at 4°C in ~15x volume of 10% (v/v) neutral buffered formalin. I performed all pathology procedures and subsequent dissections.

### **2.5.5 Tissue harvest**

Half of the dissected right lung was placed in a cryovial microcentrifuge tube then snap frozen in liquid nitrogen before transfer to -80°C storage. The second lung half was transferred to a microcentrifuge tube containing 0.5 ml RNAlater (Thermo Fisher Scientific, Waltham, MA, USA) and stored at 4°C for up to 18 hours before removal of the liquid then transferred to -80°C storage. Due to low numbers of animals with the correct genotype in bleomycin experiments utilising the COL1A2-Cre-ERT and PGK-Cre crosses, for all these animals the whole right lung was taken in liquid nitrogen. Samples of aorta, kidney, spleen and liver were also dissected and fixed for 24 hours at 4°C in ~15x volume of 10% (v/v) neutral buffered formalin.

### **2.5.6 Harvest of frozen tissue for imaging**

Snap frozen tissues for histological imaging were harvested from Cre reporter mice, which had not undergone use in experimental models. Dissection, vascular flushing and inflation of the lungs was performed as described in section 2.5.4 with the following alteration: the lungs were inflated with a 1:1 mixture of Tissue-Tek optimal cutting temperature compound (Sakura Finetek, Thatcham, UK) and water. The lungs were cut into halves and placed cut face down into a cylindrical mould, which was then filled with optimal cutting temperature compound. The mould was placed on a metal block, which was sitting in a liquid nitrogen bath. The tissue was removed once fully frozen, sealed and transferred to liquid nitrogen before storage at -80°C.

## **2.6 Animal tissue handling**

### **2.6.1 Processing formalin fixed tissues for histology**

After 24 hours fixation, neutral buffered formalin was decanted from the formalin-fixed tissues and replaced with 70% (v/v) ethanol for storage at 4°C until processing. Tissues were dissected into smaller sections for ease of embedding and cutting. The left lung was dissected

laterally into four equal parts. Tissues were dehydrated and processed into paraffin using a Leica TP1020 Semi-enclosed Benchtop Tissue Processor (Leica Microsystems, Wetzlar, Germany) according to the manufacturer's instructions. Tissues were then embedded into paraffin blocks using metal base molds (Leica Microsystems, Wetzlar, Germany). Sections of 5  $\mu\text{m}$  thickness were cut with a microtome, floated on water at 40°C and transferred to Polysine glass slides (Thermo Fisher Scientific, Waltham, MA, USA). Slides were dried overnight at 40°C then kept at room temperature until use.

### **2.6.2 Handling snap-frozen tissue for imaging**

Frozen lungs from R26R-Brainbow2.1 mouse crosses were harvested as described in section 2.5.6 then transferred from -80°C storage to -20°C storage before sectioning. Sections of 5  $\mu\text{m}$  thickness were cut in the dark with a Cryostat at -20°C and transferred to Polysine glass slides. Slides were stored at -20°C protected from light until mounting. For mounting, slides were left at room temperature for 2 minutes, then 10  $\mu\text{l}$  VECTASHIELD Vibrance Antifade Mounting Medium with DAPI (Vector Laboratories, Burlingame, CA, USA) was added. A coverslip was placed on the slide and air bubbles removed using forceps. Slides were kept at room temperature in the dark overnight to allow the mountant to cure before imaging.

### **2.6.3 Grinding frozen lung tissue**

Frozen lungs harvested as described in section 2.5.5 were transferred in small batches (5–10) from -80°C storage to liquid nitrogen contained in a portable dewar. Pestle and mortars were pre-cooled with liquid nitrogen then the lung was transferred in and ground to a fine powder. Care was taken to avoid thawing the tissue and to add more liquid nitrogen as required. Once ground, the tissue was transferred back to the cryovial microcentrifuge tube using a scalpel pre-cooled with liquid nitrogen. Tubes were then transferred back to -80°C storage until use.

#### **2.6.4 RNA extraction from lung tissue**

RNA was extracted from ground lung tissue using a Maxwell 16 miRNA Tissue Kit and a Maxwell 16 MDx Instrument (Promega, Madison, WI, United States) according to the manufacturer's instructions. Approximately 10 mg ground lung tissue was transferred with a pre-cooled spatula to a tube on ice containing 200 µl of 1-Thioglycerol/Homogenization Solution (20 µl of 1-Thioglycerol per ml of Homogenization Solution). The tissue was homogenised by repeatedly drawing through a 25G needle on a 1 ml syringe, then left on ice for an additional 15–30 seconds to ensure complete homogenization. 200 µl of Lysis Buffer and 15 µl of Proteinase K was added to the sample and vortexed for 20 seconds, then incubated for 10 minutes at room temperature. The lysate was transferred to a prepared Maxwell RSC Cartridge, which was processed using the Maxwell 16 MDx Instrument. The purified RNA was eluted into 60µl of nuclease-free water. RNA quantification, synthesis of cDNA and quantitative real-time PCR were performed as previously described (sections 2.1.5 and 2.1.6).

#### **2.6.5 Protein extraction from lung tissue**

Protein was extracted from tissue using the Tissue Protein Extraction Reagent (Thermo Fisher Scientific, Waltham, MA, USA) according to the manufacturer's instructions. 20 ml extraction reagent containing Halt Protease Inhibitor Cocktail (Thermo Fisher Scientific, Waltham, MA, USA) per g of tissue was added to a microcentrifuge tube containing lung tissue. Tissue was homogenised by repeatedly drawing through a 25G needle on a 1 ml syringe, then left on ice for an additional 15–30 seconds to ensure complete homogenization then centrifuged at 10,000 x g for 5 minutes. The supernatant containing protein lysate was transferred to a clean tube and stored at -80°C until use.

### **2.6.6 *Right ventricular hypertrophy measurement***

Atria and right ventricular free walls were dissected from hearts leaving the left ventricle (LV) and septum. RVH was measured using the ratio of right ventricular free wall weight to LV plus septum weight.

## **2.7 Histological staining of tissue sections**

### **2.7.1 *General histological techniques***

Unless otherwise stated, buffers and chemicals were obtained from Sigma Aldrich (St. Louis, MO, United States). To coverslip stained slides, they were removed from xylene and the excess xylene was blotted away. Slides were then transferred face down to a cover slip containing two drops of DPX mountant (Merck, Kenilworth, NJ, United States) and air bubbles were displaced using forceps, before drying at room temperature for a minimum of 8 hours.

### **2.7.2 *Miller's elastin stain***

Lung sections were histologically stained for morphology with Miller's elastin stain with alcian blue and Curtis' modified van Gieson (ABEVG). All steps were performed at room temperature unless stated otherwise. Sections were dewaxed with xylene twice for 10 minutes, rehydrated step-wise through 100%, 100%, 95% and 50% (v/v) ethanol for 1 minute each and finally rinsed in water for 5 minutes. Sections were oxidised with 0.25% (w/v) aqueous potassium permanganate for 3 minutes then rinsed with water for 3 minutes. Sections were bleached with 1% (w/v) aqueous oxalic acid for 3 minutes then rinsed with water for 3 minutes. Sections were stained Carazzi's haematoxylin (300 ml of 8.33% (w/v) aluminium potassium sulphate in water is added to 100 ml of 0.5% (w/v) haematoxylin in glycerol, followed by the addition of 100 ml of 0.1% (w/v) potassium iodate in water) for 2 minutes, differentiated in acid alcohol (1% (v/v) HCl in 70% (v/v) ethanol) for 5 seconds and blued under hot running tap water for 5 minutes. Sections were then stained with 1% (w/v) alcian blue (VWR International, Radnor, PA, USA) in 3% (v/v) aqueous acetic acid for 5 minutes, rinsed in water for 3 minutes and

incubated in 95% (v/v) ethanol for 3 minutes. Sections were stained with Miller's Elastin (VWR International) for 30 minutes, differentiated in 95% (v/v) ethanol for 5 seconds and rinsed in water for 3 minutes. Sections were stained with Curtis' modified Van Gieson (500 ml made using 450 ml saturate aqueous picric acid, 50 ml 1% (w/v) ponceau S and 5 ml glacial acetic acid) for 6 minutes and rinsed with water for 3 minutes. Sections were blotted dry, dehydrated step-wise through 95%, 100% and 100% (v/v) ethanol for 1 minute each then cleared with xylene twice for 10 minutes and coverslipped.

### **2.7.3 Masson's Trichrome stain**

Lung sections were histologically stained with Masson's Trichrome (MTC) to visualise collagen. All steps were performed at room temperature. All pre-made stains were obtained from the Masson-Goldner staining kit (Merck, Kenilworth, NJ, United States) unless stated otherwise. Sections were dewaxed with xylene twice for 10 minutes, rehydrated step-wise through 100%, 100%, 95% and 70% (v/v) ethanol for 1 minute each. Sections were stained with Weigert's iron haematoxylin (1:1 ratio parts A and B; made up fresh each day; Pyramid Innovation, Polegate, UK) for 5 minutes. Sections were washed in tap water for 5 minutes, then rinsed in deionised water. Sections were stained with azophloxine (azophloxine 0.6% w/v in 0.31% w/v acetic acid; Masson-Goldner staining kit) for 7 minutes, then rinsed twice in 1% (v/v) acetic acid. Sections were stained with acid G (acid G 2% w/v, phosphotungstic acid hydrate 4% w/v; Masson-Goldner staining kit) for 10 minutes then rinsed twice in 1% (v/v) acetic acid. Sections were stained with water blue (water blue 0.2% w/v in 0.2% v/v acetic acid) for 5 minutes, rinsed in 1% (v/v) acetic acid then washed for 1 minute in 1% (v/v) acetic acid. Sections were then dipped (4–5 dips; until there was no visible water) in two separate rounds of 100% (v/v) ethanol. Sections were then cleared with xylene twice for 10 minutes and coverslipped.

#### **2.7.4 General immunohistochemistry method**

All steps were performed at room temperature unless stated otherwise. Sections were cleared with xylene twice for 10 minutes, rehydrated step-wise through 100%, 100%, 95% and 70% (v/v) ethanol for 1 minute each and finally rinsed in water for 5 minutes. Endogenous peroxidases were blocked by incubation in 3% (v/v) hydrogen peroxide (diluted from 30% stock) for 10 minutes then sections were rinsed with water for 3 minutes. Sections were then outlined with a hydrophobic barrier PAP pen (Abcam, Cambridge, UK). Antigen retrieval steps were performed at this stage as required for specific antibodies. Sections were blocked with 2.5% normal serum (species determined by secondary antibody host species; Vector Laboratories, Burlingame, CA, USA) for 20 minutes. Excess blocking solution was then blotted from the slides, and excess surrounding the sections removed to leave the sections still wet. Sections were incubated with primary antibody for 1 hour, then washed three times in PBS for 5 minutes. Slides were incubated with ImmPRESS Peroxidase Polymer secondary antibody (Vector Laboratories, Burlingame, CA, USA) for 30 minutes then washed three times in PBS for 5 minutes. Detection was carried out by incubating sections in SignalStain diaminobenzidine substrate (Cell Signaling Technology, Danvers, MA, United States) for 1–5 minutes. Sections were rinsed in water for 5 minutes, then nuclei counterstained with Carazzi's Haematoxylin for 1 minute. Sections were then dehydrated step-wise through 70%, 95%, 100% and 100% (v/v) ethanol for 1 minute each, then cleared with xylene twice for 10 minutes and coverslipped.

#### **2.7.5 Alpha smooth muscle actin immunostaining**

To specifically visualise smooth muscle cells in the pulmonary arterial media, lung sections were immunohistochemically stained for  $\alpha$ -smooth muscle actin ( $\alpha$ -SMA) with the method described in section 2.7.4, with the following details. The primary antibody used was a mouse monoclonal anti-human  $\alpha$ -SMA antibody (1:150 dilution in PBS; M0851; Dako, Cambridgeshire, UK). The secondary antibody was raised in goat and accordingly goat serum was used for blocking.

### **2.7.6 TRAIL immunostaining**

Sections were immunostained for TRAIL with the method described in section 2.7.4, with the following details. The primary antibody used was a rabbit polyclonal anti-human TRAIL antibody (1:200 dilution in PBS; abx001750; Abxbexa, Cambridge, UK). The secondary antibody was raised in horse and accordingly horse serum was used for blocking.

### **2.7.7 Von Willebrand Factor immunostaining**

To visualise the endothelial layer of the pulmonary arteries, sections were immunohistochemically stained for VWF with the method described in section 2.7.4, with the following details. Antigen retrieval was carried out before blocking, with sections incubated in Menapath trypsin solution (Menarini Diagnostics, Wokingham, UK) at the stock concentration for 15 minutes at room temperature. The primary antibody used was a rabbit polyclonal anti-human VWF antibody (1:300 dilution in PBS; A082; Dako, Cambridgeshire, UK). The secondary antibody was raised in horse and accordingly horse serum was used for blocking.

### **2.7.8 Imaging of histological sections**

Sections were imaged under brightfield using an Axio Imager 2 microscope (Carl Zeiss, Oberkochen, Germany) with a 20X objective (200X effective magnification) and using Zen 2 software to produce tiled and stitched images. Briefly, whole slides were imaged using a 2.5X objective to generate a preview image. The preview images were used to draw tiled regions around the tissue sections, which were then imaged with the 20X objective. Tiles were stitched automatically during image acquisition to create a single image for each section. Compressed Zeiss CZI image files (80% quality) were saved and used for image analysis and to generate representative figures.

### **2.7.9 Imaging of fluorescence Cre reporter sections**

Sections were imaged using equipment and software as described in section 2.7.8, with brightfield illumination replaced with fluorescence imaging. A metal halide lamp (Carl Zeiss, Oberkochen, Germany) was used for illumination with images acquired separately for each channel. Optical filters were used in the microscope to detect emission at 461, 488 and 555 nm respectively.

### **2.7.10 Quantification of pulmonary vascular remodelling**

Pulmonary vascular remodelling was quantified in a blinded manner from the ABEVG histologically stained and  $\alpha$ -SMA immunostained lung sections. Sections were assessed within the Zen 2 software (Carl Zeiss). For the ABEVG histologically stained sections, the diameter of pulmonary arteries and arterioles was measured and used to divide them into two size groups (0–50  $\mu$ m and 50–100  $\mu$ m). Each vessel was scored as non-muscularised or muscularised, based on whether they had a single elastic lamina or two or more distinct elastic laminae respectively. For determining medial layer thickness in  $\alpha$ -SMA immunostained lung sections, the polygon contour tool was used to draw two shapes for each small pulmonary artery – one around the outer edge of the medial smooth muscle layer, and one around the inner edge. The medial layer area was calculated by subtracting the inner shape area from the outer area, then the medial layer area was divided by the outer area to give a ratio of the medial layer to cross-sectional area. As with the ABEVG histologically stained sections, vessels were categorised into two size groups (0–50  $\mu$ m and  $\geq$  50  $\mu$ m) based on the largest diameter obtained from the CSA measurement. For both analyses, a minimum of 20–30 pulmonary arteries were sampled from micrographs of one representative lung section and averaged to give one data point per animal. To give an overall representation of lung morphology, vessels were sampled from multiple areas of each lung section with the assistance of a grid overlaid on the image.

### **2.7.11 Quantification of PF from images**

Micrographs from lung sections stained with Masson's Trichrome as described in section 2.7.3 were used to quantify collagen staining as a measure of the extent of PF (example images shown in Figure 2.3). This was done computationally, and I was blinded until the final data were produced. Firstly, images were exported from Zen software at 25% resolution TIFF files to reduce computing time. A batch macro script was used to process the images in FIJI software (Schindelin et al. 2012, Rueden et al. 2017) with the following steps. Briefly, an image was imported into FIJI using the default settings of the Bioformats plugin (Linkert et al. 2010). A greyscale duplicate image was produced and used to make a threshold selection (0–173/255) of the whole lung section. The selection was grown using the 'Dilate' and 'Fill Holes' functions to remove gaps within the lung section, then the lung area was measured using 'Analyze Particles'. This lung area selection was used as the basis for all subsequent measurements, by cropping the image data using the 'Clear Outside' function. Next, on a duplicate of the original colour image, the background colouring was removed using 'Subtract Background' and a colour threshold (hue 118–156/255, saturation 17–255/255, brightness 9–245/255) was used to select and measure the area stained by water blue, i.e. collagen. A duplicate of the background-subtracted colour image was used to measure the white space (i.e. non-cellular) within the lung with a colour threshold (hue 0–255/255, saturation 0–30/255, brightness 245–255/255). The tissue area of the lung was calculated by subtracting the white space from the total lung area, then the collagen area was divided by the tissue area to give a collagen/lung tissue area ratio. This metric was used in order to reduce variation caused by differences in total lung size, as well as potential differences in the degree of lung inflation during fixation. For each lung, micrographs of four sections were analysed and averaged to give one data point per animal.

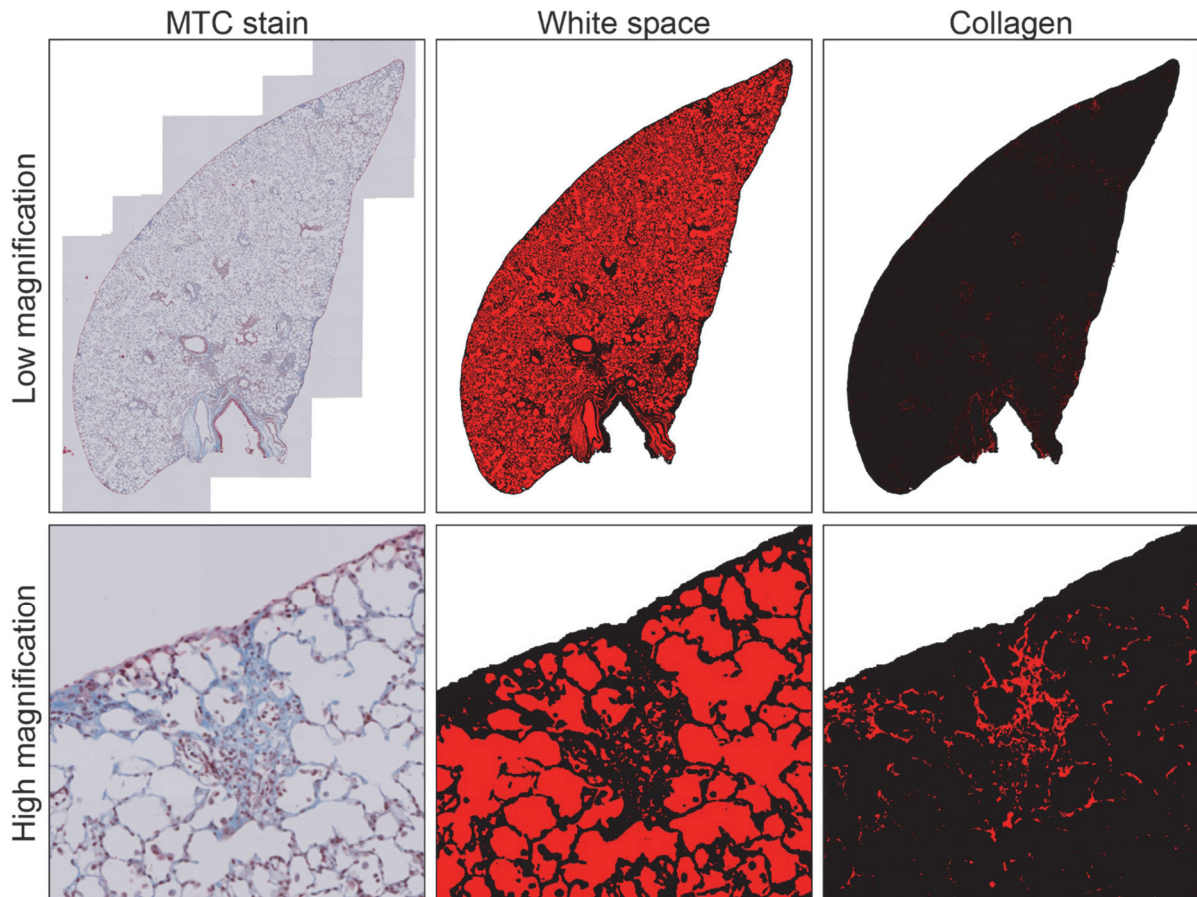


**Figure 2.3: Quantification of PF from images.** Example images demonstrating FIJI analysis to quantify fibrosis in 5  $\mu\text{m}$  mouse lung sections stained with Masson's Trichrome (MTC). Examples of threshold selections are highlighted in red for the white space (i.e. non-tissue areas) within the lung and collagen (blue stained) areas. The red areas are overlaid onto a black area representing the threshold selection for the lung section perimeter. The total collagen area for each lung was divided by the total lung tissue area to account for variation in lung sizes and degree of inflation.

## 2.8 Patient studies

### 2.8.1 Ethical approval

Clinical data and blood samples were obtained through license of materials from the STH-ObS Biobank collection, project registration STH15222, under full NHS Research Ethics Committee approval (Ethics approval No. 08/H1308/193+5).

### **2.8.2 Participants**

Patients and healthy volunteers were retrospectively enrolled from the existing Sheffield PH biobank. The following patient groups from the PH biobank were assessed in the present study: healthy volunteers, IPAH patients, SSc patients, SSc-PAH patients and a set of combined PAH patients.

### **2.8.3 Serum protein measurement**

Protein levels were measured in 1 ml serum samples from patients and healthy volunteers by Myriad RBM. Assays were performed with standard protocols on a validated Luminex-based platform.

## **2.9 Statistics**

Unless otherwise stated, data are expressed with bars representing the mean  $\pm$  standard deviation (SD). Where appropriate, the ROUT method (Motulsky and Brown 2006) with  $Q = 5\%$  was used to detect outliers for exclusion. For individual pairwise comparisons, unpaired Student's *t*-test was performed with a two-tailed *p*-value. For comparisons involving three or more groups, one-way analysis of variance (ANOVA) test was used with each group compared post hoc by the Holm-Sidak method. Significance or rejection of the null hypothesis was designated to *p*-values  $< 0.05$ . Basic statistical analyses were performed using Prism software (Version 8.2.0; GraphPad, San Diego, CA, United States).

### 3 The role of fibroblast-derived TRAIL in bleomycin-induced PF

Fibrosis of the lungs is a debilitating condition that may be idiopathic or associated with other diseases including autoimmune disorders and PAH. Patients with PF have a poor prognosis: the 5-year survival rate for IPF patients in the UK is 43%, and median survival for IPF patients is 3.9 years (McLaughlin et al. 2004). As such, there is a substantial requirement for more effective pharmaceutical treatments for PF.

PF is characterised by lung remodelling and the deposition of ECM proteins – in particular various collagens – by activated fibroblasts and myofibroblasts. The aetiology of PF is heterogeneous and various biological processes are thought to be involved. One such factor is the apoptosis-inducing cytokine TRAIL. Differences in circulating levels of TRAIL have been observed in IPF patients (Collison et al. 2019, Habel et al. 2018, McGrath et al. 2012), as well as within cells of the lung (Habel et al. 2018, McGrath et al. 2012). In pre-clinical models, mice exposed to bleomycin to induce PF have a worsened fibrotic phenotype when TRAIL is depleted by genetic deletion (McGrath et al. 2012) or by administering a neutralising antibody (Habel et al. 2018).

I hypothesised that TRAIL produced by fibroblasts within the lungs plays a protective role in modulating fibrosis in PF via apoptosis of fibroblasts, myofibroblasts or other pathogenic cells in the lung. To determine whether fibroblasts are a protective source of TRAIL in this context, a mouse strain was generated with fibroblast-specific, tamoxifen-inducible deletion of *TRAIL*. These mice were subjected to the repeated IP bleomycin model, which has been previously described as producing robust PF as well as PAH indicated by elevated RVESP and pulmonary arterial remodelling (Bryant et al. 2016, Karmouty-Quintana et al. 2015, Karmouty-Quintana et al. 2012). Additionally, a global Cre-driven *TRAIL* deletion mouse strain was

produced and subjected to the IP bleomycin model in order to recapitulate previous findings (McGrath et al. 2012) in the context of this repeated IP injection model, rather than a single dose administered intratracheally or by oropharyngeal aspiration.

### 3.1 Generation of mice with global Cre-driven *TRAIL* knockout

Offspring from the F2 cross with two genotypes were used in experiments: *TRAIL*<sup>tm1d/tm1d</sup>-PGK-Cre<sup>tg/wt</sup> (global *TRAIL* deletion) and *TRAIL*<sup>tm1c/wt</sup> (wild type control). The generation of these mice is described in Chapter 2.2.4.

#### 3.1.1 Genotyping

During breeding and before experiments, mice were genotyped by PCR detection of transgenic and wildtype alleles using DNA extracted from ear clips. PCR genotyping was performed to determine the genotypes of mice from parental strains, F1 offspring and F2 offspring (from *TRAIL*<sup>tm1d/wt</sup>-PGK-Cre<sup>tg/wt</sup> mice crossed with *TRAIL*<sup>tm1c/tm1c</sup> mice). Three separate multiplex PCR reactions were performed to detect *TRAIL*<sup>tm1c</sup> and *TRAIL*<sup>wt</sup> alleles, *TRAIL*<sup>tm1d</sup> and *TRAIL*<sup>tm1c</sup> distal LoxP alleles and PGK-Cre<sup>tg</sup> and PGK-Cre<sup>wt</sup> alleles respectively. For *TRAIL* genotyping, two PCR reactions were performed (Figure 3.1A–B). The first used a forward primer sequence upstream of the target region and a reverse primer sequence within the target region, to produce a 456 bp product for *TRAIL*<sup>wt</sup> and a larger 604 bp product for *TRAIL*<sup>tm1c</sup>, which contained the additional LoxP site upstream of the target region. No product would be produced in *TRAIL*<sup>tm1d</sup>, which lacks the target region for the reverse primer. The second *TRAIL* PCR utilised the same forward primer sequence and an additional forward primer targeting the distal LoxP sequence, with a reverse primer sequence contained within the region downstream of the target region. This PCR formed a 282 bp product for *TRAIL*<sup>tm1c</sup>, a 681 bp product for *TRAIL*<sup>tm1d</sup> and no product from *TRAIL*<sup>wt</sup>. For PGK-Cre genotyping, four primers were used: one pair specific to a genomic control region, and another pair internally targeting the PGK-Cre insert sequence (Figure 3.1C). The PCR enabled amplification of a 408 bp product for the PGK-Cre<sup>tg</sup> allele and/or a 225 bp wildtype control product. PCR conditions and primer sequences are listed in Appendix C: Genotyping PCR. Example agarose gel images of PCR genotyping from F2 offspring are shown in Figure 3.1, demonstrating the four possible genotypes from this cross: *TRAIL*<sup>tm1d/tm1d</sup>-PGK-Cre<sup>tg/wt</sup> (1), *TRAIL*<sup>tm1c/wt</sup> (2),

TRAIL<sup>tm1d/wt</sup>-PGK-Cre<sup>tg/wt</sup> (3) and TRAIL<sup>tm1c/tm1d</sup> (4). Of these, TRAIL<sup>tm1d/tm1d</sup>-PGK-Cre<sup>tg/wt</sup> and TRAIL<sup>tm1c/wt</sup> mice were used in experiments.

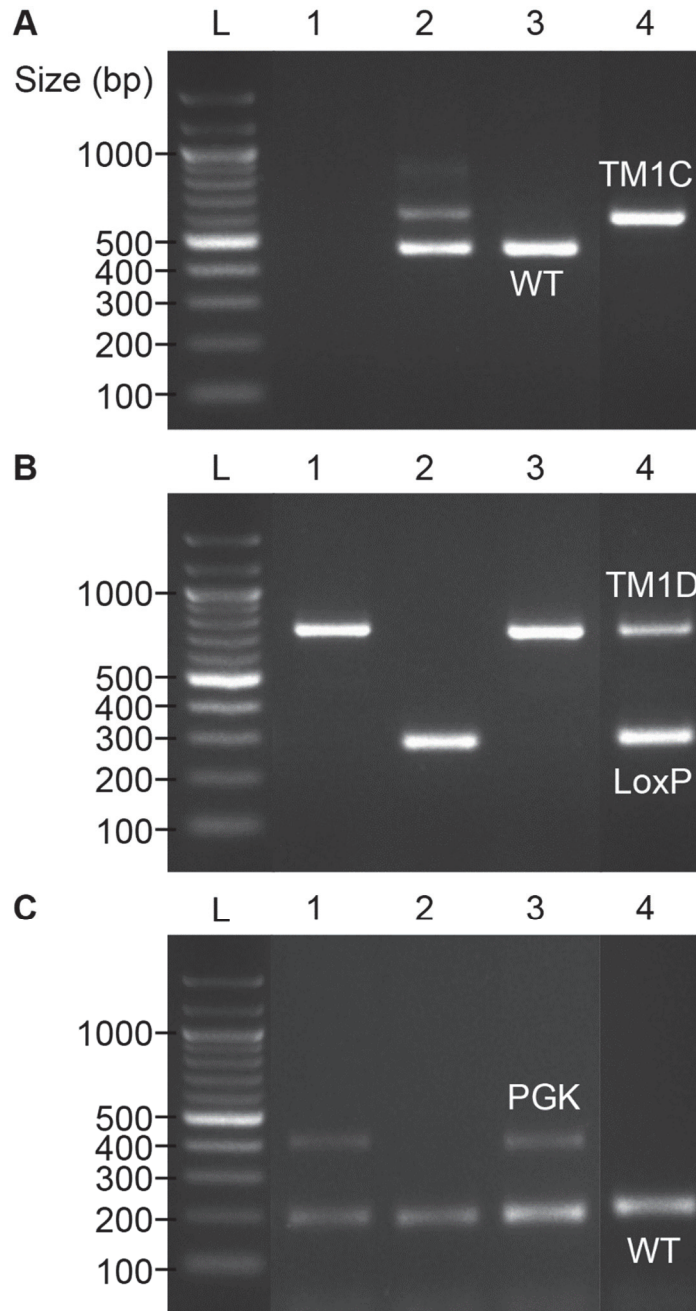


**Figure 3.1: PCR genotyping of TRAIL<sup>tm1c</sup>, TRAIL<sup>tm1d</sup> and PGK-Cre transgenic alleles.** Example images of agarose gels from PCR genotyping of four F2 offspring from TRAIL<sup>tm1d/wt</sup>-PGK-Cre<sup>tg/wt</sup> mice crossed with TRAIL<sup>tm1c/tm1c</sup> mice. Three separate PCR reactions were performed to detect (A) TRAIL<sup>tm1c</sup> and TRAIL<sup>wt</sup> alleles (bands labelled 'TM1C' and 'WT', 604 bp and 456 bp respectively), (B) TRAIL<sup>tm1d</sup> and TRAIL<sup>tm1c</sup> distal LoxP alleles (bands labelled 'TM1D' and 'LoxP', 681 bp and 282 bp respectively) and (C) PGK-Cre<sup>tg</sup> and PGK-Cre<sup>wt</sup> alleles (bands labelled 'PGK' and 'WT', 408 bp and 194 bp respectively). The lane labelled 'L' contains 100 bp ladder and lanes '1-4' contain PCR products from four separate mice, for which each PCR reaction was carried out.

### **3.1.2 Cre reporter demonstration of Cre recombination**

To confirm the localisation of PGK-Cre expression and PGK-Cre-driven recombination, R26R-Brainbow2.1 mice were crossed with PGK-Cre mice. The double transgenic offspring were utilised as a reporter strain with R26R-Brainbow2.1-driven fluorescence occurring in cells where the R26R-Brainbow2.1 flox allele becomes active after Cre recombinase-mediated recombination. Based on combinations of random Cre-driven inversion or excision recombination events at the R26R-Brainbow2.1 flox gene – which contains multiple fluorophores – cells may express fluorescence of different colours. Lung sections from double transgenic adult offspring were examined by fluorescence microscopy. As shown in Figure 3.2, green and red fluorescence indicating Cre recombination was found throughout the lungs, in all cell types examined. This confirmed that PGK-Cre expression was able to cause Cre-mediated recombination in all cell types. Nuclei were fluorescently stained blue by DAPI in the mountant.

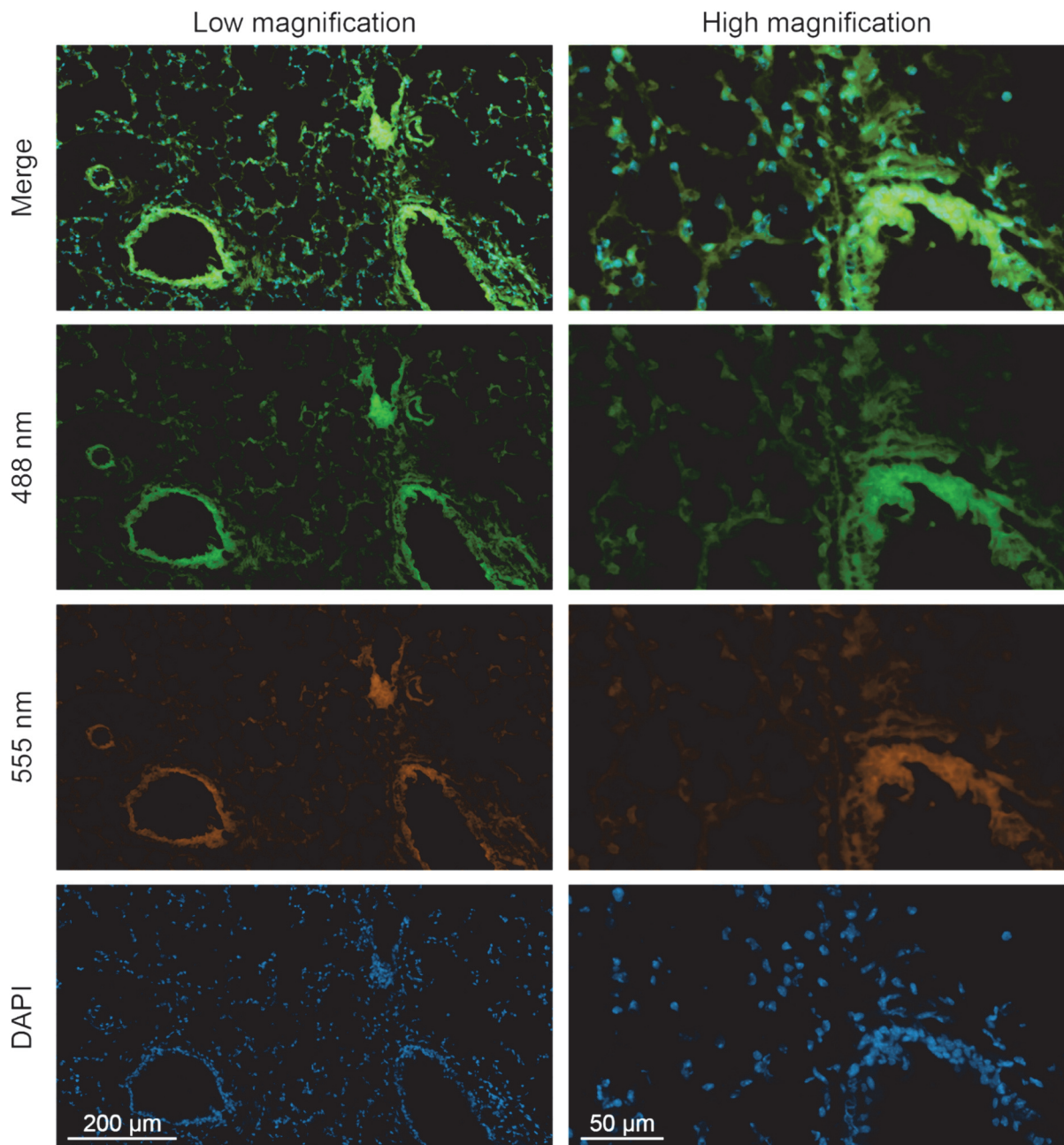


**Figure 3.2: Cre reporter demonstrates ubiquitous Cre recombination.** Fluorescence micrographs of 5  $\mu\text{m}$  lung sections from R26R-Brainbow2.1<sup>tg/wt</sup>-PGK-Cre<sup>tg/wt</sup> mice. Images were acquired at 488 nm and 555 nm (Cre recombinase-driven fluorescence) and 461 nm (DAPI nuclear stain). Images were acquired at 200X total magnification then digitally cropped.

## 3.2 Generation of mice with fibroblast-specific *TRAIL* deletion

Male offspring from the F2 cross, with tamoxifen-inducible fibroblast-specific *TRAIL* deletion ( $TRAIL^{tm1c/tm1c}$ -COL1A2-Cre-ERT<sup>tg/wt</sup>) were used in experiments. The generation of these mice is described in Chapter 2.2.4.

### 3.2.1 Genotyping

Three separate multiplex PCR reactions were performed to detect  $TRAIL^{tm1c}$  and  $TRAIL^{wt}$  alleles,  $TRAIL^{tm1d}$  and  $TRAIL^{tm1c}$  distal LoxP alleles and COL1A2-Cre-ERT<sup>tg</sup> and COL1A2-Cre-ERT<sup>wt</sup> alleles respectively (Figure 3.3). The PCR reactions were as described in Chapter 3.1.1, however as the COL1A2-Cre-ERT allele is inducible, no  $TRAIL^{tm1d}$  band was detected in DNA from ear clips of these mice (as genotyping was performed before tamoxifen was given to mice). Examples of PCR genotyping from F2 offspring are shown in Figure 3.3, demonstrating the two possible genotypes from this cross:  $TRAIL^{tm1c/tm1c}$ -COL1A2-Cre-ERT<sup>tg/wt</sup> (1) and  $TRAIL^{tm1c/tm1c}$  (2). Both of these strains were used in experiments.

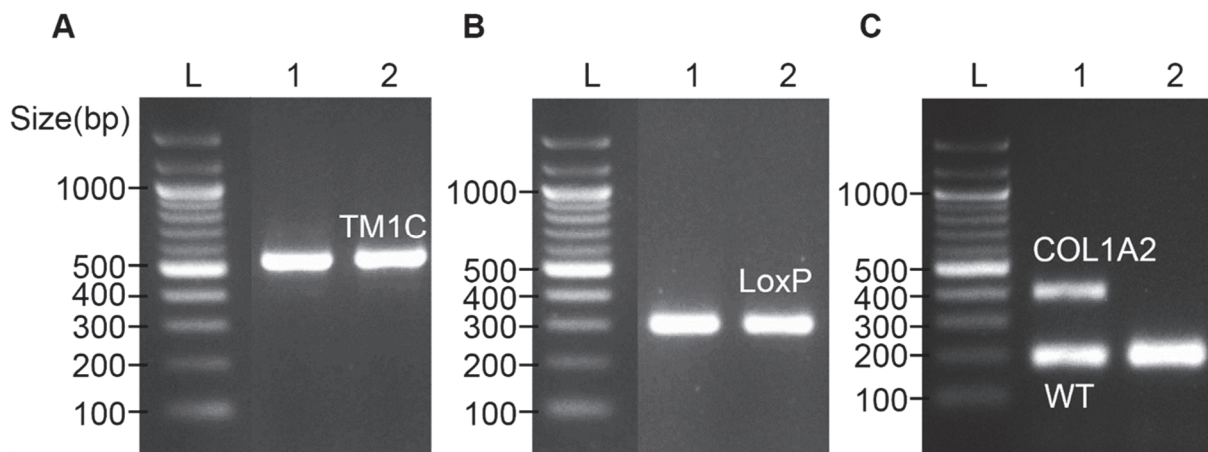


**Figure 3.3: PCR genotyping of  $TRAIL^{tm1c}$  and Col1a2-Cre-ERT transgenic alleles.** Example images of agarose gels from PCR genotyping of two F2 offspring from  $TRAIL^{tm1d/tm1c}$ -COL1A2-Cre-ERT<sup>tg/wt</sup> mice crossed with  $TRAIL^{tm1c/tm1c}$  mice. Three separate PCR reactions were performed to detect the (A)  $TRAIL^{tm1c}$  allele (band labelled 'TM1C' at 604 bp), (B)  $TRAIL^{tm1c}$  distal LoxP allele (band labelled 'LoxP', at 282 bp) and (C) COL1A2-Cre-ERT<sup>tg</sup> and COL1A2-Cre-ERT<sup>wt</sup> alleles (bands labelled 'COL1A2' and 'WT', 408 bp and 194 bp respectively). The lane labelled 'L' contains 100 bp ladder and lanes '1' and '2' contain PCR products from two separate mice, for which each PCR reaction was carried out.

### **3.2.2 *Cre reporter demonstration of Cre recombination***

To confirm the localisation of COL1A2-Cre-ERT expression and COL1A2-Cre-ERT-driven recombination, R26R-Brainbow2.1 mice were crossed with Col1a2-Cre-ERT mice. Cre expression was induced by giving 5 daily IP injections of 2 mg tamoxifen at 5–8 weeks. Lung sections from double transgenic adult offspring were examined by fluorescence microscopy. As shown in Figure 3.4, green and red fluorescence indicating Cre recombination was found in medial/adventitial connective tissue/mesenchyme surrounding large blood vessels. This is where cells from fibroblast and myofibroblast lineages would be expected to reside. Nuclei were fluorescently stained blue by DAPI in the mountant.

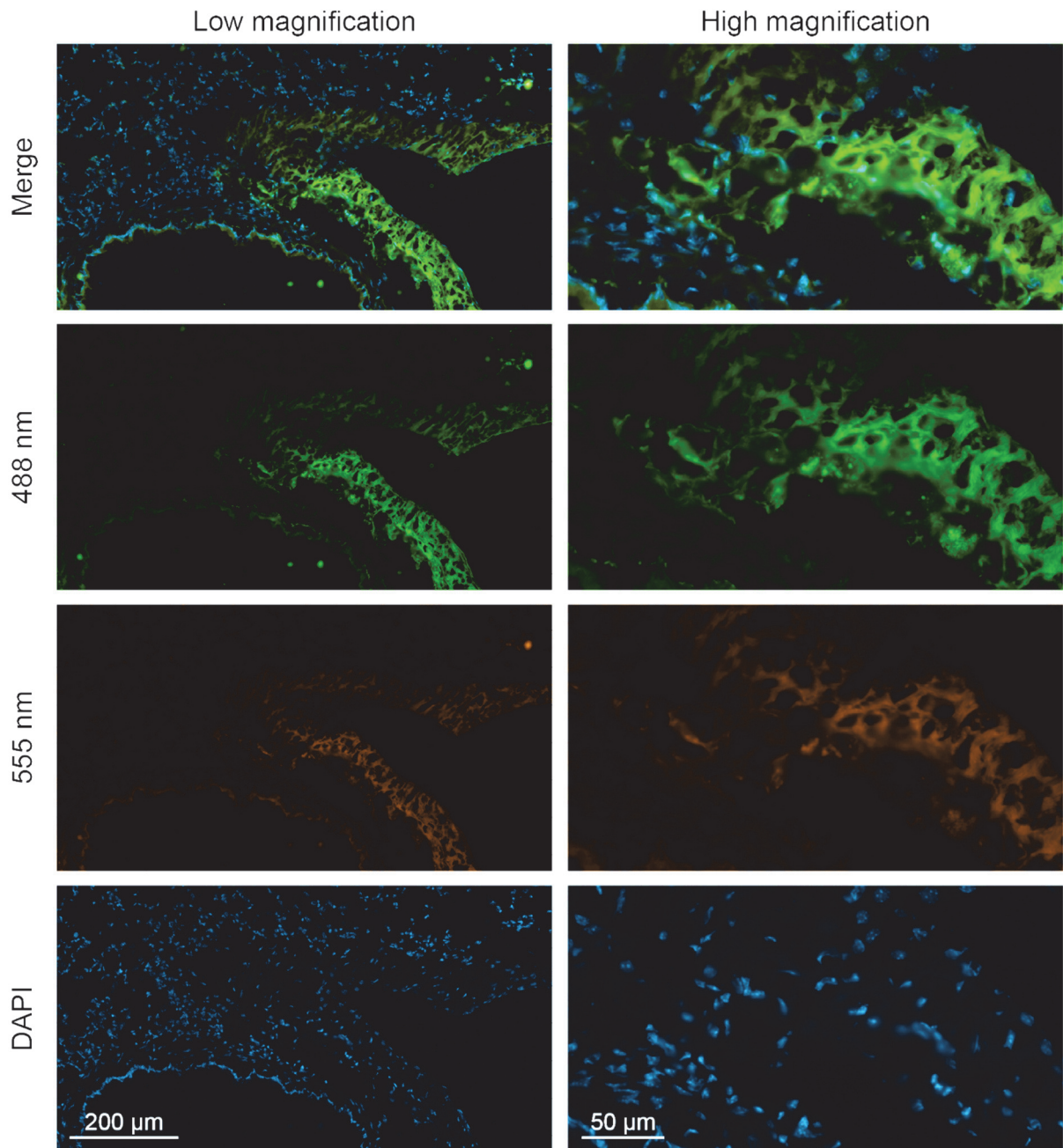


**Figure 3.4: Cre reporter demonstrates fibroblast-specific Cre recombination.** Fluorescence micrographs of 5  $\mu\text{m}$  lung sections from R26R-Brainbow2.1<sup>tg/wt</sup>-Col1a2-Cre-ERT<sup>tg/wt</sup> mice. Images were acquired at 488 nm and 555 nm (Cre recombinase-driven fluorescence) and 461 nm (DAPI nuclear stain). Images were acquired at 200X total magnification then digitally cropped.

### **3.3 Bleomycin mouse model of PF**

A time-course experiment was carried out to determine the onset and severity of PF and PAH in mice exposed to bleomycin. This experiment also served as an opportunity to optimise the protocol, which had not previously been carried out within the research group. The experimental protocol is detailed in Figure 3.5. Male C57BL/6 mice underwent IP injection with 35 mg/kg bleomycin or saline twice weekly for 1, 3 or 4 weeks (8 per group). Groups were sacrificed at day 7, day 21 and day 32 respectively. Endpoint echocardiography and cardiac catheterisation were performed to assess PAH phenotype. Animals were then sacrificed and lungs were perfusion fixed for histological staining and immunohistochemical assessment. The 32-day group was originally planned to be taken to 35 days before sacrifice, however upon visual inspection of disease severity (indicators including lethargy and breathlessness), for animal welfare purposes it was decided to sacrifice the mice at 32 days.

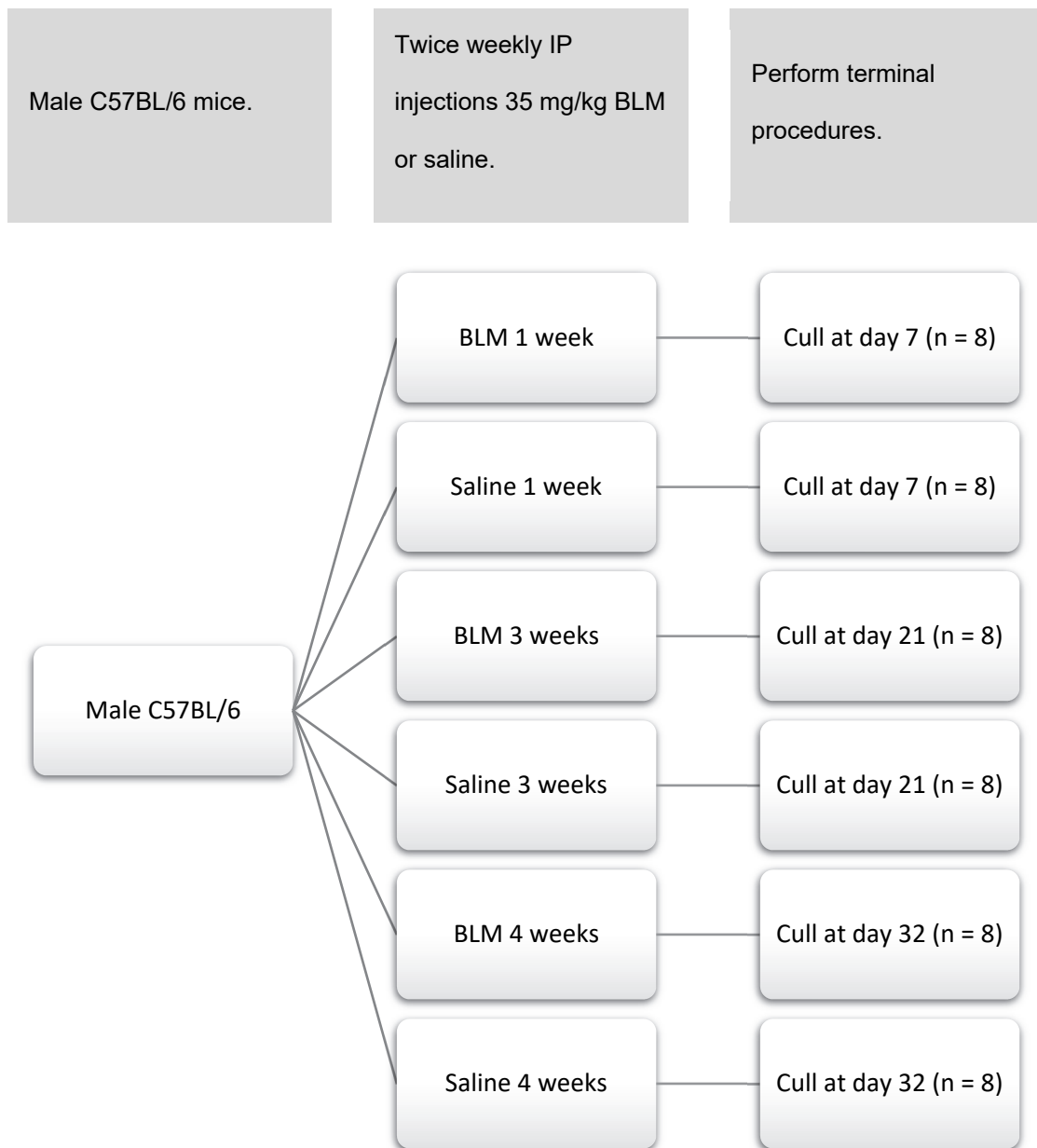


**Figure 3.5: Experimental schematic for IP bleomycin time-course.** All mice used were male C57BL/6. Mice were weaned, ear clipped and genotype confirmed by PCR. Mice were subjected to bleomycin (BLM) or saline IP injections twice weekly for up to 4 weeks and culled at day 7, 21 or 32. Terminal procedures were performed including echocardiography, cardiac catheterisation and tissue harvest.

### **3.3.1 Quantification of PF**

To visually examine the extent and onset of PF, formalin-fixed, paraffin sections of lung were stained with Masson's Trichrome (Figure 3.6A–B). This highlighted the changes in overall lung morphology and specific fibrotic lesions. In the 7-day IP bleomycin mice no fibrotic changes were observed compared to the saline control mice. At 21 days the bleomycin mice had developed increased areas of collagen deposition, primarily localised to the adventitia of pulmonary arteries. These areas also exhibited thickened alveolar septa and cellular infiltrate within the alveoli. At 32 days the bleomycin mice had large areas of extensive, contiguous fibrotic masses. In the fibrotic areas of 32-day lungs there was almost complete obliteration of alveoli, with extensive cellular infiltrate within the remaining alveoli. Blue area representing collagen staining was also quantified and normalised to total lung tissue area in FIJI software (Figure 3.6C). At 32 days the bleomycin mice had significantly increased normalised lung collagen content compared to the matched saline group (mean 0.1561 vs. 0.0410;  $p = 0.0156$ ). No quantitative differences were observed at the 7-day or 21-day timepoints between bleomycin mice and saline control mice.

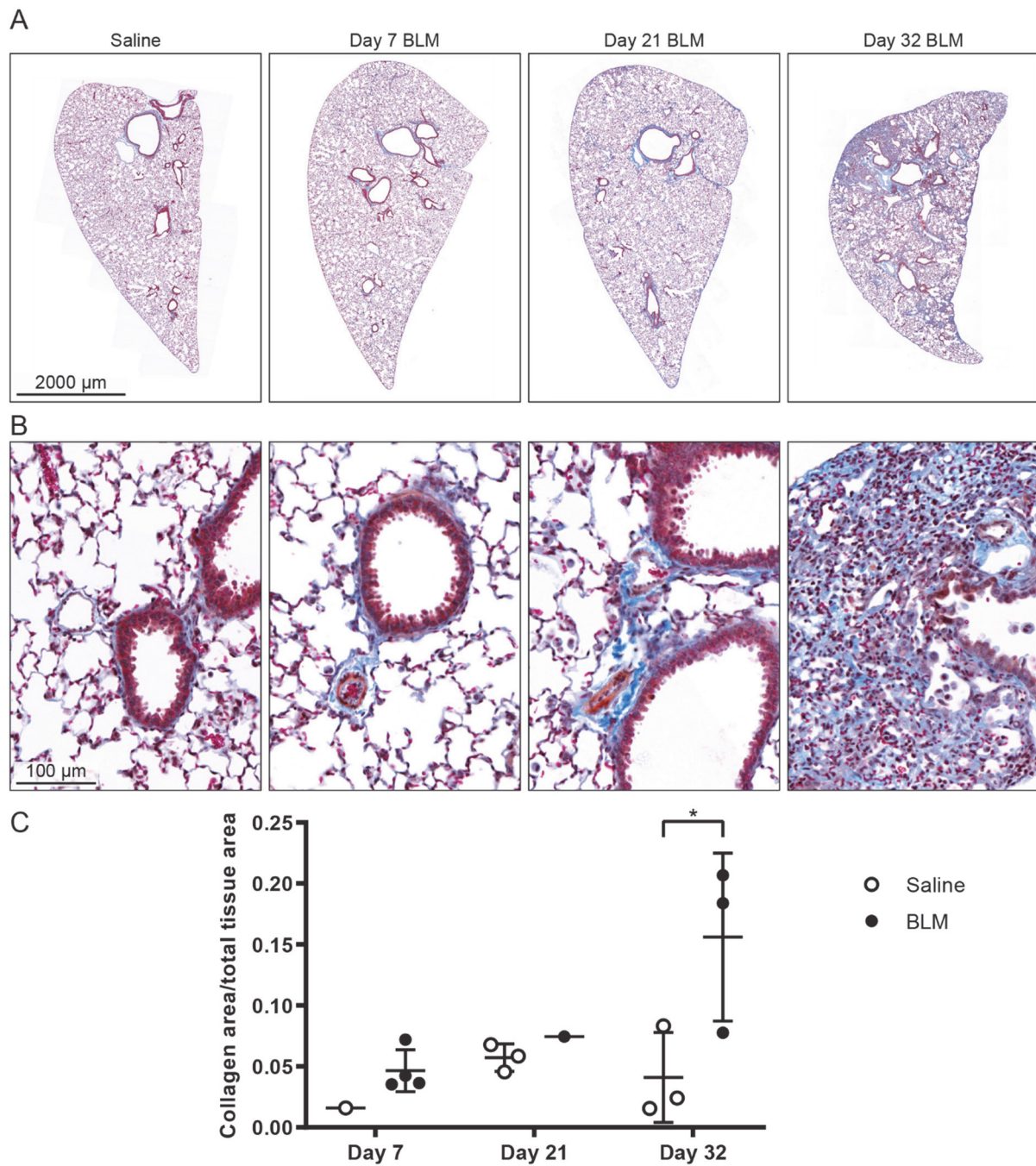


**Figure 3.6: PF in bleomycin mice.** Mice were subjected to bleomycin (BLM) or saline IP injection twice weekly for 1, 3 or 4 weeks and culled at day 7, 21 or 32 respectively. **(A–B)** Representative micrographs are shown from 5 µm thick lung sections histologically stained with Masson’s Trichrome. Collagen is stained blue, nuclei pink, cytoplasm red and muscle orange. Images were acquired at 200X total magnification then digitally cropped. **(A)** Whole lung sections showing overall difference in morphology. In **(B)** areas are magnified, highlighting pulmonary artery adventitial fibrosis at BLM day 21 and dense fibrosis at BLM day 32. **(C)** Blue area representing collagen staining was quantified and normalised to total tissue area. Collagen was measured in four lung sections from each mouse, with average values plotted for each mouse. Bars show mean ± SD, n = 1–4. \* p<0.05, two-way ANOVA with Sidak’s multiple comparisons test, bleomycin groups compared to saline control groups.

### **3.3.2 Haemodynamics**

Measurements were taken from right heart catheterisation (Figure 3.7A–E) in addition to echocardiography (Figure 3.14F–G) under anaesthesia at the time of terminal procedures to assess haemodynamic changes associated with PAH. The 32-day bleomycin mice developed significantly increased RVESP compared to saline control mice (mean 52.74 mmHg vs. 21.25 mmHg,  $p = 0.0479$ ; Figure 3.7A). While there was no significant difference in dPdt minimum, the 21-day and 32-day bleomycin groups were more disperse (standard deviations 1,871 mmHg/s and 3,109 mmHg/s respectively) compared to their time-matched saline controls (standard deviations 477 mmHg/s and 416 mmHg/s respectively), suggesting with greater group numbers a difference between treatments may have been detected. No differences due to bleomycin were detected in left heart function determined by cardiac index measured by echocardiography (cardiac output at the aortic valve normalised to body weight), suggesting that the left heart was unaffected by bleomycin insult (Figure 3.7F). Haemodynamic data were not obtained for some mice due to either technical difficulty during catheterisation, insufficient high-quality pressure-volume loops for analysis or for some control mice catheterisation was not performed. Insufficient data points were obtained from LV or aortic haemodynamic measurements to draw conclusions (data not shown).

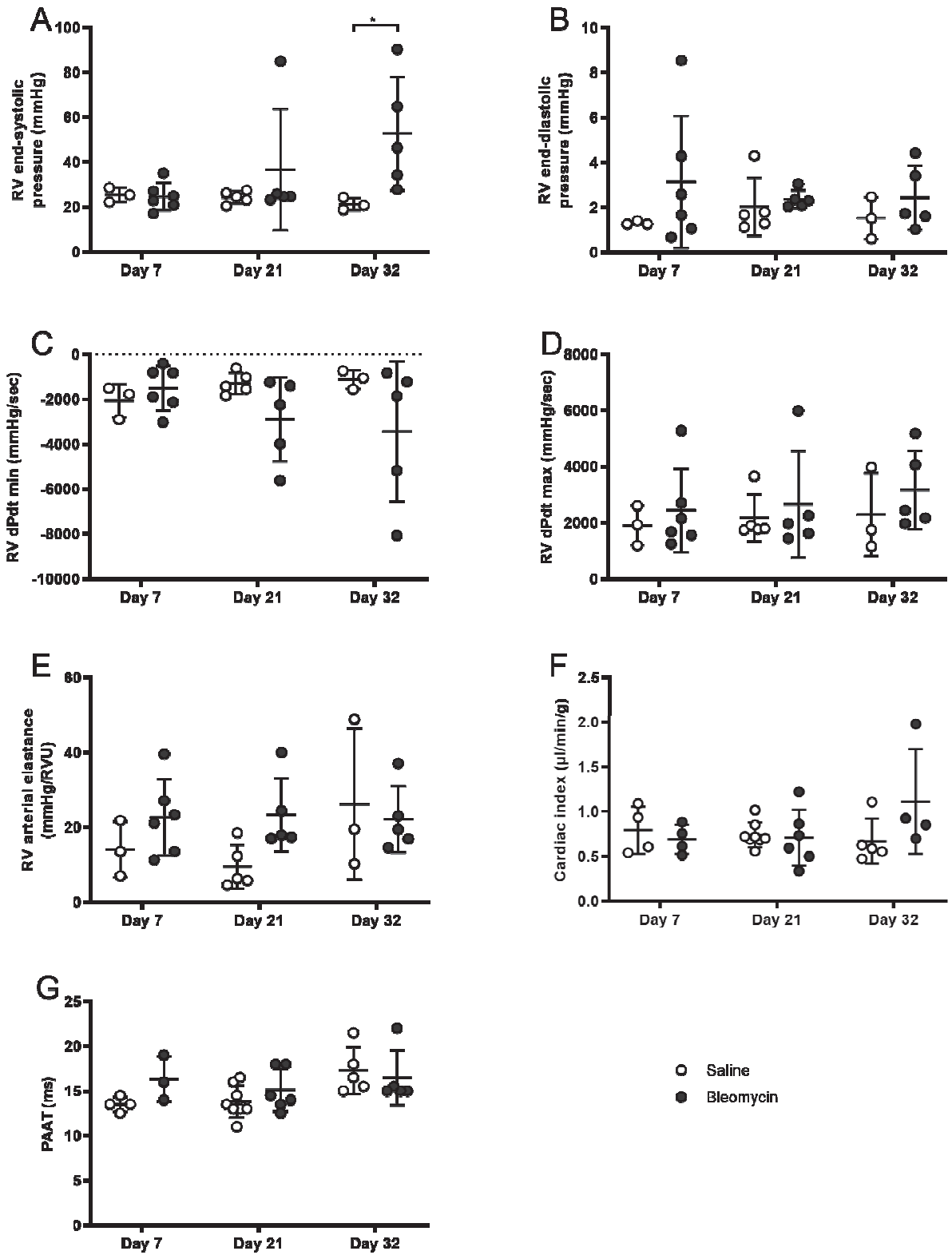


**Figure 3.7: PAH determined by haemodynamic measures after bleomycin insult.** Mice were subjected to bleomycin (BLM) or saline IP injection twice weekly for 1, 3 or 4 weeks and culled at day 7, 21 or 32 respectively. Haemodynamic measurements were taken by cardiac catheterisation (**A–E**) and echocardiography (**F–G**). Plots show (**A**) right ventricular (RV) end systolic pressure, (**B**) RV end-diastolic pressure, (**C**) RV dP/dt minimum, (**D**) RV dP/dt minimum, (**E**) RV arterial elastance, (**F**) cardiac index (cardiac output measure at the aortic valve and normalised to body weight) and (**G**) pulmonary artery acceleration time (PAAT). Points represent individual mice, n = 3–7 animals per group, bars show mean  $\pm$  SD. \*  $p < 0.05$ ; two-way ANOVA with Sidak's multiple comparisons test, bleomycin-treated groups compared to saline control groups.

### 3.3.3 Right ventricular hypertrophy

After sacrifice of animals, hearts were dissected and RVH was calculated as the ratio of RV free wall weight to LV plus septum weight. The 32-day group of bleomycin mice developed significantly increased RVH compared to saline control mice (mean 0.058 vs. 0.034,  $p = 0.0181$ ; Figure 3.8). No RVH was observed in bleomycin mice at the day 7 or day 21 timepoints.

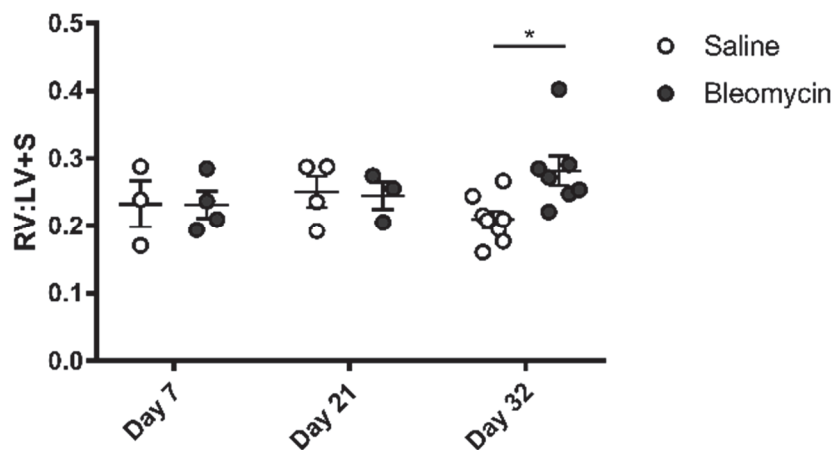


**Figure 3.8: Right ventricular hypertrophy after bleomycin insult.** Mice were subjected to bleomycin (BLM) or saline IP injection twice weekly for 1, 3 or 4 weeks and culled at day 7, 21 or 32 respectively. Hearts were dissected and right and right ventricular hypertrophy was calculated by right ventricular free wall weight normalised to left ventricle plus septum weight (RV:LV+S). Points represent individual mice,  $n = 3-6$  animals per group, bars show mean  $\pm$  SD. \*  $p < 0.05$ ; two-way ANOVA with Sidak's multiple comparisons test, bleomycin-treated groups compared to saline control groups.

### **3.3.4 Pulmonary vascular remodelling**

Pulmonary vascular remodelling was quantified in micrographs of formalin-fixed, paraffin-embedded lung sections histologically stained with ABEVG to assess vascular changes associated with PAH (Figure 3.9A–B). The diameter of pulmonary arteries and arterioles was measured and used to divide them into two size groups (0–50  $\mu\text{m}$  and  $\geq 50 \mu\text{m}$ ). Each vessel was visually scored as non-muscularised (those with a single elastic lamina) or muscularised (those with two or more distinct elastic laminae). There were significantly more muscularised small pulmonary arteries and arterioles in the bleomycin mice compared to saline control mice (Figure 3.9A) at day 21 (mean 53.4% vs. 39.4%;  $p = 0.0297$ ) and day 32 (mean 57.0% vs. 33.0%;  $p = 0.0006$ ). No differences between groups were observed in the larger vessels (Figure 3.9B). Pulmonary vascular remodelling was also assessed in micrographs lung sections immunostained for  $\alpha$ -SMA and VWF (Figure 3.9C). Representative micrographs highlight remodelling of small pulmonary arteries. Thickened media were observed by  $\alpha$ -SMA immunostaining in the 21-day and 32-day bleomycin mice, with two distinct elastic laminae visible on the ABEVG stain. Adventitial remodelling was also observed at the 21-day and 32-day timepoints.

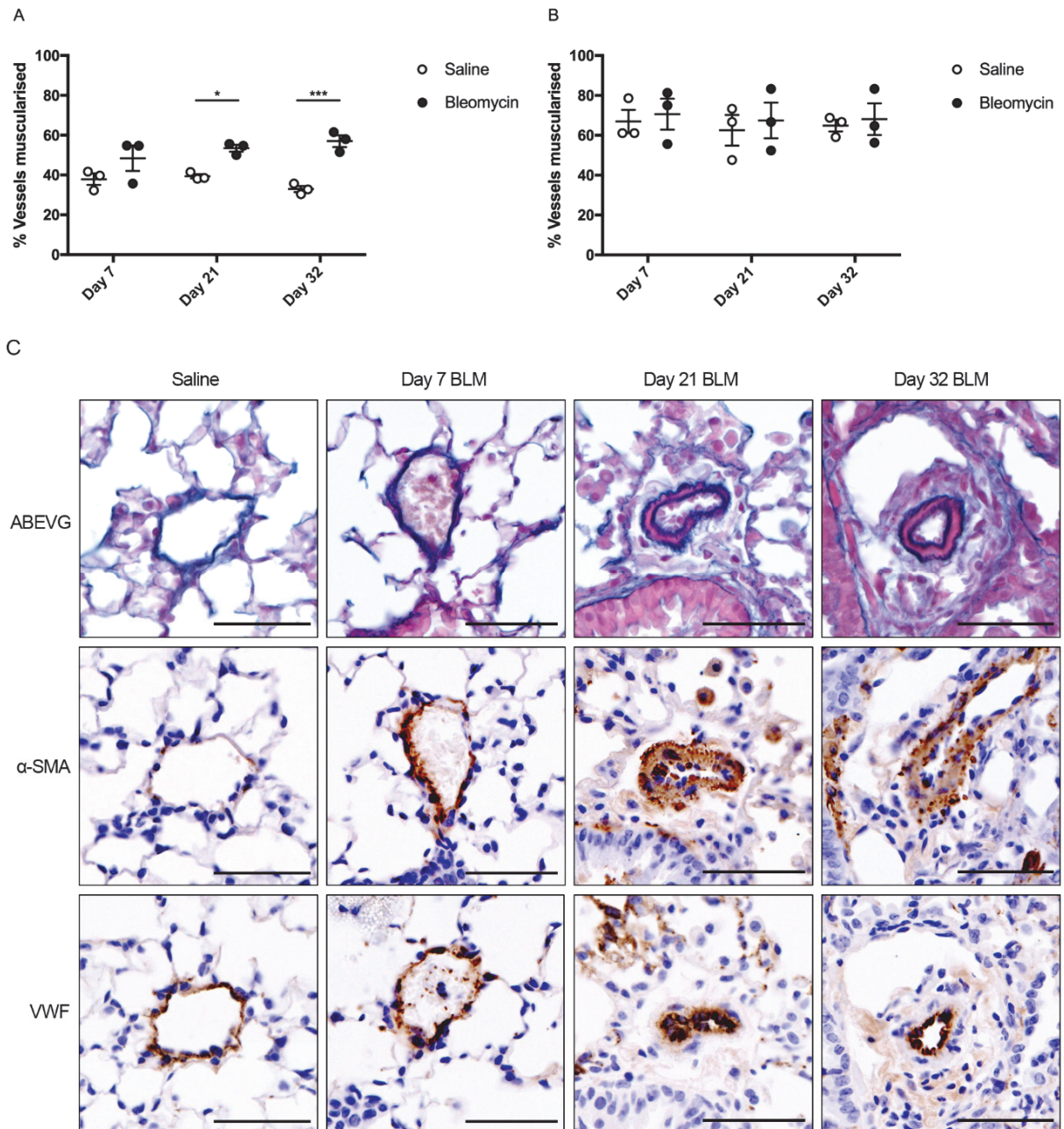


**Figure 3.9: Pulmonary vascular remodelling in bleomycin mice.** Mice were subjected to bleomycin (BLM) or saline IP injection twice weekly for 1, 3 or 4 weeks and culled at day 7, 21 or 32 respectively. **(A–B)** Pulmonary vascular remodelling determined by quantification of muscularised arteries and arterioles in lung sections stained with Miller’s elastin stain with alcian blue and van Gieson (ABEVG). Pulmonary arteries were divided into small (0–50 μm diameter; **A**) and large sizes (50–100 μm diameter; **B**). Points represent individual mice, n = 3 animals per group, bars show mean ± SD. \* p<0.05; \*\*\* p<0.001; one-way ANOVA with Sidak’s multiple comparisons test of bleomycin-treated groups compared to saline control groups. **(C)** Representative micrographs from 5 μm thick lung sections stained with ABEVG or immunostained with DAB for α-smooth muscle actin (α-SMA) or von Willebrand factor (VWF), with nuclei counterstained with Carazzi’s haematoxylin. Scale bars, 50 μm. Images were acquired at 200X total magnification then digitally cropped.

### 3.3.5 *TRAIL* mRNA expression in lungs

Real time qPCR was performed to quantify *TRAIL* mRNA expression in whole lung tissue from bleomycin mice. RNA was extracted from frozen whole lung tissue and a set quantity reverse transcribed to cDNA for qPCR analysis by TaqMan technology. *TRAIL* mRNA was detected in the lungs of mice at each bleomycin timepoint (Figure 3.10). However, due to lack of samples for 7-day saline group, this timepoint was excluded in order to have matched groups to perform the two-way ANOVA analysis. Based on this analysis, at the 32-day timepoint *TRAIL* mRNA was significantly lower in the lungs of bleomycin mice than saline controls (mean ddCt normalised to *GAPDH*  $-1.943$  vs.  $1.121$ ;  $p = 0.0468$ ). This was despite variability observed between individuals of each group, which was potentially caused by variable responses to bleomycin and thus differences in cellular phenotype (e.g. relative number of epithelial cells vs. leukocytes) of the lung tissue sampled from each animal.

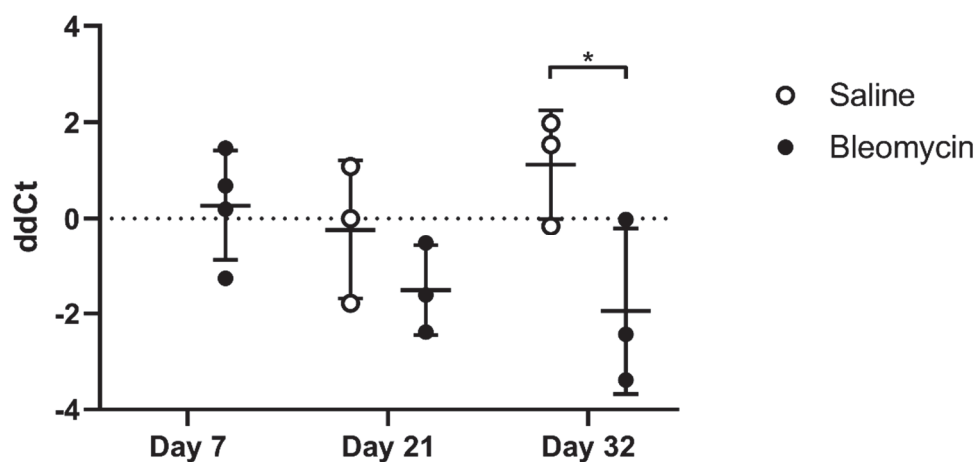


**Figure 3.10: *TRAIL* mRNA expression in lungs from bleomycin mice.** Mice were subjected to bleomycin (BLM) or saline IP injection twice weekly for 1, 3 or 4 weeks and culled at day 7, 21 or 32 respectively. *TRAIL* mRNA was measured in cDNA from whole mouse lungs by TaqMan RT-qPCR. Data shown are threshold cycle values normalised to a reference gene (*GAPDH*) then to a reference sample (delta-delta Ct; ddCt). Bars show mean  $\pm$  SD,  $n = 3-4$ , two-way ANOVA with Sidak's multiple comparisons test, bleomycin-treated groups compared to saline control groups.

### 3.4 Fibroblast-specific *TRAIL* deleted mice have worsened PF

Based on the preliminary bleomycin time-course experiment, the 5-week timepoint was found to give a robust fibrotic phenotype in the lungs, in addition to indications of PAH including haemodynamic alterations, RVH and pulmonary vascular remodelling. Therefore, this protocol was selected as suitable for subsequent experiments, in which mice with global or fibroblast-specific, tamoxifen-inducible deletion of *TRAIL* were subjected to the IP bleomycin model to determine the effect of this global or cell type-specific deletion of *TRAIL*. The experimental protocol is detailed in Figure 3.11. The strains used were  $TRAIL^{tm1c/tm1c}$  (*TRAIL* normal),  $TRAIL^{tm1c/wt}$  (*TRAIL* normal),  $TRAIL^{tm1c/tm1c}$ -COL1A2-Cre-ERT (tamoxifen-inducible fibroblast-specific *TRAIL* deletion) and  $TRAIL^{tm1d/tm1d}$ -PGK-Cre (constitutive global *TRAIL* deletion). For  $TRAIL^{tm1c/tm1c}$ -COL1A2-Cre-ERT mice and the wildtype tamoxifen control mice ( $TRAIL^{tm1c/tm1c}$ ), 5x daily 2 mg tamoxifen IP injections were given at 5–8 weeks old. At minimum 12-weeks old (median 13.6 weeks, range 11.9–14.9 weeks) and a median weight of 26.4 g (range 21.0–31.3 g), mice then underwent intraperitoneal injection with 35 mg/kg bleomycin or saline twice weekly for 4 weeks then were sacrificed at day 35. Endpoint echocardiography and cardiac catheterisation were performed to assess PAH phenotype. Animals were then sacrificed and lungs were perfusion fixed for histological staining and immunohistochemical assessment. It was originally intended for 10 mice from each group to be utilised in the experiment, however due to low numbers of  $TRAIL^{tm1d/tm1d}$ -PGK-Cre and time constraints, only 5 mice were available for this experimental group. Additionally, the choice of control groups was restricted by the number of animals available – for example, a group with  $TRAIL^{tm1c/tm1c}$ -COL1A2-Cre-ERT mice given no tamoxifen then subjected to bleomycin was not included. The choice of groups was considered to maximise the usefulness of data obtained from the experiment.

Male mice used; all strains based on C57BL/6 background.	Daily IP injections 2 mg TMX or corn oil at 5–8 weeks old (5x days).	Twice weekly IP injections 35 mg/kg BLM or saline (4x weeks), cull at day 35. Perform terminal procedures.
--	--	--

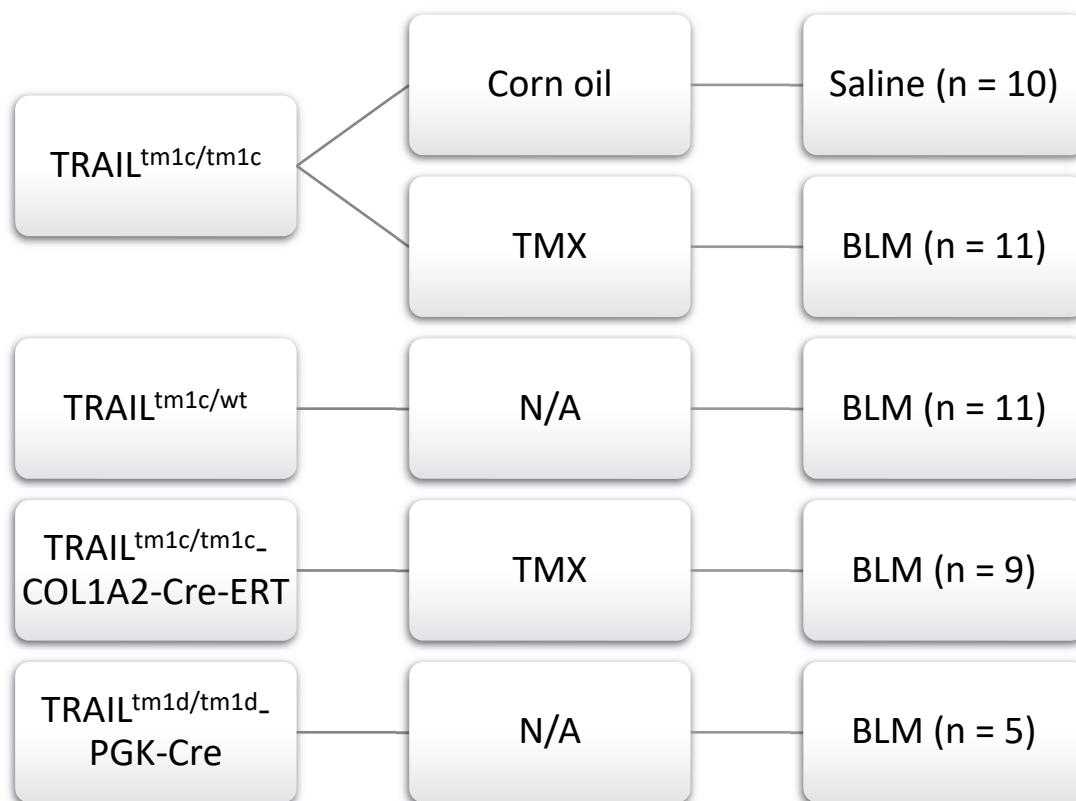


**Figure 3.11: Experimental schematic for *TRAIL* genetic deletion in bleomycin mice.** Strains utilised in the experiment either had functional TRAIL expression (TRAIL<sup>tm1c/tm1c</sup>, TRAIL<sup>tm1c/wt</sup>), tamoxifen (TMX)-inducible fibroblast-specific TRAIL deletion (TRAIL<sup>tm1c/tm1c-COL1A2-Cre-ERT</sup>) or constitutive global Cre-driven TRAIL deletion (TRAIL<sup>tm1d/tm1d-PGK-Cre</sup>). Mice were weaned, ear clipped and genotype confirmed by PCR. Two groups underwent tamoxifen (TMX) 5x daily IP injections at 5–8 weeks old. Mice were subjected to bleomycin (BLM) or saline IP injections twice weekly for 4 weeks and culled at day 35. Terminal procedures were performed including echocardiography, cardiac catheterisation and tissue harvest.

### 3.4.1 *TRAIL* expression in lungs

To confirm *TRAIL* deletion, real time qPCR and immunohistochemistry were used to determine the expression of *TRAIL* in lungs from bleomycin mice with *TRAIL* deletion, at the mRNA and protein level respectively. RNA was extracted from frozen whole lung tissue and a set quantity reverse transcribed to cDNA for qPCR analysis by TaqMan technology. At the mRNA level (Figure 3.12A), *TRAIL* was found at a significantly lower level in the lungs of *TRAIL*<sup>tm1d/tm1d</sup>-PGK-Cre mice compared to all other groups (e.g. vs. saline control group, mean ddCt normalised to *GAPDH* -12.01 vs. -0.8882;  $p < 0.0001$ ). Furthermore, in 2/5 *TRAIL*<sup>tm1d/tm1d</sup>-PGK-Cre replicates *TRAIL* mRNA was not detected at all, and these were assigned the maximum Ct value of 40 to facilitate statistical analysis (data not shown). In the other 3/5 replicates, the extremely low level of amplification may have been due to genomic DNA contamination or non-specific amplification. Nevertheless, the difference in ddCt values correspond to a theoretical 2,288-fold reduction of *TRAIL* mRNA in the *TRAIL*<sup>tm1d/tm1d</sup>-PGK-Cre. Compared to saline control mice, *TRAIL* mRNA was also significantly reduced in the lungs of *TRAIL*<sup>tm1c/tm1c</sup>-COL1A2-Cre-ERT<sup>tg/wt</sup> mice treated with tamoxifen to induce *TRAIL* deletion in fibroblasts (mean ddCt normalised to *GAPDH* -2.926 vs. -0.8882;  $p = 0.0030$ ).

Immunohistochemistry was also performed to visualise *TRAIL* protein expression in the lungs of bleomycin mice (Figure 3.12B–C). In mice without *TRAIL* deletion (*TRAIL*<sup>tm1c/wt</sup>), *TRAIL* protein was found throughout the lung, in particular concentrated within the airway epithelia, pulmonary artery media and cellular infiltrate (possibly leukocytes) within the alveoli and interstitium. In contrast, the lungs of *TRAIL*<sup>tm1d/tm1d</sup>-PGK-Cre mice showed almost no immunostaining, with no obvious concentrated areas – likely attributable to background or non-specific binding, based on the no primary antibody control staining (Figure 3.12D). No differences in *TRAIL* immunostaining could be visually detected in the lungs of *TRAIL*<sup>tm1c/tm1c</sup>-COL1A2-Cre-ERT<sup>tg/wt</sup> mice (data not shown), which may have been due to the pervasiveness of non-specific background staining.

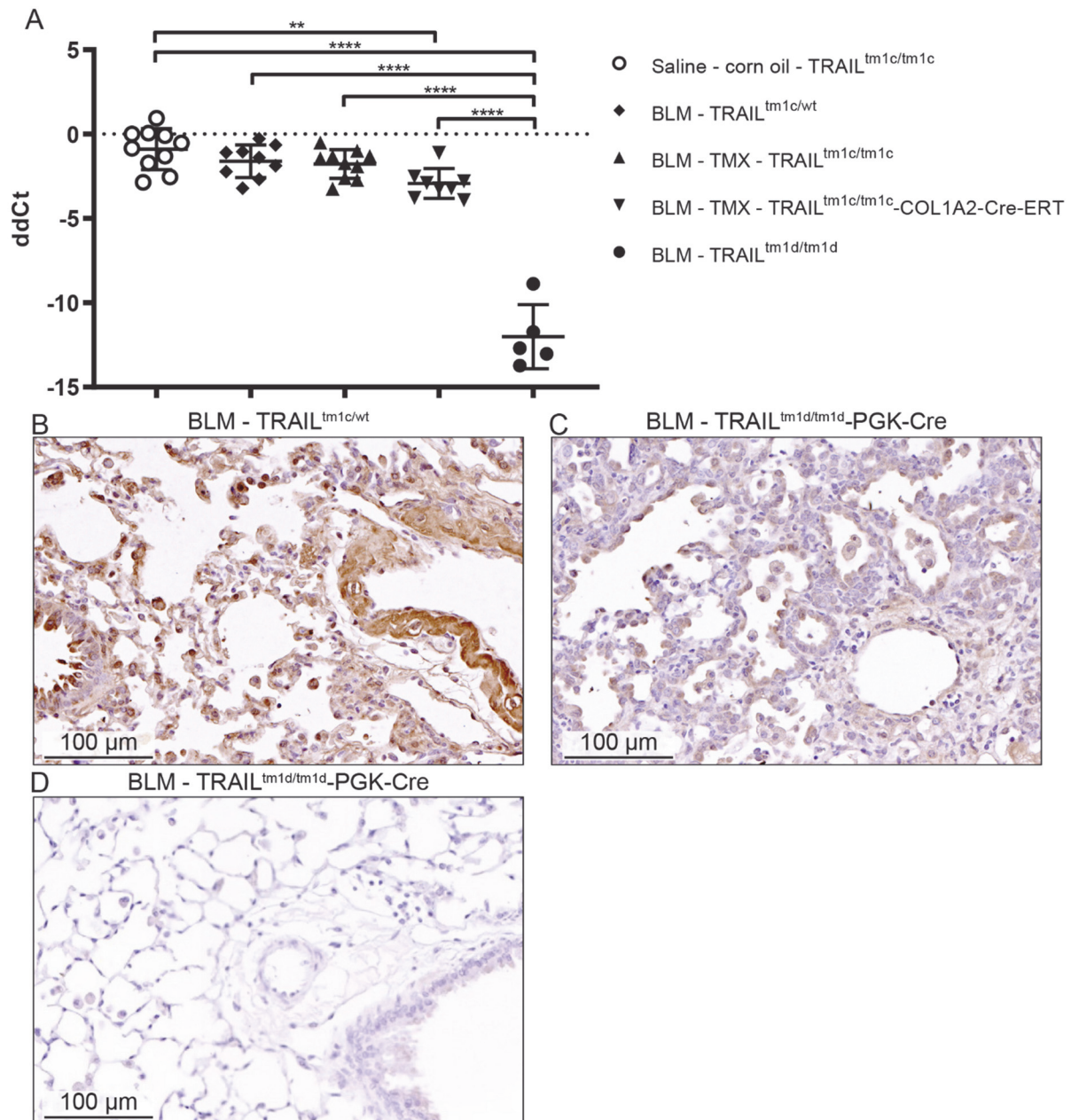


**Figure 3.12: TRAIL expression in lungs of *TRAIL*-deleted bleomycin mice.** Mice were subjected to bleomycin (BLM) or saline IP injection twice weekly for 4 weeks and culled at day 35. Two groups had previously undergone tamoxifen (TMX) 5x daily IP injections at 5–8 weeks old. **(A)** TRAIL mRNA was measured in cDNA from whole mouse lungs by TaqMan RT-qPCR. Data shown are threshold cycle values normalised to a reference gene (*GAPDH*) then to a reference sample (delta-delta Ct; ddCt). Bars show mean  $\pm$  SD, n = 3–6. \*\* p<0.01; \*\*\*\* p<0.0001, one-way ANOVA with Sidak's multiple comparisons test. Representative micrographs are shown from 5  $\mu$ m thick lung sections immunostained for TRAIL **(B–C)** or using no primary antibody **(D)** using a DAB substrate. Positive staining for TRAIL is seen as a brown stain with nuclei counterstained blue with Carazzi's haematoxylin. Images were acquired at 200X total magnification then digitally cropped.

### 3.4.2 Quantification of PF

To visually examine the severity of IP bleomycin-induced PF in the context of *TRAIL* deletion, formalin-fixed, paraffin sections of lung were stained with Masson's Trichrome. Representative micrographs of whole lung sections are shown in Figure 3.13A, with higher magnification of the same lung sections highlighted in Figure 3.13C. Small areas of collagen were observed in proximity to pulmonary arteries in the saline control group. This was in contrast with the denser and more widespread adventitial collagen, in addition to some patches of dense fibrosis, found in lungs from groups treated with IP bleomycin, but retaining *TRAIL* expression (*TRAIL*<sup>tm1c/wt</sup> and *TRAIL*<sup>tm1c/tm1c</sup> + TMX groups). Lungs from bleomycin mice with *TRAIL* deleted globally (*TRAIL*<sup>tm1d/tm1d</sup>-PGK-Cre) or specifically in fibroblasts (*TRAIL*<sup>tm1c/tm1c</sup>-COL1A2-Cre-ERT + TMX) had markedly larger areas of extensive, contiguous fibrotic masses, with obliteration of alveoli and extensive cellular infiltrate. Thickened alveolar walls were also observed throughout the lungs of these animals. Blue area representing collagen staining was also quantified (Figure 3.13B, D) and normalised to total lung tissue area in FIJI software (Figure 3.13E). All bleomycin-treated groups had significantly increased lung collagen compared to the saline control group, indicating a robust induction of PF with this model. The group with fibroblast-specific deletion of *TRAIL* (*TRAIL*<sup>tm1c/tm1c</sup>-COL1A2-Cre-ERT treated with TMX) had significantly increased lung collagen compared to the TMX-treated Cre-negative disease control group (*TRAIL*<sup>tm1c/tm1c</sup> + TMX; mean 0.0733 vs. 0.0459;  $p = 0.0477$ ). However, no significant differences in lung collagen were found between the global *TRAIL* deleted mice (*TRAIL*<sup>tm1d/tm1d</sup>-PGK-Cre) and any other bleomycin groups.

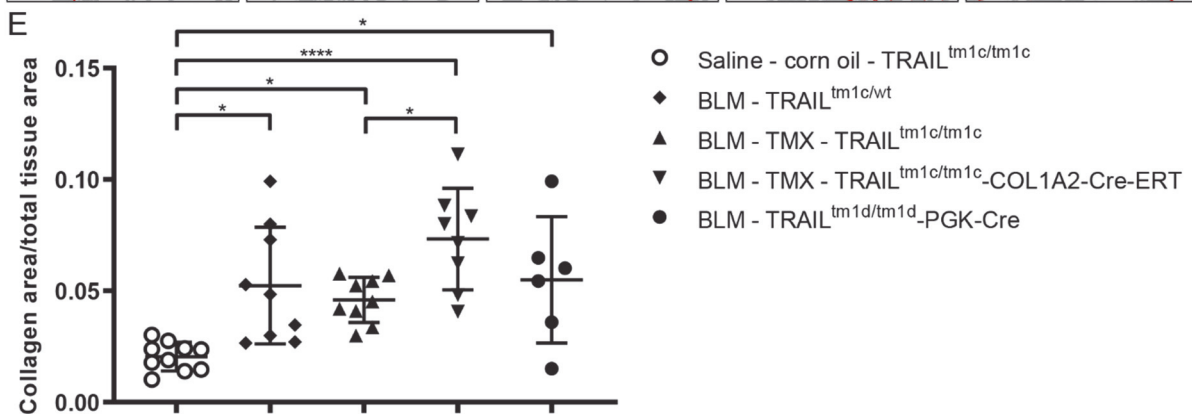
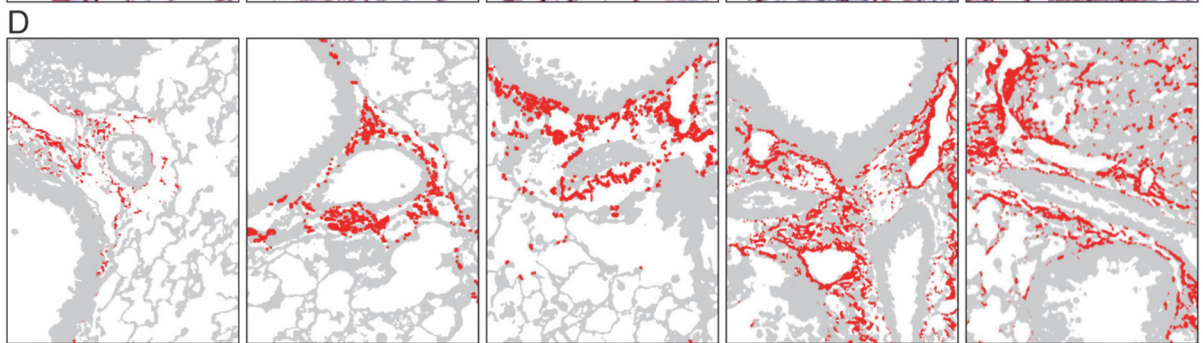
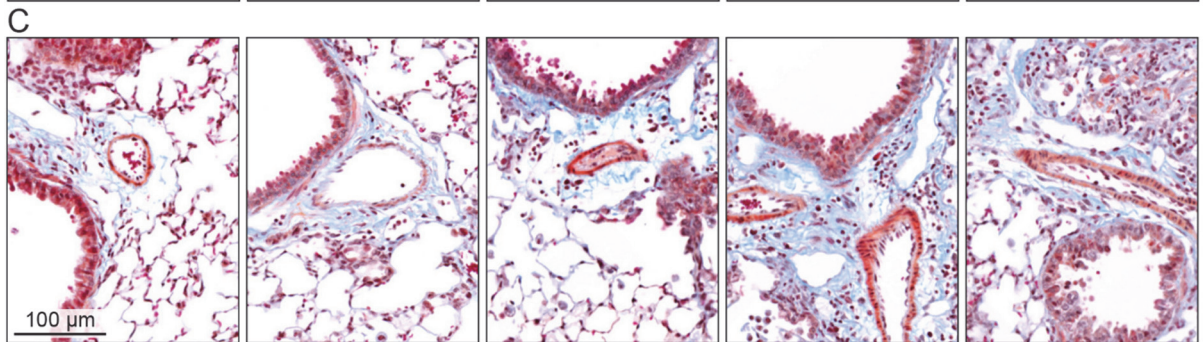
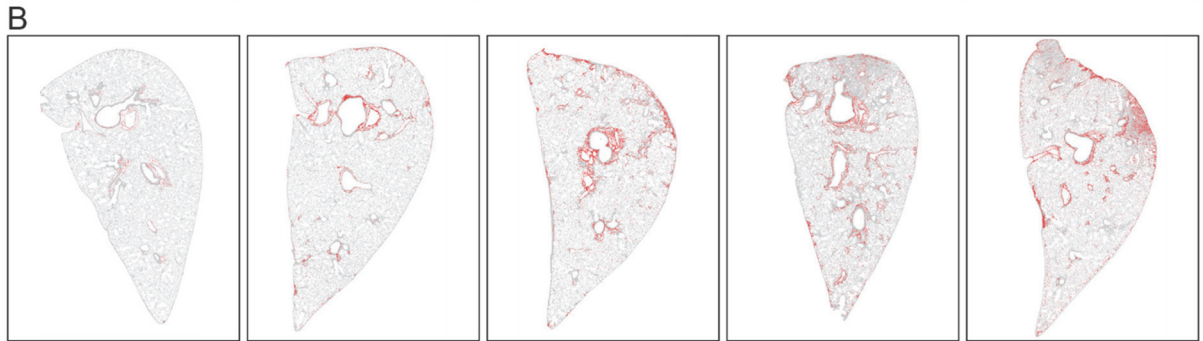
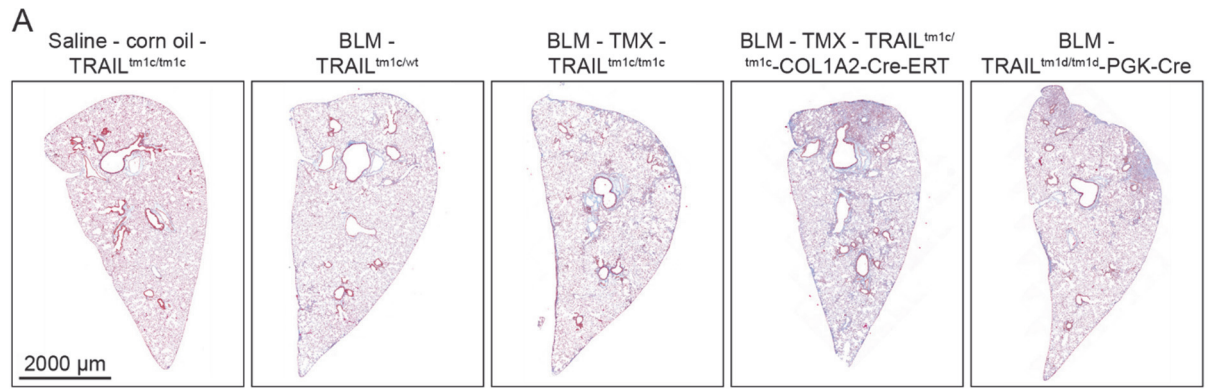


**Figure 3.13: PF in *TRAIL*-deleted bleomycin lungs.** Mice were subjected to bleomycin (BLM) or saline IP injection twice weekly for 4 weeks and culled at day 35. Two groups had previously undergone tamoxifen (TMX) 5x daily IP injections at 5–8 weeks old. **(A, C)** Representative micrographs are shown from 5  $\mu$ m thick lung sections histologically stained with Masson's Trichrome. Collagen is stained blue, nuclei pink, cytoplasm red and muscle orange. Images were acquired at 200X total magnification then digitally cropped. **(B, D)** Blue area representing collagen staining and total tissue area were quantified in FIJI software. In these example images, areas defined as collagen and non-collagen tissue and represented in red and grey, respectively. **(E)** Collagen area was normalised to total tissue area for four lung sections from each mouse, with average values plotted for each mouse. Bars show mean  $\pm$  SD, n = 6–10. \*  $p < 0.05$ ; \*\*\*\*  $p < 0.0001$ , one-way ANOVA with Sidak's multiple comparisons test comparing each group.

### 3.4.3 Haemodynamics

Earlier work in this study demonstrated the development of PAH – by haemodynamic measures and pulmonary vascular remodelling – in this particular repeated IP dose bleomycin model. Therefore, these investigations were repeated in the context of fibroblast-specific and global Cre-driven genetic deletions of *TRAIL* subjected to the same model to determine any effect on haemodynamic changes associated with PAH. Haemodynamic measurements were taken from right (Figure 3.14A–E) and left (Figure 3.14F–G) heart catheterisation in addition to echocardiography (Figure 3.14H–I) under anaesthesia at the time of terminal procedures. Pressure-volume loop analysis was performed to extract key metrics from cardiac catheterisation haemodynamic measurements. In the preliminary bleomycin time-course experiments, there was an increase in RVESP at the 32-day timepoint compared to the saline control mice. However, in this experiment no significant differences in RVESP were found in any bleomycin group compared to saline control mice (Figure 3.14A). There was however an increase in RV arterial elastance in mice without *TRAIL* deletion given tamoxifen (Figure 3.14E; mean 10.24 mmHg/RVU vs. 1.046 mmHg/RVU,  $p = 0.0074$ ). Additionally, there was a corresponding decrease in PAAT – measured by echocardiography – in all bleomycin groups apart from those with fibroblast-specific *TRAIL* deletion (Figure 3.14I). No differences due to bleomycin were detected in left heart function metrics including LVESP and mean aortic pressure (Figure 3.14F–G) by catheterisation or cardiac index measured by echocardiography (cardiac output at the aortic valve normalised to body weight), suggesting that the left heart was unaffected by bleomycin insult (Figure 3.14H).

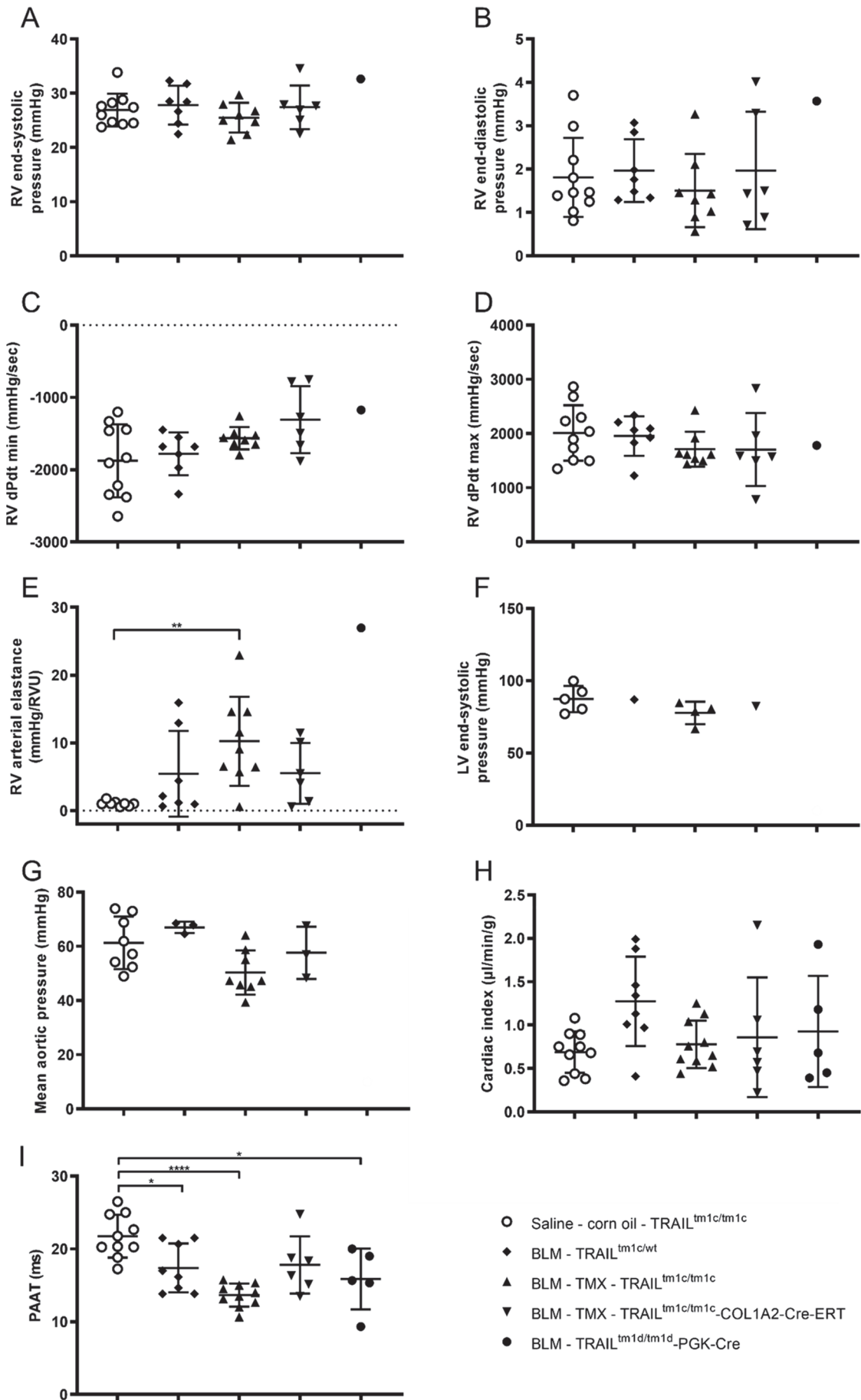


**Figure 3.14: Haemodynamic measures in *TRAIL*-deleted bleomycin mice.** Mice were subjected to bleomycin (BLM) or saline IP injection twice weekly for 4 weeks and culled at day 35. Two groups had previously undergone tamoxifen (TMX) 5x daily IP injections at 5–8 weeks old. Haemodynamic measurements were taken by cardiac catheterisation (**A–G**) and echocardiography (**H–I**). Plots show (**A**) right ventricular (RV) end systolic pressure, (**B**) RV end-diastolic pressure, (**C**) RV dP/dt minimum, (**D**) RV dP/dt maximum, (**E**) RV arterial elastance, (**F**) left ventricular (LV) end-systolic pressure, (**G**) mean aortic pressure, (**H**) cardiac index (cardiac output measure at the aortic valve and normalised to body weight) and (**I**) pulmonary artery acceleration time (PAAT). Points represent individual mice, n = 0–6 animals per group, bars show mean  $\pm$  SD. \*  $p < 0.05$ ; \*\*  $p < 0.01$ ; one-way ANOVA with Sidak's multiple comparisons test comparing each group.

### 3.4.4 Right ventricular hypertrophy

After sacrifice of animals, hearts were dissected and RVH was calculated as the ratio of RV free wall weight to LV plus septum weight (Figure 3.15). There was significant RVH compared to saline controls both in mice with *TRAIL* expression subjected to bleomycin and given tamoxifen (BLM - TMX - *TRAIL*<sup>tm1c/tm1c</sup>;  $p = 0.0250$ , mean 0.2617 vs. 0.2228) and in mice with fibroblast-specific *TRAIL* deletion subjected to bleomycin (BLM - TMX - *TRAIL*<sup>tm1c/tm1c</sup>-COL1A2-Cre-ERT;  $p = 0.0259$ , mean 0.2658 vs. 0.2228). Mice with global *TRAIL* deletion subjected to bleomycin (BLM - *TRAIL*<sup>tm1d/tm1d</sup>-PGK-Cre) and wildtype mice not given tamoxifen and subjected to bleomycin (BLM - *TRAIL*<sup>tm1c/wt</sup>) had no significant difference in RVH compared to saline control mice. A reduction in RVH in globally *TRAIL* deleted mice compared to the disease control groups without *TRAIL* deletion was not observed.

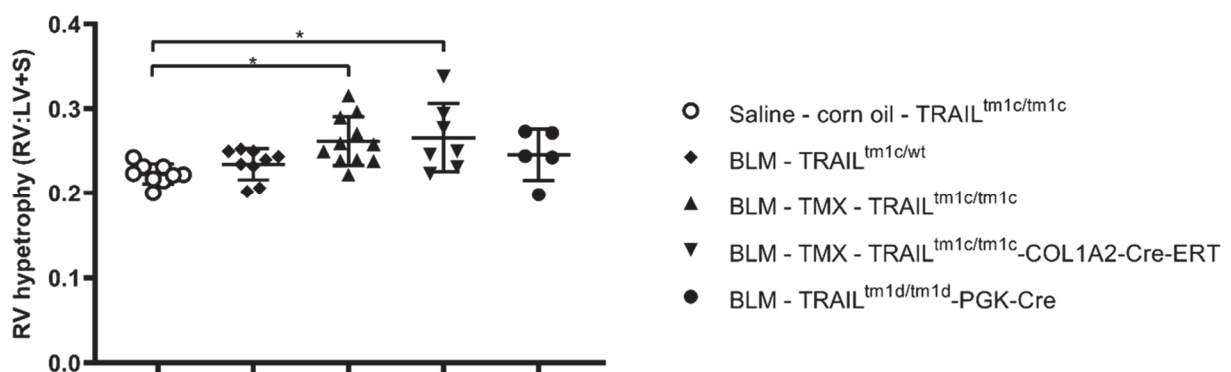
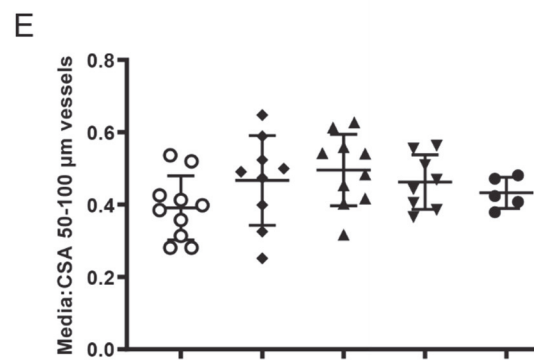
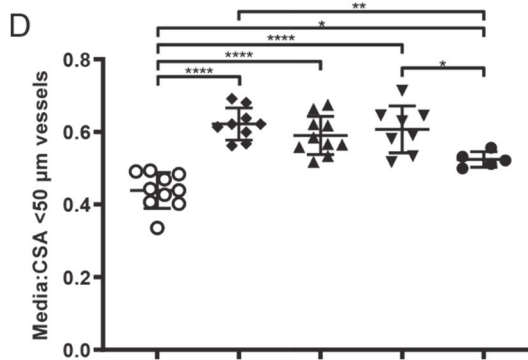
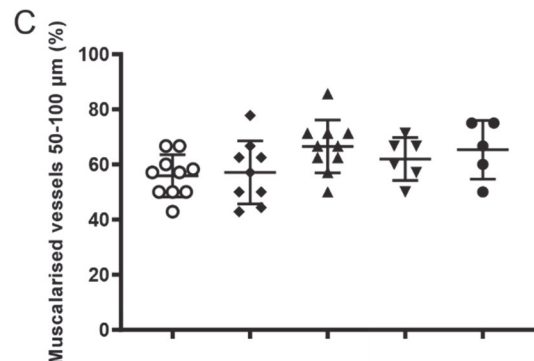
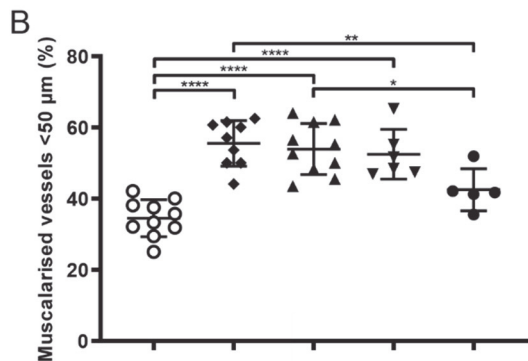
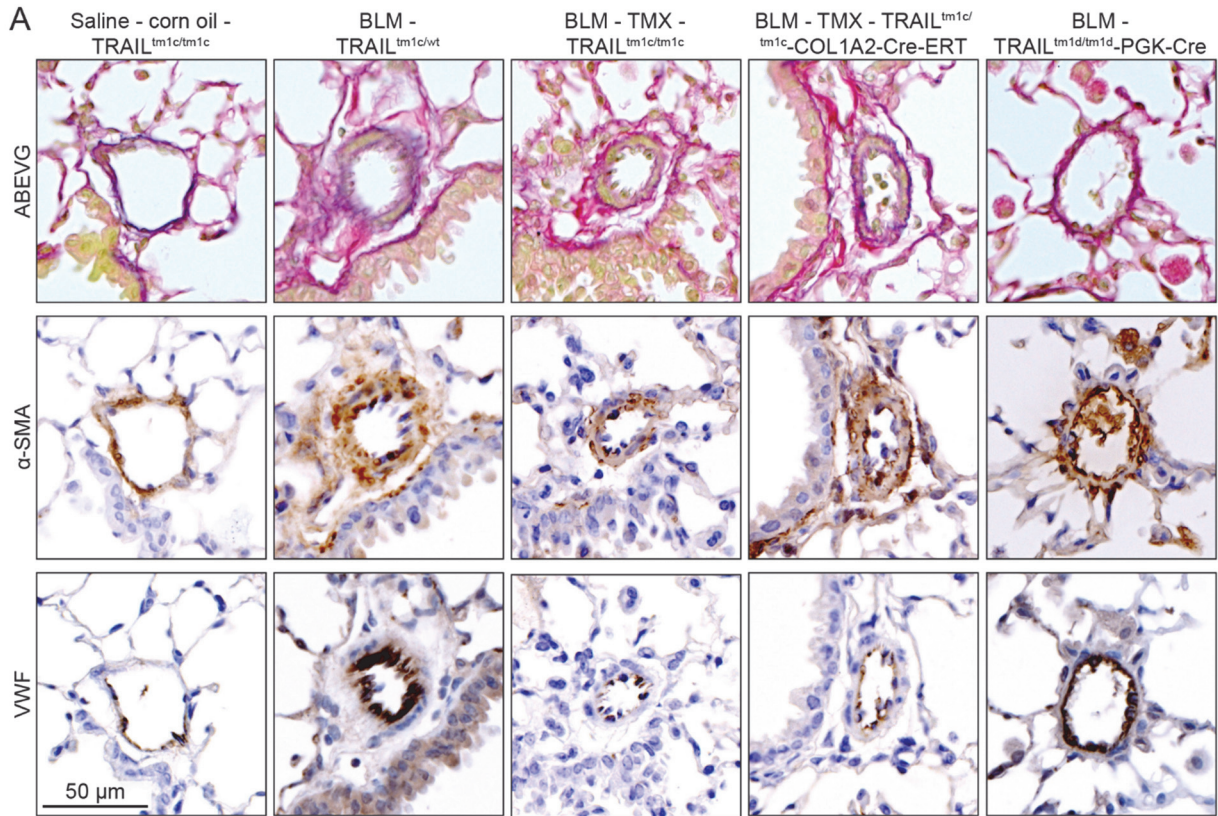


**Figure 3.15: Right ventricular hypertrophy in *TRAIL*-deleted bleomycin mice.** Mice were subjected to bleomycin (BLM) or saline IP injection twice weekly for 4 weeks and culled at day 35. Two groups had previously undergone tamoxifen (TMX) 5x daily IP injections at 5–8 weeks old. Hearts were dissected and right ventricular (RV) hypertrophy was calculated by right ventricular free wall weight normalised to left ventricle plus septum weight (RV:LV+S). Points represent individual mice,  $n = 5–11$  animals per group, bars show mean  $\pm$  SD, one-way ANOVA with Sidak's multiple comparisons test of each pairwise group combination.

### 3.4.5 Pulmonary vascular remodelling

Analysis of pulmonary vascular remodelling was carried out to determine whether genetic deletion of *TRAIL* had any effect on the vascular changes associated with PAH in the context of the IP bleomycin model. Pulmonary vascular remodelling was assessed in micrographs of formalin-fixed, paraffin-embedded lung sections histologically stained with ABEVG or immunostained for  $\alpha$ -SMA or VWF (Figure 3.16A). As shown in the example micrographs, in addition to previously illustrated PF present in this bleomycin model there was also extensive pulmonary vascular remodelling including increased muscularisation and medial thickening of small pulmonary arteries. This remodelling was also quantified by counting the proportion of muscularised vessels in ABEVG-stained sections (Figure 3.16B–C) and by measuring the medial thickness of muscularised vessels in sections immunostained for  $\alpha$ -SMA (Figure 3.16D–E). The diameter of pulmonary arteries and arterioles was measured and used to divide them into two size groups (0–50  $\mu$ m and 50–100  $\mu$ m). For ABEVG lung sections, each vessel was scored as non-muscularised (those with a single elastic lamina) or muscularised (those with two or more distinct elastic laminae). Vessels from areas with large fibrotic masses were not counted, as the large amount of adventitial and interstitial collagen and other cellular matter obscured histological details in these areas and hindered classification. There were significantly more muscularised 0–50  $\mu$ m diameter pulmonary arteries in all bleomycin groups compared to saline control mice, apart from in mice with global *TRAIL* deletion (BLM - *TRAIL*<sup>tm1d/tm1d</sup>-PGK-Cre; Figure 3.16B). Mice with global *TRAIL* deletion also had significantly fewer muscularised vessels than either the wildtype control bleomycin mice (BLM - *TRAIL*<sup>tm1c/wt</sup>; mean 42.48% vs. 55.50%,  $p = 0.0056$ ) or bleomycin mice with *TRAIL* expression given tamoxifen (BLM - TMX - *TRAIL*<sup>tm1c/tm1c</sup>; mean 42.48% vs. 53.92%,  $p = 0.0139$ ). No differences were observed between groups in the number of larger (50–100  $\mu$ m) muscularised vessels (Figure 3.16C). A similar pattern to the proportion of muscularised small vessels was also found in the measurement of medial thickening of small vessels from sections immunostained for  $\alpha$ -SMA (Figure 3.16D). In this analysis, all groups subjected to bleomycin had significantly increased medial thickening calculated as medial area normalised to CSA.

Of these groups, mice with global *TRAIL* knockout had the smallest increase in medial thickening, and this group also had significantly reduced medial thickening compared to the wildtype control bleomycin mice (BLM -  $TRAIL^{tm1c/wt}$ ; mean 0.5244 vs. 0.6221,  $p = 0.0090$ ) or the fibroblast-specific *TRAIL* deleted bleomycin group wildtype control bleomycin mice (BLM - TMX -  $TRAIL^{tm1c/tm1c}$ -COL1A2-Cre-ERT; mean 0.5244 vs. 0.6073,  $p = 0.0318$ ). No differences between any groups were observed in the larger vessels for this analysis (Figure 3.16E).



- Saline - corn oil - TRAIL<sup>tm1c/tm1c</sup>
- ◆ BLM - TRAIL<sup>tm1c/wt</sup>
- ▲ BLM - TMX - TRAIL<sup>tm1c/tm1c</sup>
- ▼ BLM - TMX - TRAIL<sup>tm1c/tm1c</sup>-COL1A2-Cre-ERT
- BLM - TRAIL<sup>tm1d/tm1d</sup>-PGK-Cre

**Figure 3.16: Pulmonary vascular remodelling in *TRAIL*-deleted bleomycin mice.** Mice were subjected to bleomycin (BLM) or saline IP injection twice weekly for 4 weeks and culled at day 35. Two groups had previously undergone tamoxifen (TMX) 5x daily IP injections at 5–8 weeks old. **(A)** Representative micrographs from 5  $\mu$ m thick lung sections stained with Miller's elastin stain with alcian blue and van Gieson (ABEVG) or immunostained for  $\alpha$ -smooth muscle actin ( $\alpha$ -SMA) or von Willebrand factor (VWF), with nuclei counterstained with Carazzi's haematoxylin. Images were acquired at 200X total magnification then digitally cropped. Pulmonary vascular remodelling was quantified by the proportion of muscularised arteries and arterioles in lung sections stained with ABEVG (**B–C**) and by the medial area over cross-sectional area (CSA) for muscularised arteries in lung sections immunostained with DAB for  $\alpha$ -SMA (**D–E**). Pulmonary arteries were divided into small (0–50  $\mu$ m diameter; **B, D**) and large sizes (50–100  $\mu$ m diameter; **C, E**). Points represent individual mice, n = 5–10 animals per group, bars show mean  $\pm$  SD. \* p<0.05; \*\* p<0.01; \*\*\* p<0.001; \*\*\*\* p<0.0001, one-way ANOVA with Sidak's multiple comparisons test of each pairwise group combination.

### 3.5 Summary

The aim of this chapter was to examine the effect of Cre-driven genetic deletion of *TRAIL* – in fibroblasts and globally – in the context of bleomycin-induced PF. In summary:

- A time-course experiment demonstrated that four twice-weekly IP injections of bleomycin produced a robust PF phenotype with associated PAH at the five-week timepoint.
- Mice with floxed *TRAIL* allele were crossed with the COL1A2-Cre-ERT and PGK-Cre lines to produce strains with tamoxifen-inducible fibroblast-specific, or constitutive global deletion of *TRAIL*, respectively.
- PF was induced by bleomycin in the *TRAIL* deletion experiment, with fibroblast-specific deletion of *TRAIL* causing exaggerated fibrosis.
- Bleomycin-induced PAH haemodynamic phenotype in the *TRAIL* deletion experiment did not fully recapitulate that of the preliminary time-course experiment. There was no significant increase in RVESP, however there was evidence of pulmonary vascular remodelling and other indices suggestive of PAH, e.g. RV arterial elastance, PAAT.
- Global deletion of *TRAIL* led to a reduction in pulmonary vascular remodelling and right ventricular hypertrophy, replicating previously published data in other mouse models (Dawson et al. 2014, Hameed et al. 2012).
- Fibroblast-specific deletion of *TRAIL* had no effect on the PAH phenotype in response to bleomycin.

## 3.6 Discussion

### 3.6.1 *Fibroblasts are a protective source of TRAIL in PF*

In this chapter I further investigated the function of TRAIL in PF by deleting *TRAIL* in fibroblasts or globally in mice and subjecting them to the bleomycin model. Fibroblast-specific deletion of *TRAIL* caused exaggerated PF as measured by lung collagen staining, suggesting that TRAIL expressed by fibroblasts is protective in PF. This result expands upon previous studies – showing that depletion of TRAIL in mice exposed to bleomycin caused a worsened fibrotic phenotype in the lungs (Habel et al. 2018, McGrath et al. 2012) – to specifically connect TRAIL from fibroblasts with this protective process. It is plausible that TRAIL-mediated apoptosis confers negative regulation of PF, as fibroblasts and myofibroblasts are key effector cells in the pathogenic deposition of collagen. Furthermore, resistance to apoptosis (Moodley et al. 2004, Thannickal and Horowitz 2006) has been recognised as a crucial factor in the aberrant and potentially senescent fibroblast function (Faner et al. 2012) underlying PF. Indeed, pulmonary fibroblasts from IPF patients have been shown to be resistant to TRAIL-induced apoptosis, with decreased expression of TRAIL receptors (Hohmann et al. 2019). Further evidence highlights a protective function of TRAIL produced by myeloid cells that are recruited to the lungs in PF – by blocking the activation of pathogenic myofibroblasts – a process that appears to be lacking in IPF patients (Habel et al. 2018). The lack of these TRAIL-mediated protective effects in IPF patients is therefore a potential pathogenic mechanism that may be targeted in PF therapeutics.

Interestingly, global *TRAIL* deletion in bleomycin mice did not cause an increase in the fibrotic phenotype like that observed in fibroblast-specific deletion of *TRAIL*. This result is also distinct from previously published studies, which demonstrated that genetic deletion or neutralisation of TRAIL heightened fibrosis in bleomycin mice (Habel et al. 2018, McGrath et al. 2012). The reasons for this outcome are unclear, but it may be due to the differing variations of the bleomycin model utilised – IP injections in the present study vs. bleomycin administered to the

airways in other studies of TRAIL function in PF (Habel et al. 2018, McGrath et al. 2012). The present work and others have highlighted the primarily pulmonary vascular-associated fibrosis in the IP bleomycin model, which is in contrast to the largely airway-linked fibrosis when bleomycin was delivered via the trachea or oropharyngeal route. A protective mechanism proposed for TRAIL in previous work was the modulation of airway and alveolar pro-inflammatory leukocyte populations such as neutrophils, thereby dampening the inflammatory aspects driving PF (McGrath et al. 2012, McGrath et al. 2011). This airway inflammation may therefore have had reduced or no impact in the context of bleomycin administered by IP injection in the present study. The lack of protective effect from global *TRAIL* deletion in the present study may have been due to TRAIL exerting other detrimental effects on the cells of the pulmonary vasculature rather than the airway epithelial cells in the context of airway delivery of bleomycin. For example, TRAIL may promote angiogenic effects via non-canonical signalling pathways, including the stimulation of proliferation in pulmonary vascular ECs (Cantarella et al. 2014, Cartland et al. 2016, Secchiero et al. 2003). The global deletion of *TRAIL* in the present study may have ameliorated processes such as these within the pulmonary vasculature, thus masking the removal of protective effects observed by the fibroblast-specific *TRAIL* deletion.

### **3.6.2 The role of TRAIL in bleomycin-induced PAH**

In addition to the PF phenotype produced in the IP bleomycin model, many studies report indications of PAH including haemodynamic measures and pulmonary vascular remodelling (Bryant et al. 2016, Karmouty-Quintana et al. 2015, Karmouty-Quintana et al. 2012). In the present study there was evidence of an early/mid stage PAH phenotype demonstrated by pulmonary vascular remodelling and RVH. The development of both PAH and autoimmune-driven PF pathologies – both processes in which TRAIL has been implicated – in these mice presented an attractive opportunity to study the interface between these diverse yet intersecting diseases. This could be especially relevant to further understanding similar disease pathobiology in patients such as the 7–12% of SSc patients who develop PAH

(Hachulla et al. 2005, Mukerjee et al. 2003). In the present study bleomycin-induced remodelling of small pulmonary arteries – a key pathogenic process in PAH – was reduced by global deletion, but not fibroblast-specific deletion of *TRAIL*. A similar effect was found in RV size, whereby bleomycin induced RVH associated with PAH, but not in mice with global *TRAIL* deletion. A reduction in RVH in globally *TRAIL* deleted mice compared to the disease control groups without *TRAIL* deletion was not observed, however in this model the RVH produced was relatively mild and differences may have been detected in the presence of a stronger phenotype. The subtle RVH phenotype may also account for the absence of a significance increase in RVH in mice with *TRAIL* expression subjected to bleomycin without tamoxifen treatment. There is therefore a disparity between the effects of *TRAIL* determined in this IP bleomycin model. Fibroblast-derived *TRAIL* was protective in the context of fibrosis but not in the PAH pathology; whereas other sources of *TRAIL* – removed by global *TRAIL* deletion – had an overriding pathogenic involvement in development of PAH. These findings are in accordance with previously described pathogenic functions for *TRAIL* in development of PAH (Dawson et al. 2014, Hameed et al. 2012). The other cell types where *TRAIL* is known to be involved in PAH include the ECs and SMCs of pulmonary arteries. Evidence for this comes from the SuHx model of PAH, but the results in the present study suggest there is an overlap between disease progression in these distinct models. The role of SMC-derived *TRAIL* in SuHx-induced PAH in mice will be examined in Chapter 4.

### **3.6.3 The IP bleomycin mouse model of PF**

In the present study a preliminary time-course experiment was performed to characterise a mouse model of fibrotic lung disease with associated PAH, which would be suitable for disentangling the role of *TRAIL* – by tissue-specific deletions – in these diseases. Bleomycin administered by IP injection, by oropharyngeal aspiration or surgically by intratracheal instillation is well established as a model of PF in preclinical animal models (Adamson and Bowden 1974, Fleischman et al. 1971, Thrall et al. 1979). While the response after 21 days post- intratracheal bleomycin instillation has been shown to be variable and possibly even

reversible (Izbicki et al. 2002), the repeated IP bleomycin model has been described as producing more chronic vascular-associated inflammation and remodelling in the lungs, with associated PAH demonstrated by haemodynamic measures and pulmonary vascular remodelling (Bryant et al. 2016, Karmouty-Quintana et al. 2015, Karmouty-Quintana et al. 2012). For these reasons, the IP bleomycin model was selected rather than the intratracheal or oropharyngeal routes of administration. The dose of 35 mg/kg bleomycin was selected based on its success when used in the previously mentioned studies. The IP bleomycin model had not been used previously in the research group, so a time-course experiment was carried out to determine the onset and pathology of PF and PAH in mice IP injected with bleomycin twice weekly for up to four weeks and culled at 7, 21 or 32 days. Development of PF was visually observed in mice at the 21-day timepoint and was quantitatively increased at 32 days, which is in line with previous timecourse studies showing PF after 21 days (Karmouty-Quintana et al. 2015, Van Rheen et al. 2011). Indicators of PAH pathology including haemodynamics, RVH and pulmonary vascular remodelling were also observed in the 32-day bleomycin group, again replicating findings from the literature (Bryant et al. 2016, Bryant et al. 2015, Karmouty-Quintana et al. 2015, Karmouty-Quintana et al. 2012). There were no differences in fibrosis, haemodynamics, pulmonary vascular remodelling or RVH between the saline control groups at any timepoint, indicating no effect due to saline IP injection alone. The development of both PF and PAH in the bleomycin mice model highlighted its potential for subsequent experiments to disentangle the differing roles of TRAIL in fibrotic lung disease and PAH.

When the IP bleomycin model was used in the context of *TRAIL* deletion, there was clear visual and quantifiable evidence for development of PF. However, the extent of collagen deposition was not as severe as in the preliminary time-course experiment. Additionally, the bleomycin-induced PAH haemodynamic phenotype in the *TRAIL* deletion experiment was not identical to that of the preliminary time-course experiment, although there was evidence for development of PAH in both experiments. In the time-course experiment there was also a

reduction in *TRAIL* mRNA detected in the lungs of bleomycin mice at 32 days, which in the *TRAIL* deletion experiment was demonstrated in the fibroblast-specific and global *TRAIL*-deleted mice but not in the bleomycin disease control mice with *TRAIL* expression. The cause of the phenotypic variation between experiments is unclear, although a potentially important factor was the greater target initial weight of mice used in the *TRAIL* deletion study, which was selected for animal welfare purposes based on the severity in the preliminary study. Another possible factor is the alternate source of bleomycin used in the *TRAIL* deletion study: in the preliminary study bleomycin was purchased from Sigma-Aldrich (St. Louis, MO), whereas in the *TRAIL* deletion study human grade medical bleomycin was produced by Kyowo Kirin (Japan) and purchased from an NHS Trust pharmacy. Both sources are described as containing a mixture of glycopeptide antibiotics – known as Bleomycin A<sub>2</sub> and Bleomycin B<sub>2</sub> – from *Streptomyces verticillus*. For both drugs, activity in units was provided by the manufacturer and used for dosage calculations. However, while the Sigma preparation lists the constituents as 55–70% Bleomycin A<sub>2</sub> and 25–32% Bleomycin B<sub>2</sub>, information was not available for the exact formulation of the Kyowo Kirin drug.

## 4 The role of VSMC-derived TRAIL in SuHx-induced PAH

A key process underlying the development and progression of PAH is the characteristic pulmonary arterial remodelling (Pietra et al. 1989). As this vascular remodelling – rather than vasodilation – so far remains largely untreated by current pharmaceuticals, there is a need for better therapies. Several factors have been described as drivers of this vascular remodelling, including the cytokine TRAIL (Hameed et al. 2012, Lawrie et al. 2011, Lawrie et al. 2008, Liu et al. 2015). TRAIL has direct effects on pulmonary vascular cells *in vitro*; it induces proliferation and migration in PAECs (Cantarella et al. 2014, Cartland et al. 2016, Secchiero et al. 2003, Zauli et al. 2003) and PASMCs (Hameed et al. 2012, Kavurma et al. 2008, Secchiero et al. 2004). Additionally, elimination of TRAIL by genetic deletion or antibody blockade causes reduced pulmonary arterial remodelling and pulmonary artery pressures in rodent models (Dawson et al. 2014, Hameed et al. 2012). Although TRAIL is expressed in most cell types, including leukocytes, bone marrow transplants have demonstrated that tissue-derived, rather than circulating TRAIL is required for development of PAH in rodent models (Hameed et al. 2012).

I hypothesised that TRAIL produced by VSMCs is crucial to development of PAH. To determine whether VSMCs are a detrimental source of TRAIL in this context, a mouse strain was generated with VSMC-specific, tamoxifen-inducible deletion of *TRAIL*. These mice were subjected to the SuHx model of PAH. For PAH, many models are available, each with their own advantages (Lawrie 2014). The recently-developed murine SuHx model (Ciuculan et al. 2011) was selected as suitable in that it produces a PAH phenotype as well as presenting the opportunity for straightforward genetic manipulation. Additionally, *TRAIL*-deficient mice subjected to the SuHx model were previously demonstrated to be protected against PAH compared to wild-type mice (Dawson et al. 2014).

## 4.1 Generation of mice with VSMC-specific *TRAIL* deletion

Male mice with tamoxifen-inducible VSMC-specific *TRAIL* deletion ( $TRAIL^{tm1c/tm1c}$ -SMMHC-Cre-ERT2<sup>tg/0</sup>) from the F2 cross were used in experiments. The generation of these mice is described in Chapter 2.2.4.

### 4.1.1 Genotyping

Three separate multiplex PCR reactions were performed to detect  $TRAIL^{tm1c}$  and  $TRAIL^{wt}$  alleles,  $TRAIL^{tm1d}$  and  $TRAIL^{tm1c}$  distal LoxP alleles and SMMHC-Cre-ERT2<sup>tg</sup> and SMMHC-Cre-ERT2<sup>wt</sup> alleles respectively (Figure 4.1). The PCR reactions for *TRAIL* alleles (Figure 4.1A–B) were as described in Chapter 3.1.1. For SMMHC-Cre-ERT2 genotyping, three primers were used: two specific to genomic regions flanking the insert site, and one targeting the insert sequence (Figure 4.1C). The PCR created a 287 bp product for the SMMHC-Cre-ERT2<sup>tg</sup> allele or a 225 bp wildtype product. PCR conditions and primer sequences are listed in Appendix C: Genotyping PCR. Example gel images from PCR genotyping are shown in Figure 4.1.

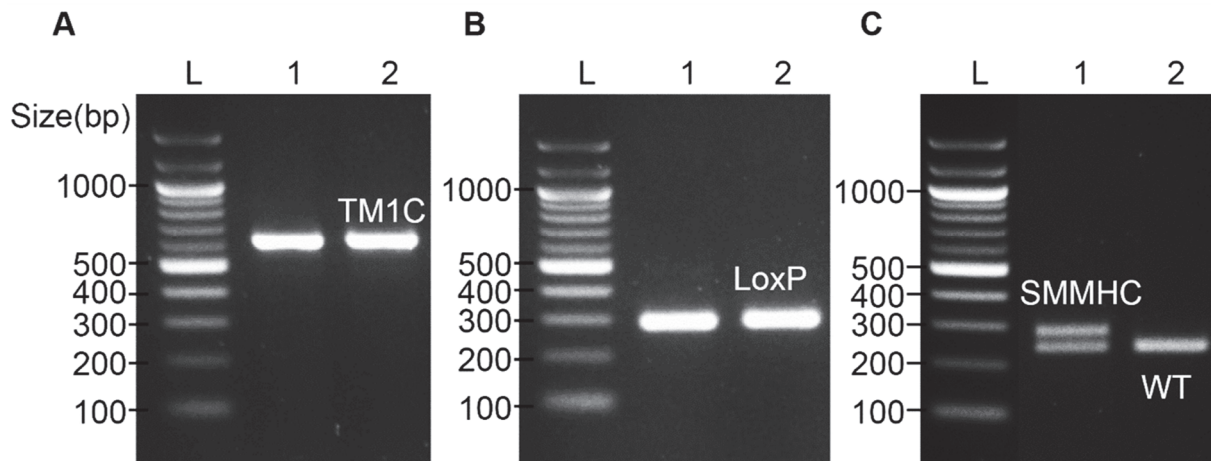


**Figure 4.1: PCR genotyping of TRAIL<sup>tm1c</sup> and SMMHC-Cre-ERT2 transgenic alleles.** Example images of agarose gels from PCR genotyping of two F2 offspring from TRAIL<sup>tm1c/tm1c</sup>-SMMHC-Cre-ERT2<sup>tg/0</sup> mice crossed with TRAIL<sup>tm1c/tm1c</sup> mice. Three separate PCR reactions were performed to detect the (A) TRAIL<sup>tm1c</sup> allele (band labelled 'TM1C' at 604 bp), (B) TRAIL<sup>tm1c</sup> distal LoxP allele (band labelled 'LoxP', at 282 bp) and (C) SMMHC-Cre-ERT2<sup>tg</sup> and SMMHC-Cre-ERT2<sup>wt</sup> alleles (bands labelled 'SMMHC' and 'WT', 287 bp and 225 bp respectively). The lane labelled 'L' contains 100 bp ladder and lanes '1' and '2' contain PCR products from two separate mice, for which each PCR reaction was carried out.

#### **4.1.2 Cre reporter demonstration of Cre recombination**

To confirm the localisation of Cre expression and Cre-driven recombination, R26R-Brainbow2.1 mice were crossed with SMMHC-Cre-ERT2 mice. Cre expression was induced by giving 5 daily intraperitoneal injections of 2 mg tamoxifen at 5–8 weeks. Lung sections from double transgenic adult offspring were examined by fluorescence microscopy. As shown in Figure 4.2, green and red fluorescence indicating Cre recombination was found in the pulmonary arterial medial layer containing SMCs. Nuclei were fluorescently stained blue by DAPI in the mountant.

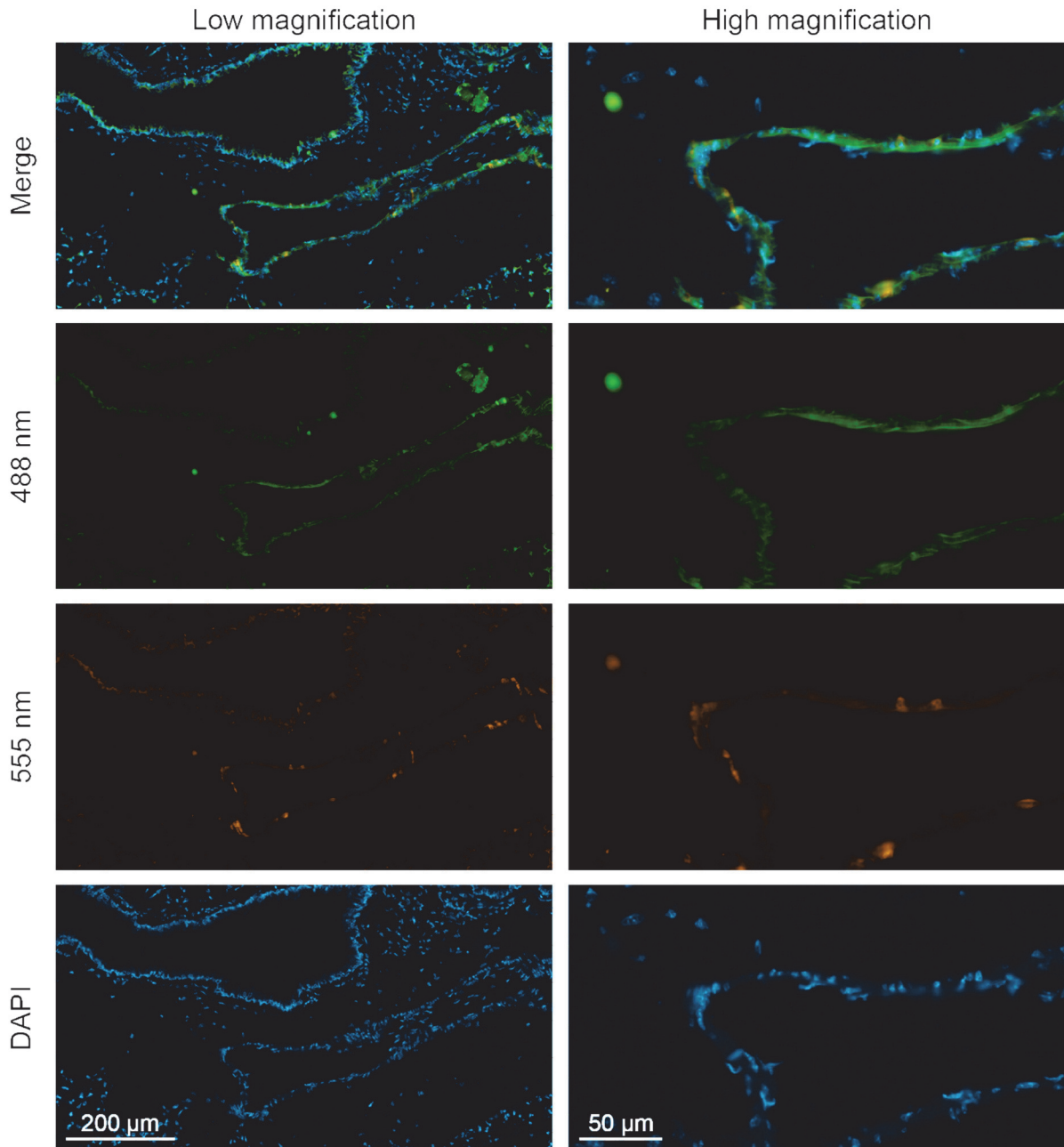


**Figure 4.2: Cre reporter demonstrates VSMC-specific Cre recombination.** Fluorescence micrographs of 5  $\mu\text{m}$  lung sections from R26R-Brainbow2.1<sup>tg/wt</sup>-SMMHC-Cre-ERT2<sup>tg/0</sup> mice. Images were acquired at 488 nm and 555 nm (Cre recombinase-driven fluorescence) and 461 nm (DAPI nuclear stain). Images were acquired at 200X total magnification then digitally cropped.

## 4.2 VSMC-specific *TRAIL* deleted mice are protected from PAH

Mice with VSMC-specific, tamoxifen-inducible deletion of *TRAIL* were subjected to the SuHx model to determine the effect of this cell type-specific deletion of *TRAIL* on the PAH phenotype. Details of the experimental protocol are summarised in Figure 4.3. The strains used were *TRAIL*<sup>tm1c/tm1c</sup> (*TRAIL* normal) and *TRAIL*<sup>tm1c/tm1c</sup>-SMMHC-Cre-ERT2 (tamoxifen-inducible VSMC-specific *TRAIL* deletion). For *TRAIL*<sup>tm1c/tm1c</sup>-SMMHC-Cre-ERT2 mice and the wildtype tamoxifen control mice (*TRAIL*<sup>tm1c/tm1c</sup>), 5x daily 2 mg tamoxifen IP injections were given at 5–8 weeks old. The other groups received 5x daily corn oil IP injections. The two *TRAIL* normal disease control groups were *TRAIL*<sup>tm1c/tm1c</sup>-SMMHC-Cre-ERT2 given corn oil and *TRAIL*<sup>tm1c/tm1c</sup> given tamoxifen. At minimum 12 weeks age (median 12.9 weeks, range 12.0–15.3 weeks) and weighing approximately 25 g (median 25.9 g, range 22.6–29.1 g) mice underwent subcutaneous injection with 20 mg/kg Sugen 5416 or saline once weekly for 3 weeks then were sacrificed at day 21. Disease groups were kept in hypoxia (10% oxygen) throughout the experiment, and normoxia control mice were kept in normal room air. Endpoint echocardiography and cardiac catheterisation were performed to assess PAH phenotype. Animals were then sacrificed and lungs were perfusion fixed for histological staining and immunohistochemical assessment.

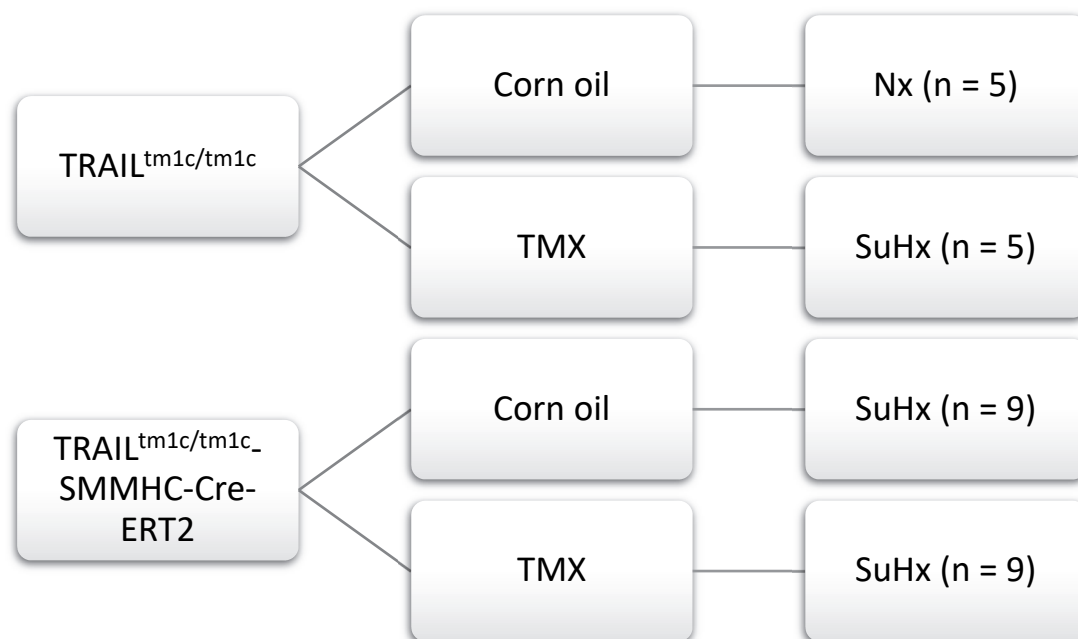
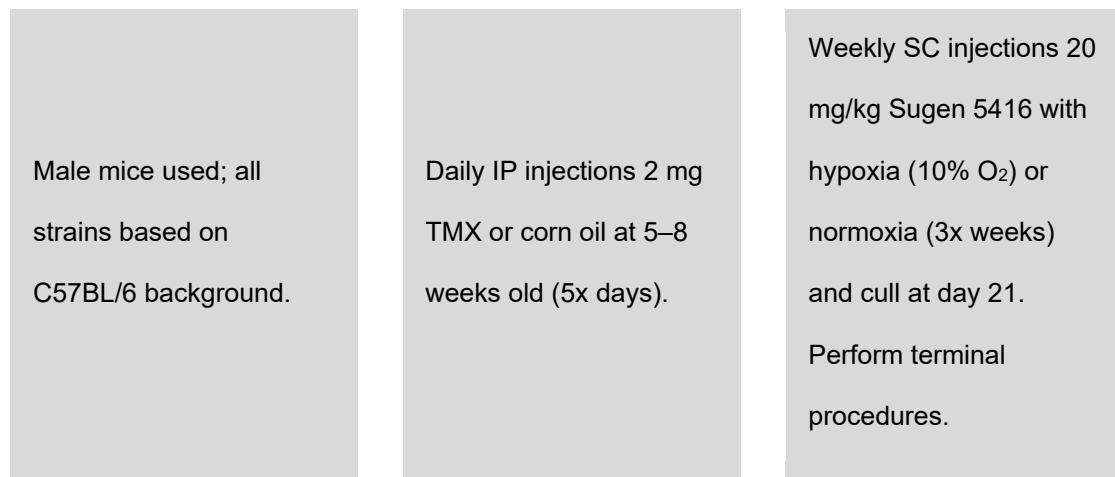


**Figure 4.3: Experimental schematic for *TRAIL* genetic deletion in SuHx mice.** Strains utilised in the experiment either had functional *TRAIL* expression ( $TRAIL^{tm1c/tm1c}$ ) or tamoxifen (TMX)-inducible vascular smooth muscle cell-specific *TRAIL* deletion ( $TRAIL^{tm1c/tm1c}$ -SMMHC-Cre-ERT2). Mice were weaned, ear clipped and genotype confirmed by PCR. Two groups underwent tamoxifen (TMX) 5x daily IP injections at 5–8 weeks old and the others received IP corn oil. Mice were subjected to 3 weekly SC Sugen 5416 injections with hypoxia (10% oxygen; SuHx) or normoxic conditions (Nx) and culled after 3 weeks. Terminal procedures were performed including echocardiography, cardiac catheterisation and tissue harvest.

#### **4.2.1 *TRAIL* expression in lungs**

Real time qPCR was performed to quantify *TRAIL* mRNA expression in whole lung tissue from SuHx mice to determine any changes in this model. RNA was extracted from frozen whole lung tissue and a set quantity reverse transcribed to cDNA for qPCR analysis by TaqMan technology. *TRAIL* mRNA was detected in the lungs of mice at each experimental group from the SuHx model (Figure 4.4A). However, no significant differences were observed between any groups within this experiment. This was in contrast to *TRAIL* RT-qPCR data from Chapter 3.4.1, whereby *TRAIL* mRNA was reduced in whole lungs from mice with fibroblast-specific *TRAIL* deletion subject to bleomycin insult (Figure 4.4B). Immunohistochemistry was also performed to visualise TRAIL protein expression in the lungs of SuHx mice (data not shown). However, at the protein level, no differences in TRAIL immunostaining could be visually detected in the lungs of any mice examined, which may have been due to the high level of non-specific background staining. It is also possible that as a soluble cytokine, the specific localisation of TRAIL is problematic.

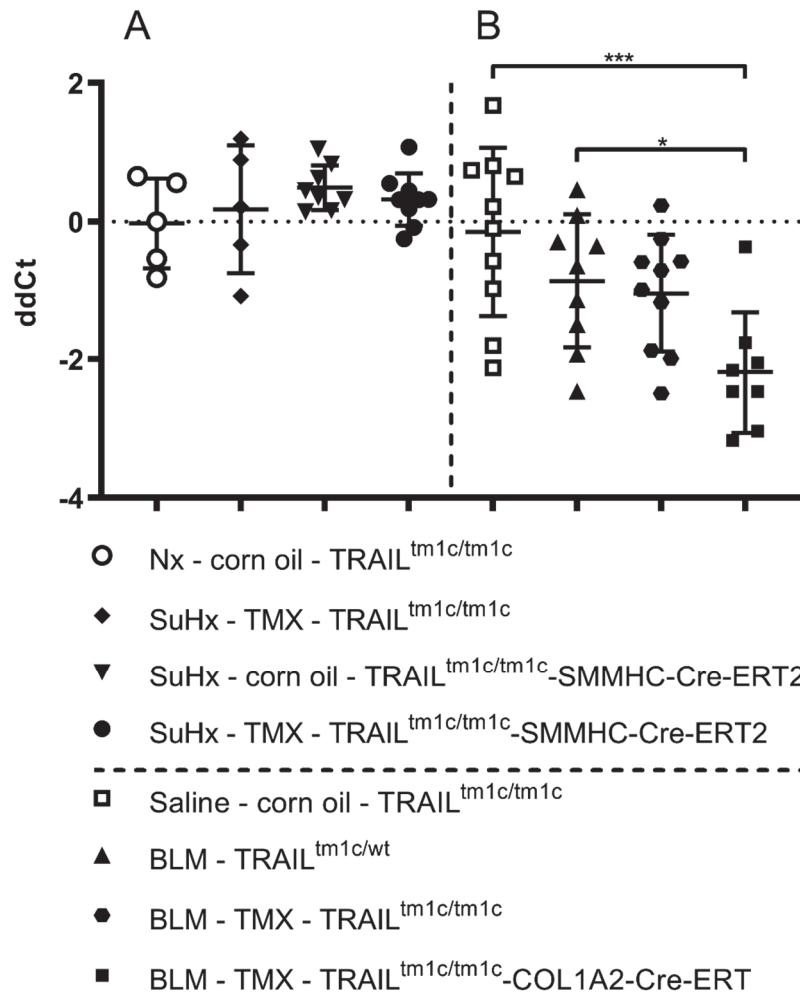


**Figure 4.4: TRAIL expression in VSMC-specific *TRAIL*-deleted SuHx lungs.** (A) Mice were subjected to 3 weekly SC Sugen 5416 injections with hypoxia (10% oxygen; SuHx) or normoxic conditions (Nx) and culled after 3 weeks. Two groups had previously undergone tamoxifen (TMX) 5x daily IP injections at 5–8 weeks old. *TRAIL* mRNA was measured in cDNA from whole mouse lungs by TaqMan RT-qPCR. (B) Also included for comparison are *TRAIL* mRNA data from Chapter 3.4.1, in which mice were subjected to bleomycin (BLM) or saline IP injection twice weekly for 4 weeks and culled at day 35. All data shown are threshold cycle values normalised to a reference gene (*GAPDH*) then to a reference sample (from the nx – corn oil –  $TRAIL^{tm1c/tm1c}$  group) to compare both experiments (delta-delta Ct; ddCt). Bars show mean  $\pm$  SD, n = 5–9. \* p<0.05, \*\*\* p<0.001, one-way ANOVA with Sidak’s multiple comparisons test comparing the mean of groups within each experiment separately.

#### 4.2.2 Haemodynamics

Haemodynamic measurements were taken from right heart catheterisation (Figure 4.5A–F) in addition to echocardiography (Figure 4.5G–H) under anaesthesia at the time of terminal procedures to determine any effect of TRAIL deletion on haemodynamic changes associated with PAH. Significantly increased RVESP was observed in mice with TRAIL expression subjected to SuHx, compared to normoxia control mice: both in those without the SMMHC-Cre-ERT2 allele given tamoxifen (Figure 4.5A; mean 38.70 mmHg vs. 27.85 mmHg,  $p = 0.0143$ ) and in those with the SMMHC-Cre-ERT2 allele given corn oil (Figure 4.5A; mean 40.28 mmHg vs. 27.85 mmHg,  $p = 0.0037$ ). Mice with VSMC-specific *TRAIL* deletion (*TRAIL*<sup>tm1c/tm1c</sup>-SMMHC-Cre-ERT2 given tamoxifen) did not have elevated RVESP compared to normoxia control mice. VSMC-deleted *TRAIL* mice also had significantly lower RVESP than both *TRAIL*<sup>tm1c/tm1c</sup> mice given tamoxifen (Figure 4.5A; mean 31.23 mmHg vs. 38.70 mmHg,  $p = 0.0386$ ) and *TRAIL*<sup>tm1c/tm1c</sup>-SMMHC-Cre-ERT2 mice given corn oil (Figure 4.5A; mean 31.23 mmHg vs. 40.28 mmHg,  $p = 0.0076$ ) and subjected to SuHx. Mice with VSMC-specific *TRAIL* deletion also had significantly higher dP/dt min than *TRAIL*<sup>tm1c/tm1c</sup>-SMMHC-Cre-ERT2 mice given corn oil and subjected to SuHx (Figure 4.5C; mean -713.1 mmHg/sec vs. -2491 mmHg/sec,  $p = 0.0330$ ). A similar pattern was seen in RV arterial elastance (Figure 4.5E), which was increased by the SuHx insult in the absence of *TRAIL* deletion, and reduced in VSMC *TRAIL*-deleted mice compared to both disease control mice groups (Figure 4.5E; e.g. VSMC-deleted mice vs. *TRAIL*<sup>tm1c/tm1c</sup>-SMMHC-Cre-ERT2 mice given tamoxifen, mean 17.56 mmHg/ $\mu$ l vs. 28.46 mmHg/ $\mu$ l,  $p = 0.0423$ ). No differences were observed due to SuHx or between diseased mice in RV end-diastolic pressure (Figure 4.5B), dP/dt max (Figure 4.5D) or RV ejection fraction (Figure 4.5F) from catheterisation or PAAT from echocardiography (Figure 4.5H). Due to insufficient data, haemodynamic measurements from catheterisation of the LV or aorta are not shown. However, echocardiographic examination demonstrated no difference in cardiac index (cardiac output at the aortic valve normalised to body weight) caused by the SuHx insult (Figure 4.5G), indicating left heart function was unaffected.

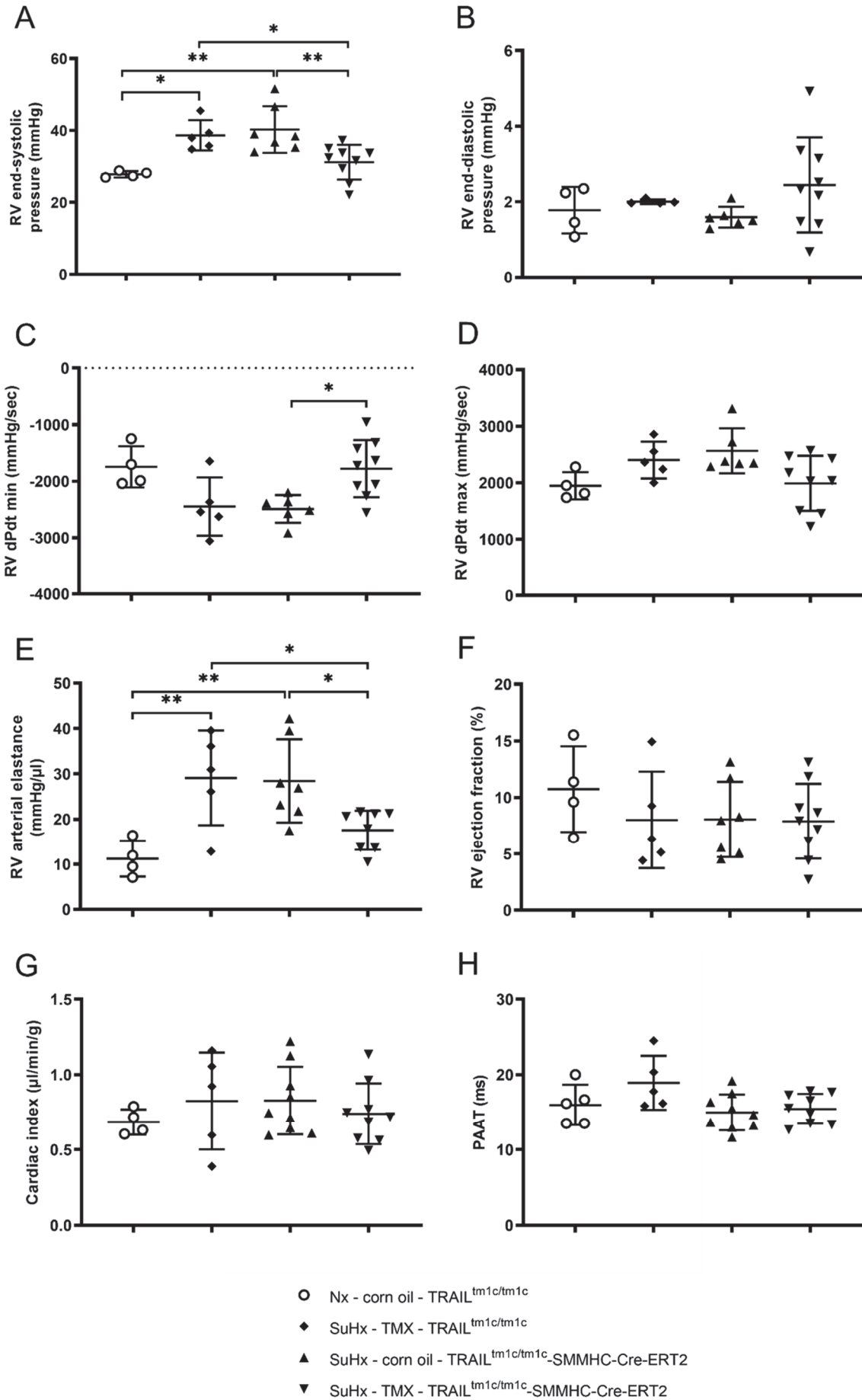


**Figure 4.5: Haemodynamic measures in VSMC-specific *TRAIL*-deleted SuHx mice.** Mice were subjected to 3 weekly SC Sugen 5416 injections with hypoxia (10% oxygen; SuHx) or normoxic conditions (Nx) and culled after 3 weeks. Two groups had previously undergone tamoxifen (TMX) 5x daily IP injections at 5–8 weeks old. Haemodynamic measurements were taken by cardiac catheterisation (**A–F**) and echocardiography (**G–H**). Plots show (**A**) right ventricular (RV) end systolic pressure, (**B**) RV end-diastolic pressure, (**C**) RV dP/dt minimum, (**D**) RV dP/dt minimum, (**E**) RV arterial elastance, (**F**) RV ejection fraction, (**G**) cardiac index (cardiac output measure at the aortic valve and normalised to body weight) and (**H**) pulmonary artery acceleration time (PAAT). Points represent individual mice, n = 4–9 animals per group, bars show mean  $\pm$  SD. \* p<0.05; \*\* p<0.01; one-way ANOVA with Sidak's multiple comparisons test comparing each group.

### 4.2.3 Right ventricular hypertrophy

To measure enlargement of the RV associated with PAH, after dissection of hearts, RVH was calculated as the ratio of right ventricular free wall weight to LV plus septum weight (Figure 4.6). The two groups subjected to SuHx, but without *TRAIL* deletion developed significantly increased RVH compared to normoxic control mice ( $TRAIL^{tm1c/tm1c}$  given TMX mean 0.3258 vs. 0.2371,  $p = 0.0305$ ;  $TRAIL^{tm1c/tm1c}$ -SMMHC-Cre-ERT2 given corn oil mean 0.3494 vs 0.2371,  $p = 0.0014$ ). Notably, SMC-specific deletion of *TRAIL* (i.e. in mice with the SMMHC-Cre-ERT2 allele that received tamoxifen) caused a reduced RVH phenotype in the context of SuHx, compared to the genetically identical mice given corn oil (mean 0.2885 vs. 0.3494,  $p = 0.0424$ ).

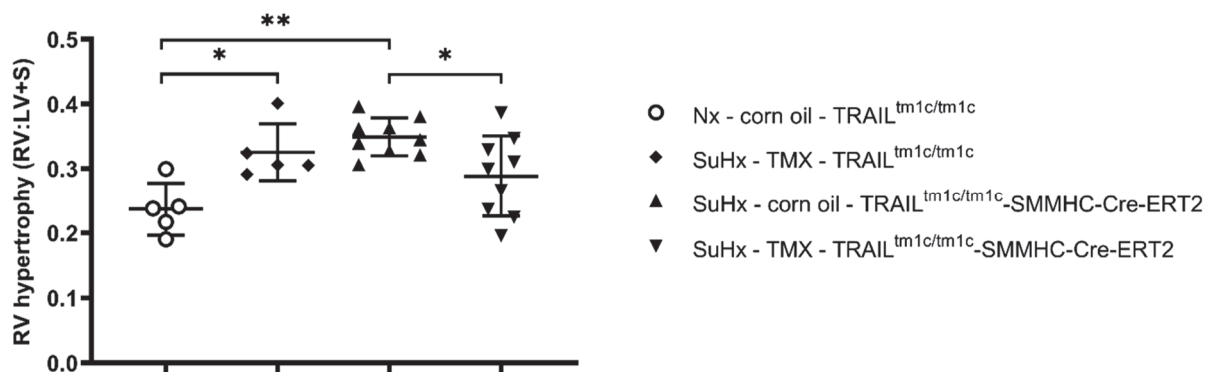
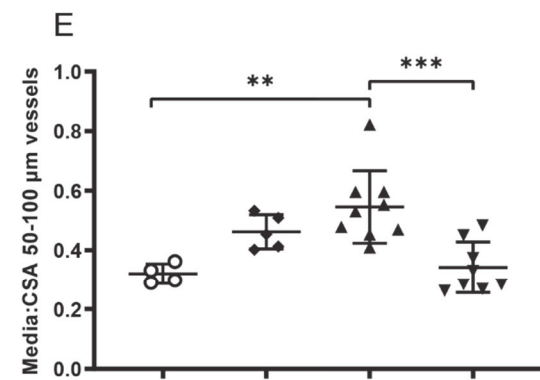
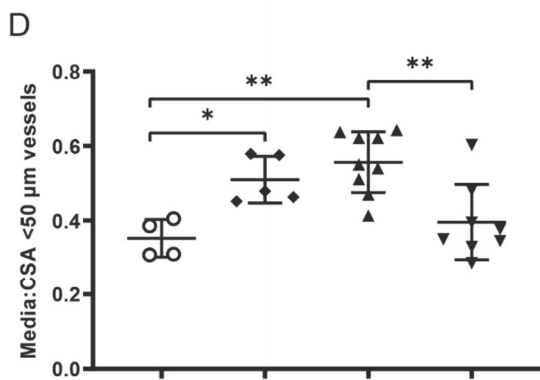
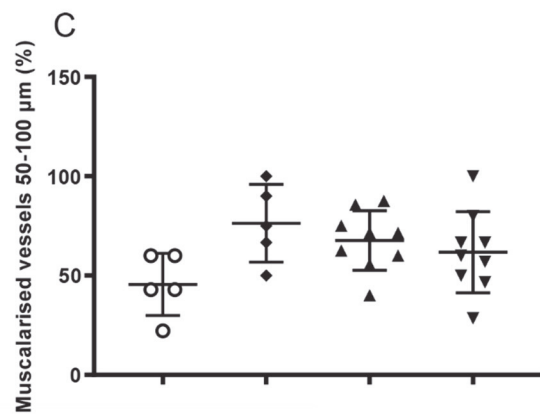
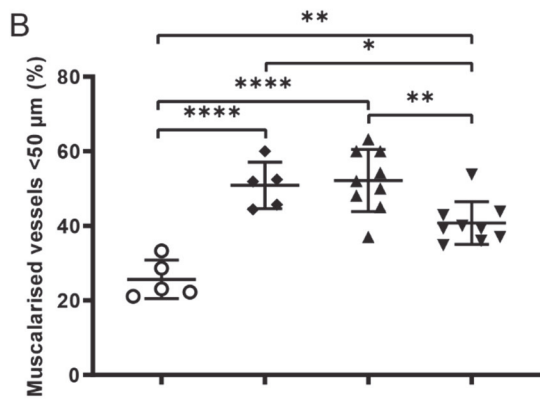
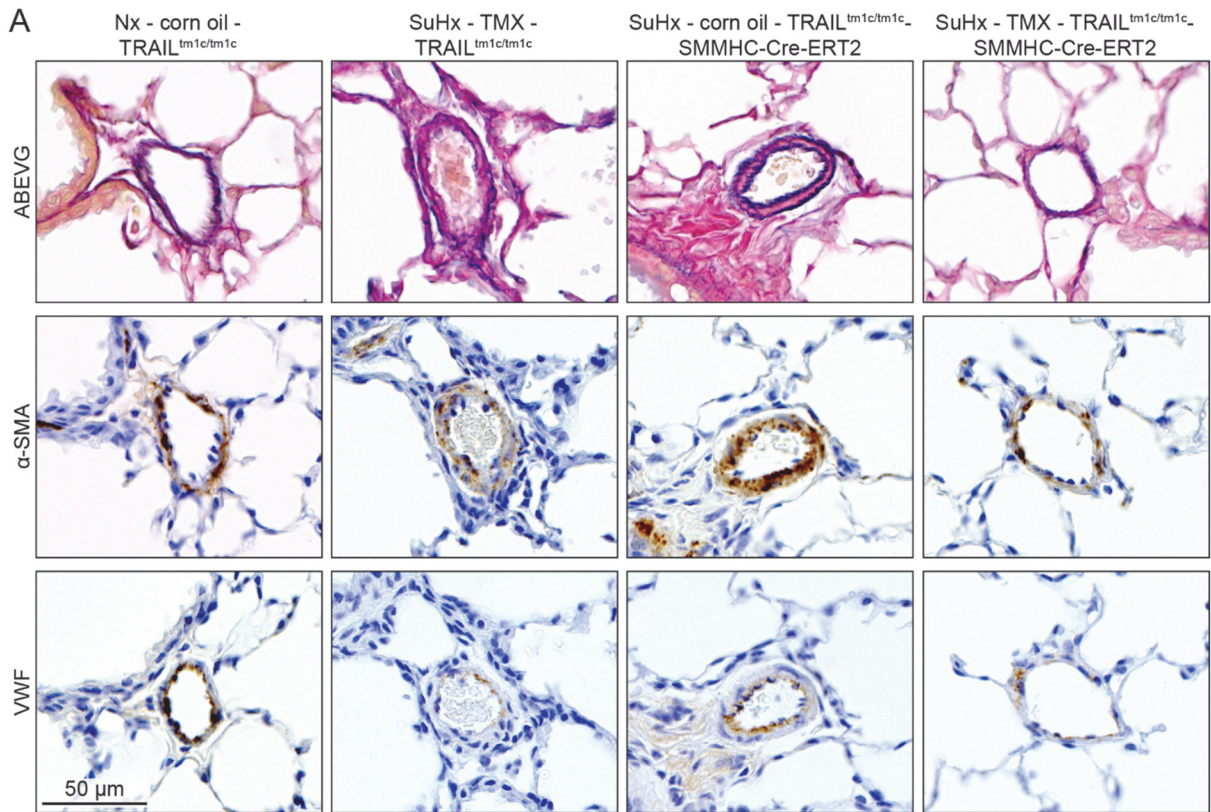


**Figure 4.6: Right ventricular hypertrophy in VSMC-specific *TRAIL*-deleted SuHx mice.** Mice were subjected to 3 weekly SC Sugen 5416 injections with hypoxia (10% oxygen; SuHx) or normoxic conditions (Nx) and culled after 3 weeks. Two groups had previously undergone tamoxifen (TMX) 5x daily IP injections at 5–8 weeks old. Hearts were dissected and right ventricular (RV) hypertrophy was calculated by right ventricular free wall weight normalised to left ventricle plus septum weight (RV:LV+S). Points represent individual mice,  $n = 5-9$  animals per group, bars show mean  $\pm$  SD. \*  $p < 0.05$ , \*\*  $p < 0.01$ ; one-way ANOVA with Sidak's multiple comparisons test of each pairwise group combination.

#### 4.2.4 Pulmonary vascular remodelling

To determine changes in PAH vascular phenotype driven by SuHx, pulmonary vascular remodelling was assessed in micrographs of formalin-fixed, paraffin-embedded lung sections histologically stained with ABEVG or immunostained for  $\alpha$ -SMA or VWF (Figure 4.7A–E). As illustrated by the example micrographs (Figure 4.7A), the SuHx insult induced pulmonary vascular remodelling including medial thickening of small (0–50  $\mu$ m) pulmonary arteries indicated by  $\alpha$ -SMA area. The appearance of thickened small pulmonary arteries was accompanied by distinct inner and outer elastic laminae. The pulmonary vascular remodelling was also quantified by counting the proportion of muscularised vessels in ABEVG-stained sections (Figure 4.7B–C) and by measuring the medial area of muscularised vessels in sections immunostained for  $\alpha$ -SMA (Figure 4.7D–E). The diameter of vessels was measured and used to divide them into two sizes (0–50  $\mu$ m and 50–100  $\mu$ m). For ABEVG lung sections, each vessel was scored as non-muscularised (those with a single elastic lamina) or muscularised (those with two or more distinct elastic laminae). Only vessels with a clear transverse cross-section were included in the analysis. There were significantly more muscularised 0–50  $\mu$ m diameter pulmonary arteries in all SuHx groups compared to normoxia control mice (Figure 4.7B). Mice with VSMC-specific *TRAIL* deletion (*TRAIL*<sup>tm1c/tm1c</sup>-SMMHC-Cre-ERT2 mice given tamoxifen) also had significantly fewer muscularised vessels than either of the SuHx mice groups without *TRAIL* deletion: those without the SMMHC-Cre-ERT2 allele given tamoxifen (mean 40.77% vs. 50.88%,  $p = 0.0243$ ) or those with the SMMHC-Cre-ERT2 allele given corn oil (mean 40.77% vs. 52.17%,  $p = 0.0041$ ). No differences in the number of larger muscularised vessels (50–100  $\mu$ m) were observed between any groups. A comparable pattern to the number of muscularised small vessels was also found in the degree of medial thickening of small vessels from sections immunostained for  $\alpha$ -SMA (Figure 4.7D). In this analysis, the two groups without *TRAIL* deletion subjected to SuHx had significantly thickened medial layers calculated as medial area normalised to CSA. The mice with VSMC-specific *TRAIL* deletion in SuHx had no difference in medial thickening to normoxia control mice, and furthermore these mice also had reduced medial thickness compared to mice with the

SMMHC-Cre-ERT2 allele given corn oil in SuHx (mean 0.3959 vs. 0.5566,  $p = 0.0028$ ). Interestingly, in the medial thickness metric for larger vessels (Figure 4.7E) there was also an increase observed in SMMHC-Cre-ERT2 allele given corn oil in SuHx (mean 0.5454 vs. 0.3205,  $p = 0.0026$ ), which was ameliorated in mice with VSMC-specific *TRAIL* deletion (mean 0.3420 vs. 0.5454,  $p = 0.0010$ ).



- Nx - corn oil - TRAIL<sup>tm1c/tm1c</sup>
- ◆ SuHx - TMX - TRAIL<sup>tm1c/tm1c</sup>
- ▲ SuHx - corn oil - TRAIL<sup>tm1c/tm1c</sup>-SMMHC-Cre-ERT2
- ▼ SuHx - TMX - TRAIL<sup>tm1c/tm1c</sup>-SMMHC-Cre-ERT2

**Figure 4.7: Vascular remodelling in VSMC-specific *TRAIL*-deleted SuHx lungs.** Mice were subjected to 3 weekly SC Sugen 5416 injections with hypoxia (10% oxygen; SuHx) or normoxic conditions (Nx) and culled after 3 weeks. Two groups had previously undergone tamoxifen (TMX) 5x daily IP injections at 5–8 weeks old. **(A)** Representative micrographs from 5  $\mu$ m thick lung sections stained with Miller's elastin stain with alcian blue and van Gieson (ABEVG) or immunostained for  $\alpha$ -smooth muscle actin ( $\alpha$ -SMA) or von Willebrand factor (VWF), with nuclei counterstained with Carazzi's haematoxylin. Images were acquired at 200X total magnification then digitally cropped. Pulmonary vascular remodelling was quantified by the proportion of muscularised arteries and arterioles in lung sections stained with ABEVG (**B–C**) and by the medial area over cross-sectional area (CSA) for muscularised arteries in lung sections immunostained with DAB for  $\alpha$ -SMA (**D–E**). Pulmonary arteries were divided into small (0–50  $\mu$ m diameter; **B, D**) and large sizes (50–100  $\mu$ m diameter; **C, E**). Points represent individual mice, n = 4–9 animals per group, bars show mean  $\pm$  SD. \* p<0.05; \*\* p<0.01; \*\*\* p<0.001; \*\*\*\* p<0.0001, one-way ANOVA with Sidak's multiple comparisons test of each pairwise group combination.

### 4.3 Summary

The aims of this chapter were to generate mice with VSMC-specific deletion of *TRAIL* and to determine any effect in the context of SuHx-induced PAH. In summary:

- Mice with floxed *TRAIL* were crossed with the SMMHC-Cre-ERT2 line to produce a strain with tamoxifen-inducible VSMC-specific deletion of *TRAIL*.
- SuHx caused a PAH haemodynamic phenotype, which was reduced in mice with deletion of *TRAIL* in VSMCs (with no effect on left heart function).
- Mice subjected to SuHx developed RVH, which was ameliorated in mice with *TRAIL* deleted in VSMCs.
- SuHx caused extensive remodelling of small pulmonary arteries, and VSMC-specific deletion of *TRAIL* reduced both the number of muscularised vessels and the medial thickness of these vessels.

## 4.4 Discussion

### 4.4.1 VSMCs are a protective source of TRAIL in PAH

In this chapter I presented data demonstrating that mice with VSMC-specific deletion of *TRAIL* were protected from SuHx-induced PAH compared to those with normal *TRAIL* expression. This was evident from improvement in multiple haemodynamic metrics, decreased RVH and a reduction in the prevalence and medial thickening of muscularised small pulmonary arteries. These results confirm that VSMCs are indeed a crucial source of *TRAIL* contributing to the PAH phenotype in the SuHx mouse model, which is in line with previous studies demonstrating that *TRAIL* drives PAH in SuHx mice (Dawson et al. 2014) and that tissue-derived rather than circulating *TRAIL* is required for PAH pathogenesis in other mouse models (Hameed et al. 2012). The magnitude of the protective effect of *TRAIL* deletion in VSMCs in these mice is striking given the relatively subtle disease phenotype compared to other models such as the monocrotaline or SuHx rat, which unlike the SuHx mouse can develop angioproliferative plexiform lesions (Abe et al. 2010b). Notably, while VSMC-specific *TRAIL* deletion reduced the establishment of PAH as determined by several metrics, it did not fully protect against disease when compared to normoxic control mice. This suggests that *TRAIL* expressed by additional key vascular cell types – such as ECs – may also be involved in driving PAH. Furthermore, the protective effect against PF of *TRAIL* deletion in fibroblasts (and suggestion of a possible effect against bleomycin-induced PAH) demonstrated in Chapter 3.4 indicates that deletion of *TRAIL* in adventitial fibroblasts and other resident vascular cells in the context of SuHx-induced PAH could be informative, as these cells are also relevant in PAH. Although deletion of *TRAIL* in ECs, fibroblasts and other cells in the SuHx model was beyond the scope of the present study, Cre driver lines are available for many cell types and future work would be beneficial in further exploring the role of *TRAIL* in PAH.

I also found that the SuHx insult did not affect *TRAIL* mRNA level in whole lung in mice with normal *TRAIL* expression or those with VSMC-specific *TRAIL* deletion. In contrast, fibroblast-

specific deletion of *TRAIL* in mice subjected to bleomycin reduced *TRAIL* mRNA at the whole lung level (but not in bleomycin insult without *TRAIL* deletion). The reasons for these findings are unclear, and I did not have data from unchallenged *TRAIL*-deleted mice to check for a potential basal change in *TRAIL* expression. A recent single cell RNA sequencing study suggested that VSMCs and fibroblasts are of similar number in an unchallenged mouse lung (Angelidis et al. 2019). Therefore, the expression of *TRAIL* may differ between these cell types in health and/or disease, and this requires further investigation. As fibroblast-specific deletion of *TRAIL* reduced *TRAIL* mRNA at the whole lung level in bleomycin mice, one possible conclusion to draw from these results is that fibroblasts are a predominant source of *TRAIL* mRNA in lungs of mice subjected to bleomycin.

Another consideration in the interpretation of the results presented here is that the targets of pathogenic VSMC-derived TRAIL in PAH remain to be elucidated. Evidence such as the pro-proliferative and/or pro-migratory effects of *in vitro* TRAIL stimulation points towards VSMCs (Secchiero et al. 2004, Kavurma et al. 2008, Hameed et al. 2012) and ECs (Secchiero et al. 2003, Zauli et al. 2003, Cantarella et al. 2014, Cartland et al. 2016) as targets of TRAIL in PAH. Additionally, antibody blockade of TRAIL in rodent PAH models has been shown to increase the number of apoptotic cells – and decrease the number of proliferating cells – within remodelled pulmonary arteries (Hameed et al. 2012). However, a direct *in vivo* effect of TRAIL on specific cell types in PAH has not yet been demonstrated. A difficulty in establishing these interactions arises from the fact that TRAIL may be membrane-bound or cleaved to form a cytokine, thus the localisation of TRAIL immunoreactivity alone may not be informative. However, a potentially valuable study would involve the genetic deletion of particular TRAIL receptors in specific cell types such as ECs and VSMCs using the Cre/lox system in the context of PAH models. Altered expression of specific TRAIL receptors has been linked to PAH pathogenesis – for example, elevated DR4 and DcR1 expression was previously detected in explanted PSMCs from IPAH patients, compared to healthy control cells (Hameed et al. 2012). Similarly, differential expression of TRAIL receptors has been linked to

pro-proliferative, pro-survival or pro-hypertrophic effects in cells involved in other varied diseases, such as: cardiomyocytes in cardiac disease (Tanner et al. 2019), AECs in IPF (Akram et al. 2014), cells in small cell lung cancer (Belyanskaya et al. 2008) and kidney proximal tubular epithelial cells in lupus nephritis (Nguyen et al. 2009). Further research into TRAIL receptors is therefore required to fully understand the pathogenic role of VSMC-derived TRAIL in PAH established in the present study. The downstream effects of TRAIL stimulation of PSMCs and the role of TRAIL-modulated targets in PAH animal models and PAH patients are further explored in Chapter 5.

#### **4.4.2 The SuHx mouse model**

In the present study, mice were subjected to the SuHx model and indications of PAH phenotype were observed including haemodynamics of the right heart and RVH, with underlying remodelling of small pulmonary arteries. The choice of mice as the model species was determined by its ease of genetic manipulation. The Cre/lox system in mice presents a somewhat simple and readily available method for achieving inducible, cell type-specific genetic deletions in a mammalian species. Due to the limited number of mice available for study, only one experimental model was able to be utilised. The SuHx mouse model was selected as a model originally developed in rats (Taraseviciene-Stewart et al. 2001) but since also adapted for mice (Ciuclan et al. 2011). In this model the targeting of the hypoxia pathway (as in the chronic hypoxic mouse model) is combined with the use of Sugen 5416, an inhibitor of VEGF receptor. The mouse SuHx model produces enhanced pulmonary vascular remodelling compared to the chronic hypoxia model in mice (Ciuclan et al. 2011), thus more closely resembling the human form of PAH. The SuHx mouse model has been widely adopted since its first use – a recent survey from the Pulmonary Vascular Research Institute found the SuHx mouse was used by approximately 39% of PH research groups in target identification studies, compared to the 56% use rate for the chronic hypoxic mouse (Lawrie 2014). The SuHx mouse model has also been utilised extensively previously within the research group (Boehm et al. 2018, Dawson et al. 2014, Farkas et al. 2019). Additionally, its use with *TRAIL*-

deleted mice reiterated a pathogenic role for TRAIL in PAH (Dawson et al. 2014) further to previous studies of TRAIL in models including the chronic hypoxic mouse and the monocrotaline rat (Hameed et al. 2012).

A further consideration is the use of the oestrogen receptor antagonist tamoxifen in the present study. PAH is sexually dimorphic and is more prevalent in women than in men (Shapiro et al. 2012) and signalling via the oestrogen alpha receptor has been linked to development of PAH (Wright et al. 2015). Animal models of PAH often only use males, however oestrogen may be important for PAH in both sexes – in female BMPR2 mutant mice, inhibition of oestrogen by use of tamoxifen, anastrozole or fulvestrant can reduce the PAH phenotype, but additionally oestrogen receptor 2 deletion is protective in male and female mice (Chen et al. 2017). A recent small phase II clinical trial also suggested that aromatase inhibition with anastrozole in postmenopausal women and men with PAH could lead to improvements in outcomes such as 6-minute walk distance (Kawut et al. 2017). However, despite the plausible potential influence of tamoxifen on the PAH phenotype in the present study, no differences due to tamoxifen were observed in haemodynamics, RVH or pulmonary vascular remodelling. This may be because tamoxifen does not have an effect on the pathways involved in this particular model, or alternatively might be due to the tamoxifen being administered to mice at 5–8 weeks of age, several weeks before the SuHx insult.

## **5 The role of TRAIL targets in PSMCs, animal models and human PAH**

In the present study I have demonstrated that fibroblast-derived TRAIL is protective in the context of IP bleomycin-induced PF in mice (Chapter 3), whereas TRAIL produced by VSMCs is pathogenic and required for the development of PAH in the SuHx mouse model (Chapter 4). These results are similar to other studies highlighting diverse roles of TRAIL in various diseases – particularly in those affecting the lung (Braithwaite et al. 2018) – but go further by suggesting that the source of TRAIL is crucial to its function in these varied disease processes. Another important aspect to understanding TRAIL function as a cytokine is its target cells and the effects induced within these cells. In the context of PAH, key cell types pathologically altered include those of the pulmonary vasculature. Indeed, TRAIL has previously been demonstrated to have direct pro-proliferative effects (e.g. by ERK1/2 phosphorylation) on VSMCs (Hameed et al. 2012, Kavurma et al. 2008, Secchiero et al. 2004) and pro-angiogenic effects on ECs (Cantarella et al. 2014, Cartland et al. 2016, Secchiero et al. 2003, Zauli et al. 2003). However, the full extent of TRAIL-induced processes in pulmonary vascular cells is not well understood. As key effector cells in PAH vascular remodelling, it is feasible that TRAIL released from PSMCs could also be inducing proliferative effects in these cells via additional, undescribed pathways. Therefore, in this chapter I explore the effects of TRAIL stimulation on human PSMC, then further characterise the TRAIL-regulated genes and pathways discovered in animal models and in human PAH.

## **5.1 TRAIL alters mRNA levels and protein phosphorylation in**

### **PASMCs**

TRAIL has previously been demonstrated to stimulate pro-proliferative, non-canonical signalling pathways in vascular cells, particularly in VSMCs (Hameed et al. 2012, Kavurma et al. 2008, Secchiero et al. 2004). Some effects of this signalling have been illustrated – such as ERK1/2 phosphorylation in PASMCs (Hameed et al. 2012) – however, the full impact of TRAIL signalling in PASMCs and in the context of PAH has not been characterised. To further explore this, I analysed microarray datasets detailing the transcriptomic effects of TRAIL stimulation of PASMCs. Microarray measurement of mRNA was carried out using cDNA created from human primary PASMCs unstimulated or stimulated with 30 ng/ml recombinant human TRAIL for 6 hours. This dose was selected as suitable for inducing a proliferative effect in PASMCs in previous studies (Hameed et al. 2012). Differential gene expression was assessed and then the set of altered genes was investigated using GO enrichment analysis and signalling pathway topology analysis, to further implicate TRAIL and TRAIL-regulated genes and biological processes in PAH pathobiology. Additionally, at 10- and 60-minute stimulation timepoints measurement of protein levels and protein phosphorylation was carried out by antibody arrays and the data combined with pathways analysis of the effects of TRAIL.

#### **5.1.1 *Microarray mRNA quantification***

To determine the transcriptomic effects of TRAIL stimulation, human primary PASMCs were stimulated with recombinant TRAIL or unstimulated as control and mRNA was isolated after 6 hours. Due to availability of arrays, and to minimise the effects of biological variation, cDNA samples from separate stimulations were pooled: 8 unstimulated samples into 4, and 6 TRAIL-stimulated samples into 2. Measurement of transcriptome was carried out using Agilent SurePrint G3 Human Gene Expression v2 single colour microarrays. Array data were background corrected, normalised then analysed to determine DE genes using the LIMMA R package. From the 35,649 probes whose target genes were found to be expressed, 3,166

were significantly altered (adjusted  $p < 0.05$ ; Figure 5.1A) when comparing TRAIL-stimulated PASMCs to unstimulated PASMCs. As would be expected from microarray gene expression analysis, due to statistical power more numerous significant changes in mRNA expression were detected for probes with larger fold changes between experimental conditions. Of the significantly DE probes, 462 had a  $\log_2$  fold change  $\geq 1$  (i.e. a 2-fold absolute difference), with 246 upregulated and 216 downregulated by TRAIL stimulation (Figure 5.1B). The probes with the 20 highest and 20 lowest  $\log_2$  fold changes after TRAIL stimulation are shown in Table 5.1. Notable genes highly upregulated by TRAIL stimulation included pro-angiogenic growth factors (*FIGF* and *PDGFD*). Genes highly downregulated by TRAIL included several cytokines (*CXCL6*, *CXCL1*, *CXCL2*, *IL6* and *IL8*), the vasorelaxant *VIPR1* and the BMP/Wnt antagonist *SOST*. Interestingly, *TRAIL* mRNA was also significantly increased after stimulation by recombinant TRAIL protein (data not shown;  $\log_2$  fold change 1.118, adjusted  $p < 0.01$ ). Commonalities in the biological functions and pathways of genes DE induced by TRAIL stimulation are further explored by GO term enrichment analysis and pathway topology analysis in Chapter 5.1.3 and Chapter 5.1.5 respectively.

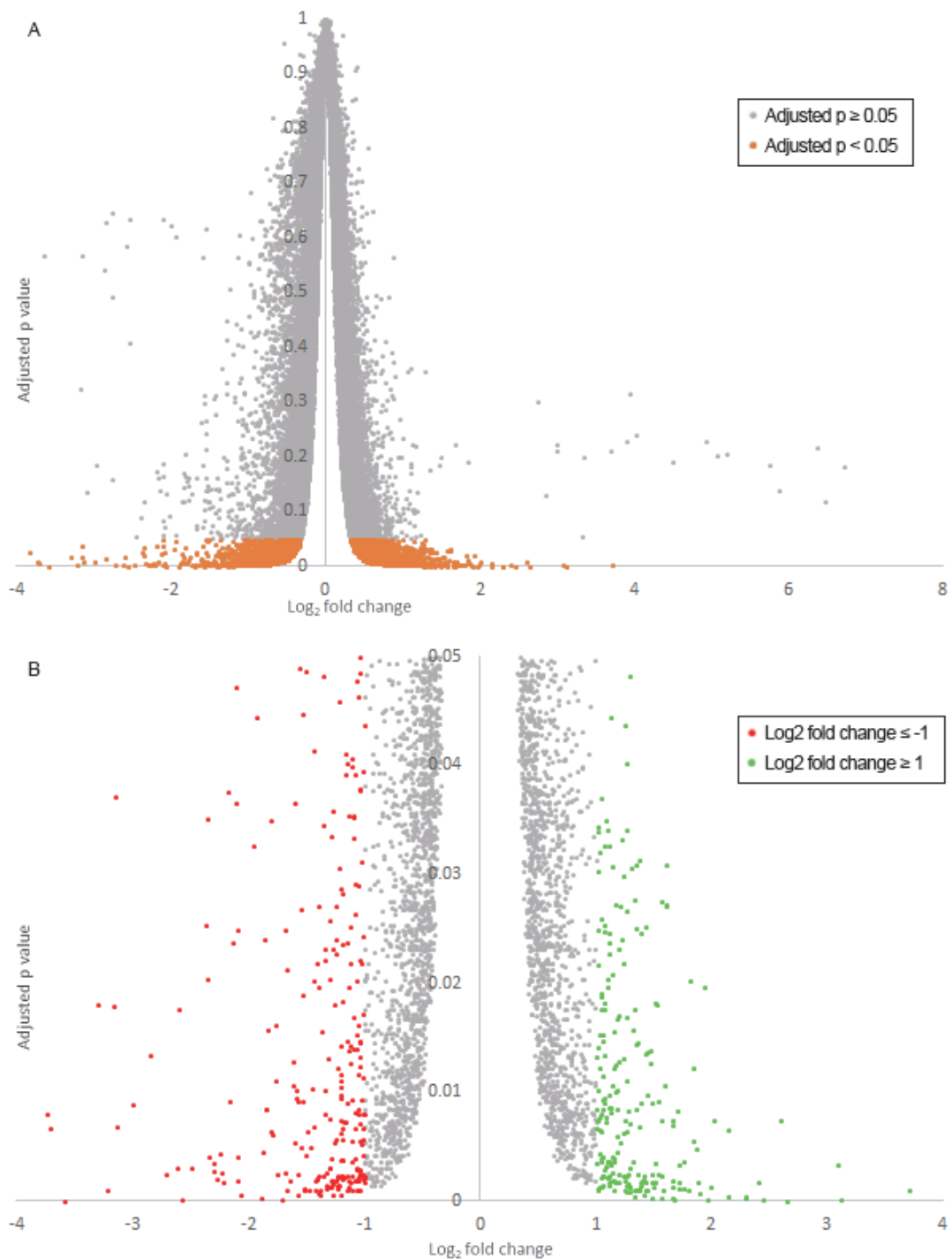


**Figure 5.1: Differentially expressed mRNA after TRAIL stimulation of PASCs.** Human primary PASCs were stimulated with recombinant TRAIL or unstimulated for 6 hours and transcriptome was measured by Agilent SurePrint G3 Human Gene Expression v2 single colour microarrays. **(A–B)** Volcano plots showing differential expression analysis by linear models for microarray analysis (LIMMA). Points represent single probes. **(A)** All probes shown, probes with adjusted  $p < 0.05$  are highlighted in orange ( $n = 3,166$ ), **(B)** probes with adjusted  $p < 0.05$  shown, probes with  $\log_2$  fold change  $\leq -1$  ( $n = 246$ ) are highlighted in red and probes with  $\log_2$  fold change  $\geq 1$  ( $n = 216$ ) are highlighted in green.  $\log_2$  fold change, TRAIL-stimulated cells vs. unstimulated cells; adjusted p-value after global FDR (5%) correction by Benjamini and Hochberg’s method.

**Table 5.1: Top differentially expressed genes after TRAIL stimulation of PSMCs**

	Log2			
Agilent probe ID	FC	Adj. p-val.	Gene symbol	Gene name
A_23_P31124	3.714	0.0009	COL21A1	Collagen, type XXI, alpha 1
A_33_P3313283	3.122	0.0002	CILP2	Cartilage intermediate layer protein 2
A_23_P82990	3.086	0.0033	OGN	Osteoglycin
A_33_P3239185	2.647	1.58X10 <sup>-5</sup>	SYT7	Synaptotagmin VII
A_33_P3279590	2.602	0.0074	OGN	Osteoglycin
A_33_P3322804	2.452	0.0002	NTRK2	Neurotrophic tyrosine kinase, receptor, type 2
A_23_P212608	2.404	0.0017	CLSTN2	Calsyntenin 2
A_23_P216429	2.294	0.0004	ASPN	Asporin
A_23_P45185	2.290	0.0002	FIGF	C-fos induced growth factor
A_23_P202448	2.151	0.0004	CXCL12	Chemokine (C-X-C motif) ligand 12
A_24_P183664	2.145	0.0065	TRIL	TLR4 interactor with leucine-rich repeats
A_23_P200741	2.017	0.0074	DPT	Dermatopontin
A_24_P156490	1.997	0.0013	KCNMA1	Calcium-activated potassium channel alpha 1
A_24_P124349	1.964	0.0002	PDGFD	Platelet derived growth factor D
A_33_P3274179	1.935	0.0196	ERV18-1	Endogenous retrovirus group 18, member 1
A_33_P3216059	1.903	0.0006	ASPN	Asporin
A_32_P181222	1.878	0.0017	KCNMA1	Calcium-activated potassium channel alpha 1
A_23_P102611	1.869	0.0048	WISP2	WNT1 inducible signaling pathway protein 2
A_19_P00320885	1.845	0.0122	XLOC_007052	
A_33_P3411244	1.841	0.0055	OR8S1	Olfactory receptor, family 8, subfamily S, mem. 1
A_23_P161218	-3.832	0.0253	ANKRD1	Ankyrin repeat domain 1
A_23_P62752	-3.740	0.0080	NPPB	Natriuretic peptide B
A_33_P3362008	-3.705	0.0066	NPPB	Natriuretic peptide B
A_33_P3265783	-3.589	1.58X10 <sup>-5</sup>	STATH	Statherin
A_33_P3227400	-3.304	0.0180	COL4A4	Collagen, type IV, alpha 4
A_24_P264943	-3.223	0.0010	COMP	Cartilage oligomeric matrix protein
A_23_P7144	-3.163	0.0179	CXCL1	Chemokine (C-X-C motif) ligand 1
A_23_P71037	-3.151	0.0371	IL6	Interleukin 6 (interferon, beta 2)
A_23_P155755	-3.134	0.0068	CXCL6	Chemokine (C-X-C motif) ligand 6
A_24_P305784	-2.993	0.0089	SPANXB2	SPANX family, member B2

A_33_P3330264	-2.844	0.0134	CXCL1	Chemokine (C-X-C motif) ligand 1
A_23_P39955	-2.715	0.0024	ACTG2	Actin, gamma-enteric smooth muscle
A_23_P107421	-2.618	0.0030	TK1	Thymidine kinase 1
A_32_P87013	-2.600	0.0176	IL8	Interleukin 8
A_24_P62783	-2.567	0.0002	FABP3	Fatty acid binding protein 3
A_23_P118571	-2.487	0.0030	SOST	Sclerostin
A_24_P257416	-2.364	0.0253	CXCL2	Chemokine (C-X-C motif) ligand 2
A_24_P299474	-2.352	0.0351	TENM2	Teneurin transmembrane protein 2
A_24_P105933	-2.348	0.0203	VIPR1	Vasoactive intestinal peptide receptor 1
A_23_P118815	-2.340	0.0040	BIRC5	Baculoviral IAP repeat containing 5 (survivin)

---

Log<sub>2</sub> FC, log<sub>2</sub> fold change between TRAIL stimulated and control cells; adj. p-val., global adjusted p-value after false discovery rate correction of p-value from moderated *t*-statistic obtained by testing for differential expression. Probes with the 20 highest and 20 lowest fold changes are shown. Some genes appear multiple times due to probe redundancy.

### 5.1.2 qPCR validation of differentially expressed genes

RT-qPCR validation was performed to confirm the DE mRNAs as defined by microarray quantification. In the microarray assays, the RNA samples (each from separate cell stimulations) were pooled: 8 unstimulated samples were pooled into 4 (2 samples per array) and 6 TRAIL-stimulated samples were pooled into 2 (3 samples per array). However, for qPCR validation the full set of 14 original RNA samples were used as templates for reverse transcription to produce fresh cDNA, and the resulting cDNA was subjected to qPCR to measure mRNA. TaqMan probes were selected to detect mRNA from 7 genes: *FIGF*, *ICAM1*, *PDGFD*, *PDGFRA*, *PDGFRB*, *SOST* and *VIPR1*. These genes were selected as they had high fold changes after TRAIL stimulation in the microarray analysis. Furthermore, based on searches of databases detailing known and predicted gene functions (e.g. NCBI Entrez Gene, UniProtKB), the selected genes were found to have potentially relevant functions in the effects of TRAIL that could warrant further investigation in this chapter. Emphasis for selection was placed on potential functional relevance of genes, rather than the very highest fold changes. The normalised, background-subtracted  $\log_2$  intensity values from microarray measurement (Figure 5.2A–G) were compared to ddCt values (normalised to *GAPDH* and a control sample) from qPCR measurement (Figure 5.2H–N). All genes investigated were found to have significantly DE mRNA as measured by qPCR, and all changes were in the same direction as those determined from the microarray data. Higher variability between replicate cDNA samples was observed in the qPCR measurement, which may be explained by the pooling of several cDNA samples for each replicate array from the microarray dataset.

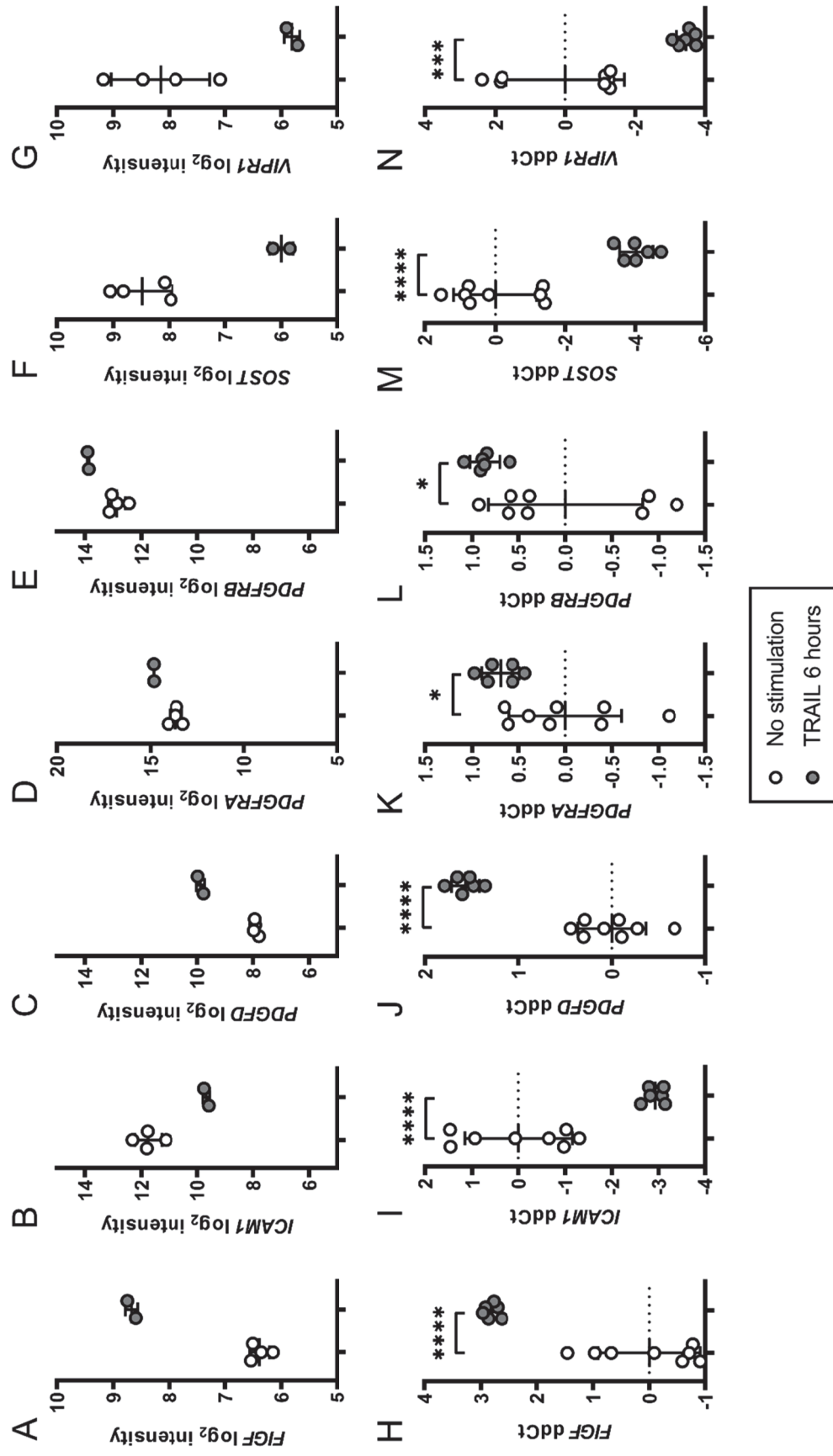


**Figure 5.2: qPCR validation of microarrays.** Human primary PASCs were stimulated with recombinant TRAIL or unstimulated for 6 hours and transcriptome measured by Agilent SurePrint G3 Human Gene Expression v2 microarrays. Linear models for microarray analysis was used to normalise and background correct array expression data. Key altered genes were from arrays (A–G) were validated by Taqman RT-qPCR (H–N). Bars show mean  $\pm$  SD,  $n = 2-4$  (cDNA pooled arrays) or 6–8 (original cDNA samples for qPCR). \*  $p < 0.05$ ; \*\*  $p < 0.01$ ; \*\*\*  $p < 0.001$ ; \*\*\*\*  $p < 0.0001$ ; \*\*\*\*\*  $p < 0.00001$ , Student's t-test of TRAIL stimulated vs. unstimulated control.

### **5.1.3 Gene ontology analysis**

To find patterns in gene expression changes after TRAIL stimulation of PSMCs, the set of all DE genes determined by LIMMA from microarrays were assessed for enrichment of GO terms using DAVID. The categories included for testing were: Genetic Association Database diseases, biological process GO terms, molecular function GO terms and KEGG pathways. These categories were selected to highlight biological processes that might be regulated by TRAIL in PSMCs. GO terms with more than 500 gene hits were excluded as they were deemed too broad to be informative. Significance threshold for enriched pathways was set to  $p < 0.05$  (Benjamini-Hochberg adjusted p-value). In this analysis, 18 terms were found to be significantly enriched after TRAIL stimulation (Table 5.2). Disease terms enriched after TRAIL stimulation in PSMCs included type 2 diabetes ( $p = 2.61 \times 10^{-6}$ ), cardiovascular diseases ( $p = 0.0013$ ) and coronary artery disease ( $p = 0.0239$ ). These may be broad terms associated with proliferating VSMCs – however, interestingly terms for steroid biosynthesis ( $p = 0.0184$ ) and metabolic pathways ( $p = 0.0325$ ) were also enriched in the context of TRAIL stimulation, suggesting a change in the metabolic phenotype of these PSMCs. Terms associated with VSMC muscularisation and contractility were enriched by TRAIL stimulation, including actin binding ( $p = 0.0066$ ), actin filament binding ( $p = 0.0092$ ) and muscle contraction ( $p = 0.0040$ ). Related terms also associated with TRAIL stimulation were those involving cytoskeletal function (structural constituent of cytoskeleton,  $p = 7.58 \times 10^{-4}$  and regulation of actin cytoskeleton,  $p = 0.0209$ ) as well as ECM-related processes (ECM organization,  $p = 0.0071$ ; ECM-receptor interaction,  $p = 0.0100$  and focal adhesion,  $p = 0.0026$ ). Further in-depth pathway topology analysis of gene expression changes induced by TRAIL stimulation is detailed in Chapter 5.1.5.

**Table 5.2: Gene ontology analysis of TRAIL-induced mRNA changes in PSMCs**

Category	Term	NDE	Fold enrichment	Adj. p-val.
GAD	Type 2 Diabetes	369	1.3270	2.61E-06
BP	Cell adhesion (GO:0007155)	95	1.7386	3.74E-04
MF	Structural constituent of cytoskeleton (GO:0005200)	33	2.5258	7.58E-04
GAD	Cardiovascular Diseases	50	2.0911	0.0013
KEGG	Focal adhesion (hsa04510)	49	1.9071	0.0026
BP	Muscle contraction (GO:0006936)	32	2.5122	0.0040
GAD	Skin cancer, non-melanoma	15	4.0884	0.0053
MF	Actin binding (GO:0003779)	59	1.7869	0.0066
BP	ECM organization (GO:0030198)	47	2.0143	0.0071
BP	Actin filament binding (GO:0051015)	34	2.1686	0.0092
KEGG	ECM-receptor interaction (hsa04512)	25	2.3039	0.0100
KEGG	Pathogenic Escherichia coli infection (hsa05130)	18	2.8297	0.0121
MF	Heparin binding (GO:0008201)	38	1.9996	0.0154
KEGG	Steroid biosynthesis (hsa00100)	10	4.0087	0.0184
KEGG	Regulation of actin cytoskeleton (hsa04810)	45	1.7180	0.0209
GAD	Coronary Artery Disease	98	1.5189	0.0239
KEGG	Phagosome (hsa04145)	34	1.8173	0.0318
KEGG	Metabolic pathways (hsa01100)	187	1.2299	0.0325

Categories: GAD, Genetic Association Database diseases; BP, biological process gene ontology (GO) terms;

MF, molecular function GO terms; KEGG, Kyoto Encyclopaedia of Genes and Genomes pathways. NDE, number of differentially expressed genes matching the term; fold enrichment, observed NDE / expected NDE; adj. p-val.,

Benjamini-Hochberg adjusted p-value for enrichment; ECM, extracellular matrix.

#### **5.1.4 Protein kinase phosphorylation changes**

To determine early changes in protein and protein phosphorylation levels, Kinex antibody arrays including 877 antibodies were used to quantify protein from unstimulated control PSMCs (n = 3) and PSMCs stimulated with recombinant TRAIL for 10 minutes (n = 4) or 60 minutes (n = 3). Z-scores were calculated for each antibody to reduce the effect of inter-array variability and these were compared between conditions using a Student's *t*-test. Proteins and phosphorylated proteins significantly altered ( $p < 0.05$ ) after either 10 or 60 minutes TRAIL stimulation vs. unstimulated control cells are shown in Table 5.3. Due to the high level of variation within the assay, global correction was not carried out and therefore the results were used only as additive data to the transcriptomic analysis. Changes in total protein and protein phosphorylation observed in this assay are combined with pathway topology analysis to highlight the extent of mRNA and protein changes within signalling pathways in Chapter 5.1.5.

**Table 5.3: Altered protein levels after TRAIL stimulation of PSMCs**

Target protein	Phospho site	TRAIL 10 min. vs unstimulated		TRAIL 60 min. vs unstimulated		Full target protein name
		Z-diff.	p-value	Z-diff.	p-value	
Adducin a/g	S662	0.34	0.035	0.12	0.364	Adducin alpha (ADD1)
APG1	Pan-specific	-0.15	0.044	-0.16	0.225	Glucose-6-phosphate 1-dehydrogenase 1, chloroplastic
AurKA	Pan-Specific	-0.02	0.905	0.22	0.036	Aurora Kinase A (serine/threonine protein kinase 6)
AurKB	Pan-Specific	0.05	0.258	0.10	0.033	Aurora Kinase B (serine/threonine protein kinase 12)
Npm1	T234/237	-0.59	0.047	-0.01	0.988	Nucleophosmin
CDK6	Pan-specific	-0.40	0.439	-0.91	0.007	Cyclin-dependent protein-serine kinase 6
CDK8	Pan-specific	-0.35	0.041	-0.37	0.019	Cyclin-dependent protein-serine kinase 8
Chk1	Pan-specific	-0.44	0.035	-0.35	0.064	Checkpoint protein-serine kinase 1
CK1d	Pan-specific	-0.26	0.007	-0.21	0.010	Casein protein-serine kinase 1 delta
Crystallin aB	Pan-specific	0.19	0.036	0.20	0.091	Crystallin alpha B (heat-shock 20 kDa like-protein)
ERB2	T686	0.10	0.018	0.13	0.018	ErbB2 (Neu) receptor-tyrosine kinase
FAK	S722	0.39	0.068	0.35	0.050	Focal adhesion protein-tyrosine kinase
Hsp27	S86	-0.10	0.861	-0.79	0.034	Heat shock 27 kDa protein beta 1 (HspB1)
JAK1	Y1022	0.18	0.449	0.47	0.048	Janus protein-tyrosine kinase 1
JAK3	Pan-specific	0.08	0.421	0.11	0.041	Janus protein-tyrosine kinase 3
Krs-1	Pan-specific	-0.34	0.560	-0.93	0.024	Protein-serine kinase suppressor of Ras 1
MAPKAPK2	Pan-specific	0.11	0.085	0.18	0.026	MAPK-activated protein kinase 2

MEK1	T386	0.15	0.159	0.28	0.044	MAPK/ERK protein-serine kinase 1 (MKK1)
Mnk2	Pan-specific	-0.60	0.031	-0.67	0.020	MAP kinase-interacting protein-serine kinase 2
Nek2	Pan-specific	-0.43	0.276	-0.84	0.000	NIMA-related protein-serine kinase 2
PAK3	Pan-specific	-0.12	0.247	0.28	0.001	p21-activated kinase 3 (beta)
PKCd	Y311	0.18	0.390	0.28	0.047	Protein-serine kinase C delta
PP4C (X/C)	Pan-specific	0.07	0.403	0.16	0.014	Protein-serine phosphatase X
PRAS40	T246	-0.03	0.860	0.25	0.004	Proline-rich Akt substrate 40 kDa (Akt1S1)
Pyk2	Pan-specific	-0.29	0.216	-0.32	0.015	Protein-tyrosine kinase 2
Raf-1	Pan-specific	-0.34	0.361	-0.69	0.018	Rad17 homolog
Rb	S780	0.26	0.056	0.27	0.027	Retinoblastoma-associated protein 1
Src	Pan-specific	-0.21	0.416	0.09	0.035	Src proto-oncogene-encoded protein
STAT3	Y704	-0.56	0.119	-0.85	0.008	Signal transducer and activator of transcription 3
WNK1	S382	0.12	0.277	0.21	0.046	Serine/threonine-protein kinase WNK1

---

Control, unstimulated PSMCs; TRAIL 10/60 min., PSMCs stimulated with TRAIL for 10 or 60 minutes; Z-diff, difference in mean Z-scores between conditions; p-value, calculated using Student's *t*-test for significance (antibodies with  $p < 0.05$  for either comparison are shown in this table).

### **5.1.5 Pathway topology analysis**

To determine changes to signalling pathways induced by TRAIL in PASCs, pathway topology enrichment analysis of DE mRNA from microarrays determined by LIMMA was carried out using the SPIA R package. The SPIA method matches DE genes to KEGG signalling pathways and incorporates two metrics – the number of genes altered within a pathway, and the predicted perturbation of the pathway (based on the total impact of gene changes within the pathway) – to assess the overall effect on the pathway. These metrics were combined using Fisher's combined probability test to give a global p-value for the probability of significantly altered pathways (Figure 5.3). After FDR correction for multiple testing, 9 pathways were determined to be significantly altered by TRAIL stimulation in PASCs. Activated pathways included gap junction (hsa04540) and focal adhesion (hsa04510), which was also the most significantly altered pathway with 40 of 201 genes DE and a global p-value of  $3.35 \times 10^{-8}$ . Inhibited pathways included chemokine signalling (hsa04062), TGF $\beta$  signalling (hsa04350), ECM-receptor interaction (hsa04512) and regulation of actin cytoskeleton (hsa04810). Notably, several of these pathways highlighted by pathway topology analysis – relating to cytoskeletal and ECM functions – were also observed in the previous GO term enrichment analysis (Chapter 5.1.3).

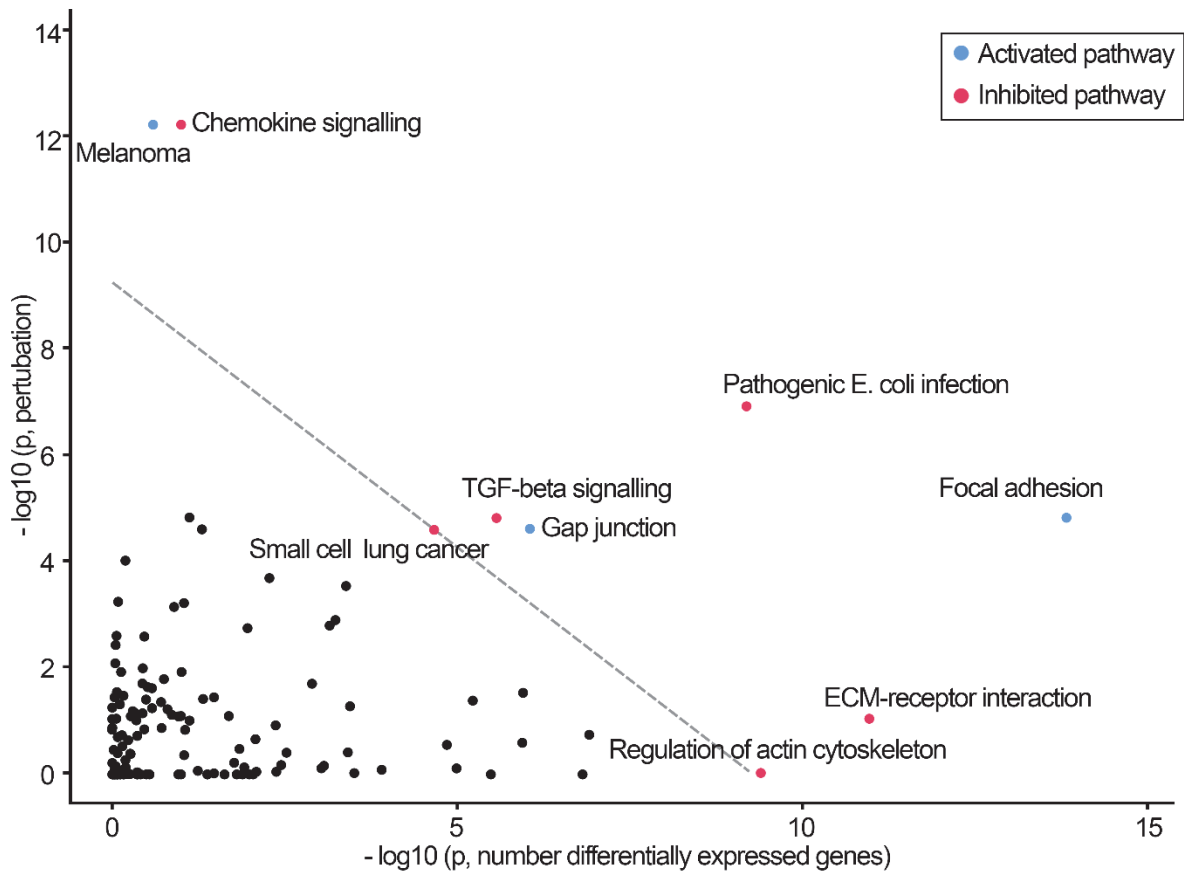


**Figure 5.3: Pathways activated by TRAIL stimulation of PSMCs.** Pathway topology analysis of differentially expressed (DE) genes using signalling pathway impact analysis (SPIA). Each point represents a Kyoto Encyclopaedia of Genes and Genomes (KEGG) pathway. The x-axis shows the  $-\log_{10}$  of the p-value of obtaining the number of DE genes (NDE) by chance. The y-axis shows the  $-\log_{10}$  of the p-value of the perturbation of a pathway by chance (PERT), considering pathway topology. Dashed line shows significance threshold after combining the NDE and PERT using Fisher's method, with global p-values after false discovery rate (FDR) correction. Of the significantly altered pathways, blue points indicate significantly activated pathways and red points indicate significantly inhibited pathways. TGF-beta, transforming growth factor  $\beta$ ; ECM, extracellular matrix.

After 6 hours of TRAIL stimulation in PASMCs, there were extensive mRNA expression alterations affecting the TGF $\beta$  signalling pathway, leading to predicted overall inhibition (Figure 5.4). Expression of mRNA from 16 genes from this pathway were altered by TRAIL, including *TGF $\beta$ 3* (downregulated) and *TGF $\beta$  receptor 1* (downregulated), as well as the transcriptional co-activator *E1A Binding Protein P300 (P300)*. Also affected was the BMP signalling incorporated in this KEGG pathway, including *BMP4* (upregulated), *BMP6* (downregulated) and the *activin receptor 2A (ACVR2A)*; upregulated). Downstream of BMP signalling, the nuclear transcriptional regulators *inhibitor of DNA binding 2 and 3 (ID2 and ID3)* were also downregulated by TRAIL.

A pathway highly upregulated by TRAIL in PASMCs was the focal adhesion pathway, including ECM components (e.g. *COL1A2*, *COL4A1*, *COL4A2*, *COL4A4* and *COL6A1*), growth factors (e.g. *VEGFA*, *FIGF* and *PDGFD*), integrins and other transmembrane receptors (e.g. *ITGA3*, *ITGA4*, *ITGA11*, *ITGB3*, *ITGB5*, *PDGFRA*, *PDGFRB*) and various intracellular components (summarised in Figure 5.5). Additionally, at the 10- or 60-minute stimulation timepoints, several changes in protein levels and phosphorylated protein levels (determined by Kinex antibody arrays; detailed in Chapter 5.1.4) were detected in the focal adhesion pathway (Figure 5.5). These included elevated phosphorylation of key protein kinase regulators of the pathway at 60 minutes after TRAIL stimulation: at the S722 amino acid residue of focal adhesion kinase (FAK) and the Y311 amino acid residue of protein kinase C delta ('PKC'). Increased phosphorylation was also observed at the T386 amino acid residue of MAPK/ERK protein-serine kinase 1 (MEK1) – an important element of the MAPK signal transduction pathway, which can regulate cell proliferation and survival.

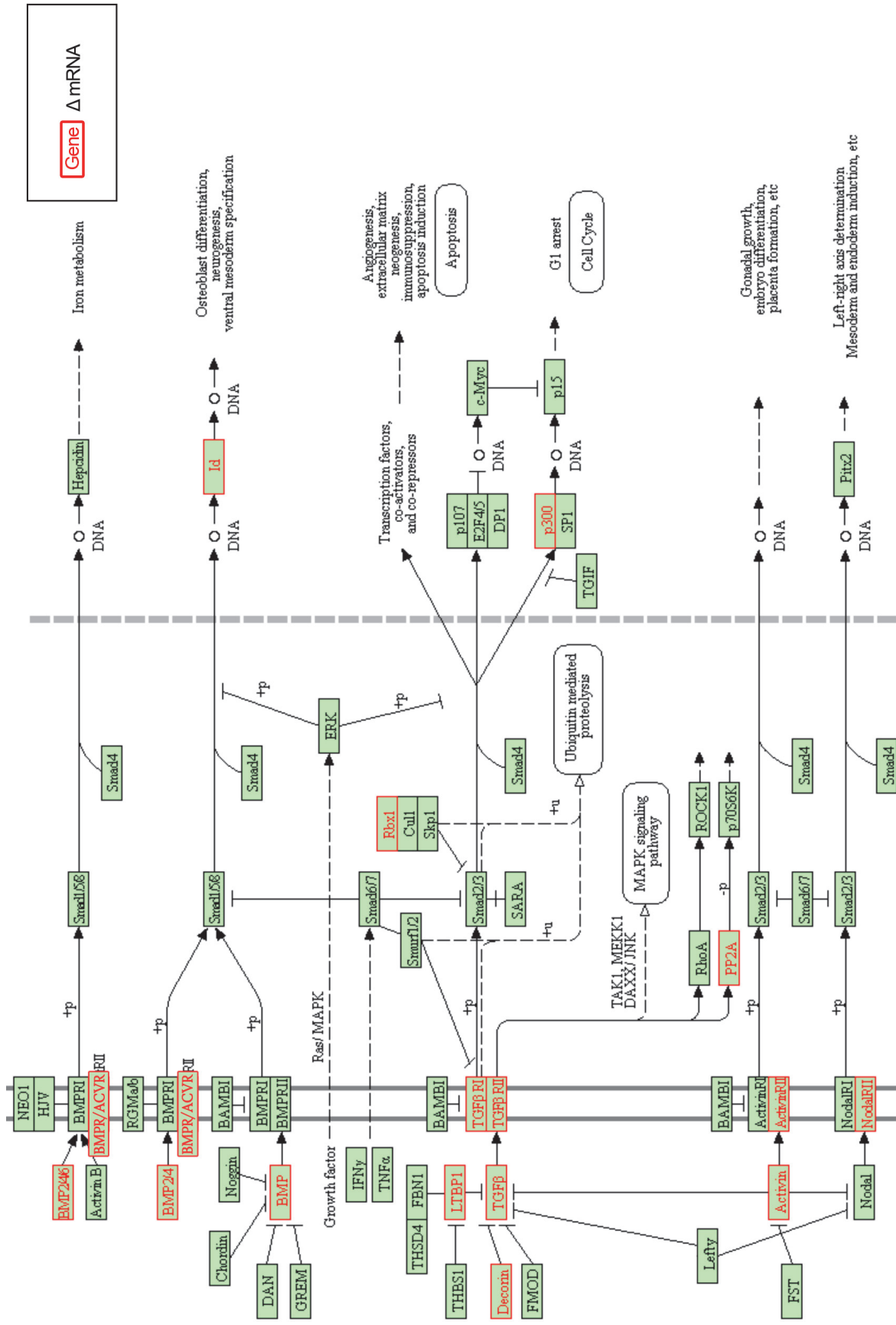


**Figure 5.4: TGFβ signalling pathway is inhibited by TRAIL stimulation of PASMCs.** Summary of the human transforming growth factor β (TGFβ) signalling KEGG pathway (hsa045350). Differentially expressed human pulmonary artery smooth muscle cells (PASMCs) vs. unstimulated control PASMCs highlighted in red. BMP, bone morphogenetic protein; BMPR/ACVR, BMP receptor 2 / activin receptor 2A; TGFβR/II, TGFβ receptor I/II; Id, inhibitor of DNA binding.

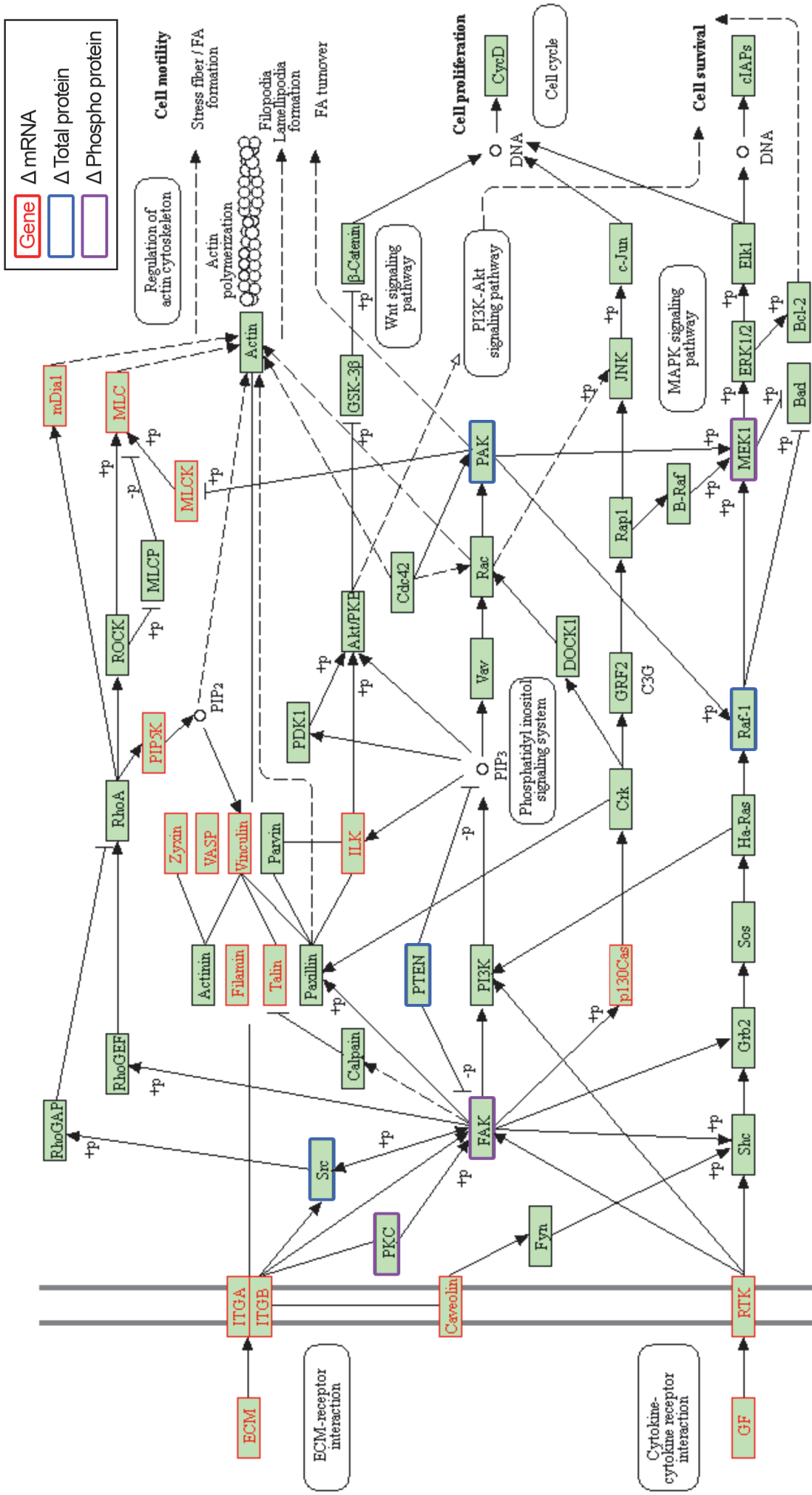


**Figure 5.5: Focal adhesion pathway is activated by TRAIL stimulation of PASM cells.** Summary of the human focal adhesion KEGG pathway (hsa04510). Differentially expressed mRNA from 6-hour TRAIL-stimulated human pulmonary artery smooth muscle cells (PASM cells) vs. unstimulated control PASM cells are highlighted in red. Altered levels of global protein or phosphorylated protein at 10- or 60-minute TRAIL stimulation are highlighted in blue or purple respectively. ECM, extracellular matrix; GF, growth factors; ITGA/B, integrins  $\alpha/\beta$ ; PKC, protein kinase C; FAK, focal adhesion kinase; MEK1, MAPK/ERK protein-kinase 1.

## 5.2 Expression of TRAIL targets are altered in animal models and PAH patients

In Chapter 5.1, genes and signalling pathways – e.g. TGF $\beta$ /BMP and focal adhesion pathways – were identified as being regulated by TRAIL in human primary PSMCs *in vitro*. While the signalling pathways identified have functions linked to PAH, further research was required to determine whether the genes are involved in PAH pathogenesis *in vivo*. As TRAIL is pathogenically linked to the development of PAH (Dawson et al. 2014, Hameed et al. 2012) and induces proliferative and pro-angiogenic changes in pulmonary vascular cells – PAECs (Cantarella et al. 2014, Cartland et al. 2016, Secchiero et al. 2003, Zauli et al. 2003) and PSMCs (Hameed et al. 2012, Kavurma et al. 2008, Secchiero et al. 2004) – I hypothesised that TRAIL might also induce changes to the genes and pathways identified in Chapter 5.1 in the context of PAH disease. To test this, the expression of TRAIL-regulated genes identified *in vitro* was examined at the mRNA level in lungs from bleomycin mice (Chapter 3) and in lungs from SuHx mice (Chapter 4) and at the protein level in serum from patients. Although the bleomycin mice in the present study had a mild PAH haemodynamic phenotype, they did develop substantial pulmonary vascular remodelling and therefore were still potentially useful in further exploring the functions of TRAIL-regulated genes. These mice also offer a system to investigate a role for TRAIL and TRAIL-regulated genes driving the vascular-associated fibrosis in the mice subjected to IP bleomycin. It is possible that the fibroblast-derived TRAIL found to be important in Chapter 3 may have effects on PSMCs. Similarly, in addition to IPAH patients these genes were also examined at the serum protein level in SSc and SSc-PAH patients. The genes selected for further investigation were 6 of those used to validate the mRNA changes from microarray measurement by RT-qPCR (Chapter 5.1.2). These were chosen based on the high fold changes induced by TRAIL stimulation in PSMCs in addition to their presence in pathways identified (Chapter 5.1) and/or functions putatively relevant to PAH pathogenesis. Protein levels were also compared to metrics of clinical severity within a PAH patient cohort to establish a possible relationship.

### 5.2.1 *TRAIL-regulated genes in bleomycin mice*

To investigate whether TRAIL-regulated genes from PASCs might play a role in bleomycin-induced PF or PAH, RNA was extracted from whole lungs of mice subjected to IP bleomycin and mRNA quantified by TaqMan RT-qPCR (Figure 5.6A–E). Also included in this analysis were samples from bleomycin mice with fibroblast-specific *TRAIL* deletion (*TRAIL*<sup>tm1c/tm1c</sup>-COL1A2-CRE-ERT mice given tamoxifen) and global *TRAIL* deletion (*TRAIL*<sup>tm1d/tm1d</sup>-PGK-Cre mice). *SOST* mRNA was reduced in lungs of both *TRAIL* normal bleomycin mice groups (Figure 5.6E) – as well as in mice with fibroblast-specific *TRAIL* deletion (mean ddCt normalised to *GAPDH* -2.606 vs. -0.4504,  $p = 0.0002$ ) – but not in mice with global deletion of *TRAIL*. The global *TRAIL* deleted mice also had significantly higher *SOST* mRNA compared to the *TRAIL* normal bleomycin control groups. No alterations in *PDGFD* mRNA levels were found due to bleomycin (Figure 5.6C), however the mice with fibroblast-specific *TRAIL* deletion had significantly reduced *PDGFD* compared to saline control mice (mean ddCt -3.424 vs. -1.517,  $p = 0.0136$ ), *TRAIL* normal bleomycin mice given tamoxifen (mean ddCt -3.424 vs. -1.131,  $p = 0.0021$ ) and globally *TRAIL* deleted bleomycin mice (mean ddCt -1.270 vs. -3.424,  $p = 0.0212$ ). *PDGFRB* mRNA was reduced in bleomycin wildtype mice (BLM - *TRAIL*<sup>tm1c/wt</sup>) compared to saline control mice (mean ddCt -2.143 vs. -0.3561  $p = 0.0068$ ), but no other differences were observed between other groups (Figure 5.6D). No mRNA alterations due to the bleomycin insult or between groups were detected in the genes *FIGF* (Figure 5.6A) or *ICAM1* (Figure 5.6B).

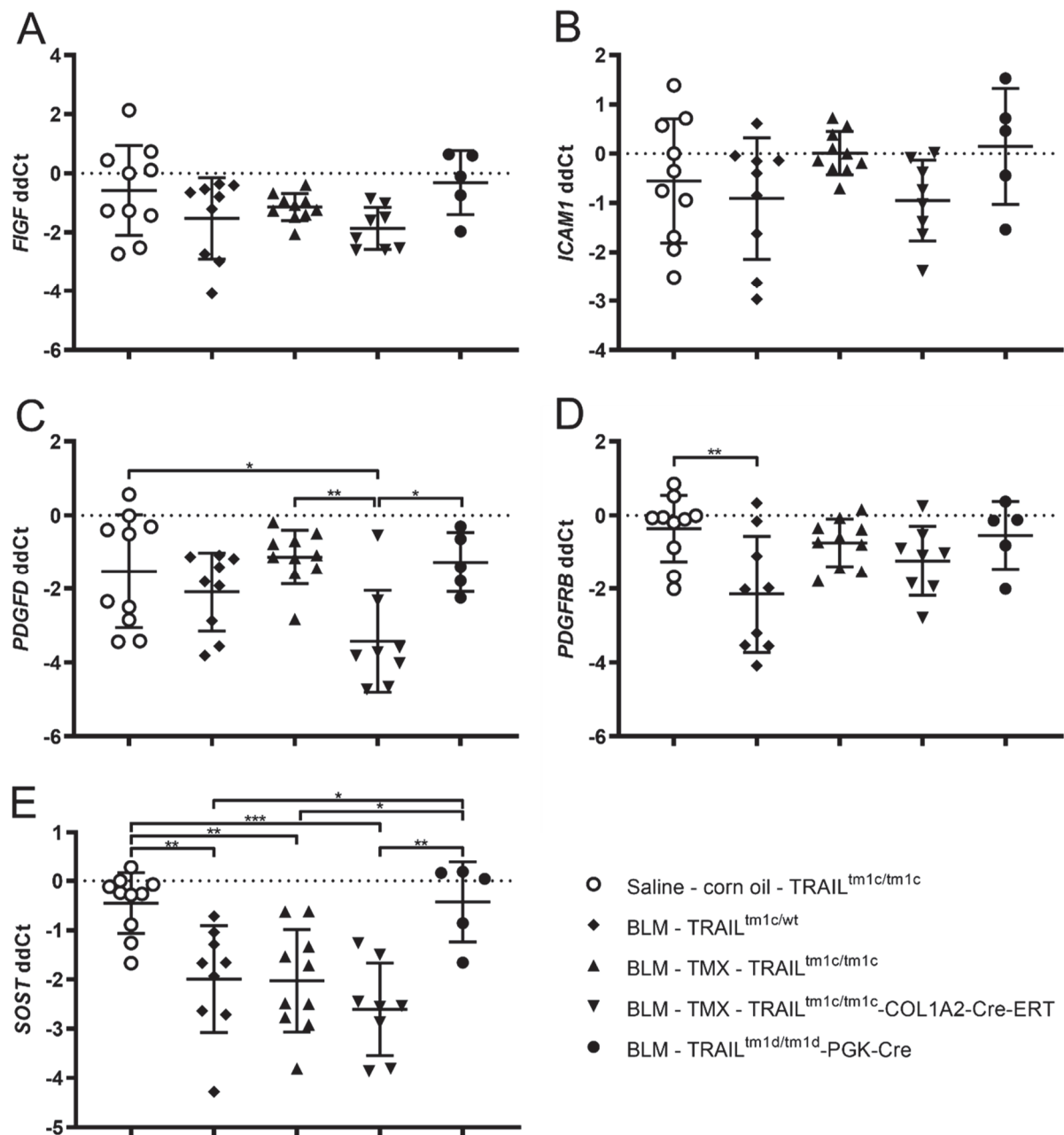


**Figure 5.6: Expression of TRAIL-regulated genes in lungs of bleomycin mice.** Mice were subjected to bleomycin (BLM) or saline IP injection twice weekly for 4 weeks and culled at day 35. Two groups had previously undergone tamoxifen (TMX) 5x daily IP injections at 5–8 weeks old. mRNA was measured in cDNA from whole mouse lungs by TaqMan RT-qPCR. Data shown are threshold cycle values normalised to a reference gene (*GAPDH*) then to a reference sample (delta-delta Ct; ddCt). Bars show mean  $\pm$  SD,  $n = 5-10$ . \*  $p < 0.05$ , \*\*  $p < 0.01$ ; \*\*\*  $p < 0.001$ , \*\*\*\*  $p < 0.0001$ , one-way ANOVA with Sidak's multiple comparisons test comparing the mean of each group.

### 5.2.2 *TRAIL-regulated genes in SuHx mice*

To investigate whether TRAIL-regulated genes from PASMCs might play a role in mice with PAH induced by SuHx, RNA was extracted from whole lungs of mice subjected to the SuHx model and mRNA quantified by TaqMan RT-qPCR (Figure 5.7A–E). This experiment also included samples from SuHx mice with VSMC-specific *TRAIL* deletion (*TRAIL*<sup>tm1c/tm1c-SMMHC-CRE-ERT2</sup> mice given tamoxifen). For the *FIGF* gene, increased mRNA was measured in lungs of all SuHx groups compared to normoxic control mice (Figure 5.7A) – including mice with VSMC-specific *TRAIL* deletion (mean ddCt -0.6548 vs. -0.06862,  $p = 0.0280$ ). However, no differences in *FIGF* were observed between SuHx groups. *SOST* mRNA was significantly increased in SuHx mice with *TRAIL* deleted in VSMCs compared to normoxic control mice (mean ddCt 0.2835 vs. -1.086,  $p = 0.0160$ ; Figure 5.7) as well as compared to Cre-negative mice in SuHx given tamoxifen (mean ddCt 0.2835 vs. -1.351,  $p = 0.0053$ ). However, *SOST* mRNA was also elevated in mice with the SMMHC-Cre-ERT2 allele given tamoxifen when compared to saline control mice or Cre-negative mice in SuHx given tamoxifen. The reason for this difference between disease control groups is unclear and cannot be accounted for by the presence of the SMMHC-Cre-ERT2 allele alone, as these mice were not given tamoxifen and so should not have any *TRAIL* deletion. No differences due to the SuHx insult were detected in the genes *ICAM1* (Figure 5.7B), *PDGFD* (Figure 5.7C) or *PDGFRB* (Figure 5.7D).

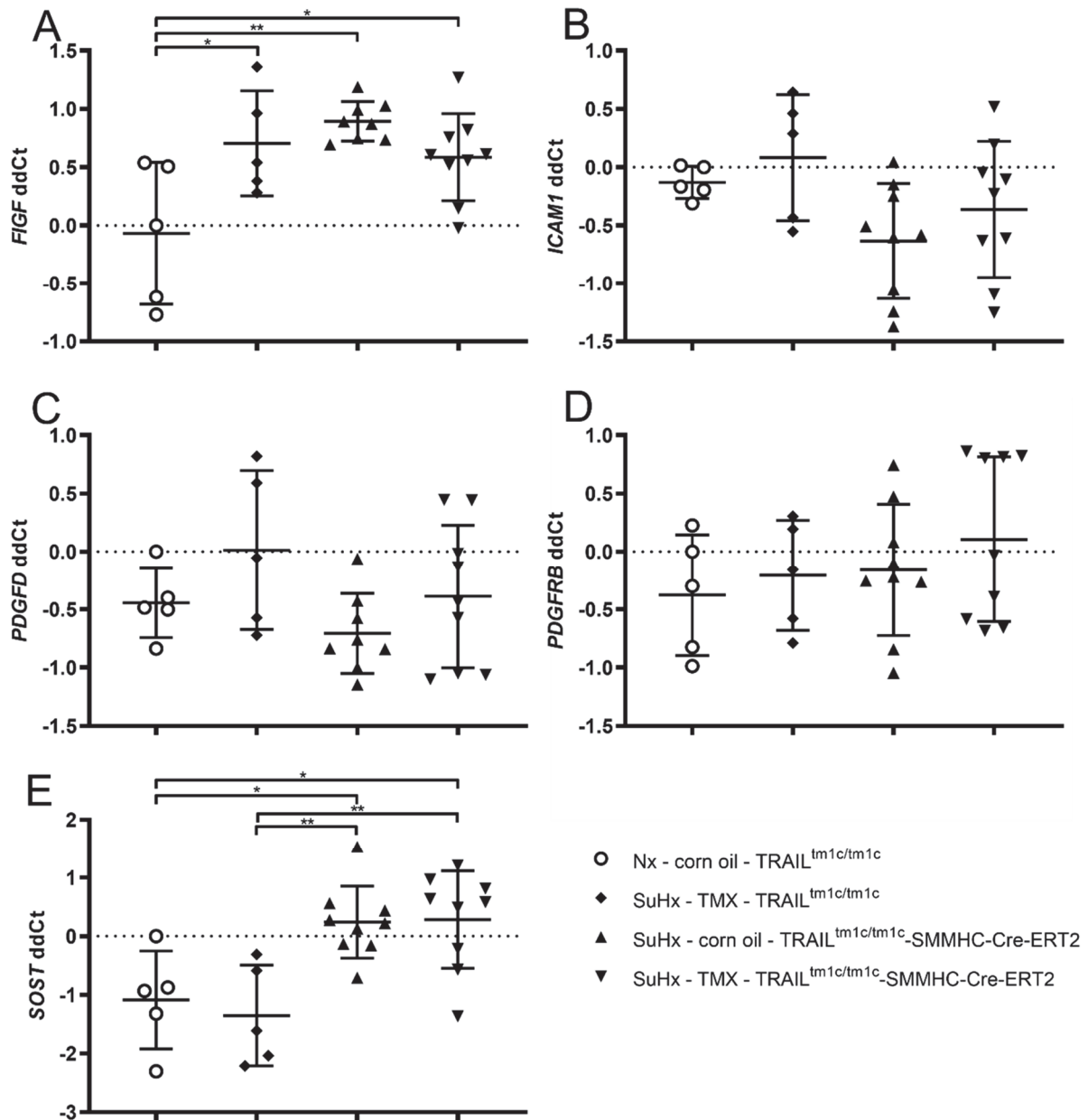


**Figure 5.7: Expression of TRAIL-regulated genes in lungs of SuHx mice.** Mice were subjected to 3 weekly SC Sugen 5416 injections with hypoxia (10% oxygen; SuHx) or normoxic conditions (Nx) and culled after 3 weeks. Two groups had previously undergone tamoxifen (TMX) 5x daily IP injections at 5–8 weeks old. mRNA was measured in cDNA from whole mouse lungs by TaqMan RT-qPCR. Data shown are threshold cycle values normalised to a reference gene (*GAPDH*) then to a reference sample (delta-delta Ct; ddCt). Bars show mean  $\pm$  SD,  $n = 5-10$ . \*  $p < 0.05$ , \*\*  $p < 0.01$ , one-way ANOVA with Sidak's multiple comparisons test comparing the mean of each group.

### **5.2.3 TRAIL-regulated genes in patient serum**

Serum protein measurement was employed as a prospective method for detecting alterations to TRAIL targets in the vasculature in PAH patients. To do this, protein levels were measured in serum samples from Sheffield PH Biobank patients (IPAH, n = 30; SSc without PAH, n = 22; SSc with PAH (SSc-PAH), n = 23) and healthy volunteers (n = 29) on a validated Luminex-based platform by Myriad RBM. SSc and SSc-PAH patients were included to explore possible differences between 'pure' IPAH and PAH with associated autoimmune disease. The protein panel for this assay was used for a separate study, so it included many other target proteins (data not shown). The proteins included for this analysis were 4 of those determined as TRAIL-regulated in the present study, in addition to a single TRAIL receptor that was measured in the assay, TRAIL-R3 (DcR1). The serum protein levels measured were visualised as violin plots, to enable clear comparisons between larger populations (Figure 5.8A–E). FIGF (Figure 5.8A) and SOST (Figure 5.8D) proteins were both elevated in serum from IPAH and SSc-PAH patients, when compared to healthy volunteers and SSc patients without PAH (e.g. SOST in IPAH vs. healthy volunteers, mean 1061 ng/ml vs. 555.1 ng/ml,  $p < 0.0001$ ; SOST in SSc-PAH vs SSc, mean 991.0 ng/ml vs. 639.2 ng/ml,  $p = 0.0057$ ). A similar pattern was observed for TRAIL-R3 protein (Figure 5.8E); however, it was found at much lower levels overall (approximately one order of magnitude). Nevertheless, significantly elevated serum TRAIL-R3 was detected in IPAH and SSc-PAH patients vs. healthy volunteers – interestingly, SSc-PAH patients also had more than IPAH patients (mean 15.79 ng/ml vs. 11.99 ng/ml,  $p = 0.0189$ ). Serum ICAM1 was also increased in the IPAH and SSc-PAH patients vs. healthy volunteers or SSc patients without PAH (Figure 5.8B). However, ICAM1 protein was also elevated in SSc patients without PAH vs. healthy volunteers (mean 152.8 ng/ml vs. 99.44 ng/ml,  $p = 0.0306$ ) – the only case in which SSc patients had an increased serum protein compared to healthy controls. However, serum levels of PDGFRB protein were reduced in all disease groups: IPAH, SSc and SSc-PAH patients (Figure 5.8C). No differences in PDGFRB level were observed between IPAH, SSc or SSc-PAH patients.

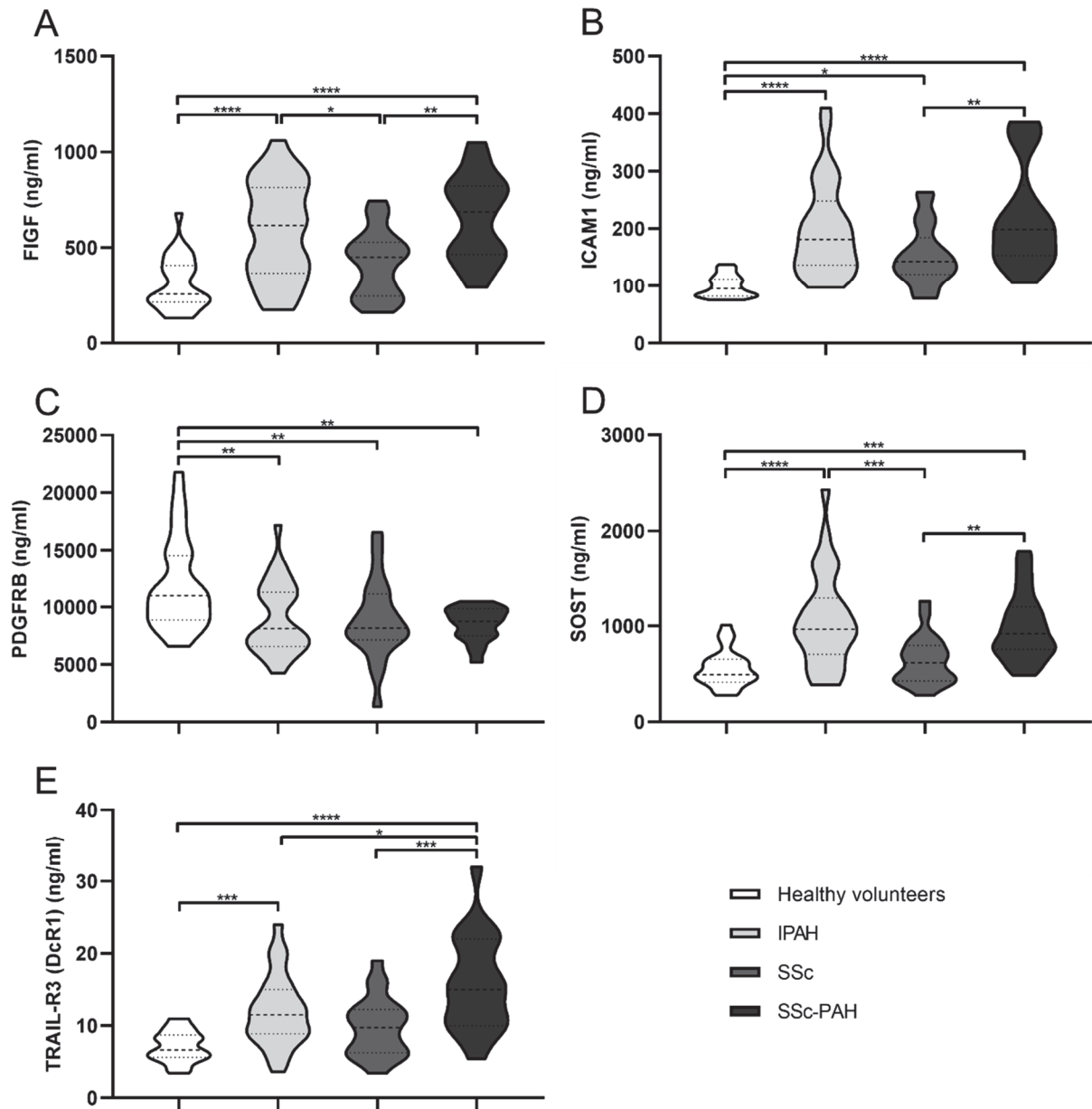


**Figure 5.8: Expression of TRAIL-regulated genes in patient serum.** Violin plots of protein levels measured in serum samples from Sheffield PH Biobank patients and healthy volunteers on a validated Luminex-based platform. Groups included are healthy volunteers (n = 29), idiopathic pulmonary arterial hypertension (IPAH; n = 30), systemic sclerosis without PAH (SSc; n = 22) and SSc with PAH (SSc-PAH; n = 23). Dashed lines show median  $\pm$  interquartile range. \* p < 0.05, \*\* p < 0.01; \*\*\* p < 0.001, \*\*\*\* p < 0.0001, one-way ANOVA with Sidak's multiple comparisons test comparing the mean of each group.

#### 5.2.4 Correlation of serum sclerostin with PAH clinical severity

As differences in serum protein levels of TRAIL-regulated genes were observed in PAH patients (Chapter 5.2.3), I went on to examine possible relationships between the protein levels and measures of clinical severity. To do this, linear regression was performed comparing the serum protein measurements with RV cardiac index and PVR in a combined cohort of PAH patients (including IPAH and SSc-PAH patients previously assessed;  $n = 68$ ). In this PAH cohort serum levels of sclerostin (SOST) protein were found to be negatively correlated with RV cardiac index ( $R^2 = 0.1819$ ,  $p = 0.0003$ ; Figure 5.9A) and positively correlated with PVR ( $R^2 = 0.08763$ ,  $p = 0.0142$ ; Figure 5.9B). Both of these associations indicate increased sclerostin protein is present in patients with worse PAH phenotype. A significant linear correlation with PAH clinical severity was not observed for FIGF, ICAM1, PDGFRB or TRAIL-R3 proteins (data not shown).

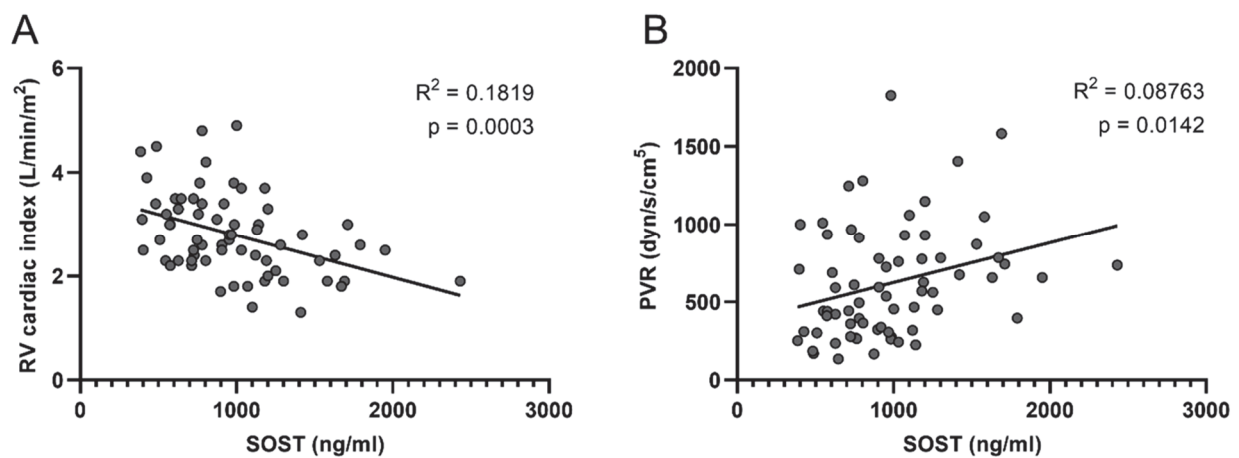


**Figure 5.9: Correlation of serum sclerostin with PAH clinical severity.** Sclerostin (SOST) protein was measured in serum samples from Sheffield PH Biobank patients on a validated Luminex-based platform. A combined PAH patient sample was studied ( $n = 68$ ), for which clinical data were also available. Linear regression analysis was performed to determine the relationship between serum SOST and metrics of PAH clinical severity: right ventricular (RV) cardiac index and pulmonary vascular resistance (PVR).

### 5.3 Summary

The aims of this chapter were to further explore the effects of TRAIL-induced signalling in human PASMCs and to validate these effects in the context of animal models and human PAH. In summary:

- TRAIL stimulation of PASMCs caused extensive protein kinase phosphorylation and transcriptomic alterations in genes and pathways known to be important in PAH e.g. TGF $\beta$ /BMP, focal adhesion and ECM regulation.
- In PASMCs TRAIL downregulates *SOST* mRNA expression. *SOST* was reduced in lungs of bleomycin mice, but not in mice with global *TRAIL* deletion. In contrast, *SOST* was upregulated in lungs of SuHx mice, including those with VSMC-specific *TRAIL* deletion (i.e. no down-regulation). Levels of serum *SOST* protein were elevated in patients with PAH and were correlated with clinical severity.
- In PASMCs, TRAIL increases the expression of *PDGFD* mRNA. *PDGFD* was downregulated in whole lungs after fibroblast-specific TRAIL deletion in bleomycin mice but not significantly altered in SuHx, suggesting that reduced PDGFD may be associated with increased fibrosis.
- *FIGF* mRNA was not significantly regulated in the bleomycin model but was increased in SuHx mice lungs. However, there was no significant difference in expression following TRAIL deletion in fibroblasts (bleomycin model) or VSMCs (SuHx). FIGF was also elevated in the serum of patients with PAH.
- Other TRAIL targets e.g. ICAM1, and the TRAIL receptor TRAIL-R3 were elevated in serum from patients with PAH.

## 5.4 Discussion

### 5.4.1 *TRAIL inhibits TGF $\beta$ /BMP signalling*

In this chapter I presented transcriptomic and protein phosphorylation data from TRAIL-stimulated PSMCs, in order to expand upon the known effects of TRAIL in these cells, such as ERK1/2 phosphorylation (Hameed et al. 2012). In the present study, TRAIL stimulation of PSMCs caused extensive transcriptomic changes in genes and pathways known to be important in PAH. For example, TRAIL inhibited the TGF $\beta$ /BMP signalling pathway; changing expression of several transcripts. The importance of BMP signalling has been highlighted in heritable PAH patients, where causative loss-of-function mutations affecting the BMP receptor and TGF $\beta$  receptor superfamily are found in 60% of patients, but are also found in 10–20% of patients with IPAH (International et al. 2000, Deng et al. 2000). In the present study, TRAIL also induced downregulation of mRNA from extracellular factors *TGF $\beta$ 3* and *BMP6* and the receptors *TGF $\beta$ R1* and *ACVR2A* from this pathway in PSMCs. Downstream effectors of the pathway were also affected by TRAIL: the transcriptional co-activator *P300* and nuclear transcriptional regulators *Id2* and *Id3*.

TRAIL stimulation of PSMCs also downregulated expression of *sclerostin* (*SOST*) mRNA, and *sclerostin* mRNA was reduced in lungs of mice with bleomycin-induced PF and PAH, but not in mice with global *TRAIL* deletion, suggesting a link between TRAIL-regulated sclerostin and development of disease. In SuHx mice lungs, *sclerostin* mRNA was upregulated in two of the three disease groups, but apparently was not affected by VSMC-specific *TRAIL* deletion. Sclerostin is known as an osteocyte-secreted glycoprotein linked to BMP signalling, which acts as a negative regulator of bone formation by suppressing mineralisation of osteoblasts (Poole et al. 2005). Mutations leading to loss of sclerostin in humans cause sclerosteosis, a condition characterised by high bone mass (Brunkow et al. 2001). In the context of bone formation, based on its sequence similarity with other proteins, sclerostin was originally suggested to suppress osteocyte differentiation and function via antagonism of BMP signalling

(Brunkow et al. 2001, Winkler et al. 2003). However, it was later suggested that sclerostin is actually an antagonist of Wnt signalling, which is closely linked to BMP signalling (Li et al. 2005, van Bezooijen et al. 2004, van Bezooijen et al. 2007). Wnt signalling has also been linked to PAH pathobiology – e.g. upregulation of Wnt pathway components was observed in explanted IPAH plexiform lesions (Laumanns et al. 2009) and Wnt signalling was subsequently associated with BMP2-induced PAEC proliferation and survival (de Jesus Perez et al. 2009). In PASMCs, BMP signalling has also been demonstrated to induce Wnt signalling to suppress proliferation, but enhance motility (Perez et al. 2011). To provide further evidence for importance of TRAIL-regulated genes in human PAH, I also measured the serum protein levels of several of these genes in PAH and other patients. Interestingly, sclerostin protein was elevated in serum from PAH and SSc-PAH patients, compared to healthy volunteers or SSc patients without PAH. Within a PAH patient cohort, serum sclerostin was associated with clinical severity of PAH measured by PVR and RV cardiac index.

Furthermore, increased serum sclerostin levels have also been linked to the presence of atherosclerosis and cardiovascular disease in humans (Morales-Santana et al. 2013, Novo-Rodríguez and García-Fontana 2018) and to cardiovascular mortality (Novo-Rodríguez and García-Fontana 2018). Expression of osteocyte phenotype markers including sclerostin has also been associated with calcification of VSMCs linked to atherosclerosis (Zhu et al. 2011). A connection between development of atherosclerosis and PAH has been demonstrated by the development of PAH in atherosclerosis-prone ApoE<sup>-/-</sup> mice fed a high-fat diet (Hansmann et al. 2007) or more severely in ApoE<sup>-/-</sup> mice fed a high-fat, high-cholesterol diet (Lawrie et al. 2011). In the present study TRAIL stimulated altered gene expression in PASMCs significantly associated with GO terms for diseases including type 2 diabetes, cardiovascular diseases and coronary artery disease, in addition to biological processes such as metabolic pathways and steroid biosynthesis, suggesting a TRAIL-mediated change in the metabolic phenotype of these PASMCs. This is in accordance with further evidence for metabolic dysfunction as a driver of PAH. For example, treatment of rats with dichloroacetate, an inhibitor of glycolysis,

was shown to reverse experimental hypoxic PH (Michelakis et al. 2002) and in humans, a shift from oxidative phosphorylation to glycolytic state (the Warburg effect) has been observed in IPAH lungs and also in explanted PAECs (Xu et al. 2007). Treatment of IPAH patients with dichloroacetate also improved PVR and functional capacity – albeit with a varied response, purportedly due to genetic variation (Michelakis et al. 2017). Furthermore, experimental inhibition of BMP2 induces mitochondrial dysfunction and glycolysis in PAECs (Diebold et al. 2015), suggesting a link between BMP signalling and metabolic dysfunction. Interestingly, in the present study expression of the vascular cellular adhesion molecule ICAM1 was downregulated by TRAIL in PSMCs and elevated in serum of PAH patients. ICAM1 is predominantly recognised for its role in promoting adhesion of leukocytes when expressed by ECs and circulating soluble ICAM1 levels have been linked to cardiovascular disease (Hwang et al. 1997, Jude et al. 2002, Ridker et al. 2000) and risk of cardiovascular events and mortality (Luc et al. 2003, Ridker et al. 1998).

The evidence presented here implicates TRAIL in modulating the TGF $\beta$ /BMP signalling pathways in PSMCs. Sclerostin is also indicated as a novel biomarker for PAH, although the relationship between decreased sclerostin in PSMCs induced by TRAIL, decreased sclerostin in bleomycin mice lungs, increased sclerostin in SuHx mice lungs and increased sclerostin found in PAH patient serum is unclear. It is possible that sclerostin is a protective factor released by other vascular cells such as PAECs into the circulation. Given its influence on BMP and Wnt signalling, further functional investigation is warranted into the role of sclerostin in the PAH molecular processes.

#### **5.4.2 TRAIL activates focal adhesion**

In the present study TRAIL activated the focal adhesion pathway in PSMCs, with altered expression of numerous transcripts within the pathway in addition to activation of FAK and MEK1 proteins indicated by increased phosphorylation. Furthermore, GO terms relating to ECM and cytoskeletal functions were enriched in the DE PSMC transcriptome after TRAIL

stimulation. The focal adhesion pathway and FAK in particular is important in the regulation of cell migration through interactions with growth factors and with the ECM via integrins (Sieg et al. 2000). Enhanced motility in SMCs is also a key process in the pulmonary vascular remodelling found in PAH (Tajsic and Morrell 2011). Furthermore, dysregulated focal adhesion has been indicated in PAH – unlike healthy PSMCs, explanted PSMCs from PAH patients can spontaneously migrate in the absence of growth factors (Wilson et al. 2015) and additionally elevated FAK activation has been observed in PSMCs from PAH patients compared to healthy controls (Paulin et al. 2014). Experimental inhibition of FAK in PSMCs *in vitro* can reduce proliferation and migration (Lin et al. 2017, Paulin et al. 2014) and therapeutic inhibition of FAK by inhaled FAK-siRNA or orally-delivered FAK inhibitor has been demonstrated to improve PAH in monocrotaline rats, with reduced haemodynamic measures, vascular medial hypertrophy and RVH (Paulin et al. 2014). This link between TRAIL and focal adhesion in PSMCs therefore presents a novel mechanism potentially driving PAH.

In the present study TRAIL stimulation of PSMCs altered expression of various growth factors, including ones able to activate the focal adhesion pathway. TRAIL induced upregulation of *FIGF* (also known as *VEGFD*) and *PDGFD* (and its receptors *PDGRFA* and *PDGFRB*). FIGF is a pro-angiogenic member of the platelet-derived growth factor family and although other members of the family have been implicated in PAH, the function of FIGF is less well understood. FIGF has been implicated in cardiac repair/remodelling – in the context of myocardial infarction, FIGF stimulates myofibroblast growth, migration, and collagen synthesis (Zhao et al. 2013). FIGF is also upregulated in the RV of PAH patients (Williams et al. 2018). In the present study, mRNA levels of these growth factors were also examined in lungs of mice subjected to models of PF and PAH. *FIGF* mRNA was upregulated in lungs of SuHx mice and also at the protein level in serum of PAH patients, suggesting a link between TRAIL-induced *FIGF* and development of PAH, distinct from cardiac remodelling and potentially via the focal adhesion pathway. Interestingly, the growth factor *PDGFD* was downregulated in the lungs of fibroblast-specific *TRAIL* deleted bleomycin mice. Fibroblast-

specific *TRAIL* deleted mice also had reduced IP bleomycin-induced vascular-associated PF, but no reduction in pulmonary vascular remodelling (described in Chapter 3). Together these data highlight a further potential mechanism for TRAIL-regulated protection against fibrosis.

### **5.4.3 A molecular signature of TRAIL stimulation in PSMCs**

In this chapter the effects of TRAIL stimulation in primary human PSMCs was examined using a combined approach of mRNA microarray and protein antibody array assays. Many studies utilise PSMCs explanted from PAH patients, or normal PSMCs that have been genetically altered – e.g. by mutation of *BMP2* – to study the function of diseased PSMCs. While the present study used commercially available PSMCs from non-PAH patients, the stimulation by TRAIL was intended to produce a pathogenic effect that might be comparable to that which PSMCs experience in vessels of PAH patients, where the presence of TRAIL has previously been observed (Hameed et al. 2012). After microarray measurement of transcriptome, LIMMA analysis of gene expression allowed many mRNA changes to be detected, despite the small number of array replicates. LIMMA employs an empirical Bayes approach to estimate sample variances within a pooled estimate, enabling more stable inference with small numbers of arrays (Ritchie et al. 2015, Smyth 2004). While the functional relevance of individual DE genes could be inferred from their known or predicted functions, a more powerful approach is to assess the enrichment of GO terms – annotated classes of genes with related functions – within the whole altered transcriptome (The Gene Ontology Consortium 2018). Pathway topology analysis using SPIA (Tarca et al. 2009) is a similar method, which has the additional advantage of estimating the perturbation effects on a pathway of changes in gene expression, using networks determined from curated pathways. GO enrichment and pathway topology analyses were employed in the present study, implicating intersecting and distinct biological processes as regulated by TRAIL in PSMCs.

## 6 General discussion

In this thesis I have presented evidence for divergent functions for TRAIL in PF and PAH. Based on previous studies highlighting a pathogenic role for tissue-derived TRAIL in human PAH and experimental rodent models of PAH (Hameed et al. 2012) and a protective function for TRAIL in IPF patients and bleomycin mice (McGrath et al. 2012), I hypothesised that as key effector cells differ between PAH and PF, so TRAIL from different cell types plays differing roles in the aetiology of these diseases. To test this hypothesis, I employed the Cre/lox system to generate mice with cell type-specific genetic deletions of *TRAIL*. These were subjected to models of PF and PAH as a means to highlight the roles of TRAIL from these specific cell types. In Chapter 3, mice with either fibroblast-specific or global *TRAIL* deletion were subjected to bleomycin-induced PF. Mice with normal TRAIL expression developed extensive PF whereas mice with TRAIL deleted in fibroblasts had more severe fibrosis. Furthermore, fibroblast-specific *TRAIL* deletion reduced *TRAIL* mRNA at the whole lung level. These data suggested that fibroblasts are a major source of TRAIL in the bleomycin model, and this TRAIL plays a protective role in the development of PF induced by bleomycin. My proposed protective mechanism is that TRAIL dampens fibrosis by inducing apoptosis of fibroblasts and/or nearby cells either by autocrine or paracrine signalling. Senescent, pro-fibrotic fibroblasts are found in the lungs of IPF patients, and their ablation in bleomycin mice improves lung function (Lehmann et al. 2017, Schafer et al. 2017). Removal of pathogenic fibroblasts also seems to be impaired in IPF patients, and furthermore these fibroblasts are resistant to TRAIL-induced apoptosis, with decreased expression of TRAIL receptors (Hohmann et al. 2019). These data demonstrate mechanistic links between TRAIL function and pathogenic fibroblasts in PF, which requires additional study to verify (expanded in Chapter 6.2).

The global deletion of *TRAIL* in the present study did not protect against PF, whereas specific loss of *TRAIL* in fibroblasts led to worsened fibrosis. The lack of protective effect against PF phenotype following global *TRAIL* deletion (unlike with the fibroblast deletion) is in contrast to

previous work finding this outcome (McGrath et al. 2012). My other novel finding from the bleomycin model was that global *TRAIL* deletion reduced the medial thickening of small pulmonary arteries and RVH associated with PAH – effects that interestingly were not observed in mice with fibroblast-specific *TRAIL* deletion. This protective effect of global *TRAIL* deletion was not reported previously with *TRAIL* deletion in bleomycin mice (McGrath et al. 2012). These discrepancies highlight both the complexity in cell-type specific roles of TRAIL, and possibly subtle differences in PF phenotype with different route of bleomycin administration (repeated IP bleomycin in the present study vs. single intratracheal injection used by McGrath et al. (2012)). The protective mechanism against PF proposed for TRAIL in previous work was the modulation of airway and alveolar immune cell populations such as neutrophils, thereby dampening the inflammatory aspects driving PF (McGrath et al. 2012). From the data presented here it is not possible to determine whether similar effects were produced in mice with *TRAIL* deleted from fibroblasts or globally. It would therefore be interesting to further examine this inflammatory modulation effect – e.g. by immunohistochemistry to detect specific leukocytes such as neutrophils and macrophages – in available tissue samples from these experiments, such as paraffin-embedded mouse lung sections (as bronchoalveolar lavage samples were not taken due to limited numbers).

Previous data from genetic deletion or antibody blockade of TRAIL expression in animal models demonstrated that TRAIL drives the pulmonary vascular remodelling in PAH (Hameed et al. 2012). In Chapter 4 I identified the pathogenic role of VSMC-derived TRAIL in mice subjected to the SuHx model, demonstrated by haemodynamics, RVH and pulmonary vascular remodelling. These data build on previous findings that predominantly tissue-derived TRAIL is responsible for driving PAH pathogenesis (Hameed et al. 2012), to demonstrate that specifically TRAIL expressed by VSMCs is key in driving the development of PAH in this experimental model. To identify potential mechanisms of the TRAIL-driven PAH phenotype I examined TRAIL target genes in PSMCs. TRAIL has previously been demonstrated to drive pro-migratory and pro-proliferative signalling pathways in PSMCs, by mechanisms including

activation of protein kinases such as ERK and MAPK (Hameed et al. 2012, Kavurma et al. 2008, Secchiero et al. 2004). In Chapter 5 the effects of TRAIL on PASMCs were further explored, using an *in vitro* TRAIL stimulation model in order to determine novel signalling pathways activated by TRAIL. Interestingly, phosphorylation of multiple protein kinases – including the cyclin-dependent kinases 6 and 8 (CDK6, CDK8) – were altered by TRAIL in PASMCs. These proteins are key regulators of cell cycle progression, which is particularly relevant in cell growth and also in cancer. The proliferative, apoptosis-resistant state of pulmonary vascular cells in PAH has been compared to that of cancer cells due to the similar cellular effects and biological processes involved (Boucherat et al. 2017). Furthermore, PH associated with vascular remodelling and perivascular inflammation has recently been described in lung cancer patients, and lung cancer cells induced migration and proliferation of PASMCs *in vitro* (Pullamsetti et al. 2017). As described in Chapter 1.4.2.1, TRAIL has been well studied as a tumour suppressor that can paradoxically also promote survival and apoptosis-resistance in cancerous cells. TRAIL therefore presents a common link between PAH and cancer, and the regulation of cell cycle proteins by TRAIL in PASMCs presented in this study highlights a potential mechanism for the pathogenic role of VSMC-derived TRAIL in PAH.

I also demonstrated that TRAIL induces extensive alterations to genes and protein kinase phosphorylation within signalling pathways in PASMCs, e.g. TGF $\beta$ /BMP signalling was a key pathway regulated by TRAIL that has also been implicated in PAH pathobiology (Morrell 2006). The TGF $\beta$  superfamily, which contains TGF $\beta$  proteins, BMPs and activins are structurally similar cytokines that can regulate varied cellular processes such as apoptosis, proliferation and migration. TGF $\beta$  superfamily members bind to type II receptors and recruits and activates the type I receptor; this phosphorylates Smad proteins, which then translocate into the nucleus and regulate gene expression via interactions with transcription factors, co-activators and co-repressors. I found that TRAIL alters expression of ligands, receptors and nuclear effectors within the TGF $\beta$ /BMP signalling pathway in PASMCs. Interestingly, BMP

signalling has also been linked to self-renewal vs. pathological response to injury in AECs – an important aspect of PF pathobiology (Zepp et al. 2017). This highlights commonalities in processes underlying progressive pulmonary diseases such as PAH and PF, and the effect of TRAIL on AECs presents another potential aspect for further investigation.

In the present study, the expression of several TRAIL-regulated genes was also altered in animal models of PF and PAH and in serum of PAH patients, suggesting potential links to disease pathobiology. One such gene was *sclerostin*, a Wnt signalling pathway antagonist that has previously been linked to bone formation (Poole et al. 2005) and cardiovascular disease (Morales-Santana et al. 2013, Novo-Rodríguez and García-Fontana 2018). In the present study sclerostin was regulated by TRAIL in PSMCs and modulated in lungs of bleomycin and SuHx mice, and additionally serum levels of sclerostin were correlated with clinical severity in PAH patients. As Wnt signalling has been linked to PAH pathobiology, it could present a link between TRAIL, sclerostin and human PAH. As with sclerostin in this study, evidence for the nature of the role of Wnt signalling in PAH is mixed: BMP2 has been shown to induce Wnt signalling leading to PAEC proliferation (de Jesus Perez et al. 2009), whereas BMP and Wnt signalling can suppress proliferation in PSMCs (Perez et al. 2011). Although in this study the TGF $\beta$ /BMP signalling pathways were predicted to be downregulated overall by TRAIL, this is a simplification that may mask individual variations within the pathway. Furthermore, antagonism between the TGF $\beta$  and BMP signalling pathways has been demonstrated (Sheares et al. 2004). Further work is therefore required to elucidate the role of TRAIL-regulated sclerostin and TGF $\beta$ /BMP signalling in PAH (Chapter 6.2).

Interestingly, another protein linked to bone formation, OPG, has been closely linked to PAH pathogenesis. OPG is a secreted glycoprotein that is widely expressed across tissues, and was originally studied for its role in regulation of bone formation (Simonet et al. 1997). OPG was noted as a soluble decoy receptor of TRAIL that is able to block TRAIL-mediated apoptosis (Emery et al. 1998), however paradoxically OPG is now known to drive PAH biology

in a similar manner to TRAIL. A role for OPG in PAH was first suggested by increased circulating OPG found in PAH patient serum (Condliffe et al. 2012, Jia et al. 2017, Lawrie et al. 2008) and explanted PSMCs from PAH patients had elevated expression of OPG (Condliffe et al. 2012). Furthermore, OPG is upregulated in animal models including SuHx mice (Arnold et al. 2019, Jia et al. 2017) and monocrotaline rats (Arnold et al. 2019), and stimulation of PSMCs induces proliferation and migration (Lawrie et al. 2008) – a similar effect to that of TRAIL. As recent direct evidence for the role of OPG in PAH, genetic deletion of OPG was demonstrated to attenuate SuHx-induced PAH in mice (Arnold et al. 2019, Jia et al. 2017) and treatment of multiple rodent PAH models with a humanised anti-OPG antibody attenuated established PAH-associated pulmonary vascular remodelling (Arnold et al. 2019). Notably, in the mouse SuHx model, bone marrow-derived OPG was found to drive PAH (Arnold et al. 2019), conversely to TRAIL where its effect has been demonstrated as primarily tissue-driven (Hameed et al. 2012) – and in the present study, specifically by VSMCs. Also, despite its link to TRAIL as a decoy receptor, the involvement of OPG in PAH has most recently been demonstrated to be independent of TRAIL, instead acting by binding to the Fas receptor to induce proliferation, migration and survival pathways (Arnold et al. 2019).

Focal adhesion and ECM regulation were another set of functions I found to be extensively regulated by TRAIL in PSMCs. This included alterations in gene expression and phosphorylation of key regulators such as FAK. Interestingly these ECM-related pathways are linked to the development of PAH as well as PF. I also demonstrated that TRAIL altered expression of growth factors connected with these pathways – e.g. *FIGF* and *PDGFD* (and its receptors *PDGRFA* and *PDGFRB*) – in PSMCs. Additionally, *FIGF* and *PDGFD* were altered in patient serum, suggesting a possible role in disease. While *FIGF* protein was increased in IPAH and SSc-PAH patients, *PDGFRB* protein was reduced in IPAH, SSc and SSc-PAH patients compared to healthy volunteers. This highlights a potential commonality for PDGF signalling between idiopathic and autoimmune-associated PAH, which requires further study. Interestingly, in fos-related antigen-2 (*Fra-2*) transgenic mice – which develop disease

resembling SSc-associated PAH (Maurer et al. 2012) – treatment with the anti-fibrotic drug nintedanib reduces pulmonary VSMC proliferation and vascular remodelling as well as PF (Huang et al. 2017). Nintedanib has been demonstrated as an inhibitor of VEGF and PDGF receptors (Hilberg et al. 2008), which link into the focal adhesion pathway described here. Together, these results highlight a potential link between fibroblast-derived TRAIL, PDGFD and fibrogenesis in PAH and PF.

## **6.1 Limitations**

Animal models present an invaluable tool in biomedical research by enabling the study of disease pathways. They allow perturbation of normal pathways – e.g. by genetic manipulation or pharmaceuticals – to unravel the underlying processes of diseases. However, as with any research involving animal models, the conclusions drawn from this study must be carefully considered in context. Translation of potential targets from animal models to successful clinical trials is poor, which may in part be due to the quality of the model systems utilised (van der Worp et al. 2010). This is particularly evident in PH research, where animal models may not fully recapitulate the processes underlying disease, at times depending on the varying animal physiology. For instance, in PH research where possible the SuHx rat is often selected over the mouse, due to the more severe form of disease characterised by worsened pulmonary vascular remodelling such as the appearance of angioproliferative plexiform lesions (Abe et al. 2010b) not present in mouse models. Another consideration is that many models of PH target a single pathway: for example, by hypoxia, administering drugs or genetic modifications. Thus, any particular individual model may not fully resemble the complex and possibly unknown molecular pathology of human PH. Despite the limitations of the mouse models utilised in the present study, they nevertheless offered an extremely useful tool to investigate TRAIL functions by means of cell type-specific genetic deletions using the Cre/lox system, which would not be possible in larger animals.

A further consideration for the present study was the floxed and tissue-specific Cre recombinase driver mouse lines utilised to study the effects of *TRAIL* deletion. The floxed *TRAIL* line and Cre lines utilised were selected based on previous evidence of *TRAIL* functions and hypotheses for what were deemed to be the most likely important sources of *TRAIL*. However, an exhaustive study could have sought to delete *TRAIL* from each relevant cell type – i.e. vascular ECs, SMCs and fibroblasts – for PAH (where pathogenic *TRAIL* was shown to be tissue-derived), potentially in addition to leukocyte lineages for PF. Furthermore, deletion of the two mouse decoy receptors for *TRAIL* and the single death domain-containing receptor, mDR5, using floxed lines could have been useful to study the targets of *TRAIL* in these disease models. However, due to restrictions of time and costs, these aspects of study were beyond the scope of this thesis.

A possible limitation was in the measurement of PF in mice subjected to bleomycin. I determined that measurement of collagen content from Masson's Trichrome micrographs was a simple and robust method for determining the extent of fibrosis in the lungs. However, other characteristic features of PF – such as collagen distribution, alveolar septum thickening/obliteration or influx of leukocytes – would not be quantified using this method. It is possible that differences in these other PF features might have been present in mice with global *TRAIL* deletion, despite no difference being observed in collagen content. Future analyses could include manual pathological scoring e.g. using a modified Ashcroft scale that has been proven in experimental animal models (Hubner et al. 2008). Due to low numbers of transgenic mice it was also not possible to examine inflammation, e.g. by differential leukocyte counts within bronchoalveolar lavage fluid. It would be potentially interesting to examine the effect of the mouse *TRAIL* deletions presented here on bleomycin-associated inflammation as has been previously described (McGrath et al. 2012).

In the present study, R26R-Brainbow2.1 fluorescent reporter mice were crossed with the Cre driver mice to illustrate the localisation of Cre-driven recombination in the expected areas of

the lung. However, specific deletions of *TRAIL* were not demonstrated in either VSMCs or fibroblasts – the two cell types targeted in these experiments. Differences in the localisation of TRAIL were not observed by immunohistochemical staining, possibly due to non-specific antibody binding or cleaved TRAIL released from other cells being bound the cells of interest. If crossed with the Cre lines, a reporter floxed *TRAIL* mouse such as one with the *TRAIL*<sup>tm1a</sup> allele could have presented direct evidence of cells with Cre recombination occurring. When subjected to Cre-mediated recombination, the *TRAIL*<sup>tm1a</sup> allele is converted to a *TRAIL*<sup>tm1b</sup> allele, thereby inducing expression of a LacZ cassette, which can be detected histologically by beta-galactosidase staining. Nevertheless, the tissue specificity of the Cre lines used in the present study has previously been well characterised (Lallemand et al. 1998, Wirth et al. 2008, Zheng et al. 2002), and furthermore the effectiveness of the *TRAIL*<sup>tm1c</sup> floxed line was demonstrated in the present study by the removal of *TRAIL* mRNA in *TRAIL*<sup>tm1c</sup> mice crossed with the PGK-Cre global Cre strain.

A potential limitation was found in the small numbers of separate biological replicates of PSMCs used for transcriptomic and protein measurements. This was more apparent in the measurement of total protein and protein phosphorylation by Kinex antibody arrays – the data from which was highly variable and caused difficulty in drawing confident statistical conclusions. Besides the small numbers analysed, another factor was the high variability of antibody-based measurements. In comparison, the mRNA microarrays were able to detect over 3,000 DE genes after TRAIL stimulation of PSMCs, despite the smaller number of replicates analysed than with the antibody arrays. As well as the differences in technology, the use of the LIMMA package allowed detection of DE genes from microarray data even with smaller numbers of arrays (Ritchie et al. 2015, Smyth 2004).

## 6.2 Future work

In this thesis I have presented evidence supporting new insights into TRAIL functions in PAH and PF. These findings raise further questions regarding TRAIL and further research is warranted to fully understand the roles of TRAIL in lung diseases. Therefore, in this section I detail areas where future work could be beneficial.

In the present study, important facets of TRAIL function were highlighted in VSMCs and fibroblasts for PAH and PF, respectively. As described in Chapter 6.1, deletion of the *TRAIL* gene in other key vascular cell types – such as ECs – would be useful in fully understanding the milieu of TRAIL signalling within these diseases. This was particularly emphasised in the IP bleomycin mouse model, where differences in the phenotypes of fibroblast-specific and global *TRAIL* deleted mice suggested other additional cell types as sources of TRAIL. Likewise, the target cells affected by TRAIL in these models remain to be elucidated. This could be facilitated by further study of TRAIL receptor expression in pulmonary vascular cells, in addition to cell type-specific deletion of TRAIL receptors. However, the functional overlap and differences between the human and mouse TRAIL receptors are not fully understood (Schneider et al. 2003), and further characterisation of the mouse TRAIL receptors in the context of PAH and PF is required. There is now also the possibility for genetic manipulation in specific cell types in rats – a potentially more physiologically relevant model species for PAH, which also possesses four TRAIL receptors – using the CRISPR-Cas9 system (Li et al. 2013).

The effects of TRAIL signalling illustrated by stimulation of human PASMCs also warrant further study. Commercial primary PASMCs from healthy lungs were used in the *in vitro* TRAIL stimulation experiments, and whether the response of these cells reflects that of cells from PAH patients is unclear. Therefore, future work could aim to replicate these findings using pulmonary vascular cells from explanted PAH lung tissue. Furthermore, the effects of TRAIL

stimulation on other important cells such as ECs and fibroblasts – and how these effects compare to those found in PSMCs – would be an interesting aspect to investigate in future work. In particular the effects of TRAIL on fibroblasts would be useful in further exploring the mechanism of fibroblast-derived TRAIL-mediated protection from bleomycin-induced fibrosis in mice. As I proposed that this protection is facilitated by increased TRAIL-mediated apoptosis of fibroblasts, this could be validated by staining lung sections with an apoptosis marker such as terminal deoxynucleotidyl transferase dUTP nick end labelling (TUNEL) and counter-immunostaining for a fibroblast-specific marker such as vimentin.

A further consideration is that *in vitro* assays with homogeneous cell populations do not necessarily represent the full extent of physiological signalling *in vivo*. It would therefore potentially be informative to carry out single cell sequencing of lung tissue from mice with *TRAIL* deletions subjected to models of PF and PAH. Transition and clonal expansion of pulmonary vascular cells such as SMCs are additional processes that has been implicated in formation of pulmonary vascular lesions in PAH (Sheikh et al. 2015). Furthermore, recent research into atherosclerotic plaque highlights the ability of VSMCs to transform into other cell types e.g. myofibroblasts (Wirka et al. 2019) or macrophage-like cells (Shankman et al. 2015). It could therefore be interesting to study a potential effect of TRAIL on these processes *in vivo*, besides previously demonstrated effects on migration and proliferation. The R26R-Brainbow2.1 fluorescent reporter mice present a useful tool for lineage tracking that could be crossed with *TRAIL*-deleted mice to determine any effects. A similar lineage tracking investigation was demonstrated in the formation of neointimal lesions by VSMC progenitor cells after carotid ligation injury (Chappell et al. 2016), a similar process to the pathological remodelling found in PAH.

In the present study, evidence for the role of sclerostin in PF and PAH was demonstrated: expression of the TRAIL-regulated gene *SOST* was altered at the mRNA level in whole lung from bleomycin and SuHx mice and at the protein level in serum of patients. It could be

informative to study the expression and localisation of sclerostin in human disease, for example by immunohistochemistry to detect proteins within the lungs of patients or within explanted cells. Functional assays such as inhibition or depletion of sclerostin in cellular models and animal models would provide direct evidence for sclerostin function. Reports in the literature have linked genetic deletion of *sclerostin* in mice to bone formation functions (Li et al. 2008, Qin et al. 2016). However, studies specifically examining cardiovascular or pulmonary vascular functions in *SOST*<sup>-/-</sup> mice – either unchallenged or subjected to insult to drive disease – have not been published. Further investigations could also be carried out into the signalling pathways associated with sclerostin, such as Wnt and BMP signalling. As the gene products from these pathways were not examined exhaustively, it would be useful to carry out protein measurements for them in further TRAIL stimulation experiments, and in the context of disease. The expression of these pathway members could also be studied in human disease or using single cell sequencing of experimental disease lungs as described in this section, in order to further understand the role of TRAIL in PF and PAH. Together, the data in this thesis highlight new mechanisms for TRAIL involvement in PF and PAH and introduce new potential targets for therapeutic intervention.

## 7 Bibliography

- Abe, K., Toba, M., Alzoubi, A., Ito, M., Fagan, K.A., Cool, C.D., Voelkel, N.F., Mcmurtry, I.F. & Oka, M. (2010a). Formation of Plexiform Lesions in Experimental Severe Pulmonary Arterial Hypertension. *Circulation*. **121**(25), 2747-2754.
- Abe, K., Toba, M., Alzoubi, A., Ito, M., Fagan, K.A., Cool, C.D., Voelkel, N.F., Mcmurtry, I.F. & Oka, M. (2010b). Formation of plexiform lesions in experimental severe pulmonary arterial hypertension. *Circulation*. **121**(25), 2747-2754.
- Adamson, I.Y. & Bowden, D.H. (1974). The pathogenesis of bleomycin-induced pulmonary fibrosis in mice. *Am. J. Pathol.* **77**(2), 185-197.
- Akram, K.M., Lomas, N.J., Forsyth, N.R. & Spiteri, M.A. (2014). Alveolar epithelial cells in idiopathic pulmonary fibrosis display upregulation of TRAIL, DR4 and DR5 expression with simultaneous preferential over-expression of pro-apoptotic marker p53. *Int. J. Clin. Exp. Pathol.* **7**(2), 552-564.
- Alladina, S.J., Song, J.H., Davidge, S.T., Hao, C. & Easton, A.S. (2005). TRAIL-induced apoptosis in human vascular endothelium is regulated by phosphatidylinositol 3-kinase/Akt through the short form of cellular FLIP and Bcl-2. *J. Vasc. Res.* **42**(4), 337-347.
- Angelidis, I., Simon, L.M., Fernandez, I.E., Strunz, M., Mayr, C.H., Greiffo, F.R., Tsitsiridis, G., Ansari, M., Graf, E., Strom, T.-M., Nagendran, M., Desai, T., Eickelberg, O., Mann, M., Theis, F.J. & Schiller, H.B. (2019). An atlas of the aging lung mapped by single cell transcriptomics and deep tissue proteomics. *Nat Commun.* **10**(1), 963.
- Arnold, N.D., Pickworth, J.A., West, L.E., Dawson, S., Carvalho, J.A., Casbolt, H., Braithwaite, A.T., Iremonger, J., Renshall, L., Germaschewski, V., Mccourt, M., Bland-Ward, P., Kowash, H., Hameed, A.G., Rothman, A.M.K., Frid, M.G., Roger Thompson, A.A., Evans, H.R., Southwood, M., Morrell, N.W., Crossman, D.C., Whyte, M.K.B., Stenmark, K.R., Newman, C.M., Kiely, D.G., Francis, S.E. & Lawrie, A. (2019). A therapeutic antibody targeting osteoprotegerin attenuates severe experimental pulmonary arterial hypertension. *Nat Commun.* **10**(1), 5183.
- Ashkenazi, A., Pai, R.C., Fong, S., Leung, S., Lawrence, D.A., Marsters, S.A., Blackie, C., Chang, L., Mcmurtrey, A.E., Hebert, A., Deforge, L., Koumenis, I.L., Lewis, D., Harris, L., Bussiere, J., Koeppen, H., Shahrokh, Z. & Schwall, R.H. (1999). Safety and antitumor activity of recombinant soluble Apo2 ligand. *J. Clin. Invest.* **104**(2), 155-162.
- Atkinson, C., Stewart, S., Upton, P.D., Machado, R., Thomson, J.R., Trembath, R.C. & Morrell, N.W. (2002). Primary pulmonary hypertension is associated with reduced pulmonary vascular expression of type II bone morphogenetic protein receptor. *Circulation*. **105**(14), 1672-1678.
- Azab, N.A., Rady, H.M. & Marzouk, S.A. (2012). Elevated serum TRAIL levels in scleroderma patients and its possible association with pulmonary involvement. *Clin. Rheumatol.* **31**(9), 1359-1364.
- Azijli, K., Yuvaraj, S., Peppelenbosch, M.P., Wurdinger, T., Dekker, H., Joore, J., Van Dijk, E., Quax, W.J., Peters, G.J., De Jong, S. & Kruyt, F.A. (2012). Kinome profiling of non-

- canonical TRAIL signaling reveals RIP1-Src-STAT3-dependent invasion in resistant non-small cell lung cancer cells. *J. Cell Sci.* **125**(Pt 19), 4651-4661.
- Baader, E., Toloczko, A., Fuchs, U., Schmid, I., Beltinger, C., Ehrhardt, H., Debatin, K.M. & Jeremias, I. (2005). Tumor necrosis factor-related apoptosis-inducing ligand-mediated proliferation of tumor cells with receptor-proximal apoptosis defects. *Cancer Res.* **65**(17), 7888-7895.
- Belyanskaya, L.L., Ziogas, A., Hopkins-Donaldson, S., Kurtz, S., Simon, H.U., Stahel, R. & Zangemeister-Wittke, U. (2008). TRAIL-induced survival and proliferation of SCLC cells is mediated by ERK and dependent on TRAIL-R2/DR5 expression in the absence of caspase-8. *Lung Cancer.* **60**(3), 355-365.
- Berg, D., Stuhmer, T., Siegmund, D., Muller, N., Giner, T., Dittrich-Breiholz, O., Kracht, M., Bargou, R. & Wajant, H. (2009). Oligomerized tumor necrosis factor-related apoptosis inducing ligand strongly induces cell death in myeloma cells, but also activates proinflammatory signaling pathways. *FEBS J.* **276**(23), 6912-6927.
- Berglund, L., Bjorling, E., Oksvold, P., Fagerberg, L., Asplund, A., Szigyarto, C.A., Persson, A., Ottosson, J., Wernerus, H., Nilsson, P., Lundberg, E., Sivertsson, A., Navani, S., Wester, K., Kampf, C., Hober, S., Ponten, F. & Uhlen, M. (2008). A gene-centric Human Protein Atlas for expression profiles based on antibodies. *Mol. Cell. Proteomics.* **7**(10), 2019-2027.
- Boehm, M., Arnold, N., Braithwaite, A., Pickworth, J., Lu, C., Novoyatleva, T., Kiely, D.G., Grimminger, F., Ghofrani, H.A., Weissmann, N., Seeger, W., Lawrie, A., Schermuly, R.T. & Kojonazarov, B. (2018). Eplerenone attenuates pathological pulmonary vascular rather than right ventricular remodeling in pulmonary arterial hypertension. *BMC Pulm. Med.* **18**(1), 41.
- Boucherat, O., Vitry, G., Trinh, I., Paulin, R., Provencher, S. & Bonnet, S. (2017). The cancer theory of pulmonary arterial hypertension. *Pulm Circ.* **7**(2), 285-299.
- Boucly, A., Weatherald, J., Savale, L., Jais, X., Cottin, V., Prevot, G., Picard, F., De Groote, P., Jevnikar, M., Bergot, E., Chaouat, A., Chabanne, C., Bourdin, A., Parent, F., Montani, D., Simonneau, G., Humbert, M. & Sitbon, O. (2017). Risk assessment, prognosis and guideline implementation in pulmonary arterial hypertension. *Eur. Respir. J.* **50**(2), 1700889.
- Braithwaite, A.T., Marriott, H.M. & Lawrie, A. (2018). Divergent Roles for TRAIL in Lung Diseases. *Front. Med.* **5**, 212.
- Brincks, E.L., Gurung, P., Langlois, R.A., Hemann, E.A., Legge, K.L. & Griffith, T.S. (2011). The magnitude of the T cell response to a clinically significant dose of influenza virus is regulated by TRAIL. *J. Immunol.* **187**(9), 4581-4588.
- Brincks, E.L., Katewa, A., Kucaba, T.A., Griffith, T.S. & Legge, K.L. (2008a). CD8 T cells utilize TRAIL to control influenza virus infection. *J. Immunol.* **181**(7), 4918-4925.
- Brincks, E.L., Kucaba, T.A., Legge, K.L. & Griffith, T.S. (2008b). Influenza-induced expression of functional tumor necrosis factor-related apoptosis-inducing ligand on human peripheral blood mononuclear cells. *Hum. Immunol.* **69**(10), 634-646.
- Brunkow, M.E., Gardner, J.C., Van Ness, J., Paeper, B.W., Kovacevich, B.R., Proll, S., Skonier, J.E., Zhao, L., Sabo, P.J., Fu, Y., Alisch, R.S., Gillett, L., Colbert, T., Tacconi,

- P., Galas, D., Hamersma, H., Beighton, P. & Mulligan, J. (2001). Bone dysplasia sclerosteosis results from loss of the SOST gene product, a novel cystine knot-containing protein. *Am. J. Hum. Genet.* **68**(3), 577-589.
- Bryant, A.J., Carrick, R.P., McConaha, M.E., Jones, B.R., Shay, S.D., Moore, C.S., Blackwell, T.R., Gladson, S., Penner, N.L., Burman, A., Tanjore, H., Hemnes, A.R., Karwandyar, A.K., Polosukhin, V.V., Talati, M.A., Dong, H.J., Gleaves, L.A., Carrier, E.J., Gaskill, C., Scott, E.W., Majka, S.M., Fessel, J.P., Haase, V.H., West, J.D., Blackwell, T.S. & Lawson, W.E. (2016). Endothelial HIF signaling regulates pulmonary fibrosis-associated pulmonary hypertension. *Am. J. Physiol. Lung Cell Mol. Physiol.* **310**(3), L249-262.
- Bryant, A.J., Robinson, L.J., Moore, C.S., Blackwell, T.R., Gladson, S., Penner, N.L., Burman, A., McClellan, L.J., Polosukhin, V.V., Tanjore, H., McConaha, M.E., Gleaves, L.A., Talati, M.A., Hemnes, A.R., Fessel, J.P., Lawson, W.E., Blackwell, T.S. & West, J.D. (2015). Expression of mutant bone morphogenetic protein receptor II worsens pulmonary hypertension secondary to pulmonary fibrosis. *Pulm Circ.* **5**(4), 681-690.
- Cantarella, G., Di Benedetto, G., Ribatti, D., Saccani-Jotti, G. & Bernardini, R. (2014). Involvement of caspase 8 and c-FLIPL in the proangiogenic effects of the tumour necrosis factor-related apoptosis-inducing ligand (TRAIL). *FEBS J.* **281**(5), 1505-1513.
- Cantarella, G., Risuglia, N., Dell'eva, R., Lempereur, L., Albini, A., Pennisi, G., Scoto, G.M., Noonan, D.N. & Bernardini, R. (2006). TRAIL inhibits angiogenesis stimulated by VEGF expression in human glioblastoma cells. *Br. J. Cancer.* **94**(10), 1428-1435.
- Cartland, S.P., Genner, S.W., Zahoor, A. & Kavurma, M.M. (2016). Comparative Evaluation of TRAIL, FGF-2 and VEGF-A-Induced Angiogenesis In Vitro and In Vivo. *Int J Mol Sci.* **17**(12).
- Chappell, J., Harman, J.L., Narasimhan, V.M., Yu, H., Foote, K., Simons, B.D., Bennett, M.R. & Jørgensen, H.F. (2016). Extensive Proliferation of a Subset of Differentiated, yet Plastic, Medial Vascular Smooth Muscle Cells Contributes to Neointimal Formation in Mouse Injury and Atherosclerosis Models. *Circ. Res.* **119**(12), 1313-1323.
- Chen, X., Austin, E.D., Talati, M., Fessel, J.P., Farber-Eger, E.H., Brittain, E.L., Hemnes, A.R., Loyd, J.E. & West, J. (2017). Oestrogen inhibition reverses pulmonary arterial hypertension and associated metabolic defects. *Eur. Respir. J.* **50**(2).
- Chilosi, M., Poletti, V., Murer, B., Lestani, M., Cancellieri, A., Montagna, L., Piccoli, P., Cangi, G., Semenzato, G. & Doglioni, C. (2002). Abnormal re-epithelialization and lung remodeling in idiopathic pulmonary fibrosis: the role of deltaN-p63. *Lab. Invest.* **82**(10), 1335-1345.
- Chilosi, M., Poletti, V., Zamo, A., Lestani, M., Montagna, L., Piccoli, P., Pedron, S., Bertaso, M., Scarpa, A., Murer, B., Cancellieri, A., Maestro, R., Semenzato, G. & Doglioni, C. (2003). Aberrant Wnt/beta-catenin pathway activation in idiopathic pulmonary fibrosis. *Am. J. Pathol.* **162**(5), 1495-1502.
- Chinnaiyan, A.M., Prasad, U., Shankar, S., Hamstra, D.A., Shanaiah, M., Chenevert, T.L., Ross, B.D. & Rehemtulla, A. (2000). Combined effect of tumor necrosis factor-related apoptosis-inducing ligand and ionizing radiation in breast cancer therapy. *Proc. Natl. Acad. Sci. U. S. A.* **97**(4), 1754-1759.

- Christman, B.W., Mcpherson, C.D., Newman, J.H., King, G.A., Bernard, G.R., Groves, B.M. & Loyd, J.E. (1992). An imbalance between the excretion of thromboxane and prostacyclin metabolites in pulmonary hypertension. *N. Engl. J. Med.* **327**(2), 70-75.
- Ciuculan, L., Bonneau, O., Hussey, M., Duggan, N., Holmes, A.M., Good, R., Stringer, R., Jones, P., Morrell, N.W., Jarai, G., Walker, C., Westwick, J. & Thomas, M. (2011). A novel murine model of severe pulmonary arterial hypertension. *Am. J. Respir. Crit. Care Med.* **184**(10), 1171-1182.
- Collison, A., Li, J., Pereira De Siqueira, A., Zhang, J., Toop, H.D., Morris, J.C., Foster, P.S. & Mattes, J. (2014). Tumor necrosis factor-related apoptosis-inducing ligand regulates hallmark features of airways remodeling in allergic airways disease. *Am. J. Respir. Cell Mol. Biol.* **51**(1), 86-93.
- Collison, A.M., Li, J., De Siqueira, A.P., Lv, X., Toop, H.D., Morris, J.C., Starkey, M.R., Hansbro, P.M., Zhang, J. & Mattes, J. (2019). TRAIL signals through the ubiquitin ligase MID1 to promote pulmonary fibrosis. *BMC Pulm. Med.* **19**(1), 31.
- Condliffe, R., Pickworth, J.A., Hopkinson, K., Walker, S.J., Hameed, A.G., Suntharalingam, J., Soon, E., Treacy, C., Pepke-Zaba, J., Francis, S.E., Crossman, D.C., Newman, C.M., Elliot, C.A., Morton, A.C., Morrell, N.W., Kiely, D.G. & Lawrie, A. (2012). Serum osteoprotegerin is increased and predicts survival in idiopathic pulmonary arterial hypertension. *Pulm Circ.* **2**(1), 21-27.
- Cool, C.D., Stewart, J.S., Werahera, P., Miller, G.J., Williams, R.L., Voelkel, N.F. & Tuder, R.M. (1999). Three-dimensional reconstruction of pulmonary arteries in plexiform pulmonary hypertension using cell-specific markers. Evidence for a dynamic and heterogeneous process of pulmonary endothelial cell growth. *Am. J. Pathol.* **155**(2), 411-419.
- Cretney, E., Takeda, K., Yagita, H., Glaccum, M., Peschon, J.J. & Smyth, M.J. (2002). Increased susceptibility to tumor initiation and metastasis in TNF-related apoptosis-inducing ligand-deficient mice. *J. Immunol.* **168**(3), 1356-1361.
- Crosby, A., Jones, F.M., Southwood, M., Stewart, S., Schermuly, R., Butrous, G., Dunne, D.W. & Morrell, N.W. (2010). Pulmonary vascular remodeling correlates with lung eggs and cytokines in murine schistosomiasis. *Am. J. Respir. Crit. Care Med.* **181**(3), 279-288.
- D'alonzo, G.E., Barst, R.J., Ayres, S.M., Bergofsky, E.H., Brundage, B.H., Detre, K.M., Fishman, A.P., Goldring, R.M., Groves, B.M., Kernis, J.T. & Et Al. (1991). Survival in patients with primary pulmonary hypertension. Results from a national prospective registry. *Ann. Intern. Med.* **115**(5), 343-349.
- Daniels, R.A., Turley, H., Kimberley, F.C., Liu, X.S., Mongkolsapaya, J., Ch'en, P., Xu, X.N., Jin, B.Q., Pezzella, F. & Screaton, G.R. (2005). Expression of TRAIL and TRAIL receptors in normal and malignant tissues. *Cell Res.* **15**(6), 430-438.
- Dawson, S., Arnold, N., Pickworth, J., Francis, S. & Lawrie, A. (2014). TRAIL Deficient Mice Are Protected from Sugen/Hypoxia Induced Pulmonary Arterial Hypertension. *Diseases.* **2**(3), 260.
- De Jesus Perez, V.A., Alastalo, T.P., Wu, J.C., Axelrod, J.D., Cooke, J.P., Amieva, M. & Rabinovitch, M. (2009). Bone morphogenetic protein 2 induces pulmonary angiogenesis via Wnt-beta-catenin and Wnt-RhoA-Rac1 pathways. *J. Cell Biol.* **184**(1), 83-99.

- Degli-Esposti, M.A., Smolak, P.J., Walczak, H., Waugh, J., Huang, C.P., Dubose, R.F., Goodwin, R.G. & Smith, C.A. (1997). Cloning and characterization of TRAIL-R3, a novel member of the emerging TRAIL receptor family. *J. Exp. Med.* **186**(7), 1165-1170.
- Deng, Z., Morse, J.H., Slager, S.L., Cuervo, N., Moore, K.J., Venetos, G., Kalachikov, S., Cayanis, E., Fischer, S.G., Barst, R.J., Hodge, S.E. & Knowles, J.A. (2000). Familial primary pulmonary hypertension (gene PPH1) is caused by mutations in the bone morphogenetic protein receptor-II gene. *Am. J. Hum. Genet.* **67**(3), 737-744.
- Dickens, L.S., Boyd, R.S., Jukes-Jones, R., Hughes, M.A., Robinson, G.L., Fairall, L., Schwabe, J.W., Cain, K. & Macfarlane, M. (2012). A death effector domain chain DISC model reveals a crucial role for caspase-8 chain assembly in mediating apoptotic cell death. *Mol. Cell.* **47**(2), 291-305.
- Diebold, I., Hennigs, J.K., Miyagawa, K., Li, C.G., Nickel, N.P., Kaschwich, M., Cao, A., Wang, L., Reddy, S., Chen, P.I., Nakahira, K., Alcazar, M.A., Hopper, R.K., Ji, L., Feldman, B.J. & Rabinovitch, M. (2015). BMPR2 preserves mitochondrial function and DNA during reoxygenation to promote endothelial cell survival and reverse pulmonary hypertension. *Cell Metab.* **21**(4), 596-608.
- Douglas, W.W., Ryu, J.H., Swensen, S.J., Offord, K.P., Schroeder, D.R., Caron, G.M. & Deremee, R.A. (1998). Colchicine versus prednisone in the treatment of idiopathic pulmonary fibrosis. A randomized prospective study. Members of the Lung Study Group. *Am. J. Respir. Crit. Care Med.* **158**(1), 220-225.
- Du, L., Sullivan, C.C., Chu, D., Cho, A.J., Kido, M., Wolf, P.L., Yuan, J.X., Deutsch, R., Jamieson, S.W. & Thistlethwaite, P.A. (2003). Signaling molecules in nonfamilial pulmonary hypertension. *N. Engl. J. Med.* **348**(6), 500-509.
- Eddahibi, S., Guignabert, C., Barlier-Mur, A.M., Dewachter, L., Fadel, E., Dartevielle, P., Humbert, M., Simonneau, G., Hanoun, N., Saurini, F., Hamon, M. & Adnot, S. (2006). Cross talk between endothelial and smooth muscle cells in pulmonary hypertension: critical role for serotonin-induced smooth muscle hyperplasia. *Circulation.* **113**(15), 1857-1864.
- Ehrhardt, H., Fulda, S., Schmid, I., Hiscott, J., Debatin, K.M. & Jeremias, I. (2003). TRAIL induced survival and proliferation in cancer cells resistant towards TRAIL-induced apoptosis mediated by NF-kappaB. *Oncogene.* **22**(25), 3842-3852.
- Emery, J.G., McDonnell, P., Burke, M.B., Deen, K.C., Lyn, S., Silverman, C., Dul, E., Appelbaum, E.R., Eichman, C., Diprinzio, R., Dodds, R.A., James, I.E., Rosenberg, M., Lee, J.C. & Young, P.R. (1998). Osteoprotegerin is a receptor for the cytotoxic ligand TRAIL. *J. Biol. Chem.* **273**(23), 14363-14367.
- Faner, R., Rojas, M., Macnee, W. & Agusti, A. (2012). Abnormal lung aging in chronic obstructive pulmonary disease and idiopathic pulmonary fibrosis. *Am. J. Respir. Crit. Care Med.* **186**(4), 306-313.
- Farha, S., Saygin, D., Park, M.M., Cheong, H.I., Asosingh, K., Comhair, S.A., Stephens, O.R., Roach, E.C., Sharp, J., Highland, K.B., Difilippo, F.P., Neumann, D.R., Tang, W.H.W. & Erzurum, S.C. (2017). Pulmonary arterial hypertension treatment with carvedilol for heart failure: a randomized controlled trial. *JCI Insight.* **2**(16).
- Farkas, D., Thompson, A.a.R., Bhagwani, A.R., Hultman, S., Ji, H., Kotha, N., Farr, G., Arnold, N.D., Braithwaite, A., Casbolt, H., Cole, J.E., Sabroe, I., Monaco, C., Cool, C.D.,

- Goncharova, E.A., Lawrie, A. & Farkas, L. (2019). Toll-like Receptor 3 Is a Therapeutic Target for Pulmonary Hypertension. *199*(2), 199-210.
- Finnberg, N., Klein-Szanto, A.J. & El-Deiry, W.S. (2008). TRAIL-R deficiency in mice promotes susceptibility to chronic inflammation and tumorigenesis. *J. Clin. Invest.* **118**(1), 111-123.
- Fisher, M., Nathan, S.D., Hill, C., Marshall, J., Dejonckheere, F., Thuresson, P.O. & Maher, T.M. (2017). Predicting Life Expectancy for Pirfenidone in Idiopathic Pulmonary Fibrosis. *J Manag Care Spec Pharm.* **23**(3-b Suppl), S17-s24.
- Fleischman, R.W., Baker, J.R., Thompson, G.R., Schaeppi, U.H., Illievski, V.R., Cooney, D.A. & Davis, R.D. (1971). Bleomycin-induced interstitial pneumonia in dogs. *Thorax.* **26**(6), 675-682.
- Galie, N., Corris, P.A., Frost, A., Girgis, R.E., Granton, J., Jing, Z.C., Klepetko, W., Mcgoon, M.D., Mclaughlin, V.V., Preston, I.R., Rubin, L.J., Sandoval, J., Seeger, W. & Keogh, A. (2013). Updated Treatment Algorithm of Pulmonary Arterial Hypertension. *J. Am. Coll. Cardiol.* **62**(25), D60-D72.
- Geiger, R., Berger, R.M., Hess, J., Bogers, A.J., Sharma, H.S. & Mooi, W.J. (2000). Enhanced expression of vascular endothelial growth factor in pulmonary plexogenic arteriopathy due to congenital heart disease. *J. Pathol.* **191**(2), 202-207.
- Girkin, J.L., Hatchwell, L.M., Collison, A.M., Starkey, M.R., Hansbro, P.M., Yagita, H., Foster, P.S. & Mattes, J. (2017). TRAIL signaling is proinflammatory and proviral in a murine model of rhinovirus 1B infection. *Am. J. Physiol. Lung Cell Mol. Physiol.* **312**(1), L89-L99.
- Gochuico, B.R., Zhang, J., Ma, B.Y., Marshak-Rothstein, A. & Fine, A. (2000). TRAIL expression in vascular smooth muscle. *Am. J. Physiol. Lung Cell Mol. Physiol.* **278**(5), L1045-1050.
- Good, R.B., Gilbane, A.J., Trinder, S.L., Denton, C.P., Coghlan, G., Abraham, D.J. & Holmes, A.M. (2015). Endothelial to Mesenchymal Transition Contributes to Endothelial Dysfunction in Pulmonary Arterial Hypertension. *Am. J. Pathol.* **185**(7), 1850-1858.
- Gräf, S., Haimel, M., Bleda, M., Hadinnapola, C., Southgate, L., Li, W., Hodgson, J., Liu, B., Salmon, R.M., Southwood, M., Machado, R.D., Martin, J.M., Treacy, C.M., Yates, K., Daugherty, L.C., Shamardina, O., Whitehorn, D., Holden, S., Aldred, M., Bogaard, H.J., Church, C., Coghlan, G., Condliffe, R., Corris, P.A., Danesino, C., Eyries, M., Gall, H., Ghio, S., Ghofrani, H.-A., Gibbs, J.S.R., Girerd, B., Houweling, A.C., Howard, L., Humbert, M., Kiely, D.G., Kovacs, G., Mackenzie Ross, R.V., Moledina, S., Montani, D., Newnham, M., Olschewski, A., Olschewski, H., Peacock, A.J., Pepke-Zaba, J., Prokopenko, I., Rhodes, C.J., Scelsi, L., Seeger, W., Soubrier, F., Stein, D.F., Suntharalingam, J., Swietlik, E.M., Toshner, M.R., Van Heel, D.A., Vonk Noordegraaf, A., Waisfisz, Q., Wharton, J., Wort, S.J., Ouwehand, W.H., Soranzo, N., Lawrie, A., Upton, P.D., Wilkins, M.R., Trembath, R.C. & Morrell, N.W. (2018). Identification of rare sequence variation underlying heritable pulmonary arterial hypertension. *Nat Commun.* **9**(1), 1416.
- Habel, D.M., Moreira, A.P., Ismailoglu, U.B., Dunleavy, M.P., Cavassani, K.A., Van Rooijen, N., Coelho, A.L. & Hogaboam, C.M. (2018). TRAIL-Dependent Resolution of Pulmonary Fibrosis. *Mediators Inflamm.* **2018**, 7934362.

- Hachulla, E., Carpentier, P., Gressin, V., Diot, E., Allanore, Y., Sibilia, J., Launay, D., Mouthon, L., Jegou, P., Cabane, J., De Groote, P., Chabrol, A., Lazareth, I., Guillevin, L., Clerson, P., Humbert, M. & Itiner, A.I.R.S.S.I. (2009). Risk factors for death and the 3-year survival of patients with systemic sclerosis: the French ItinerAIR-Sclerodermie study. *Rheumatology (Oxford)*. **48**(3), 304-308.
- Hachulla, E., Gressin, V., Guillevin, L., Carpentier, P., Diot, E., Sibilia, J., Kahan, A., Cabane, J., Frances, C., Launay, D., Mouthon, L., Allanore, Y., Tiev, K.P., Clerson, P., De Groote, P. & Humbert, M. (2005). Early detection of pulmonary arterial hypertension in systemic sclerosis: a French nationwide prospective multicenter study. *Arthritis Rheum.* **52**(12), 3792-3800.
- Hagen, M., Fagan, K., Steudel, W., Carr, M., Lane, K., Rodman, D.M. & West, J. (2007). Interaction of interleukin-6 and the BMP pathway in pulmonary smooth muscle. *Am. J. Physiol. Lung Cell Mol. Physiol.* **292**(6), L1473-1479.
- Hameed, A.G., Arnold, N.D., Chamberlain, J., Pickworth, J.A., Paiva, C., Dawson, S., Cross, S., Long, L., Zhao, L., Morrell, N.W., Crossman, D.C., Newman, C.M., Kiely, D.G., Francis, S.E. & Lawrie, A. (2012). Inhibition of tumor necrosis factor-related apoptosis-inducing ligand (TRAIL) reverses experimental pulmonary hypertension. *J. Exp. Med.* **209**(11), 1919-1935.
- Hansmann, G., Wagner, R.A., Schellong, S., Perez, V.A., Urashima, T., Wang, L., Sheikh, A.Y., Suen, R.S., Stewart, D.J. & Rabinovitch, M. (2007). Pulmonary arterial hypertension is linked to insulin resistance and reversed by peroxisome proliferator-activated receptor-gamma activation. *Circulation*. **115**(10), 1275-1284.
- Harith, H.H., Di Bartolo, B.A., Cartland, S.P., Genner, S. & Kavoura, M.M. (2016). Insulin promotes vascular smooth muscle cell proliferation and apoptosis via differential regulation of tumor necrosis factor-related apoptosis-inducing ligand. *J Diabetes*. **8**(4), 568-578.
- Hashimoto, N., Jin, H., Liu, T., Chensue, S.W. & Phan, S.H. (2004). Bone marrow-derived progenitor cells in pulmonary fibrosis. *J. Clin. Invest.* **113**(2), 243-252.
- Hashimoto, N., Phan, S.H., Imaizumi, K., Matsuo, M., Nakashima, H., Kawabe, T., Shimokata, K. & Hasegawa, Y. (2010). Endothelial-mesenchymal transition in bleomycin-induced pulmonary fibrosis. *Am. J. Respir. Cell Mol. Biol.* **43**(2), 161-172.
- Hatano, S. & Strasser, T. 1975. *Primary Pulmonary Hypertension: Report on a WHO Meeting, Geneva, 15-17 October 1973*, World Health Organization.
- Haw, T.J., Starkey, M.R., Nair, P.M., Pavlidis, S., Liu, G., Nguyen, D.H., Hsu, A.C., Hanish, I., Kim, R.Y., Collison, A.M., Inman, M.D., Wark, P.A., Foster, P.S., Knight, D.A., Mattes, J., Yagita, H., Adcock, I.M., Horvat, J.C. & Hansbro, P.M. (2016). A pathogenic role for tumor necrosis factor-related apoptosis-inducing ligand in chronic obstructive pulmonary disease. *Mucosal Immunol.* **9**(4), 859-872.
- Herold, S., Steinmueller, M., Von Wulffen, W., Cakarova, L., Pinto, R., Pleschka, S., Mack, M., Kuziel, W.A., Corazza, N., Brunner, T., Seeger, W. & Lohmeyer, J. (2008). Lung epithelial apoptosis in influenza virus pneumonia: the role of macrophage-expressed TNF-related apoptosis-inducing ligand. *J. Exp. Med.* **205**(13), 3065-3077.
- Hilberg, F., Roth, G.J., Krssak, M., Kautschitsch, S., Sommergruber, W., Tontsch-Grunt, U., Garin-Chesa, P., Bader, G., Zoepfel, A., Quant, J., Heckel, A. & Rettig, W.J. (2008).

BIBF 1120: Triple Angiokinase Inhibitor with Sustained Receptor Blockade and Good Antitumor Efficacy. *Cancer Res.* **68**(12), 4774-4782.

- Hoepfer, M.M., Bogaard, H.J., Condliffe, R., Frantz, R., Khanna, D., Kurzyna, M., Langleben, D., Manes, A., Satoh, T., Torres, F., Wilkins, M.R. & Badesch, D.B. (2013). Definitions and diagnosis of pulmonary hypertension. *J. Am. Coll. Cardiol.* **62**(25 Suppl), D42-50.
- Hoepfer, M.M., Kramer, T., Pan, Z., Eichstaedt, C.A., Spiesshoefer, J., Benjamin, N., Olsson, K.M., Meyer, K., Vizza, C.D., Vonk-Noordegraaf, A., Distler, O., Opitz, C., Gibbs, J.S.R., Delcroix, M., Ghofrani, H.A., Huscher, D., Pittrow, D., Rosenkranz, S. & Grunig, E. (2017). Mortality in pulmonary arterial hypertension: prediction by the 2015 European pulmonary hypertension guidelines risk stratification model. *Eur. Respir. J.* **50**(2), 1700740.
- Hohmann, M.S., Habel, D.M., Coelho, A.L., Verri, W.A., Jr. & Hogaboam, C.M. (2019). Quercetin Enhances Ligand-induced Apoptosis in Senescent Idiopathic Pulmonary Fibrosis Fibroblasts and Reduces Lung Fibrosis In Vivo. *Am. J. Respir. Cell Mol. Biol.* **60**(1), 28-40.
- Horowitz, J.C., Lee, D.Y., Waghray, M., Keshamouni, V.G., Thomas, P.E., Zhang, H., Cui, Z. & Thannickal, V.J. (2004). Activation of the pro-survival phosphatidylinositol 3-kinase/AKT pathway by transforming growth factor-beta1 in mesenchymal cells is mediated by p38 MAPK-dependent induction of an autocrine growth factor. *J. Biol. Chem.* **279**(2), 1359-1367.
- Huang Da, W., Sherman, B.T. & Lempicki, R.A. (2009). Systematic and integrative analysis of large gene lists using DAVID bioinformatics resources. *Nat. Protoc.* **4**(1), 44-57.
- Huang, J., Maier, C., Zhang, Y., Soare, A., Dees, C., Beyer, C., Harre, U., Chen, C.W., Distler, O., Schett, G., Wollin, L. & Distler, J.H.W. (2017). Nintedanib inhibits macrophage activation and ameliorates vascular and fibrotic manifestations in the Fra2 mouse model of systemic sclerosis. *Ann. Rheum. Dis.* **76**(11), 1941-1948.
- Hubner, R.H., Gitter, W., El Mokhtari, N.E., Mathiak, M., Both, M., Bolte, H., Freitag-Wolf, S. & Bewig, B. (2008). Standardized quantification of pulmonary fibrosis in histological samples. *Biotechniques.* **44**(4), 507-511, 514-507.
- Humbert, M., Monti, G., Brenot, F., Sitbon, O., Portier, A., Grangeot-Keros, L., Duroux, P., Galanaud, P., Simonneau, G. & Emilie, D. (1995). Increased interleukin-1 and interleukin-6 serum concentrations in severe primary pulmonary hypertension. *Am. J. Respir. Crit. Care Med.* **151**(5), 1628-1631.
- Humbert, M., Sitbon, O., Chaouat, A., Bertocchi, M., Habib, G., Gressin, V., Yaici, A., Weitzenblum, E., Cordier, J.F., Chabot, F., Dromer, C., Pison, C., Reynaud-Gaubert, M., Haloun, A., Laurent, M., Hachulla, E. & Simonneau, G. (2006). Pulmonary arterial hypertension in France: results from a national registry. *Am. J. Respir. Crit. Care Med.* **173**(9), 1023-1030.
- Hutchinson, J., Fogarty, A., Hubbard, R. & Mckeever, T. (2015). Global incidence and mortality of idiopathic pulmonary fibrosis: a systematic review. *Eur. Respir. J.* **46**(3), 795-806.
- Hwang, S.J., Ballantyne, C.M., Sharrett, A.R., Smith, L.C., Davis, C.E., Gotto, A.M., Jr. & Boerwinkle, E. (1997). Circulating adhesion molecules VCAM-1, ICAM-1, and E-selectin in carotid atherosclerosis and incident coronary heart disease cases: the Atherosclerosis Risk In Communities (ARIC) study. *Circulation.* **96**(12), 4219-4225.

- Hymowitz, S.G., Christinger, H.W., Fuh, G., Ultsch, M., O'Connell, M., Kelley, R.F., Ashkenazi, A. & De Vos, A.M. (1999). Triggering cell death: the crystal structure of Apo2L/TRAIL in a complex with death receptor 5. *Mol. Cell.* **4**(4), 563-571.
- International, P.P.H.C., Lane, K.B., Machado, R.D., Pauciulo, M.W., Thomson, J.R., Phillips, J.A., 3rd, Loyd, J.E., Nichols, W.C. & Trembath, R.C. (2000). Heterozygous germline mutations in BMPR2, encoding a TGF-beta receptor, cause familial primary pulmonary hypertension. *Nat. Genet.* **26**(1), 81-84.
- Ishikawa, E., Nakazawa, M., Yoshinari, M. & Minami, M. (2005). Role of tumor necrosis factor-related apoptosis-inducing ligand in immune response to influenza virus infection in mice. *J. Virol.* **79**(12), 7658-7663.
- Izbicki, G., Segel, M.J., Christensen, T.G., Conner, M.W. & Breuer, R. (2002). Time course of bleomycin-induced lung fibrosis. *Int. J. Exp. Pathol.* **83**(3), 111-119.
- Jacobs, W., Van De Veerdonk, M.C., Trip, P., De Man, F., Heymans, M.W., Marcus, J.T., Kawut, S.M., Bogaard, H.J., Boonstra, A. & Vonk Noordegraaf, A. (2014). The right ventricle explains sex differences in survival in idiopathic pulmonary arterial hypertension. *Chest.* **145**(6), 1230-1236.
- Jasmin, J.F., Lucas, M., Cernacek, P. & Dupuis, J. (2001). Effectiveness of a nonselective ET(A/B) and a selective ET(A) antagonist in rats with monocrotaline-induced pulmonary hypertension. *Circulation.* **103**(2), 314-318.
- Jia, D., Zhu, Q., Liu, H., Zuo, C., He, Y., Chen, G. & Lu, A. (2017). Osteoprotegerin Disruption Attenuates HySu-Induced Pulmonary Hypertension Through Integrin alphavbeta3/FAK/AKT Pathway Suppression. *Circ. Cardiovasc. Genet.* **10**(1).
- Johnstone, R.W., Frew, A.J. & Smyth, M.J. (2008). The TRAIL apoptotic pathway in cancer onset, progression and therapy. *Nat. Rev. Cancer.* **8**(10), 782-798.
- Jude, E.B., Douglas, J.T., Anderson, S.G., Young, M.J. & Boulton, A.J. (2002). Circulating cellular adhesion molecules ICAM-1, VCAM-1, P- and E-selectin in the prediction of cardiovascular disease in diabetes mellitus. *Eur. J. Intern. Med.* **13**(3), 185-189.
- Kanehisa, M. & Goto, S. (2000). KEGG: kyoto encyclopedia of genes and genomes. *Nucleic Acids Res.* **28**(1), 27-30.
- Karmouty-Quintana, H., Philip, K., Acero, L.F., Chen, N.Y., Weng, T., Molina, J.G., Luo, F., Davies, J., Le, N.B., Bunge, I., Volcik, K.A., Le, T.T., Johnston, R.A., Xia, Y., Eltzschig, H.K. & Blackburn, M.R. (2015). Deletion of ADORA2B from myeloid cells dampens lung fibrosis and pulmonary hypertension. *FASEB J.* **29**(1), 50-60.
- Karmouty-Quintana, H., Zhong, H., Acero, L., Weng, T., Melicoff, E., West, J.D., Hemnes, A., Grenz, A., Eltzschig, H.K., Blackwell, T.S., Xia, Y., Johnston, R.A., Zeng, D., Belardinelli, L. & Blackburn, M.R. (2012). The A2B adenosine receptor modulates pulmonary hypertension associated with interstitial lung disease. *FASEB J.* **26**(6), 2546-2557.
- Kasper, M. & Haroske, G. (1996). Alterations in the alveolar epithelium after injury leading to pulmonary fibrosis. *Histol. Histopathol.* **11**(2), 463-483.
- Kavurma, M.M., Schoppet, M., Bobryshev, Y.V., Khachigian, L.M. & Bennett, M.R. (2008). TRAIL stimulates proliferation of vascular smooth muscle cells via activation of NF-

- kappaB and induction of insulin-like growth factor-1 receptor. *J. Biol. Chem.* **283**(12), 7754-7762.
- Kawut, S.M., Archer-Chicko, C.L., Demichele, A., Fritz, J.S., Klinger, J.R., Ky, B., Palevsky, H.I., Palmisciano, A.J., Patel, M., Pinder, D., Propert, K.J., Smith, K.A., Stanczyk, F., Tracy, R., Vaidya, A., Whittenhall, M.E. & Ventetuolo, C.E. (2017). Anastrozole in Pulmonary Arterial Hypertension. A Randomized, Double-Blind, Placebo-controlled Trial. *195*(3), 360-368.
- Kawut, S.M., Taichman, D.B., Archer-Chicko, C.L., Palevsky, H.I. & Kimmel, S.E. (2003). Hemodynamics and survival in patients with pulmonary arterial hypertension related to systemic sclerosis. *Chest.* **123**(2), 344-350.
- Kay, J.M., Harris, P. & Heath, D. (1967). Pulmonary hypertension produced in rats by ingestion of *Crotalaria spectabilis* seeds. *Thorax.* **22**(2), 176-179.
- King, T.E., Jr., Bradford, W.Z., Castro-Bernardini, S., Fagan, E.A., Glaspole, I., Glassberg, M.K., Gorina, E., Hopkins, P.M., Kardatzke, D., Lancaster, L., Lederer, D.J., Nathan, S.D., Pereira, C.A., Sahn, S.A., Sussman, R., Swigris, J.J. & Noble, P.W. (2014). A phase 3 trial of pirfenidone in patients with idiopathic pulmonary fibrosis. *N. Engl. J. Med.* **370**(22), 2083-2092.
- Kotelkin, A., Prikhod'ko, E.A., Cohen, J.I., Collins, P.L. & Bukreyev, A. (2003). Respiratory syncytial virus infection sensitizes cells to apoptosis mediated by tumor necrosis factor-related apoptosis-inducing ligand. *J. Virol.* **77**(17), 9156-9172.
- Kreymborg, K., Uchida, S., Gellert, P., Schneider, A., Boettger, T., Voswinckel, R., Wietelmann, A., Szibor, M., Weissmann, N., Ghofrani, A.H., Schermuly, R., Schranz, D., Seeger, W. & Braun, T. (2010). Identification of right heart-enriched genes in a murine model of chronic outflow tract obstruction. *J. Mol. Cell. Cardiol.* **49**(4), 598-605.
- Kuwano, K., Kunitake, R., Maeyama, T., Hagimoto, N., Kawasaki, M., Matsuba, T., Yoshimi, M., Inoshima, I., Yoshida, K. & Hara, N. (2001). Attenuation of bleomycin-induced pneumopathy in mice by a caspase inhibitor. *Am. J. Physiol. Lung Cell Mol. Physiol.* **280**(2), L316-325.
- Lallemand, Y., Luria, V., Haffner-Krausz, R. & Lonai, P. (1998). Maternally expressed PGK-Cre transgene as a tool for early and uniform activation of the Cre site-specific recombinase. *Transgenic Res.* **7**(2), 105-112.
- Laumanns, I.P., Fink, L., Wilhelm, J., Wolff, J.C., Mitnacht-Kraus, R., Graef-Hoehst, S., Stein, M.M., Bohle, R.M., Klepetko, W., Hoda, M.A., Schermuly, R.T., Grimminger, F., Seeger, W. & Voswinckel, R. (2009). The noncanonical WNT pathway is operative in idiopathic pulmonary arterial hypertension. *Am. J. Respir. Cell Mol. Biol.* **40**(6), 683-691.
- Launay, J.M., Herve, P., Peoc'h, K., Tournois, C., Callebert, J., Nebigil, C.G., Etienne, N., Drouet, L., Humbert, M., Simonneau, G. & Maroteaux, L. (2002). Function of the serotonin 5-hydroxytryptamine 2B receptor in pulmonary hypertension. *Nat. Med.* **8**(10), 1129-1135.
- Lawrie, A. (2014). A report on the use of animal models and phenotyping methods in pulmonary hypertension research. *Pulm Circ.* **4**(1), 2-9.

- Lawrie, A., Hameed, A.G., Chamberlain, J., Arnold, N., Kennerley, A., Hopkinson, K., Pickworth, J., Kiely, D.G., Crossman, D.C. & Francis, S.E. (2011). Paigen diet-fed apolipoprotein E knockout mice develop severe pulmonary hypertension in an interleukin-1-dependent manner. *Am. J. Pathol.* **179**(4), 1693-1705.
- Lawrie, A., Waterman, E., Southwood, M., Evans, D., Suntharalingam, J., Francis, S., Crossman, D., Croucher, P., Morrell, N. & Newman, C. (2008). Evidence of a role for osteoprotegerin in the pathogenesis of pulmonary arterial hypertension. *Am. J. Pathol.* **172**(1), 256-264.
- Le Pavec, J., Girgis, R.E., Lechtzin, N., Mathai, S.C., Launay, D., Hummers, L.K., Zaiman, A., Sitbon, O., Simonneau, G., Humbert, M. & Hassoun, P.M. (2011). Systemic sclerosis-related pulmonary hypertension associated with interstitial lung disease: impact of pulmonary arterial hypertension therapies. *Arthritis Rheum.* **63**(8), 2456-2464.
- Lee, C.G., Cho, S.J., Kang, M.J., Chapoval, S.P., Lee, P.J., Noble, P.W., Yehualaeshet, T., Lu, B., Flavell, R.A., Milbrandt, J., Homer, R.J. & Elias, J.A. (2004). Early growth response gene 1-mediated apoptosis is essential for transforming growth factor beta1-induced pulmonary fibrosis. *J. Exp. Med.* **200**(3), 377-389.
- Lehmann, M., Korfei, M., Mutze, K., Klee, S., Skronska-Wasek, W., Alsafadi, H.N., Ota, C., Costa, R., Schiller, H.B., Lindner, M., Wagner, D.E., Guenther, A. & Koenigshoff, M. (2017). Senolytic drugs target alveolar epithelial cell function and attenuate experimental lung fibrosis ex vivo. *Eur. Respir. J.* **50**(2), 1602367.
- Li, D., Qiu, Z., Shao, Y., Chen, Y., Guan, Y., Liu, M., Li, Y., Gao, N., Wang, L., Lu, X., Zhao, Y. & Liu, M. (2013). Heritable gene targeting in the mouse and rat using a CRISPR-Cas system. *Nat. Biotechnol.* **31**, 681-683.
- Li, X., Ominsky, M.S., Niu, Q.T., Sun, N., Daugherty, B., D'agostin, D., Kurahara, C., Gao, Y., Cao, J., Gong, J., Asuncion, F., Barrero, M., Warmington, K., Dwyer, D., Stolina, M., Morony, S., Sarosi, I., Kostenuik, P.J., Lacey, D.L., Simonet, W.S., Ke, H.Z. & Paszty, C. (2008). Targeted deletion of the sclerostin gene in mice results in increased bone formation and bone strength. *J. Bone Miner. Res.* **23**(6), 860-869.
- Li, X., Zhang, Y., Kang, H., Liu, W., Liu, P., Zhang, J., Harris, S.E. & Wu, D. (2005). Sclerostin binds to LRP5/6 and antagonizes canonical Wnt signaling. *J. Biol. Chem.* **280**(20), 19883-19887.
- Lin, C., Li, X., Luo, Q., Yang, H., Li, L., Zhou, Q., Li, Y., Tang, H. & Wu, L. (2017). RELM-beta promotes human pulmonary artery smooth muscle cell proliferation via FAK-stimulated surviving. *Exp. Cell Res.* **351**(1), 43-50.
- Linkert, M., Rueden, C.T., Allan, C., Burel, J.M., Moore, W., Patterson, A., Loranger, B., Moore, J., Neves, C., Macdonald, D., Tarkowska, A., Sticco, C., Hill, E., Rossner, M., Eliceiri, K.W. & Swedlow, J.R. (2010). Metadata matters: access to image data in the real world. *J. Cell Biol.* **189**(5), 777-782.
- Liu, H., Yang, E., Lu, X., Zuo, C., He, Y., Jia, D., Zhu, Q., Yu, Y. & Lv, A. (2015). Serum levels of tumor necrosis factor-related apoptosis-inducing ligand correlate with the severity of pulmonary hypertension. *Pulm. Pharmacol. Ther.* **33**, 39-46.
- Livak, K.J. & Schmittgen, T.D. (2001). Analysis of relative gene expression data using real-time quantitative PCR and the 2<sup>-</sup>(Delta Delta C(T)) Method. *Methods.* **25**(4), 402-408.

- Livet, J., Weissman, T.A., Kang, H., Draft, R.W., Lu, J., Bennis, R.A., Sanes, J.R. & Lichtman, J.W. (2007). Transgenic strategies for combinatorial expression of fluorescent proteins in the nervous system. *Nature*. **450**(7166), 56-62.
- Lopes, A.A., Maeda, N.Y. & Bydlowski, S.P. (1998). Abnormalities in circulating von Willebrand factor and survival in pulmonary hypertension. *Am. J. Med.* **105**(1), 21-26.
- Luc, G., Arveiler, D., Evans, A., Amouyel, P., Ferrieres, J., Bard, J.M., Elkhailil, L., Fruchart, J.C. & Ducimetiere, P. (2003). Circulating soluble adhesion molecules ICAM-1 and VCAM-1 and incident coronary heart disease: the PRIME Study. *Atherosclerosis*. **170**(1), 169-176.
- Macchia, A., Marchioli, R., Marfisi, R., Scarano, M., Levantesi, G., Tavazzi, L. & Tognoni, G. (2007). A meta-analysis of trials of pulmonary hypertension: a clinical condition looking for drugs and research methodology. *Am. Heart J.* **153**(6), 1037-1047.
- Macfarlane, M., Ahmad, M., Srinivasula, S.M., Fernandes-Alnemri, T., Cohen, G.M. & Alnemri, E.S. (1997). Identification and molecular cloning of two novel receptors for the cytotoxic ligand TRAIL. *J. Biol. Chem.* **272**(41), 25417-25420.
- Manetti, M., Romano, E., Rosa, I., Guiducci, S., Bellando-Randone, S., De Paulis, A., Ibbamanneschi, L. & Matucci-Cerinic, M. (2017). Endothelial-to-mesenchymal transition contributes to endothelial dysfunction and dermal fibrosis in systemic sclerosis. *Ann. Rheum. Dis.* **76**(5).
- Marsters, S.A., Sheridan, J.P., Pitti, R.M., Huang, A., Skubatch, M., Baldwin, D., Yuan, J., Gurney, A., Goddard, A.D., Godowski, P. & Ashkenazi, A. (1997). A novel receptor for Apo2L/TRAIL contains a truncated death domain. *Curr. Biol.* **7**(12), 1003-1006.
- Maurer, B., Reich, N., Juengel, A., Kriegsmann, J., Gay, R.E., Schett, G., Michel, B.A., Gay, S., Distler, J.H. & Distler, O. (2012). Fra-2 transgenic mice as a novel model of pulmonary hypertension associated with systemic sclerosis. *Ann. Rheum. Dis.* **71**(8), 1382-1387.
- Mcgrath, E.E., Lawrie, A., Marriott, H.M., Mercer, P., Cross, S.S., Arnold, N., Singleton, V., Thompson, A.A., Walmsley, S.R., Renshaw, S.A., Sabroe, I., Chambers, R.C., Dockrell, D.H. & Whyte, M.K. (2012). Deficiency of tumour necrosis factor-related apoptosis-inducing ligand exacerbates lung injury and fibrosis. *Thorax*. **67**(9), 796-803.
- Mcgrath, E.E., Marriott, H.M., Lawrie, A., Francis, S.E., Sabroe, I., Renshaw, S.A., Dockrell, D.H. & Whyte, M.K. (2011). TNF-related apoptosis-inducing ligand (TRAIL) regulates inflammatory neutrophil apoptosis and enhances resolution of inflammation. *J. Leukoc. Biol.* **90**(5), 855-865.
- Mclaughlin, V.V., Presberg, K.W., Doyle, R.L., Abman, S.H., Mccrory, D.C., Fortin, T. & Ahearn, G. (2004). Prognosis of pulmonary arterial hypertension - ACCP evidence-based clinical practice guidelines. *Chest*. **126**(1), 78S-92S.
- Merino, D., Lalaoui, N., Morizot, A., Schneider, P., Solary, E. & Micheau, O. (2006). Differential inhibition of TRAIL-mediated DR5-DISC formation by decoy receptors 1 and 2. *Mol. Cell. Biol.* **26**(19), 7046-7055.
- Michelakis, E.D., Gurtu, V., Webster, L., Barnes, G., Watson, G., Howard, L., Cupitt, J., Paterson, I., Thompson, R.B., Chow, K., O'regan, D.P., Zhao, L., Wharton, J., Kiely, D.G., Kinnaird, A., Boukouris, A.E., White, C., Nagendran, J., Freed, D.H., Wort, S.J.,

- Gibbs, J.S.R. & Wilkins, M.R. (2017). Inhibition of pyruvate dehydrogenase kinase improves pulmonary arterial hypertension in genetically susceptible patients. *Sci. Transl. Med.* **9**(413), eaao4583.
- Michelakis, E.D., Mcmurtry, M.S., Wu, X.C., Dyck, J.R., Moudgil, R., Hopkins, T.A., Lopaschuk, G.D., Puttagunta, L., Waite, R. & Archer, S.L. (2002). Dichloroacetate, a metabolic modulator, prevents and reverses chronic hypoxic pulmonary hypertension in rats: role of increased expression and activity of voltage-gated potassium channels. *Circulation.* **105**(2), 244-250.
- Miyashita, T., Kawakami, A., Nakashima, T., Yamasaki, S., Tamai, M., Tanaka, F., Kamachi, M., Ida, H., Migita, K., Origuchi, T., Nakao, K. & Eguchi, K. (2004). Osteoprotegerin (OPG) acts as an endogenous decoy receptor in tumour necrosis factor-related apoptosis-inducing ligand (TRAIL)-mediated apoptosis of fibroblast-like synovial cells. *Clin. Exp. Immunol.* **137**(2), 430-436.
- Moeller, A., Ask, K., Warburton, D., Gauldie, J. & Kolb, M. (2008). The bleomycin animal model: a useful tool to investigate treatment options for idiopathic pulmonary fibrosis? *Int. J. Biochem. Cell Biol.* **40**(3), 362-382.
- Moodley, Y.P., Caterina, P., Scaffidi, A.K., Misso, N.L., Papadimitriou, J.M., Mcanulty, R.J., Laurent, G.J., Thompson, P.J. & Knight, D.A. (2004). Comparison of the morphological and biochemical changes in normal human lung fibroblasts and fibroblasts derived from lungs of patients with idiopathic pulmonary fibrosis during FasL-induced apoptosis. *J. Pathol.* **202**(4), 486-495.
- Moore, B., Lawson, W.E., Oury, T.D., Sisson, T.H., Raghavendran, K. & Hogaboam, C.M. (2013). Animal models of fibrotic lung disease. *Am. J. Respir. Cell Mol. Biol.* **49**(2), 167-179.
- Moore, B.B. & Hogaboam, C.M. (2008). Murine models of pulmonary fibrosis. *Am. J. Physiol. Lung Cell Mol. Physiol.* **294**(2), L152-160.
- Morales-Santana, S., Garcia-Fontana, B., Garcia-Martin, A., Rozas-Moreno, P., Garcia-Salcedo, J.A., Reyes-Garcia, R. & Munoz-Torres, M. (2013). Atherosclerotic disease in type 2 diabetes is associated with an increase in sclerostin levels. *Diabetes Care.* **36**(6), 1667-1674.
- Morissette, M.C., Parent, J. & Milot, J. (2011). The emphysematous lung is abnormally sensitive to TRAIL-mediated apoptosis. *Respir. Res.* **12**, 105.
- Morissette, M.C., Vachon-Beaudoin, G., Parent, J., Chakir, J. & Milot, J. (2008). Increased p53 level, Bax/Bcl-x(L) ratio, and TRAIL receptor expression in human emphysema. *Am. J. Respir. Crit. Care Med.* **178**(3), 240-247.
- Morrell, N.W. (2006). Pulmonary Hypertension Due to BMPR2 Mutation. *Proceedings of the American Thoracic Society.* **3**(8), 680-686.
- Motulsky, H.J. & Brown, R.E. (2006). Detecting outliers when fitting data with nonlinear regression - a new method based on robust nonlinear regression and the false discovery rate. *BMC Bioinformatics.* **7**, 123.
- Mukerjee, D., St George, D., Coleiro, B., Knight, C., Denton, C.P., Davar, J., Black, C.M. & Coghlan, J.G. (2003). Prevalence and outcome in systemic sclerosis associated

pulmonary arterial hypertension: application of a registry approach. *Ann. Rheum. Dis.* **62**(11), 1088-1093.

- Nathan, S.D., Albera, C., Bradford, W.Z., Costabel, U., Glaspole, I., Glassberg, M.K., Kardatzke, D.R., Daigl, M., Kirchgaessler, K.U., Lancaster, L.H., Lederer, D.J., Pereira, C.A., Swigris, J.J., Valeyre, D. & Noble, P.W. (2017). Effect of pirfenidone on mortality: pooled analyses and meta-analyses of clinical trials in idiopathic pulmonary fibrosis. *Lancet Respir Med.* **5**(1), 33-41.
- Nguyen, V., Cudrici, C., Zernetkina, V., Niculescu, F., Rus, H., Drachenberg, C. & Rus, V. (2009). TRAIL, DR4 and DR5 are upregulated in kidneys from patients with lupus nephritis and exert proliferative and proinflammatory effects. *Clin. Immunol.* **132**(1), 32-42.
- Novo-Rodríguez, C. & García-Fontana, B. (2018). Circulating levels of sclerostin are associated with cardiovascular mortality. **13**(6), e0199504.
- Olson, A.L., Brown, K.K. & Fischer, A. (2012). Connective tissue disease-associated lung disease. *Immunol. Allergy Clin. North Am.* **32**(4), 513-536.
- Pan, G., Ni, J., Wei, Y.F., Yu, G., Gentz, R. & Dixit, V.M. (1997a). An antagonist decoy receptor and a death domain-containing receptor for TRAIL. *Science.* **277**(5327), 815-818.
- Pan, G., Ni, J., Yu, G., Wei, Y.F. & Dixit, V.M. (1998). TRUNDD, a new member of the TRAIL receptor family that antagonizes TRAIL signalling. *FEBS Lett.* **424**(1-2), 41-45.
- Pan, G., O'rourke, K., Chinnaiyan, A.M., Gentz, R., Ebner, R., Ni, J. & Dixit, V.M. (1997b). The receptor for the cytotoxic ligand TRAIL. *Science.* **276**(5309), 111-113.
- Paulin, R., Meloche, J., Courboulain, A., Lambert, C., Haromy, A., Courchesne, A., Bonnet, P., Provencher, S., Michelakis, E.D. & Bonnet, S. (2014). Targeting cell motility in pulmonary arterial hypertension. *Eur. Respir. J.* **43**(2), 531-544.
- Peacock, A.J., Murphy, N.F., McMurray, J.J., Caballero, L. & Stewart, S. (2007). An epidemiological study of pulmonary arterial hypertension. *Eur. Respir. J.* **30**(1), 104-109.
- Perez, V.A., Ali, Z., Alastalo, T.P., Ikeno, F., Sawada, H., Lai, Y.J., Kleisli, T., Spiekerkoetter, E., Qu, X., Rubinos, L.H., Ashley, E., Amieva, M., Dedhar, S. & Rabinovitch, M. (2011). BMP promotes motility and represses growth of smooth muscle cells by activation of tandem Wnt pathways. *J. Cell Biol.* **192**(1), 171-188.
- Peteranderl, C., Morales-Nebreda, L., Selvakumar, B., Lecuona, E., Vadasz, I., Morty, R.E., Schmoltdt, C., Bepalowa, J., Wolff, T., Pleschka, S., Mayer, K., Gattenloehner, S., Fink, L., Lohmeyer, J., Seeger, W., Sznajder, J.I., Mutlu, G.M., Budinger, G.R. & Herold, S. (2016). Macrophage-epithelial paracrine crosstalk inhibits lung edema clearance during influenza infection. *J. Clin. Invest.* **126**(4), 1566-1580.
- Petrovski, S., Todd, J.L., Durheim, M.T., Wang, Q., Chien, J.W., Kelly, F.L., Frankel, C., Mebane, C.M., Ren, Z., Bridgers, J., Urban, T.J., Malone, C.D., Copeland, A.F., Brinkley, C., Allen, A.S., O'riordan, T., Mchutchison, J.G., Palmer, S.M. & Goldstein, D.B. (2017). An Exome Sequencing Study to Assess the Role of Rare Genetic Variation in Pulmonary Fibrosis. *Am. J. Respir. Crit. Care Med.* **196**(1), 82-93.

- Phillips, R.J., Burdick, M.D., Hong, K., Lutz, M.A., Murray, L.A., Xue, Y.Y., Belperio, J.A., Keane, M.P. & Strieter, R.M. (2004). Circulating fibrocytes traffic to the lungs in response to CXCL12 and mediate fibrosis. *J. Clin. Invest.* **114**(3), 438-446.
- Pietra, G.G., Edwards, W.D., Kay, J.M., Rich, S., Kernis, J., Schloo, B., Ayres, S.M., Bergofsky, E.H., Brundage, B.H., Detre, K.M. & Et Al. (1989). Histopathology of primary pulmonary hypertension. A qualitative and quantitative study of pulmonary blood vessels from 58 patients in the National Heart, Lung, and Blood Institute, Primary Pulmonary Hypertension Registry. *Circulation.* **80**(5), 1198-1206.
- Pitti, R.M., Marsters, S.A., Ruppert, S., Donahue, C.J., Moore, A. & Ashkenazi, A. (1996). Induction of apoptosis by Apo-2 ligand, a new member of the tumor necrosis factor cytokine family. *J. Biol. Chem.* **271**(22), 12687-12690.
- Plataki, M., Koutsopoulos, A.V., Darivianaki, K., Delides, G., Siafakas, N.M. & Bouros, D. (2005). Expression of apoptotic and antiapoptotic markers in epithelial cells in idiopathic pulmonary fibrosis. *Chest.* **127**(1), 266-274.
- Poole, K.E., Van Bezooijen, R.L., Loveridge, N., Hamersma, H., Papapoulos, S.E., Lowik, C.W. & Reeve, J. (2005). Sclerostin is a delayed secreted product of osteocytes that inhibits bone formation. *FASEB J.* **19**(13), 1842-1844.
- Pullamsetti, S.S., Kojonazarov, B., Storn, S., Gall, H., Salazar, Y., Wolf, J., Weigert, A., El-Nikhely, N., Ghofrani, H.A., Krombach, G.A., Fink, L., Gattenlöhner, S., Rapp, U.R., Schermuly, R.T., Grimminger, F., Seeger, W. & Savai, R. (2017). Lung cancer-associated pulmonary hypertension: Role of microenvironmental inflammation based on tumor cell-immune cell cross-talk. *Sci. Transl. Med.* **9**(416), eaai9048.
- Qin, W., Zhao, W., Li, X., Peng, Y., Harlow, L.M., Li, J., Qin, Y., Pan, J., Wu, Y., Ran, L., Ke, H.Z., Cardozo, C.P. & Bauman, W.A. (2016). Mice with sclerostin gene deletion are resistant to the severe sublesional bone loss induced by spinal cord injury. *Osteoporos. Int.* **27**(12), 3627-3636.
- Raghu, G., Anstrom, K.J., King, T.E., Jr., Lasky, J.A. & Martinez, F.J. (2012). Prednisone, azathioprine, and N-acetylcysteine for pulmonary fibrosis. *N. Engl. J. Med.* **366**(21), 1968-1977.
- Raghu, G., Collard, H.R., Egan, J.J., Martinez, F.J., Behr, J., Brown, K.K., Colby, T.V., Cordier, J.F., Flaherty, K.R., Lasky, J.A., Lynch, D.A., Ryu, J.H., Swigris, J.J., Wells, A.U., Ancochea, J., Bouros, D., Carvalho, C., Costabel, U., Ebina, M., Hansell, D.M., Johkoh, T., Kim, D.S., King, T.E., Jr., Kondoh, Y., Myers, J., Muller, N.L., Nicholson, A.G., Richeldi, L., Selman, M., Dudden, R.F., Griss, B.S., Protzko, S.L. & Schunemann, H.J. (2011). An official ATS/ERS/JRS/ALAT statement: idiopathic pulmonary fibrosis: evidence-based guidelines for diagnosis and management. *Am. J. Respir. Crit. Care Med.* **183**(6), 788-824.
- Raghu, G., Van Den Blink, B., Hamblin, M.J., Brown, A.W., Golden, J.A., Ho, L.A., Wijsenbeek, M.S., Vasakova, M., Pesci, A., Antin-Ozerkis, D.E., Meyer, K.C., Kreuter, M., Moran, D., Santin-Janin, H., Aubin, F., Mulder, G.J., Gupta, R. & Richeldi, L. (2019). Long-term treatment with recombinant human pentraxin 2 protein in patients with idiopathic pulmonary fibrosis: an open-label extension study. *Lancet Respir Med.* **7**(8), 657-664.
- Raghu, G., Van Den Blink, B., Hamblin, M.J., Brown, A.W., Golden, J.A., Ho, L.A., Wijsenbeek, M.S., Vasakova, M., Pesci, A., Antin-Ozerkis, D.E., Meyer, K.C., Kreuter, M., Santin-Janin, H., Mulder, G.J., Bartholmai, B., Gupta, R. & Richeldi, L. (2018). Effect of

Recombinant Human Pentraxin 2 vs Placebo on Change in Forced Vital Capacity in Patients With Idiopathic Pulmonary Fibrosis: A Randomized Clinical Trial. *JAMA*. **319**(22), 2299-2307.

Ranchoux, B., Antigny, F., Rucker-Martin, C., Hautefort, A., Pechoux, C., Bogaard, H.J., Dorfmueller, P., Remy, S., Lecerf, F., Plante, S., Chat, S., Fadel, E., Houssaini, A., Anegon, I., Adnot, S., Simonneau, G., Humbert, M., Cohen-Kaminsky, S. & Perros, F. (2015). Endothelial-to-mesenchymal transition in pulmonary hypertension. *Circulation*. **131**(11), 1006-1018.

Rhodes, C.J., Batai, K., Bleda, M., Haimel, M., Southgate, L., Germain, M., Pauciulo, M.W., Hadinnapola, C., Aman, J., Girerd, B., Arora, A., Knight, J., Hanscombe, K.B., Karnes, J.H., Kaakinen, M., Gall, H., Ulrich, A., Harbaum, L., Cebola, I., Ferrer, J., Lutz, K., Swietlik, E.M., Ahmad, F., Amouyel, P., Archer, S.L., Argula, R., Austin, E.D., Badesch, D., Bakshi, S., Barnett, C., Benza, R., Bhatt, N., Bogaard, H.J., Burger, C.D., Chakinala, M., Church, C., Coghlan, J.G., Condliffe, R., Corris, P.A., Danesino, C., Debette, S., Elliott, C.G., Elwing, J., Eyries, M., Fortin, T., Franke, A., Frantz, R.P., Frost, A., Garcia, J.G.N., Ghio, S., Ghofrani, H.-A., Gibbs, J.S.R., Harley, J., He, H., Hill, N.S., Hirsch, R., Houweling, A.C., Howard, L.S., Ivy, D., Kiely, D.G., Klinger, J., Kovacs, G., Lahm, T., Laudes, M., Machado, R.D., Mackenzie Ross, R.V., Marsolo, K., Martin, L.J., Moledina, S., Montani, D., Nathan, S.D., Newnham, M., Olschewski, A., Olschewski, H., Oudiz, R.J., Ouwehand, W.H., Peacock, A.J., Pepke-Zaba, J., Rehman, Z., Robbins, I., Roden, D.M., Rosenzweig, E.B., Saydain, G., Scelsi, L., Schilz, R., Seeger, W., Shaffer, C.M., Simms, R.W., Simon, M., Sitbon, O., Suntharalingam, J., Tang, H., Tchourbanov, A.Y., Thenappan, T., Torres, F., Toshner, M.R., Treacy, C.M., Vonk Noordegraaf, A., Waisfisz, Q., Walsworth, A.K., et al. (2019). Genetic determinants of risk in pulmonary arterial hypertension: international genome-wide association studies and meta-analysis. *The Lancet Respiratory Medicine*. **7**(3), 227-238.

Rich, S. (2007). The value of approved therapies for pulmonary arterial hypertension. *Am. Heart J.* **153**(6), 889-890.

Richeldi, L., Du Bois, R.M., Raghu, G., Azuma, A., Brown, K.K., Costabel, U., Cottin, V., Flaherty, K.R., Hansell, D.M., Inoue, Y., Kim, D.S., Kolb, M., Nicholson, A.G., Noble, P.W., Selman, M., Taniguchi, H., Brun, M., Le Maulf, F., Girard, M., Stowasser, S., Schlenker-Herceg, R., Disse, B. & Collard, H.R. (2014). Efficacy and safety of nintedanib in idiopathic pulmonary fibrosis. *N. Engl. J. Med.* **370**(22), 2071-2082.

Ridker, P.M., Hennekens, C.H., Buring, J.E. & Rifai, N. (2000). C-reactive protein and other markers of inflammation in the prediction of cardiovascular disease in women. *N. Engl. J. Med.* **342**(12), 836-843.

Ridker, P.M., Hennekens, C.H., Roitman-Johnson, B., Stampfer, M.J. & Allen, J. (1998). Plasma concentration of soluble intercellular adhesion molecule 1 and risks of future myocardial infarction in apparently healthy men. *Lancet*. **351**(9096), 88-92.

Ritchie, M.E., Phipson, B., Wu, D., Hu, Y., Law, C.W., Shi, W. & Smyth, G.K. (2015). limma powers differential expression analyses for RNA-sequencing and microarray studies. *Nucleic Acids Res.* **43**(7), e47.

Robertson, N.M., Zangrilli, J.G., Steplewski, A., Hastie, A., Lindemeyer, R.G., Planeta, M.A., Smith, M.K., Innocent, N., Musani, A., Pascual, R., Peters, S. & Litwack, G. (2002). Differential expression of TRAIL and TRAIL receptors in allergic asthmatics following

- segmental antigen challenge: evidence for a role of TRAIL in eosinophil survival. *J. Immunol.* **169**(10), 5986-5996.
- Roth, R.A., Dotzlaw, L.A., Baranyi, B., Kuo, C.H. & Hook, J.B. (1981). Effect of monocrotaline ingestion on liver, kidney, and lung of rats. *Toxicol. Appl. Pharmacol.* **60**(2), 193-203.
- Rudarakanchana, N., Flanagan, J.A., Chen, H., Upton, P.D., Machado, R., Patel, D., Trembath, R.C. & Morrell, N.W. (2002). Functional analysis of bone morphogenetic protein type II receptor mutations underlying primary pulmonary hypertension. *Hum. Mol. Genet.* **11**(13), 1517-1525.
- Rueden, C.T., Schindelin, J., Hiner, M.C., DeZonia, B.E., Walter, A.E., Arena, E.T. & Eliceiri, K.W. (2017). ImageJ2: ImageJ for the next generation of scientific image data. *BMC Bioinformatics.* **18**(1), 529.
- Sato, S., Shinohara, S., Hayashi, S., Morizumi, S., Abe, S., Okazaki, H., Chen, Y., Goto, H., Aono, Y., Ogawa, H., Koyama, K., Nishimura, H., Kawano, H., Toyoda, Y., Uehara, H. & Nishioka, Y. (2017). Anti-fibrotic efficacy of nintedanib in pulmonary fibrosis via the inhibition of fibrocyte activity. *Respir. Res.* **18**(1), 172.
- Savale, L., Tu, L., Rideau, D., Izziki, M., Maitre, B., Adnot, S. & Eddahibi, S. (2009). Impact of interleukin-6 on hypoxia-induced pulmonary hypertension and lung inflammation in mice. *Respir. Res.* **10**, 6.
- Schafer, M.J., White, T.A., Iijima, K., Haak, A.J., Ligresti, G., Atkinson, E.J., Oberg, A.L., Birch, J., Salmonowicz, H., Zhu, Y., Mazula, D.L., Brooks, R.W., Fuhrmann-Stroissnigg, H., Pirtskhalava, T., Prakash, Y.S., Tchkonja, T., Robbins, P.D., Aubry, M.C., Passos, J.F., Kirkland, J.L., Tschumperlin, D.J., Kita, H. & Lebrasseur, N.K. (2017). Cellular senescence mediates fibrotic pulmonary disease. *Nat Commun.* **8**, 14532.
- Schindelin, J., Arganda-Carreras, I., Frise, E., Kaynig, V., Longair, M., Pietzsch, T., Preibisch, S., Rueden, C., Saalfeld, S., Schmid, B., Tinevez, J.Y., White, D.J., Hartenstein, V., Eliceiri, K., Tomancak, P. & Cardona, A. (2012). Fiji: an open-source platform for biological-image analysis. *Nat Methods.* **9**(7), 676-682.
- Schneider, P., Olson, D., Tardivel, A., Browning, B., Lugovskoy, A., Gong, D., Dobles, M., Hertig, S., Hofmann, K., Van Vlijmen, H., Hsu, Y.M., Burkly, L.C., Tschopp, J. & Zheng, T.S. (2003). Identification of a new murine tumor necrosis factor receptor locus that contains two novel murine receptors for tumor necrosis factor-related apoptosis-inducing ligand (TRAIL). *J. Biol. Chem.* **278**(7), 5444-5454.
- Screaton, G.R., Mongkolsapaya, J., Xu, X.N., Cowper, A.E., McMichael, A.J. & Bell, J.I. (1997). TRICK2, a new alternatively spliced receptor that transduces the cytotoxic signal from TRAIL. *Curr. Biol.* **7**(9), 693-696.
- Secchiero, P., Gonelli, A., Carnevale, E., Milani, D., Pandolfi, A., Zella, D. & Zauli, G. (2003). TRAIL promotes the survival and proliferation of primary human vascular endothelial cells by activating the Akt and ERK pathways. *Circulation.* **107**(17), 2250-2256.
- Secchiero, P., Zerbinati, C., Rimondi, E., Corallini, F., Milani, D., Grill, V., Forti, G., Capitani, S. & Zauli, G. (2004). TRAIL promotes the survival, migration and proliferation of vascular smooth muscle cells. *Cell. Mol. Life Sci.* **61**(15), 1965-1974.
- Shankman, L.S., Gomez, D., Cherepanova, O.A., Salmon, M., Alencar, G.F., Haskins, R.M., Swiatlowska, P., Newman, A.a.C., Greene, E.S., Straub, A.C., Isakson, B., Randolph,

- G.J. & Owens, G.K. (2015). KLF4 Dependent Phenotypic Modulation of SMCs Plays a Key Role in Atherosclerotic Plaque Pathogenesis. *Nat. Med.* **21**(6), 628-637.
- Shapiro, S., Traiger, G.L., Turner, M., Mcgoon, M.D., Wason, P. & Barst, R.J. (2012). Sex differences in the diagnosis, treatment, and outcome of patients with pulmonary arterial hypertension enrolled in the registry to evaluate early and long-term pulmonary arterial hypertension disease management. *Chest.* **141**(2), 363-373.
- Sheares, K.K., Jeffery, T.K., Long, L., Yang, X. & Morrell, N.W. (2004). Differential effects of TGF-beta1 and BMP-4 on the hypoxic induction of cyclooxygenase-2 in human pulmonary artery smooth muscle cells. *Am. J. Physiol. Lung Cell Mol. Physiol.* **287**(5), L919-927.
- Sheikh, A.Q., Misra, A., Rosas, I.O., Adams, R.H. & Greif, D.M. (2015). Smooth muscle cell progenitors are primed to muscularize in pulmonary hypertension. *Sci. Transl. Med.* **7**(308), 308ra159.
- Sieg, D.J., Hauck, C.R., Ilic, D., Klingbeil, C.K., Schaefer, E., Damsky, C.H. & Schlaepfer, D.D. (2000). FAK integrates growth-factor and integrin signals to promote cell migration. *Nat. Cell Biol.* **2**(5), 249-256.
- Simonet, W.S., Lacey, D.L., Dunstan, C.R., Kelley, M., Chang, M.S., Luthy, R., Nguyen, H.Q., Wooden, S., Bennett, L., Boone, T., Shimamoto, G., Derosé, M., Elliott, R., Colombero, A., Tan, H.L., Trail, G., Sullivan, J., Davy, E., Bucay, N., Renshaw-Gegg, L., Hughes, T.M., Hill, D., Pattison, W., Campbell, P., Sander, S., Van, G., Tarpley, J., Derby, P., Lee, R. & Boyle, W.J. (1997). Osteoprotegerin: a novel secreted protein involved in the regulation of bone density. *Cell.* **89**(2), 309-319.
- Simonneau, G. & Montani, D. (2019). Haemodynamic definitions and updated clinical classification of pulmonary hypertension. **53**(1).
- Sitbon, O., Channick, R., Chin, K.M., Frey, A., Gaine, S., Galie, N., Ghofrani, H.A., Hoeper, M.M., Lang, I.M., Preiss, R., Rubin, L.J., Di Scala, L., Tapson, V., Adzerikho, I., Liu, J., Moiseeva, O., Zeng, X., Simonneau, G., Mclaughlin, V.V. & Investigators, G. (2015). Selexipag for the Treatment of Pulmonary Arterial Hypertension. *N. Engl. J. Med.* **373**(26), 2522-2533.
- Sitbon, O., Humbert, M., Jais, X., loos, V., Hamid, A.M., Provencher, S., Garcia, G., Parent, F., Herve, P. & Simonneau, G. (2005). Long-term response to calcium channel blockers in idiopathic pulmonary arterial hypertension. *Circulation.* **111**(23), 3105-3111.
- Smyth, G.K. (2004). Linear models and empirical bayes methods for assessing differential expression in microarray experiments. *Stat. Appl. Genet. Mol. Biol.* **3**, Article3.
- Song, S., Choi, K., Ryu, S.W., Kang, S.W. & Choi, C. (2011). TRAIL promotes caspase-dependent pro-inflammatory responses via PKCdelta activation by vascular smooth muscle cells. *Cell Death Dis.* **2**, e223.
- Starkey, M.R., Nguyen, D.H., Essilfie, A.T., Kim, R.Y., Hatchwell, L.M., Collison, A.M., Yagita, H., Foster, P.S., Horvat, J.C., Mattes, J. & Hansbro, P.M. (2014). Tumor necrosis factor-related apoptosis-inducing ligand translates neonatal respiratory infection into chronic lung disease. *Mucosal Immunol.* **7**(3), 478-488.

- Steen, V.D. & Medsger, T.A. (2007). Changes in causes of death in systemic sclerosis, 1972-2002. *Ann. Rheum. Dis.* **66**(7), 940-944.
- Steiner, M.K., Syrkina, O.L., Kolliputi, N., Mark, E.J., Hales, C.A. & Waxman, A.B. (2009). Interleukin-6 overexpression induces pulmonary hypertension. *Circ. Res.* **104**(2), 236-244, 228p following 244.
- Steinwede, K., Henken, S., Bohling, J., Maus, R., Ueberberg, B., Brumshagen, C., Brincks, E.L., Griffith, T.S., Welte, T. & Maus, U.A. (2012). TNF-related apoptosis-inducing ligand (TRAIL) exerts therapeutic efficacy for the treatment of pneumococcal pneumonia in mice. *J. Exp. Med.* **209**(11), 1937-1952.
- Stenmark, K.R., Meyrick, B., Galie, N., Mooi, W.J. & Mcmurtry, I.F. (2009). Animal models of pulmonary arterial hypertension: the hope for etiological discovery and pharmacological cure. *Am. J. Physiol. Lung Cell Mol. Physiol.* **297**(6), L1013-1032.
- Strongman, H., Kausar, I. & Maher, T.M. (2018). Incidence, Prevalence, and Survival of Patients with Idiopathic Pulmonary Fibrosis in the UK. *Adv. Ther.* **35**(5), 724-736.
- Suliman, A., Lam, A., Datta, R. & Srivastava, R.K. (2001). Intracellular mechanisms of TRAIL: apoptosis through mitochondrial-dependent and -independent pathways. *Oncogene.* **20**(17), 2122-2133.
- Tajsic, T. & Morrell, N.W. (2011). Smooth muscle cell hypertrophy, proliferation, migration and apoptosis in pulmonary hypertension. *Compr Physiol.* **1**(1), 295-317.
- Tanner, M.A., Thomas, T.P. & Grisanti, L.A. (2019). Death receptor 5 contributes to cardiomyocyte hypertrophy through epidermal growth factor receptor transactivation. *J. Mol. Cell. Cardiol.*
- Taraseviciene-Stewart, L., Kasahara, Y., Alger, L., Hirth, P., Mc Mahon, G., Waltenberger, J., Voelkel, N.F. & Tuder, R.M. (2001). Inhibition of the VEGF receptor 2 combined with chronic hypoxia causes cell death-dependent pulmonary endothelial cell proliferation and severe pulmonary hypertension. *FASEB J.* **15**(2), 427-438.
- Tarca, A.L., Draghici, S., Khatri, P., Hassan, S.S., Mittal, P., Kim, J.S., Kim, C.J., Kusanovic, J.P. & Romero, R. (2009). A novel signaling pathway impact analysis. *Bioinformatics.* **25**(1), 75-82.
- Thambiayya, K. (2015). Endothelial dysfunction in pulmonary arterial hypertension (PAH). *The FASEB Journal.* **29**(1 Supplement).
- Thannickal, V.J. & Horowitz, J.C. (2006). Evolving concepts of apoptosis in idiopathic pulmonary fibrosis. *Proc Am Thorac Soc.* **3**(4), 350-356.
- The gene ontology consortium (2018). The Gene Ontology Resource: 20 years and still GOing strong. *Nucleic Acids Res.* **47**(D1), D330-D338.
- Thrall, R.S., McCormick, J.R., Jack, R.M., McCreynolds, R.A. & Ward, P.A. (1979). Bleomycin-induced pulmonary fibrosis in the rat: inhibition by indomethacin. *Am. J. Pathol.* **95**(1), 117-130.
- Trauzold, A., Siegmund, D., Schniewind, B., Sipos, B., Egberts, J., Zorenkov, D., Emme, D., Roder, C., Kalthoff, H. & Wajant, H. (2006). TRAIL promotes metastasis of human pancreatic ductal adenocarcinoma. *Oncogene.* **25**(56), 7434-7439.

- Tuder, R.M., Chacon, M., Alger, L., Wang, J., Taraseviciene-Stewart, L., Kasahara, Y., Cool, C.D., Bishop, A.E., Geraci, M., Semenza, G.L., Yacoub, M., Polak, J.M. & Voelkel, N.F. (2001). Expression of angiogenesis-related molecules in plexiform lesions in severe pulmonary hypertension: evidence for a process of disordered angiogenesis. *J. Pathol.* **195**(3), 367-374.
- Uhal, B.D., Joshi, I., Hughes, W.F., Ramos, C., Pardo, A. & Selman, M. (1998). Alveolar epithelial cell death adjacent to underlying myofibroblasts in advanced fibrotic human lung. *Am. J. Physiol.* **275**(6), L1192-1199.
- Uhlen, M., Zhang, C., Lee, S., Sjostedt, E., Fagerberg, L., Bidkhor, G., Benfeitas, R., Arif, M., Liu, Z., Edfors, F., Sanli, K., Von Feilitzen, K., Oksvold, P., Lundberg, E., Hober, S., Nilsson, P., Mattsson, J., Schwenk, J.M., Brunnstrom, H., Glimelius, B., Sjoblom, T., Edqvist, P.H., Djureinovic, D., Micke, P., Lindskog, C., Mardinoglu, A. & Ponten, F. (2017). A pathology atlas of the human cancer transcriptome. *Science.* **357**(6352).
- Van Bezooijen, R.L., Roelen, B.A., Visser, A., Van Der Wee-Pals, L., De Wilt, E., Karperien, M., Hamersma, H., Papapoulos, S.E., Ten Dijke, P. & Lowik, C.W. (2004). Sclerostin is an osteocyte-expressed negative regulator of bone formation, but not a classical BMP antagonist. *J. Exp. Med.* **199**(6), 805-814.
- Van Bezooijen, R.L., Svensson, J.P., Eefting, D., Visser, A., Van Der Horst, G., Karperien, M., Quax, P.H., Vrieling, H., Papapoulos, S.E., Ten Dijke, P. & Lowik, C.W. (2007). Wnt but not BMP signaling is involved in the inhibitory action of sclerostin on BMP-stimulated bone formation. *J. Bone Miner. Res.* **22**(1), 19-28.
- Van Der Worp, H.B., Howells, D.W., Sena, E.S., Porritt, M.J., Rewell, S., O'collins, V. & Macleod, M.R. (2010). Can animal models of disease reliably inform human studies? *PLoS Med.* **7**(3), e1000245.
- Van Rheen, Z., Fattman, C., Domarski, S., Majka, S., Klemm, D., Stenmark, K.R. & Nozik-Grayck, E. (2011). Lung extracellular superoxide dismutase overexpression lessens bleomycin-induced pulmonary hypertension and vascular remodeling. *Am. J. Respir. Cell Mol. Biol.* **44**(4), 500-508.
- Varfolomeev, E., Maecker, H., Sharp, D., Lawrence, D., Renz, M., Vucic, D. & Ashkenazi, A. (2005). Molecular determinants of kinase pathway activation by Apo2 ligand/tumor necrosis factor-related apoptosis-inducing ligand. *J. Biol. Chem.* **280**(49), 40599-40608.
- Vaughan, A.E., Brumwell, A.N., Xi, Y., Gotts, J.E., Brownfield, D.G., Treutlein, B., Tan, K., Tan, V., Liu, F.C., Looney, M.R., Matthay, M.A., Rock, J.R. & Chapman, H.A. (2015). Lineage-negative progenitors mobilize to regenerate lung epithelium after major injury. *Nature.* **517**(7536), 621-625.
- Walczak, H., Miller, R.E., Ariail, K., Gliniak, B., Griffith, T.S., Kubin, M., Chin, W., Jones, J., Woodward, A., Le, T., Smith, C., Smolak, P., Goodwin, R.G., Rauch, C.T., Schuh, J.C. & Lynch, D.H. (1999). Tumoricidal activity of tumor necrosis factor-related apoptosis-inducing ligand in vivo. *Nat. Med.* **5**(2), 157-163.
- Wang, R., Ibarra-Sunga, O., Verlinski, L., Pick, R. & Uhal, B.D. (2000). Abrogation of bleomycin-induced epithelial apoptosis and lung fibrosis by captopril or by a caspase inhibitor. *Am. J. Physiol. Lung Cell Mol. Physiol.* **279**(1), L143-151.

- Wang, Y., Kuan, P.J., Xing, C., Cronkhite, J.T., Torres, F., Rosenblatt, R.L., Dimaio, J.M., Kinch, L.N., Grishin, N.V. & Garcia, C.K. (2009). Genetic defects in surfactant protein A2 are associated with pulmonary fibrosis and lung cancer. *Am. J. Hum. Genet.* **84**(1), 52-59.
- Weckmann, M., Collison, A., Simpson, J.L., Kopp, M.V., Wark, P.A., Smyth, M.J., Yagita, H., Matthaei, K.I., Hansbro, N., Whitehead, B., Gibson, P.G., Foster, P.S. & Mattes, J. (2007). Critical link between TRAIL and CCL20 for the activation of TH2 cells and the expression of allergic airway disease. *Nat. Med.* **13**(11), 1308-1315.
- Weissman, T.A., Sanes, J.R., Lichtman, J.W. & Livet, J. (2011). Generating and imaging multicolor Brainbow mice. *Cold Spring Harb Protoc.* **2011**(7), 763-769.
- Wharton, J., Strange, J.W., Moller, G.M., Growcott, E.J., Ren, X., Franklyn, A.P., Phillips, S.C. & Wilkins, M.R. (2005). Antiproliferative effects of phosphodiesterase type 5 inhibition in human pulmonary artery cells. *Am. J. Respir. Crit. Care Med.* **172**(1), 105-113.
- Wiley, S.R., Schooley, K., Smolak, P.J., Din, W.S., Huang, C.P., Nicholl, J.K., Sutherland, G.R., Smith, T.D., Rauch, C., Smith, C.A. & Goodwin, R.G. (1995). Identification and characterization of a new member of the TNF family that induces apoptosis. *Immunity.* **3**(6), 673-682.
- Williams, J.L., Cavus, O., Loccoh, E.C., Adelman, S., Daugherty, J.C., Smith, S.A., Canan, B., Janssen, P.M.L., Koenig, S., Kline, C.F., Mohler, P.J. & Bradley, E.A. (2018). Defining the molecular signatures of human right heart failure. *Life Sci.* **196**, 118-126.
- Willis, B.C., Liebler, J.M., Luby-Phelps, K., Nicholson, A.G., Crandall, E.D., Du Bois, R.M. & Borok, Z. (2005). Induction of epithelial-mesenchymal transition in alveolar epithelial cells by transforming growth factor-beta1: potential role in idiopathic pulmonary fibrosis. *Am. J. Pathol.* **166**(5), 1321-1332.
- Wilson, J.L., Rupasinghe, C., Usheva, A., Warburton, R., Kaplan, C., Taylor, L., Hill, N., Mierke, D.F. & Polgar, P. (2015). Modulating the dysregulated migration of pulmonary arterial hypertensive smooth muscle cells with motif mimicking cell permeable peptides. *Curr Top Pept Protein Res.* **16**, 1-17.
- Winkler, D.G., Sutherland, M.K., Geoghegan, J.C., Yu, C., Hayes, T., Skonier, J.E., Shpektor, D., Jonas, M., Kovacevich, B.R., Staehling-Hampton, K., Appleby, M., Brunkow, M.E. & Latham, J.A. (2003). Osteocyte control of bone formation via sclerostin, a novel BMP antagonist. *EMBO J.* **22**(23), 6267-6276.
- Wirka, R.C., Wagh, D., Paik, D.T., Pjanic, M., Nguyen, T., Miller, C.L., Kundu, R., Nagao, M., Collier, J., Koyano, T.K., Fong, R., Woo, Y.J., Liu, B., Montgomery, S.B., Wu, J.C., Zhu, K., Chang, R., Alamprese, M., Tallquist, M.D., Kim, J.B. & Quertermous, T. (2019). Atheroprotective roles of smooth muscle cell phenotypic modulation and the TCF21 disease gene as revealed by single-cell analysis. *Nat. Med.* **25**(8), 1280-1289.
- Wirth, A., Benyo, Z., Lukasova, M., Leutgeb, B., Wettschureck, N., Gorbey, S., Orsy, P., Horvath, B., Maser-Gluth, C., Greiner, E., Lemmer, B., Schutz, G., Gutkind, J.S. & Offermanns, S. (2008). G12-G13-LARG-mediated signaling in vascular smooth muscle is required for salt-induced hypertension. *Nat. Med.* **14**(1), 64-68.
- Wright, A.F., Ewart, M.A., Mair, K., Nilsen, M., Dempsie, Y., Loughlin, L. & Maclean, M.R. (2015). Oestrogen receptor alpha in pulmonary hypertension. *Cardiovasc. Res.* **106**(2), 206-216.

- Wu, Y., Shen, Y., Zhang, J., Wan, C., Wang, T., Xu, D., Yang, T. & Wen, F. (2015). Increased serum TRAIL and DR5 levels correlated with lung function and inflammation in stable COPD patients. *Int. J. Chron. Obstruct. Pulmon. Dis.* **10**, 2405-2412.
- Xu, W., Koeck, T., Lara, A.R., Neumann, D., Difilippo, F.P., Koo, M., Janocha, A.J., Masri, F.A., Arroliga, A.C., Jennings, C., Dweik, R.A., Tuder, R.M., Stuehr, D.J. & Erzurum, S.C. (2007). Alterations of cellular bioenergetics in pulmonary artery endothelial cells. *Proc. Natl. Acad. Sci. U. S. A.* **104**(4), 1342-1347.
- Xu, Y., Mizuno, T., Sridharan, A., Du, Y., Guo, M., Tang, J., Wikenheiser-Brokamp, K.A., Perl, A.T., Funari, V.A., Gokey, J.J., Stripp, B.R. & Whitsett, J.A. (2016). Single-cell RNA sequencing identifies diverse roles of epithelial cells in idiopathic pulmonary fibrosis. *JCI Insight.* **1**(20), e90558.
- Yang, X., Long, L., Southwood, M., Rudarakanchana, N., Upton, P.D., Jeffery, T.K., Atkinson, C., Chen, H., Trembath, R.C. & Morrell, N.W. (2005). Dysfunctional Smad signaling contributes to abnormal smooth muscle cell proliferation in familial pulmonary arterial hypertension. *Circ. Res.* **96**(10), 1053-1063.
- Yeager, M.E., Halley, G.R., Golpon, H.A., Voelkel, N.F. & Tuder, R.M. (2001). Microsatellite instability of endothelial cell growth and apoptosis genes within plexiform lesions in primary pulmonary hypertension. *Circ. Res.* **88**(1), E2-E11.
- Yu, Y., Fantozzi, I., Remillard, C.V., Landsberg, J.W., Kunichika, N., Platoshyn, O., Tigno, D.D., Thistlethwaite, P.A., Rubin, L.J. & Yuan, J.X. (2004). Enhanced expression of transient receptor potential channels in idiopathic pulmonary arterial hypertension. *Proc. Natl. Acad. Sci. U. S. A.* **101**(38), 13861-13866.
- Zauli, G., Pandolfi, A., Gonelli, A., Di Pietro, R., Guarnieri, S., Ciabattini, G., Rana, R., Vitale, M. & Secchiero, P. (2003). Tumor necrosis factor-related apoptosis-inducing ligand (TRAIL) sequentially upregulates nitric oxide and prostanoid production in primary human endothelial cells. *Circ. Res.* **92**(7), 732-740.
- Zepp, J.A., Zacharias, W.J., Frank, D.B., Cavanaugh, C.A., Zhou, S., Morley, M.P. & Morrissey, E.E. (2017). Distinct Mesenchymal Lineages and Niches Promote Epithelial Self-Renewal and Myofibrogenesis in the Lung. *Cell.* **170**(6), 1134-1148.
- Zhang, H.Y. & Phan, S.H. (1999). Inhibition of myofibroblast apoptosis by transforming growth factor beta(1). *Am. J. Respir. Cell Mol. Biol.* **21**(6), 658-665.
- Zhao, T., Zhao, W., Chen, Y., Liu, L., Ahokas, R.A. & Sun, Y. (2013). Differential expression of vascular endothelial growth factor isoforms and receptor subtypes in the infarcted heart. *Int. J. Cardiol.* **167**(6), 2638-2645.
- Zheng, B., Zhang, Z., Black, C.M., De Crombrughe, B. & Denton, C.P. (2002). Ligand-dependent genetic recombination in fibroblasts : a potentially powerful technique for investigating gene function in fibrosis. *Am. J. Pathol.* **160**(5), 1609-1617.
- Zhu, D., Mackenzie, N.C., Millan, J.L., Farquharson, C. & Macrae, V.E. (2011). The appearance and modulation of osteocyte marker expression during calcification of vascular smooth muscle cells. *PLoS One.* **6**(5), e19595.
- Zuo, W., Zhang, T., Wu, D.Z., Guan, S.P., Liew, A.A., Yamamoto, Y., Wang, X., Lim, S.J., Vincent, M., Lessard, M., Crum, C.P., Xian, W. & Mckeon, F. (2015). p63(+)/Krt5(+)

distal airway stem cells are essential for lung regeneration. *Nature*. **517**(7536), 616-620.

## 8 Appendices

### 8.1 Appendix A: Taqman RT-qPCR

#### 8.1.1 Taqman RT-qPCR probes

Target	Species	Assay number
<i>GAPDH</i>	Mouse	Mm99999915_g1
<i>FIGF</i>	Mouse	Mm01131929_m1
<i>SOST</i>	Mouse	Mm00470479_m1
<i>PDGFD</i>	Mouse	Mm00546829_m1
<i>PDGFRB</i>	Mouse	Mm00435553_m1
<i>ICAM1</i>	Mouse	Mm00516023_m1
<i>TNFSF10</i>	Mouse	Mm01283606_m1
<i>FIGF</i>	Human	Hs01128657_m1
<i>ICAM1</i>	Human	Hs00164932_m1
<i>PDGFD</i>	Human	Hs00228671_m1
<i>PDGFRA</i>	Human	Hs00998018_m1
<i>PDGFRB</i>	Human	Hs01019589_m1
<i>SOST</i>	Human	Hs00228830_m1
<i>VIPR1</i>	Human	Hs00910453_m1

#### 8.1.2 Taqman RT-qPCR reaction

Reagent	µl per reaction
Probe (20X)	0.5
MM (2X)	5
<i>cDNA</i>	4.5
Total	10

Temp.	Time	Cycles
50°C	2 min	
95°C	10 min	
95°C	15 sec	40X
60°C	1 min	

## 8.2 Appendix B: R scripts

### 8.2.1 LIMMA mRNA microarray analysis

Measurement of mRNA expression from microarrays was carried out using the LIMMA R package. The Biocmanager package was used for package management.

*LIMMA: <https://bioconductor.org/packages/release/bioc/html/limma.html>*

*Biocmanager: <https://cran.r-project.org/web/packages/BiocManager/index.html>*

```
# set main folder
main.dir <- "."
setwd(main.dir)

# requirements
if (!requireNamespace("BiocManager", quietly = T))
install.packages("BiocManager")
library('BiocManager')
BiocManager::install()
library(limma)

# read Agilent array data
Agilent_ProbeIDs <- read.delim(paste(main.dir,
"targets", "Agilent_gene_list.txt", sep = "/"), header = T)
colnames(Agilent_ProbeIDs) <- gsub("ProbeID", "ProbeName",
colnames(Agilent_ProbeIDs))

# read targets file
targets <- readTargets(paste(main.dir, "targets", "targetsExpression.txt",
sep = "/"))
```

```

# read in array data
x <- read.maimages(targets, path = paste(main.dir, "data", sep = "/"),
source = "agilent", green.only = T)

# background correct and normalise arrays
y <- backgroundCorrect(x, method = "normexp", offset = 16)
y <- normalizeBetweenArrays(y, method = "cyclicloess")

# average spots per probe
y.ave <- avereps(y, ID = y$genes$ProbeName)

# matrix for linear modeling
f <- factor(targets$Condition, levels = unique(targets$Condition))
design <- model.matrix(~0 + f)
colnames(design) <- levels(f)

## fit intensity values to linear model
fit <- lmFit(y.ave, design)

# crate contrast for comparison
contrast.matrix <- makeContrasts("trail-control", levels = design)
fit2 <- contrasts.fit(fit, contrast.matrix)
fit2 <- eBayes(fit2)

# volcano plot of all probes
volcanoplot(fit2, "trail-control")

# decide tests
results <- decideTests(fit2)

# results table
output.trail <- topTable(fit2, adjust = "BH", coef = "trail-control",
genelist = y.ave$genes, number = Inf)
write.csv(output.trail, file =
paste(main.dir, "TRAILvsControl_Expression_Results.txt", sep = "/"),
row.names=F)

```

### **8.2.2 SPIA pathway topology analysis**

Pathway topology analysis was performed using the SPIA R package with KEGG pathways. The Ensembl Biomart R package was used to download matching Entrez IDs for Agilent microarray probe IDs. The plyr R package was used for data manipulation. The Biocmanager package was used for package management.

*SPIA: <http://bioconductor.org/packages/release/bioc/html/SPIA.html>*

*Biomart: <https://bioconductor.org/packages/release/bioc/html/biomaRt.html>*

*Plyr: <https://cran.r-project.org/web/packages/plyr/index.html>*

*Biocmanager: <https://cran.r-project.org/web/packages/BiocManager/index.html>*

```
# set main folder
main.dir <- "."
setwd(main.dir)

# requirements
if (!requireNamespace("BiocManager", quietly = TRUE))
install.packages("BiocManager")
library('BiocManager')
BiocManager::install("SPIA")
install.packages('plyr')
library("SPIA")
library('biomaRt')
library('plyr')

# run SPIA using pathways data generated from (up-to-date) xml files
obtained from http://www.kegg.jp/
kegg.dir <- "./hsa83.0_2017-07-01"
kgml.dir <- paste(kegg.dir, "kgml", sep = "/")
kegg.spia <- paste(kegg.dir, "spia", sep = "/")
makeSPIAdata(kgml.path = kgml.dir, organism = "hsa", out.path = kegg.spia)

# read limma export table
expr.table <- read.csv(file = paste(main.dir,
"TRAILvsControl_Expression_Results.txt"), header = T)
```

```

# convert agilent probe IDs to entrez with biomaRt
ensembl = useEnsembl(biomart = "ensembl", dataset="hsapiens_gene_ensembl")
genes.entrez <- getBM(attributes = c('agilent_sureprint_g3_ge_8x60k_v2',
  'entrezgene'), filters = 'agilent_sureprint_g3_ge_8x60k_v2', values =
  expr.table$ProbeName, mart = ensembl)
colnames(genes.entrez) <- c('ProbeName', 'entrez')

# merge entrez ID into expression table
expr.table.2 <- merge(expr.table, genes.entrez, by = 'ProbeName', all.x =
  FALSE, all.y = FALSE)

# remove rows without entrez ID
top <- expr.table.2[!is.na(expr.table.2$entrez), ]

# average fold change for duplicate probes
top.aveFC <- ddply(top, "entrez", numcolwise(sum))

# define DE genes for SPIA
data <- top.aveFC
sig = 0.05
nrow(data[data$adj.P.Val < sig, ])
tg1 <- data[data$adj.P.Val < sig, ]

# extract fold changes from DE genes
de.genes = tg1$logFC
names(de.genes) <- as.vector(tg1$entrez)

# all genes list
all.genes = data$entrez

# run spia with generated pathway data
res <- spia(de = de.genes, all = all.genes, organism= "hsa", nB = 2000,
  plots = TRUE, verbose = TRUE, beta = NULL, combine = "fisher", data.dir =
  paste(kegg.spia, "/", sep = ""))

# save pathways table
write.csv(res, file = paste(main.dir, keggversion, "pathways.csv",
  sep="/"))

# save spia plot
pdf(file = paste(main.dir, keggversion, "spia.pdf", sep = "/"))

```

```

plotP(res, threshold = 0.05)
dev.off()

# save res object for future use
saveRDS(res, file = paste(main.dir, keggversion, "res", sep = "/"))

```

## 8.3 Appendix C: Genotyping PCR

### 8.3.1 Genotyping PCR primers

Name	Sequence
CSD-Tnfsf10-F	TTCCCTCAATCCCAACCTCCTTTCC
CSD-Tnfsf10-ttR	CCCTGCCCCAGATTTTGTAGTAACC
CSD-loxF	GAGATGGCGCAACGCAATTAATG
CSD-Tnfsf10-R	CAGGGGTAGGTAGATAGCTTGCTGG
HELpr010	GCATTACCGGTCGATGCAACGAGTGATGAG
HELpr011	GAGTGAACGAACCTGGTCGAAATCAGTGCG
HELpr012	TGGACAGGACTGGACCTCTGCTTTCCTAGA
HELpr013	TAGAGCTTTGCCACATCACAGGTCATTCAG
SMWT1	TGACCCCATCTCTTCACTCC
SMWT2	AACTCCACGACCACCTCATC
PHCreAS1	AGTCCCTCACATCCTCAGGTT

### 8.3.2 *TRAIL<sup>tm1c</sup>* & *TRAIL<sup>WT</sup>* PCR reaction

Reagent	µl per reaction
REExtract-N-Amp PCR mix (2X)	10
Nuclease-free water	4.4
CSD-Tnfsf10-F (10 uM)	0.8
CSD-Tnfsf10-ttR (10 uM)	0.8
<i>DNA</i>	4
Total	20

Temp.	Time	Cycles
94°C	5 min	
94°C	15 sec	
65...56°C	30 sec	10X
72°C	40 sec	
94°C	15 sec	
55°C	30 sec	30X
72°C	40 sec	
72°C	5 min	
4°C	hold	

Expected products:

- TRAIL<sup>tm1c</sup> (604 bp)
- TRAIL<sup>WT</sup> (456 bp)

### 8.3.3 TRAIL<sup>tm1d</sup> & distal LoxP site PCR reaction

Reagent	µl per reaction
REExtract-N-Amp PCR mix (2X)	10
Nuclease-free water	4.4
CSD-loxF (10 uM)	0.4
CSD-Tnfsf10-F (10 uM)	0.4
CSD-Tnfsf10-R (10 uM)	0.8
DNA	4
Total	20

Temp.	Time	Cycles
94°C	5 min	
94°C	15 sec	
65...56°C	30 sec	10X
72°C	40 sec	
94°C	15 sec	
55°C	30 sec	30X
72°C	40 sec	
72°C	5 min	
4°C	hold	

Expected products:

- TRAIL<sup>tm1d</sup> (681 bp)
- Distal loxP (282 bp)

#### 8.3.4 COL1A2-Cre-ERT / PGK-Cre & WT control PCR reaction

Reagent	µl per reaction
REExtract-N-Amp PCR mix (2X)	10
HELpr010 (10 uM)	2
HELpr011 (10 uM)	2
HELpr012 (10 uM)	1
HELpr013 (10 uM)	1
DNA	4
Total	20

Temp.	Time	Cycles
93°C	1 min	
93°C	20 sec	30X
68°C	3 min	
4°C	hold	

Expected products:

- COL1A2-Cre-ERT / PGK-Cre (408 bp)
- WT control (194 bp)

### 8.3.5 SMMHC-Cre-ERT2<sup>tg</sup> / SMMHC-Cre-ERT2<sup>wt</sup> PCR reaction

Reagent	µl per reaction
REDExtract-N-Amp PCR mix (2X)	10
Nuclease-free water	1
SMWT1 (10 µM)	2
SMWT2 (10 µM)	1
PHCreAS1 (10 µM)	2
DNA	4
Total	20

Temp.	Time	Cycles
95°C	2 min	
95°C	45 sec	30X
58°C	45 sec	
72°C	2 min	
72°C	5 min	
4°C	hold	

Expected products:

- SMMHC-Cre-ERT2<sup>tg</sup> (300 bp)
- SMMHC-Cre-ERT2<sup>wt</sup> (200 bp)